U.S. GEOLOGICAL SURVEY CIRCULAR 937

Proceedings of the 1980 Workshop of the International Association of Seismology and Physics of the Earth's Interior on the Seismic Modeling of Laterally Varying Structures: Contributions Based on Data from the 1978 Saudi Arabian Refraction Profile

Proceedings of the 1980 Workshop of the International Association of Seismology and Physics of the Earth's Interior on the Seismic Modeling of Laterally Varying Structures: Contributions Based on Data from the 1978 Saudi Arabian Refraction Profile

Walter D. Mooney and Claus Prodehl, Editors

U.S. GEOLOGICAL SURVEY CIRCULAR 937

1984

Department of the Interior
WILLIAM P. CLARK, *Secretary*

U.S. Geological Survey
Dallas L. Peck, *Director*

Library of Congress Cataloging in Publication Data

International Association of Seismology and Physics of the Earth's Interior. Workshop (1980 : Park City, Utah)
Proceedings of the 1980 Workshop of the International Association of Seismology and Physics of the Earth's Interior on the seismic modeling of laterally varying structures.

(U.S. Geological Survey Circular 937)
Includes bibliographical references.
Supt. of Docs. no.: I 19.4/2:937
1. Seismology—Saudi Arabia—Congresses. 2. Seismic refraction method—Congresses. 3. Geology—Saudi Arabia—Congresses. I. Mooney, Walter D. II. Prodehl, Claus, 1936- . III. Title. IV. Series: United States. Geological Survey. Circular 937.
QE537.2.S33I57 1980 551.8'0953 84-600241

Free on application to Distribution Branch, Text Products Section, U.S. Geological Survey, 604 South Pickett Street, Alexandria, VA 22304

CONTENTS

FOREWORD

This volume is a collection of contributions presented at the 1980 IASPEI (International Association of Seismology and Physics of the Earth's Interior) workshop of the Commission on Controlled Source Seismology (CCSS), addressing seismic modeling of laterally varying structures. The participants of this workshop described research on state-of-the-art geophysical techniques applied to seismic refraction data. The data were collected during 1978 under a work agreement between the Directorate General of Mineral Resources, Kingdom of Saudi Arabia, and the U.S. Geological Survey. The results from this international cooperative effort at interpretation are presented herein.

The participants of this workshop were asked for contributions leading to an understanding of the crustal structure along the Saudi Arabian seismic refraction profile. As no specific format was solicited from participants, the proceedings contain contributions of varying lengths and formats. Crustal model illustrations and figures comparing the contributed crustal interpretations prepared by the editors are included.

The efforts and contributions of IASPEI participants uniquely advance insight into Saudi Arabian crustal structure along the 1978 profile. It is hoped that these workshop presentations will stimulate further work in the general area of seismic modeling of laterally varying structures and in the study of the crustal structure of the Red Sea and the Saudi Arabian Peninsula.

On behalf of all the participants of the workshop, we would like to thank the editors for taking the time to prepare this volume.

Stephan Mueller
Irina Kosminskaya
Co-chairmen, Commission on Controlled Source Seismology

PROCEEDINGS OF THE 1980 WORKSHOP OF THE INTERNATIONAL ASSOCIATION OF SEISMOLOGY AND PHYSICS OF THE EARTH'S INTERIOR ON THE SEISMIC MODELING OF LATERALLY VARYING STRUCTURES: CONTRIBUTIONS BASED ON DATA FROM THE 1978 SAUDI ARABIAN REFRACTION PROFILE

INTRODUCTION

By W. D. Mooney

During the past ten years significant progress has been made in the methods of collection and analysis of seismic refraction and reflection data. This progress has led to the development of new models for the structure and composition of the earth's crust, based on sophisticated analysis of numerous profiles in many areas of geologic importance. The third triennial meeting of the IASPEI Commission on Controlled Source Seismology convened in Park City, Utah, on August 11-17, 1980, to bring together seismologists and geologists to assess the status of controlled source techniques (including explosions, air guns, and vibrators) and to evaluate their usefulness for modeling seismic velocity structure and composition of the crust and upper mantle. Progress and problems in modeling two- and three-dimensional structures received particular attention.

Park City was an ideal location for the conference, as examples of the complex structures that we are presently attempting to model can be seen in that area. The effects on the crust of tectonic forces were easily discernible from the air during the approach to the Salt Lake City airport, as they were on the ground during the field trip into the Wasatch Mountains led by R. B. Smith of the University of Utah. Forty-six seismologists from 11 countries attended the conference and a few more sent written contributions.

Two-and-one-half days of the five-day conference were devoted to discussing interpretations of the seismic refraction data collected in Saudi Arabia by the U.S. Geological Survey in 1978 (Blank and others, 1979). The complete refraction data set had been distributed to the participants before the meeting, giving each seismologist (or team of seismologists) time to analyze the same data. Therefore, the participants were able to discuss issues of interpretation in more detail than is possible in traditional workshops which are based on diverse data sets.

Because the known surface geology must constrain seismic interpretation, the session opened with a discussion of the geologic framework of Saudi Arabia and the southeastern Red Sea. (All participants received the U.S. Geological Survey's 1963 geologic map of Saudi Arabia.) H. R. Blank introduced the geologic problems of Saudi Arabia, and M. Q. Assad outlined the planning and goals of the 900-km-long refraction profile (fig. 1), after which a series of speakers explained their team's interpretation of the data and the methods they used to derive velocity-depth structures. Six participants presented their deep seismic reflection techniques, and five presented new theoretical approaches on the interpretation of explosion seismic data. Five other participants discussed the uniqueness and physical significance of structural models. These presentations led to general discussions on the principles of correlation and subsequent inversion techniques.

In the course of the presentations it became evident that the differences between the models usually resulted from differing phase correlation. The term "phase correlation" refers to the process of identifying, within a seismic record section, those arrivals that refract or reflect from the same velocity feature of the crust or mantle. For example, the P* phase refracts in the middle crust while the PmP phase reflects from the crust-mantle boundary. A knowledge of the expected amplitude and frequency of a particular phase, based on experience and theoretical considerations, facilitates its correlation within the record section, but the complexity of the typically observed wave fields leads to a degree of subjectivity in the interpretation of the phases. Given identical phase correlations, different methods of traveltime and amplitude analysis of these phases will produce nearly the same models. However, different phase correlations will result in markedly divergent models regardless of further analysis methods. This is seen when comparing the models of the Arabian Shield (fig. 2A) to those of the continent-Red Sea transition (fig. 2B). For the most part, the teams of interpreters agreed on the phase correlation of the profiles between shotpoints 1 and 5, and the similarity of the resultant models reflect this agreement. However, the correlations and interpretations of the data crossing the continent-Red Sea transition were diverse and ultimately led to quite different models for that region (fig. 2B).

To summarize, the CCSS workshop interpretation of the Saudi Arabian data showed the following:

1. The upper crust of the shield is 21 km thick and has an average velocity of 6.25 km/s. In some regions there are small velocity discontinuities and low-velocity zones.

2. The lower crust of the shield (19 km thick) is separated from the upper crust by a seismic discontinuity where the velocity increases by 0.3 km/s. The average velocity of the lower crust is about 6.7 km/s. Velocities greater than 7.0 km/s may be present in the lowermost crust.

3. The M-discontinuity is probably a transition zone 2-5 km thick at an average depth of about 40 km. The uppermost mantle velocity probably increases laterally from 8.0 km/s beneath the Red Sea to 8.2 km/s beneath the Arabian Platform.

4. The structure of the continent-Red Sea transition remains uncertain with the currently available data. The range of proposed models is indicated in figure 2B. Improved models would result from the recommendations below.

5. There is considerable evidence for fine structure in the upper mantle, including low-velocity zones and velocity discontinuities between 40 and 70 km depth.

The participants of the meeting recommended the following methods for future seismic refraction and reflection work in areas with strongly laterally heterogeneous velocity structure, such as the continent-Red Sea transition in western Saudi Arabia:

1. Parallel-to-structure refraction profiles are needed, in the present case, along the coastal plain and in the Red Sea.

2. Perpendicular-to-structure profiles must be densely recorded and should include considerable data redundancy.

3. Seismic reflection profiles would help resolve details in the areas of greatest structural complexity. In the present case, reflection profiles across the Hijaz-Asir escarpment (fig. 1) would shed light on the structure of this rift boundary.

REFERENCES

Blank, H. R., Healy, J. H., Roller, J. C., Lamson, R. J., Fischer, F., McClearn, R., and Allen, S., 1979, Seismic refraction profile, Kingdom of Saudi Arabia--Field operations, instrumentation and initial results: U.S. Geological Survey Saudi Arabian Mission Project Report 259, 49 p.

U.S. Geological Survey and Arabian-American Oil Company, 1963, Geologic map of the Arabian Peninsula: U.S. Geological Survey Miscellaneous Geologic Investigations Map I-270A, scale 1:2,000,000.

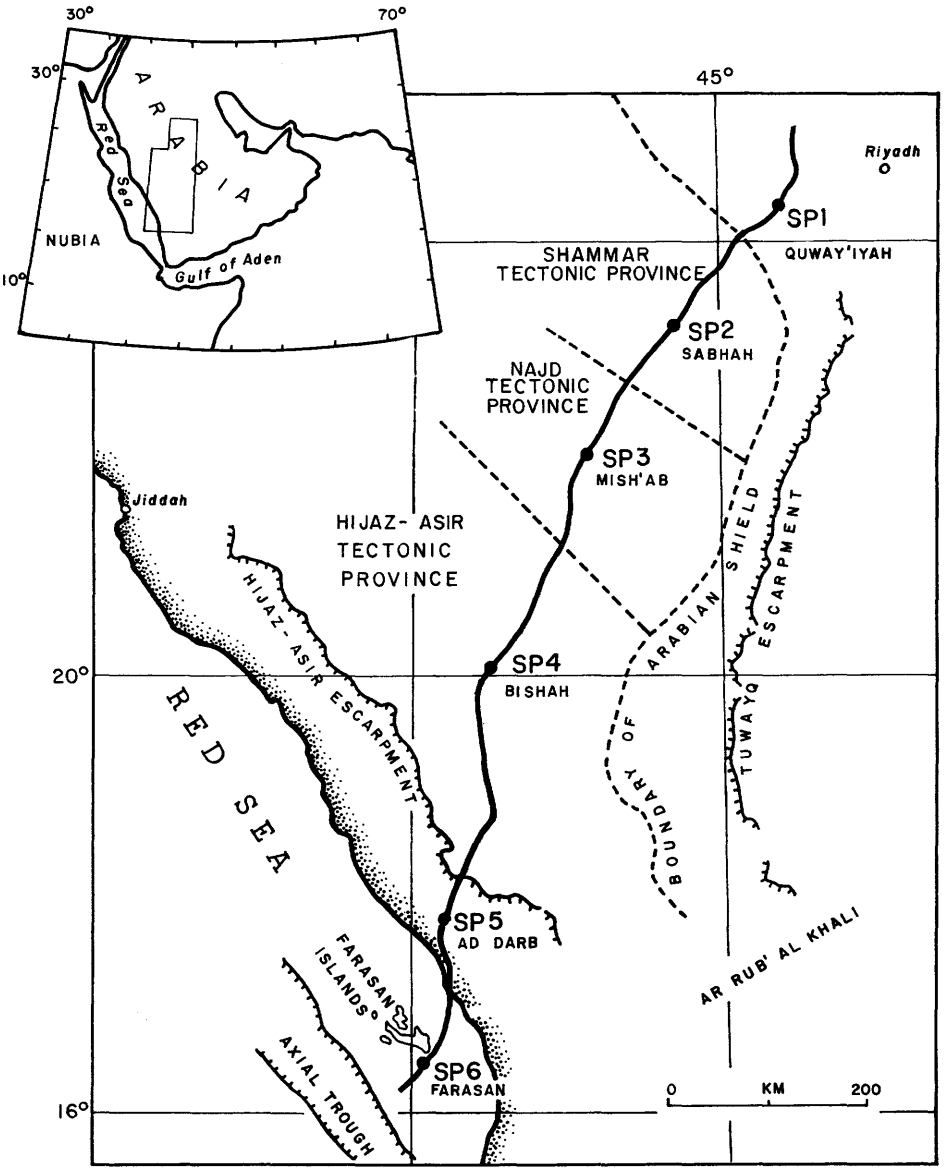

Figure 1. Location map of the 1978 USGS/DGMR-conducted seismic refraction profile across western Saudi Arabia and the southeastern Red Sea, interpreted by the IASPEI CCSS workshop participants, showing the shotpoints (SP), the profile line (heavy line), and the tectonic provinces.

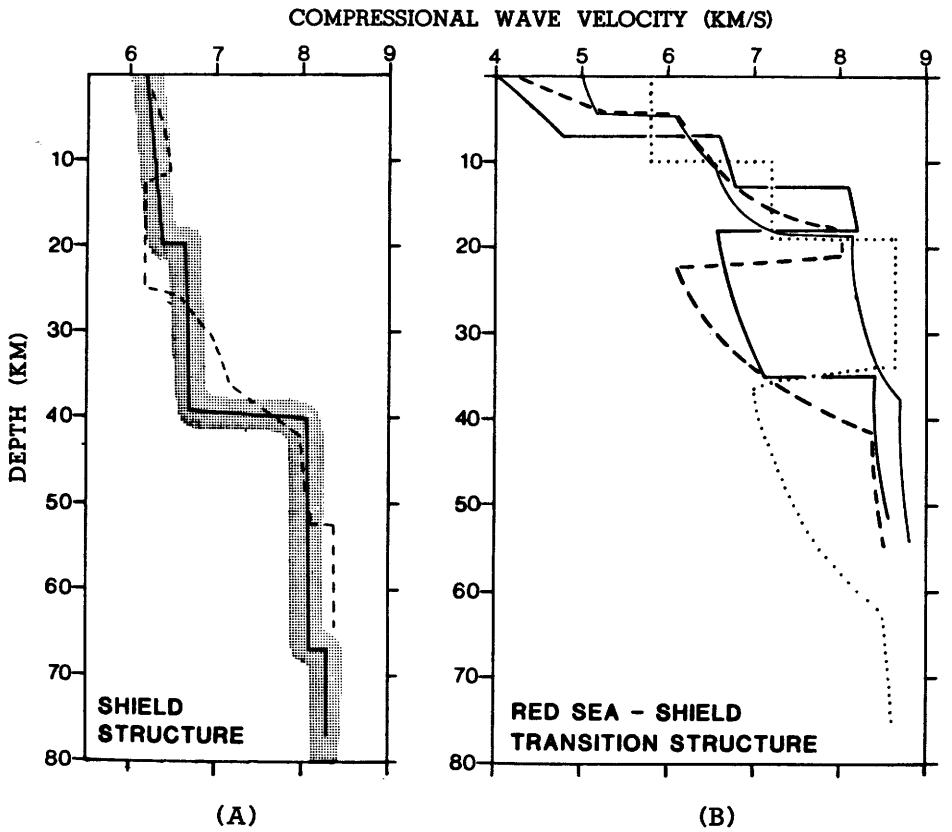

Figure 2. A, P-wave velocity-depth structure of the Arabian Shield presented by workshop participants. Shaded region outlines the range of velocities of most models, solid line is a typical example of a velocity structure, and dashed line is an alternative model. B, Four P-wave velocity structures for the Arabian Shield-Red Sea transition. Data were sparse in this laterally inhomogeneous region, causing interpretations to differ radically.

ACKNOWLEDGMENTS

The participants thank the officers of the Commission on Controlled Source Seismology, particularly co-chairmen S. Mueller, from Eidgenössische Technische Hochschule (ETH)-Zurich, Switzerland, and I. P. Kosminskaya, from the Institute of the Physics of the Earth, Moscow, USSR, and secretary J. Ansorge, also from ETH-Zurich, Switzerland, for their support and contributions to the IASPEI workshop. We also thank D. P. Hill, Menlo Park, California, J. A. Orcutt, La Jolla, California, and R. B. Smith, Salt Lake City, Utah, for the local planning and organizing of the August 1980 workshop.

The U.S. Geological Survey Saudi Arabian Mission personnel, in particular G. E. Andreason, H. R. Blank, and D. F. Davidson, gave their continuous support from the planning of the seismic refraction survey across Saudi Arabia to the completion of the IASPEI workshop. The research presented by the IASPEI participants at the workshop significantly contributed to the understanding of the crustal structure of Saudi Arabia along the seismic refraction profile.

We thank F. McKisic for arranging financial support from the Office of Naval Research which, together with that from the U.S. Geological Survey, made the IASPEI workshop possible. We thank the Directorate General of Mineral Resources, Saudi Arabia, for permission to use the seismic refraction data for this workshop.

PRELIMINARY INTERPRETATION OF SAUDI ARABIAN SEISMIC REFRACTION DATA

By J. Ansorge[1], E. Banda[1], H. Benz[2], S. Mueller[1], and R. B. Smith[2]

[1]Institute of Geophysics, Swiss Federal Institute of Technology
CH-8093, Zurich, Switzerland

[2]Department of Geology and Geophysics, University of Utah
Salt Lake City, Utah 84112

INTRODUCTORY REMARKS

For a preliminary interpretation the following methods have been applied to the record sections from shotpoint 1 to shotpoint 5:

--Correlation of first and later traveltime branches,
--Comparisons of correlated phases with those on adjacent and reversed profiles,
--Computation of traveltimes by trial and error for flat and parallel layered models,
--Adjustment of models to make the best fit with observed traveltimes, distances, and amplitude characteristics,
--Computation of synthetic seismogram sections for a few selected profiles.

The individual velocity-depth models have been combined into a preliminary crustal cross section.

The entire profile (shot 1 - shot 6) has been grouped into three sections according to similar characteristics and numbers of traveltime branches.

Northern sections: profiles 1 SW, 2 NE, 2 SW
Central section: profiles 3 SW, 4 NE, 4 SW, 5 NE
Southern sections: profiles 5 SW, 6 NE

NORTHERN SECTION

The very thin sedimentary or weathered layer near the surface has been ignored. Below this layer the velocity increases rapidly from 6.0 km/s to 6.2 km/s at a depth of about 2 km. This layer can be interpreted either as a weathered part of the basement or a separate layer overlying a basement with a velocity of 6.2 km/s. A more detailed interpretation of the available seismic and geologic data may answer this question. The critical distance of the underlying refractor with a velocity of 6.4 km/s suggests the existence of a low-velocity layer with a thickness of about 5 km and an assumed velocity of 5.6 km/s. Both the low-velocity layer and the underlying 6.4 km/s layer are depressed by about 3 km from shotpoint 1 to shotpoint 2.

The transition to the lower crust occurs at a depth of about 27 km with a sharp increase in velocity from 6.4 km/s to 6.8 km/s.

The traveltimes of Pn and PmP indicate a thinning of the crust from 40 km under shotpoint 1 to 37 km west of shotpoint 2.

CENTRAL SECTION

A rather homogeneous crust characterizes the central section over a distance of about 500 km from shotpoint 3 to north of shotpoint 5.

A near-surface layer with a velocity of 6.0 km/s varies in thickness from zero at shotpoint 5 to 3.5 km south of shotpoint 4. This layer is clearly separated from material with a velocity of 6.3 km/s. This separation correlates with outcrops of greenstone on profile 5 North with a velocity at the surface of 6.3 km/s. The crust-mantle boundary lies at about 37 km depth between shotpoint 3 and shotpoint 5. The mean Pn velocity north of shotpoint 5 is 8.1 km/s.

A velocity of 6.5 km/s between depths of 12 and 22 km in the upper crust under shotpoint 5 might be interpreted as a transitional feature to the Red Sea rift.

SOUTHERN SECTION

The data from profiles 5 SW and 6 NE document a highly complex and laterally varying crustal structure. The thickness of the young sediments increases from zero at shotpoint 5 to about 3 km north of shotpoint 6. The observations of PmP and Pn indicate a crustal thickness of about 22 km with a mean crustal velocity of 6.5 km/s and a Pn velocity of about 7.8 km/s. Secondary phases arriving with an apparent velocity of 8.0 to 8.1 km/s after the relatively early Pn of 7.8 km/s are evidence for a further differentiation in the uppermost mantle beneath the thin crust characteristic of the Red Sea rift.

LATERAL VARIATION OF THE CRUSTAL STRUCTURE

From the crustal structure deduced for each of the three sections the presence of significant lateral variations over the entire profile is evident.

The main features characterizing the lateral variations are as follows: (1) a low-velocity layer exists under the northern section only; (2) the southern boundary of this section shows an abrupt offset of about 6 km in the lower crust, possibly related to the transition from the Arabian platform to the shield; (3) the transition from the shield structure to the Red Sea rift begins north of shotpoint 5 with the appearance of a refractor of a velocity of 6.5 km/s at about 12 km depth; (4) south of shotpoint 5 thickening sediments characterize the transition to the Red Sea rift; (5) the Pn velocity decreases from 8.1 to 7.8 km/s beneath the margin of the rift.

CORRELATIONS

Shot 1 - South

$t = 0 + \Delta/6.0$
$t = 0.28 + \Delta/6.22$
$t = 1.3 + \Delta/6.38$
$t = 3.63 + \Delta/6.85$
$t = 7.87 + \Delta/8.3$

Shot 2 - North

$t = 0 + \Delta/6.0$
$t = 0.2 + \Delta/6.21$
$t = 0.53 + \Delta/6.42$
$t = 3.6 + \Delta/6.78$

Shot 2 - South

$t = 0 + \Delta/6.0$
$t = 0.34 + \Delta/6.17$
$t = 1.62 + \Delta/6.37$
$t = 2.73 + \Delta/6.67$
$t = 7.19 + \Delta/8.04$

Shot 3 - North

P $t = 0.08 + \Delta/6.0$
S $t = 0.08 + \Delta/3.51$
R $t = \Delta/2.96$
$V_p V_s = 1.71$ $V_R/V_S = 0.84$

Shot 3 - South

$t = 0.05 + \Delta/6.0$
$t = 0.3 + \Delta/6.33$
$t = 2.25 + \Delta/6.68$
$t = 6.8 + \Delta/8.14$

Shot 4 - North

$t = 0 + \Delta/6.0$
$t = 0.1 + \Delta/6.23$
$t = 2.6 + \Delta/6.75$

Shot 4 - South

$t = 0 + \Delta/6.0$
$t = 0.37 + \Delta/6.33$
$t = 2.63 + \Delta/6.78$

Shot 5 - North

$t = \Delta/6.33$
$t = 0.69 + \Delta/6.5$
$t = 6.4 + \Delta/7.9$

Shot 1 - South

Depth (km)	V_p(km/s)
.00	6.00
3.19	6.00
3.19	6.19
7.00	6.25
7.00	5.60
11.00	5.60
11.00	6.38
26.80	6.38
26.80	6.85
40.50	6.85
40.50	8.30
45.00	8.30

Shot 2 - North

Depth (km)	V_p(km/s)
.00	6.00
2.44	6.00
2.44	6.18
9.00	6.25
9.00	5.60
13.00	5.60
13.00	6.42
28.00	6.42
28.00	6.78
38.00	6.78
38.00	8.20
45.00	8.20

Shot 2 - South

Depth (km)	V_p(km/s)
.00	6.00
4.38	6.00
4.38	6.14
10.00	6.20
10.00	5.60
14.00	5.60
14.00	6.37
21.30	6.37
21.30	6.67
37.00	6.67
37.00	8.04
40.00	8.04

Shot 3 - South

Depth (km)	V_p(km/s)
.00	6.00
2.82	6.00
2.82	6.30
22.16	6.36
22.16	6.68
35.50	6.68
35.50	8.14
45.00	8.14

Shot 4 - North

Depth (km)	V_p(km/s)
.00	6.00
1.11	6.00
1.11	6.20
22.50	6.26
22.20	6.75
37.00	6.75
37.00	8.14
45.00	8.14

Shot 4 - South

Depth (km)	V_p(km/s)
.00	6.00
3.48	6.00
3.48	6.30
21.81	6.36
21.81	6.78
37.00	6.78
37.00	8.10
45.00	8.10

Shot 5 - North

Depth (km)	V_p(km/s)
.00	6.31
11.80	6.35
11.80	6.50
22.00	6.50
22.00	6.80
37.00	6.80
37.00	7.90
40.00	7.90

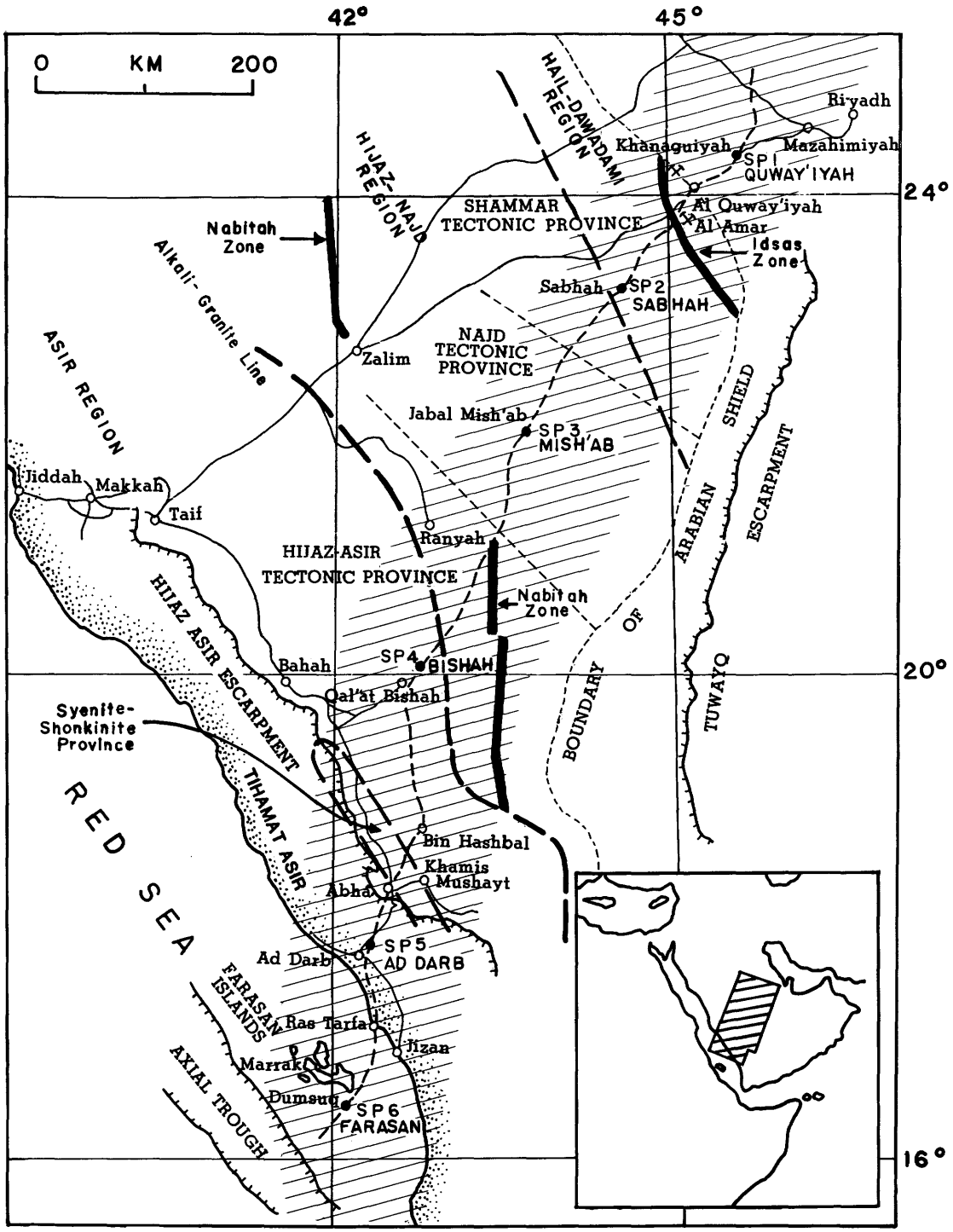

Figure 3. Index map of western Saudi Arabia showing the seismic refraction line (dashed) and shotpoints (SP).

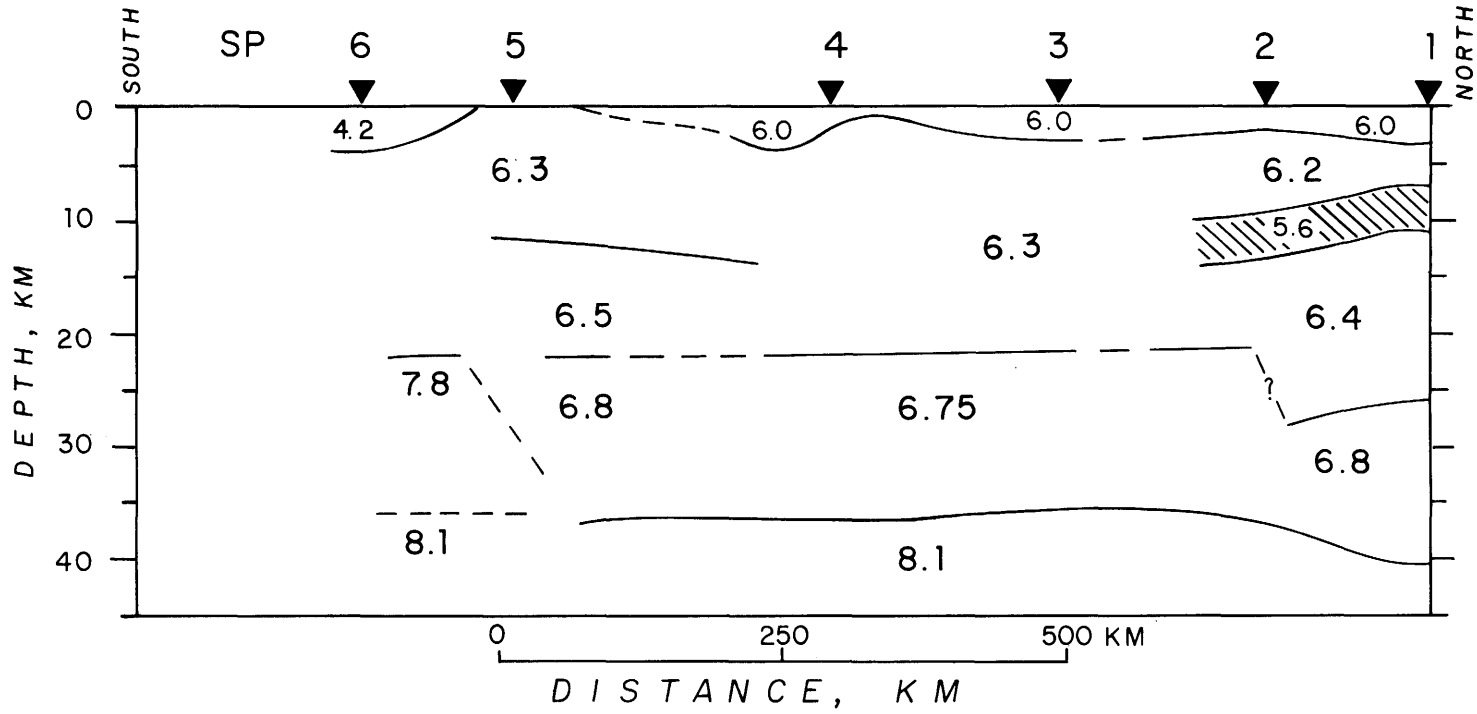

Figure 4. Cartoon cross section of the Saudi Arabian seismic refraction profile showing major layer velocities and prominent changes in crustal structure.

TWO-DIMENSIONAL INVERSE KINEMATIC PROBLEM--APPLICATION TO THE SAUDI ARABIAN REFRACTION PROFILE

By Petr Firbas

Geofyzika Brno
Ječná 29a, 612 46 Brno, Czechoslovakia

An iterative method for solving the inverse kinematic problem for the two-dimensional laterally inhomogeneous medium is proposed here based on the linearization approach and the ray theory. Model calculation results and the velocity model for a part of a refraction profile across Czechoslovakia are presented. The computer program solving the inverse kinematic problem based on the above-mentioned algorithm is tentatively applied to the Saudi Arabian refraction profile data. Preliminary results are presented as a velocity contour map and verified by ray tracing.

Nowadays the solution of the inverse seismic problem represents a high priority task. In carrying out a seismic survey we are nearly always concerned with a heterogeneous medium, and our aim is to establish these lateral inhomogeneities, no matter whether the point of our interest is the deep seismic soundings, seismic prospecting for engineering purposes, or prospecting for oil or minerals.

The kinematic parameters (that is, the times of seismic wave propagation from various shot points to various geophone locations) seem to be the most reliable input data for solving the inverse problem. We may utilize the arrivals of seismic waves of various types, but it is evident that the time of the first arrival can be determined with the highest precision.

It follows from our model calculations that, especially in the case of the laterally inhomogeneous medium without distinct seismic interface, knowledge of refracted wave arrivals nearly always enables us to resolve substantial lateral inhomogeneities. The model obtained using refraction wave arrivals can be improved in a few steps, in each of which the direct problem is repeatedly solved (computation of synthetic seismograms for laterally inhomogeneous medium (Červený, 1979) and ray tracing (Pšenčik, 1976)). At these iterative steps all the other information gained by profile measurements can be used.

A mathematical procedure solving the above stated inverse problem has been proposed. The procedure is based on the linearization of the multidimensional inverse kinematic problem. The linearization approach was introduced by V. G. Romanov (Alekseev and others, 1970). The ray theory (Červený and others, 1977) has been applied for the computation of rays and refracted wave arrivals. The mathematical procedure proposed is an iterative one, and at each step we are minimizing a quadratic form so that we are forced to solve a relatively large system of linear equations. The perturbation part of the two-dimensional slowness function is expressed at each step in the form of a twofold series of polynomials being orthogonal in a rectangular area. The rectangular area was obtained through a transformation of an irregular area covered by rays of refracted waves. A detailed description of the mathematical procedure proposed will be published elsewhere. The linearization approach has already been successfully used to solve the inverse kinematic problem by Alekseev and others (1970), but with a different algorithm.

Let us first present a model example of the solution of the inverse kinematic problem for a laterally inhomogeneous medium. For that purpose a theoretical velocity model of an anticline (fig. 5) was chosen. The theoretical traveltime curves of the refracted waves were computed (fig. 6).

As the input data for the algorithm proposed must be in the form of discrete points, the traveltime curves computed were sampled and the refracted wave arrival time values for a series of epicentral distances R were obtained for all shotpoints. These values are plotted in figure 7 in the form of the so-called "special time field." Individual discrete points derived from the traveltime curves are represented by means of graphic symbols. Lines in figure 7 connect the points corresponding to the same epicentral distances R.

As a starting approximation, a laterally homogeneous model derived by a modified Wiechert-Herglotz method was used. After the first iteration the laterally inhomogeneous velocity distribution shown in figure 8 was obtained. The first-order perturbation function was expressed in the form of a twofold series of the Legendre polynomials. The maximum rank of the polynomials was 5 in the x-axis direction and 3 in the z-axis direction. For an easier comparison of the theoretical and computed velocity models a contour map of relative deviations between these two models is presented in figure 9. (Relative deviation values are expressed in percent. The maximum relative deviation is about 1.5 percent.)

Although the algorithm described is still in the development stage, it has already been used for the computation of velocity distribution models along some regional profiles. As an example, a computed velocity distribution along the northern part of the Trans-Carpathian profile K-III across Czechoslovakia is presented in figure 10. The computed model shows an area of a relatively strong lateral inhomogeneity, the area where the high velocity crystalline basement reaches the surface, the area being surrounded on both sides by low velocity sediments (Beránek and others, 1979).

The proposed mathematical procedure for solving the inverse kinematic problem requires a relatively dense system of traveltime curves of refracted waves. The more the traveltime curves cross a particular geophone location, the better the resulting computed velocity model and the higher the resolving power of the solution will be.

In the case of the Saudi Arabian refraction profile, this condition is not fulfilled because refracted waves from only about two shotpoints were recorded at each geophone location; nevertheless, we tentatively tried to apply our computer program.

In the wave fields the arrivals of the principal waves were distinguished. The traveltime curves were digitized on a digitizer with the sampling interval of 1 km. From the refracted traveltime curves, which are plotted on an unreduced scale in figure 11, the special time field (see fig. 12) was constructed. As input data we obtained the arrivals of 100 rays of refracted waves evenly distributed along the whole profile.

From this special time field (fig. 12) we can conclude that the crust in the area between shotpoints 1 and 5 is relatively laterally homogeneous and that in the area between shotpoints 5 and 6 we can expect lower velocities in the upper part and a sharp rise in the velocities in greater depths.

The computed velocity distribution is shown in figure 13. The first-order perturbation function was expressed in the form of a twofold series of Legendre polynomials of maximum rank 5 in both x and z axes.

The computed velocity model presented has to be regarded as preliminary because our computer program was used for the input data without any corrections, and only the first-order perturbation function was computed. In spite of that, we obtained a velocity model showing in rough outline distinct lateral inhomogeneities down to the depth of 32 km. A large lateral inhomogeneity can be seen, particularly in the area between shotpoints 5 and 6.

The character of the record sections permits us to assume the existence of an inner discontinuity in the crust. As the computed two-dimensional velocity model is represented by a smooth function, we can expect the appropriate velocity contrast to the depicted as a smooth velocity transition zone separating two areas of different nature in the crust.

We attempted to verify the computed velocity model by ray tracing (Pšenčik, 1976). Ray diagrams for all shotpoints were computed. An example of the ray diagram for shotpoint 1 is shown in figure 14. The agreement between the measured traveltime curves (plotted as a line) and the calculated arrivals can be seen in figure 15. (This picture is plotted in the reduced scale with the reduction velocity of 6.0 km/s.) The differences are comparatively small for the upper part of the crust and increase somewhat for greater depths.

The method proposed is iterative. The results presented above represent only the first approximation. The resulting model gives a good picture of large lateral inhomogeneities, but the differences between the theoretical and experimental traveltimes are still relatively high in certain parts of the profile (see fig. 15).

The next step is to improve the computed two-dimensional model by calculating the higher order perturbation functions. Before we do so, the relief and other corrections should be applied. At each step, the ray-tracing and synthetic seismogram calculations will be used to distinguish distinct seismic boundaries in the crust and to verify the model.

No attempts have been made yet to determine the Moho geometry and the structure of the uppermost mantle along the profile. This will be done after the structure of the crust has been determined to the desired accuracy.

Acknowledgments

I am greatly indebted to V. Červený for valuable discussions and for his kind help during the preparation of this paper. Thanks are also due to B. Beránek for his encouragements, I. Pšenčik for his ray-tracing computer program, and to all coworkers for their help. The management of Geofyzika Brno gave permission to submit the paper to the workshop meeting.

REFERENCES

Alekseev, A. S., Lavrentev, M. M., Muchometov, R. G., Nersesov, I. L., Romanov, V. G., 1970, Method for numerical investigation of horizontal non-homogeneities of the Earth's mantle by seismological data: Proceedings of the X assembly of the ESC, Leningrad, 3-11 September 1968, Academy of Sciences of the USSR, Moscow, v. 1, p. 26-36. (In Russian, English abstract.)

Beránek, B., Leško, B., and Mayerová, M., 1979, Interpretation of seismic measurements along the Trans-Carpathian profile K-III, in Geodynamic investigations in Czechoslovakia, final report: Vaněk, J., Babuška, V., and Plančár, J., eds., VEDA, Bratislava, p. 201-206.

Červený, V., 1977, Ray theoretical seismograms for laterally inhomogeneous structures: Journal of Geophysics, v. 46, p. 335-342.

Červený, V., Molotkov, I. A., and Pšenčik, I., 1977, Ray method in seismology: Univerzita Karlova, Praha, 214 p.

Pšenčik, I., 1976, Program RATLIM, rays, amplitudes, and traveltimes in laterally inhomogeneous media: Uppsala, unpublished report.

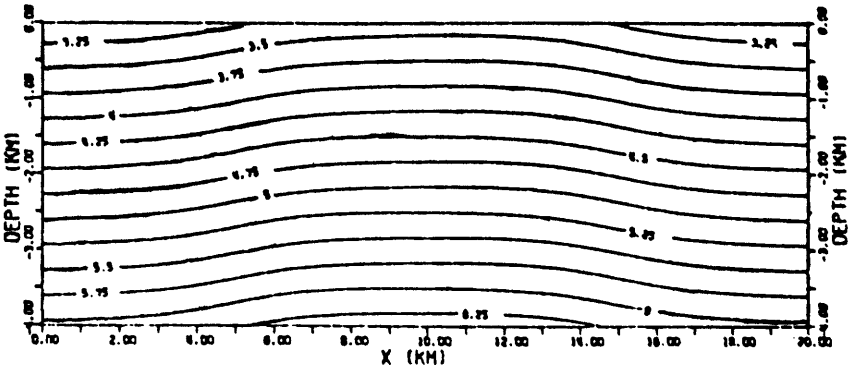

ANTICLINE I

THEORETICAL VELOCITY MODEL

$V=A+ B*Z + 2*C*ARCTG(D*(X-E))/P] +2*F*ARCTG(G*(X-H))/P]$

Figure 5. Velocity contours of the theoretical model.

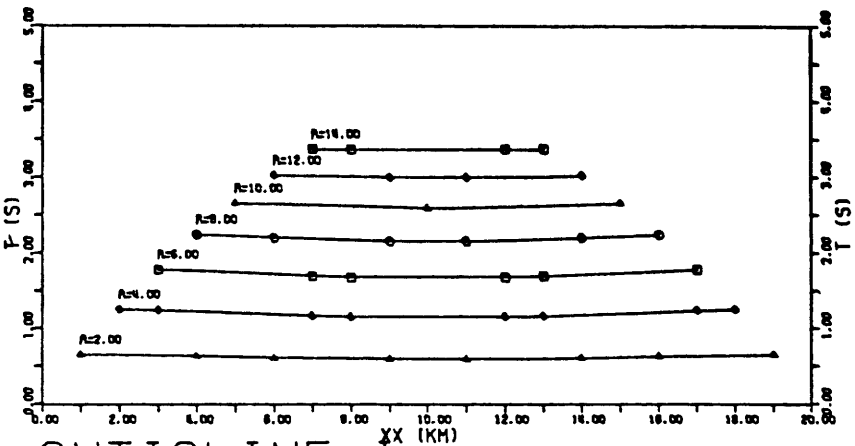

ANTICLINE I

SPECIAL TIME FIELD

Figure 6. Theoretical traveltimes for the model of figure 5.

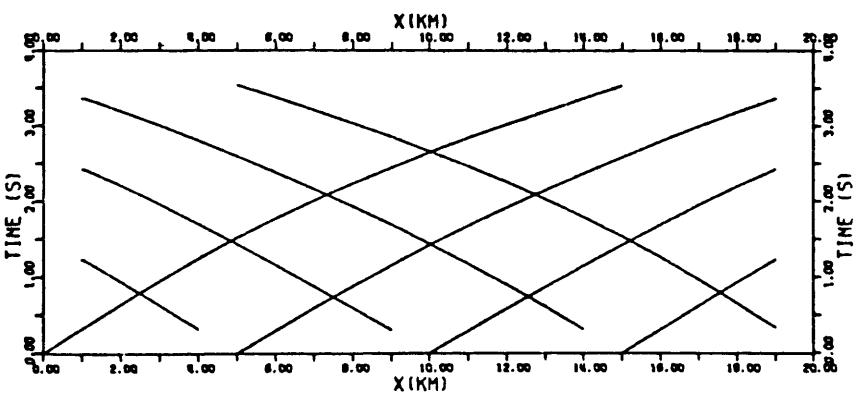

ANTICLINE I

TRAVELTIME CURVES OF THE PROFILE

Figure 7. Special time field derived from figure 6.

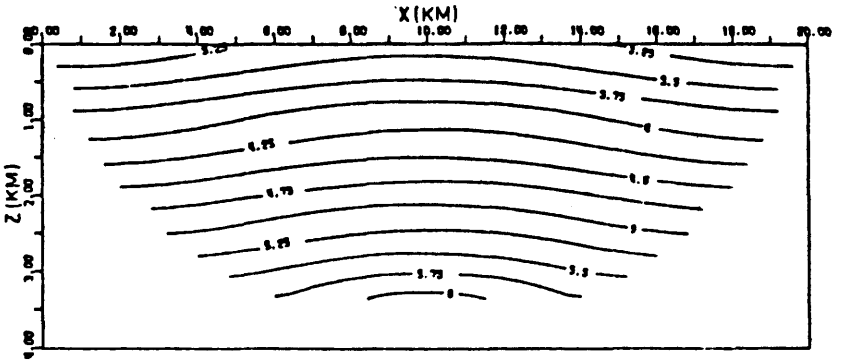

ANTICLINE I TTCS1
COMPUTED VELOCITY MODEL
NT= 5 MT= 3

Figure 8. Velocity model derived from inversion of traveltimes.

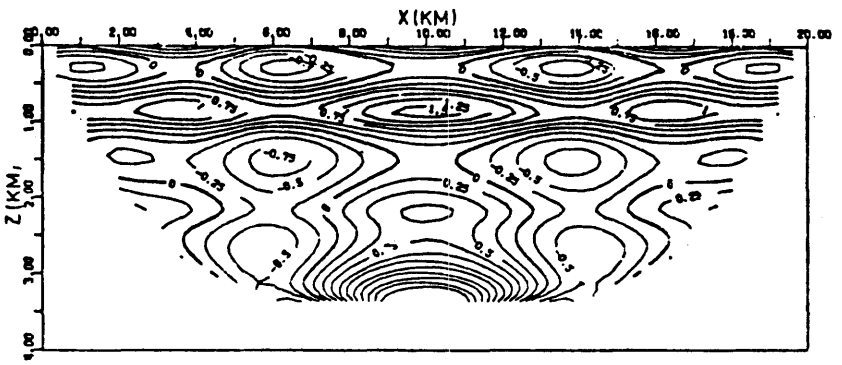

ANTICLINE I TTCS1
RELATIVE VELOCITY DEVIATIONS
NT= 5 MT= 3

Figure 9. Comparison of the theoretical and computed velocity models.

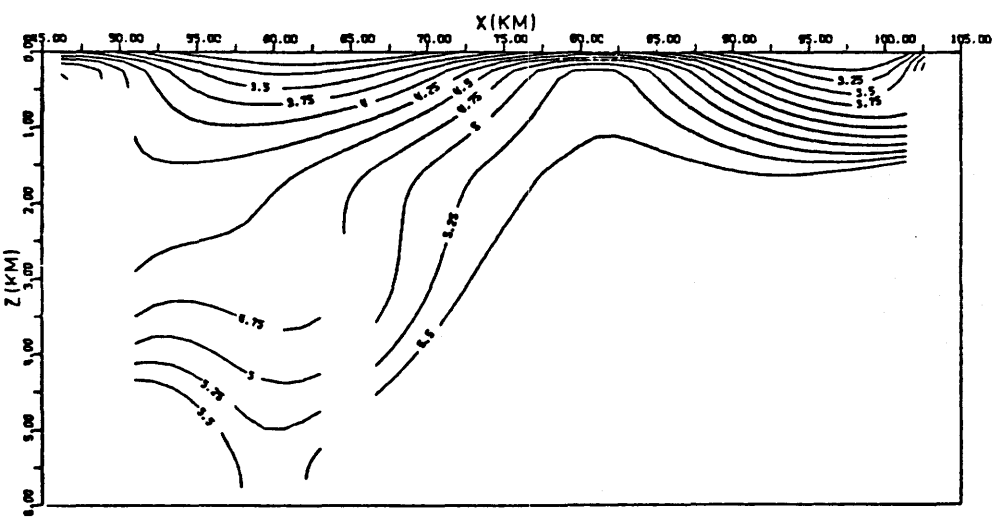

TRANSCARPATHIAN PROFILE K-III
COMPUTED VELOCITY MODEL
NT= 6 MT= 5

Figure 10. Computed velocity model for the Trans-Carpathian profile K-111.

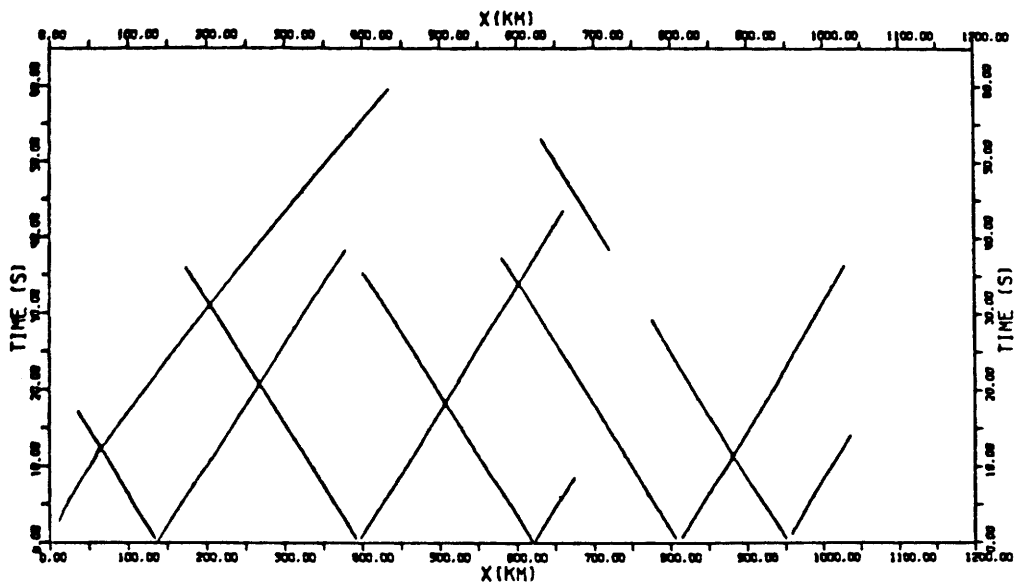

SAUDI ARABIA REFRACTION PROF.
TRAVELTIME CURVES OF THE PROFILE

Figure 11. Traveltime curves for the Saudi Arabian profile.

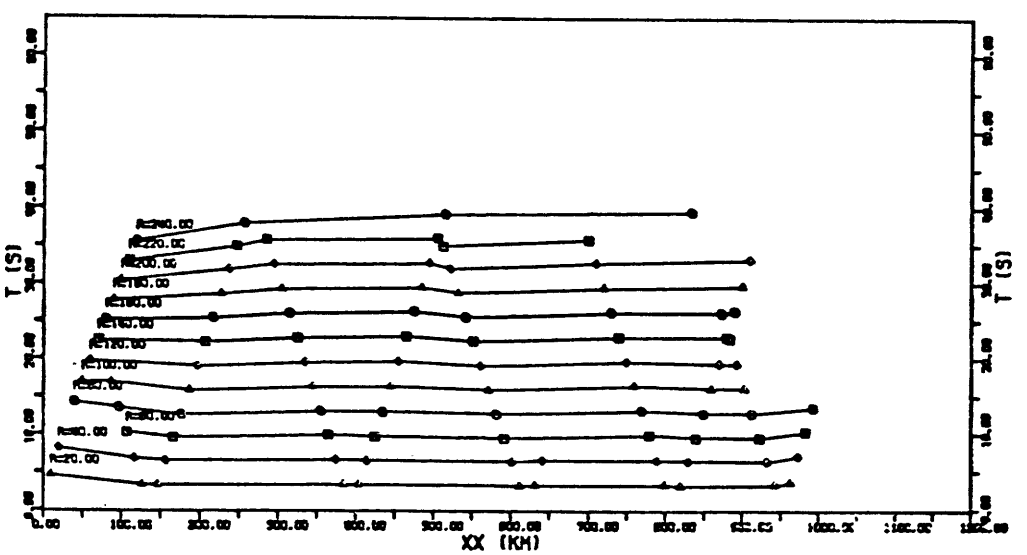

SAUDI ARABIA SPEC 13-20.0
SPECIAL TIME FIELD

Figure 12. Special time field derived from figure 11.

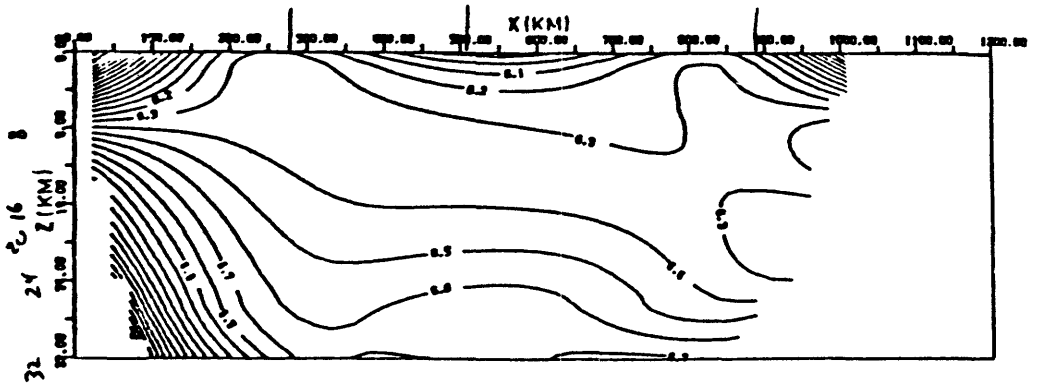

Figure 13. Velocity model derived from inversion of the special time field (figure 12).

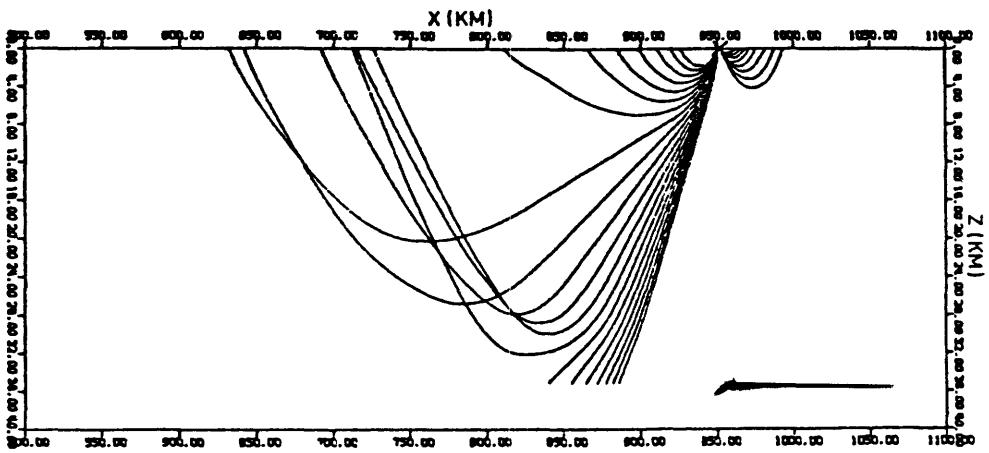

Figure 14. Ray diagram for shotpoint 1.

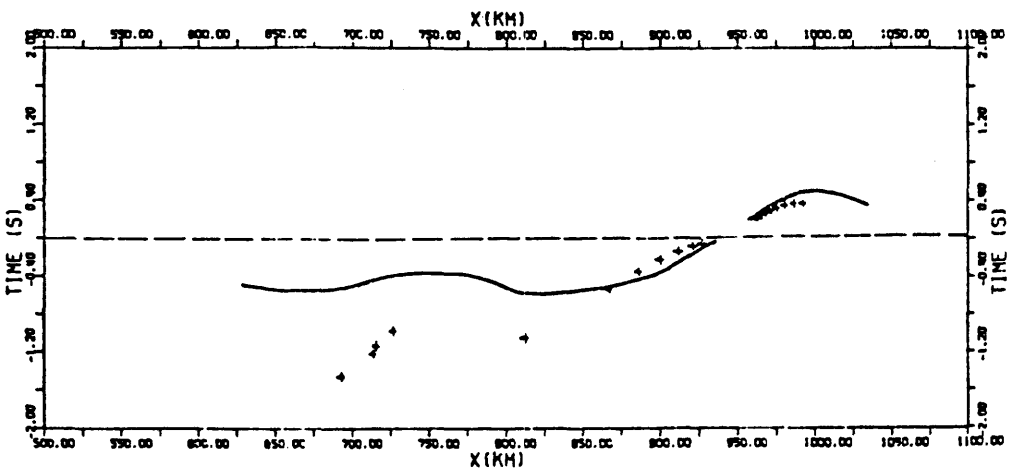

Figure 15. Comparison of observed and calculated traveltimes for shotpoint 1.

CRUSTAL STRUCTURE OF THE RED SEA-ARABIAN SHIELD TRANSITION[1]

by D. A. Forsyth, A. Green, and A. Mair

Division of Seismology, Earth Physics Branch,
EMR 1 Observatory Crescent, Ottawa K1A 0Y3, Canada

Analysis of refraction records from (the southwestern three) shotpoints 4, 5, and 6 of the refraction profile across Saudi Arabia shows a complex structure in transition from oceanic to continental crust. Modeling was accomplished by comparing the data with (1) traveltime curves for laterally homogeneous models, and (2) traveltime curves computed by ray tracing through models with lateral changes in velocity.

Beneath the Farasan Bank in the eastern Red Sea a sedimentary layer with a velocity of about 4.1 km/s extends to a depth of 1.3 km. The model has a second layer with a velocity of 4.7 km/s transitional to 5.8 km/s near the coast. The lower crustal layer has a velocity of 7.2 km/s and extends from 8 to 15 km beneath the Farasan Bank. Both the mid-crustal "discontinuity" and the Moho dip toward the continent at 2-3°. The upper mantle between shotpoints 6 and 5 appears to have a velocity of 8.6-8.7 km/s.

Over the western Arabian Shield the near-surface velocity is 5.8 km/s. The upper crustal material with a velocity of 6.2 km/s overlies 6.5 km/s material at a depth of about 16 km near shotpoint 5. The mid-crustal boundary and the Moho appear to dip northeastward at 1-2°. An upper mantle velocity near 8.2 km/s extends from 35 km east of shotpoint 5 to 45 km near shotpoint 6.

The refraction data permit only a general description of the oceanic to continental transition. Preliminary ray tracing indicates that lower velocity material is required at upper mantle depths beneath shotpoint 5 to account for the delayed arrivals observed between 240 and 450 km from shotpoint 6.

Following the refraction interpretation, a geological literature search has revealed a conceptual model by Coleman and others (1975) that is remarkably similar to the seismic model.

REFERENCE

Coleman, R. G., Fleck, R. J., Hedge, C. E., and Ghent, E. D., 1975, The volcanic rocks of southwest Saudi Arabia and the opening of the Red Sea: U.S. Geological Survey Saudi Arabian Project Report 194, 60 p.

---

[1] Contribution of the Earth Physics Branch No. 962.

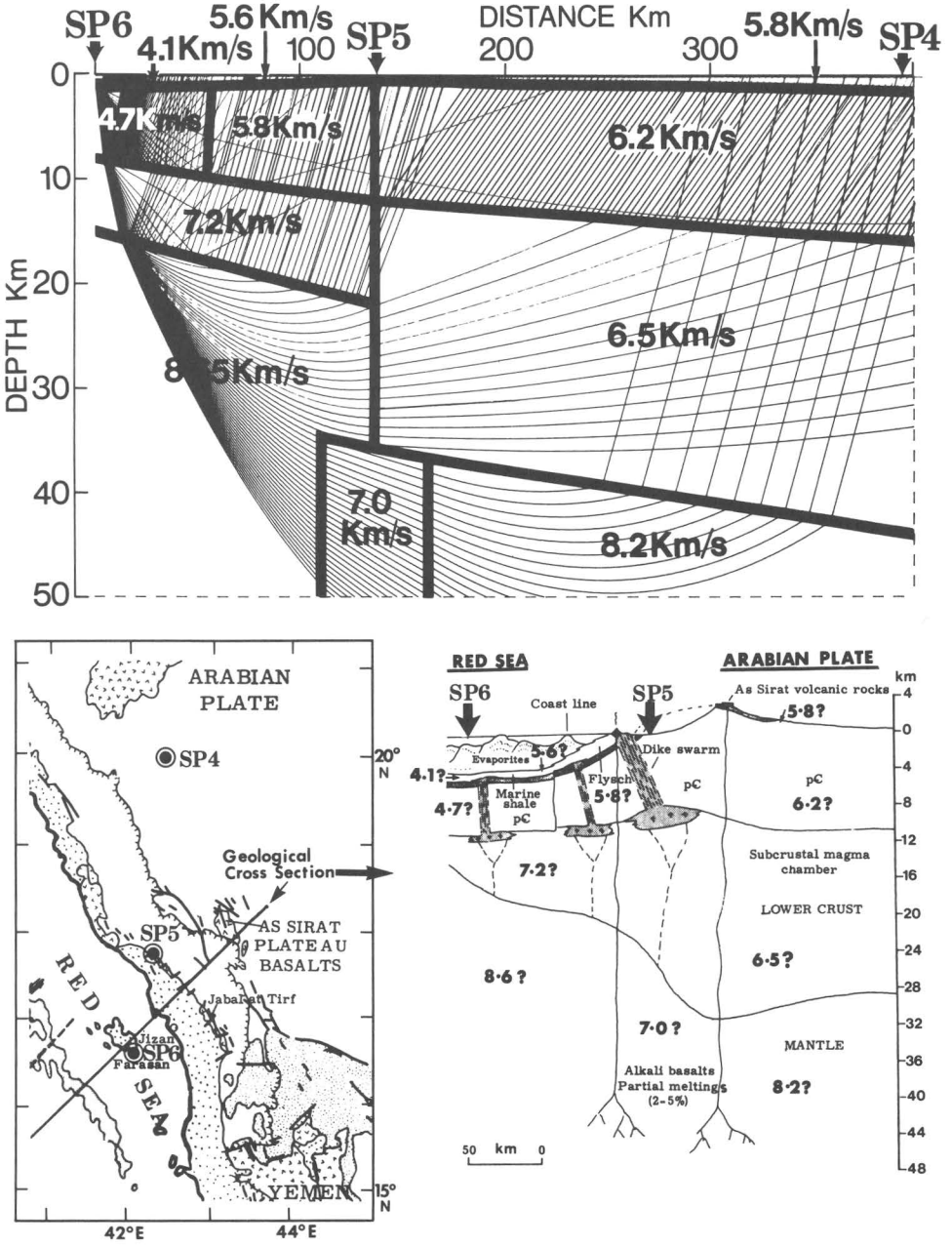

Figure 16. Interpreted crustal velocity structure (top), profile location (bottom left), and geologic interpretation (bottom right).

A CRUSTAL SECTION FOR THE ARABIAN SHIELD AND ADJACENT RED SEA MARGIN DERIVED FROM FIRST-ARRIVAL DATA

By M. E. Gettings

U.S. Geological Survey
Saudi Arabian Mission
Jiddah, Saudi Arabia

Production of a regional crustal model for the Arabian Shield and bordering provinces is a major objective of the Saudi Arabian Mission of the U.S. Geological Survey. Regional geologic, seismic refraction, gravity, and aeromagnetic studies form the principal data base for construction of the crustal model, and in order to provide a starting model for interpretation of regional gravity and heat flow patterns, a preliminary analysis of the results of the Saudi Arabian long-range seismic refraction profile was carried out. The objective was to produce a generalized crustal section consistent with the refraction data. At the time of this work the only record sections available were the uncorrected field data sections contained in Blank and others (1979); consequently, only an elementary analysis based on first-arrival times was attempted.

The procedure followed was to pick first arrivals on the record sections as carefully as possible and fit average, maximum, and minimum lines to the approximately linear segments, which were then converted to velocities with uncertainties. The velocities and intercept times so defined were then interpreted in terms of two homogeneous horizontally layered models extending northeast and southwest, respectively, from each shotpoint. If appropriate, sloping interfaces were then used to refine the interpretation between shotpoints. A time delay of about 0.25 s at 210 km southwest of shotpoint 3 and another delay of nearly 1 s about 100 km northeast of shotpoint 5 were interpreted as step-like changes in layer thicknesses. However, in most cases traveltime delays and advances were ignored and lines defining velocities were drawn in a least-squares sense by inspection. Some of the clearer secondary arrivals were used to help constrain the lines used in the velocity determinations. In several cases alternate interpretations with varying numbers of layers were attempted. The velocity-depth models about each shotpoint were then plotted and the crustal section of figure 17 was produced by visual generalization of those features which are common between adjacent shotpoints. The models yielded higher crustal velocities between shotpoints 1 and 2 than shown in figure 17, particularly in the lower crust. However, to keep the model as simple as possible, a lateral discontinuity was not introduced, and the velocity variation is reflected only in the larger uncertainty of P* and a shallowing of the boundary between Pg and P* in this part of the profile.

The gravity profile (fig. 17) was also used to constrain the model; within the uncertainties of density contrast that result from uncertainties in average velocities and their conversion to density values, the model fits the gravity data southwest of shotpoint 3. Rock compositions in the shield area were deduced from the models of Schmidt and others (1978) and were considered in the conversion of velocities to densities (see Nafe and Drake, 1968).

In this model, the gross structure of the Arabian Shield is characterized by a two-layer crust with a lateral velocity discontinuity about 30 km southwest of shotpoint 3. To the northeast of this boundary, Pg is 6.12 km/s in a

layer 18 to 22 km thick, and P* is 6.55 km/s in a layer 14 to 22 km thick. Southwest of the discontinuity, Pg is 6.24 km/s in a layer 22 to 24 km thick, underlain by a 14- to 23-km-thick layer with P* equal to 6.83 km/s. Near shotpoint 5, both layers thin appreciably. The higher average values for the southwestern block are inferred to be due to a more mafic average crustal composition.

West of shotpoint 5, the drill hole data at Mansiyah I (Gillman, 1968) help constrain the interpretation of the seismic refraction data for the rift crust. The section shown in figure 17 differs somewhat from the compilation of oceanic crustal velocites of Le Pichon and others (1976, p. 173; see also Worzel, 1974). Velocities in layer 1 (sedimentary layer) are quite high, due at least in part to the large proportion of halite and anhydrite (>1,500 m; Gillman, 1968) in the section. The layer 2 velocity of 6.1 km/s is in the high end of the velocity range for this layer, and the layer itself is about twice the average thickness for this layer. The layer 3 velocity of 6.7 km/s is near the mean, and this layer is also significantly thicker than average. Mantle velocity is average for that beneath oceanic crust, and indeed, mantle velocities are almost constant at the oceanic average value (within uncertainties) for the entire section including the shield area.

Due to the preliminary nature of the record sections and the rather elementary interpretation procedures used, this interpretation of the seismic data is only tentative. No weathering corrections or allowances for delays due to surface lithologic variations have been made, and because large segments of the profile traverse areas of unconsolidated cover, particularly between shotpoints 5 and 6 (coastal plain) and between shotpoints 3 and 4, such corrections may be substantial. Also, no allowance has been made for topographic relief, which is about 2,000 m between shotpoints 4 and 5. The uncertainties in the depths and thicknesses of the layers are probably on the order of $\pm$ 15 percent.

REFERENCES

Blank, H. R., Healy, J. H., Roller, J. C., Lamson, R., Fischer, F., McClearn, R. and Allen, S., 1979, Seismic refraction profile, Kingdom of Saudi Arabia, field operations, instrumentation, and initial results: U.S. Geological Survey Saudi Arabian Mission Project Report 259, 49 p.; also, 1979, U.S. Geological Survey Open-File Report 79-1568.

Gillman, M., 1968, Primary results of a geological and geophysical reconnaissance of the Jizan coastal plain in Saudi Arabia: American Institute of Mining and Metallurgical Engineers, Society of Petroleum Geologists, Saudi Arabian Section, Proceedings of the 2nd Regional Symposium, Dhahran, Saudi Arabia, p. 189-208.

Le Pichon, X., Francheteau, J., and Bonnin, J., 1976, Plate Tectonics: Elsevier, Amsterdam, 2nd ed., 311 p.

Nafe, J. E. and Drake, C. L., 1968, Physical properties of rocks of basaltic composition, in Hess, H. H. and Poldervaart, A., eds., Basalts: The Poldervaart treatise on rocks of basaltic composition: Interscience Publishers, New York, v. 2, p. 483-502.

Schmidt, D. L., Hadley, D. G., and Stoeser, D. B., 1978, Late Proterozoic crustal history of the Arabian Shield, southern Najd province, Kingdom of Saudi Arabia, in Evolution and mineralization of the Arabian-Nubian Shield: Pergamon Press, Oxford-New York, v. 2, p. 41-58.

Worzel, J. L., 1974, Standard oceanic and continental structure, in Burke, C. A. and Drake, C. L., eds., Geology of continental margins: Springer-Verlag, New York, p. 59-66.

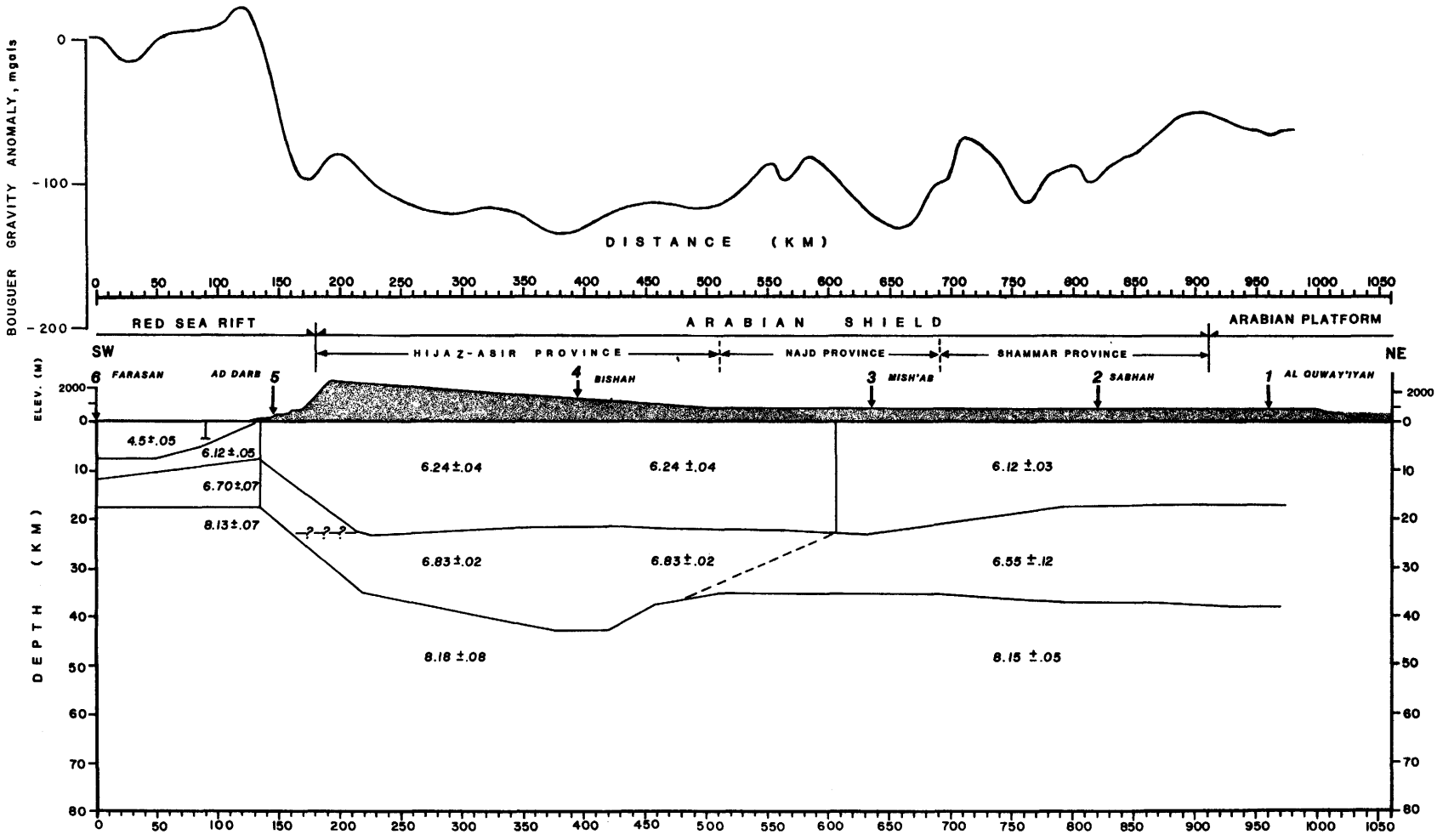

Figure 17. Simple Bouguer gravity anomaly profile and crustal section for the Arabian Shield and adjacent Red Sea margin deduced from long-range seismic refraction and gravity data.

A SEISMIC REFRACTION PROFILE ACROSS THE ARABIAN SHIELD

By A. Ginzburg

Department of Geophysics and Planetary Sciences
Tel Aviv University
Ramat Aviv, Tel Aviv 69978, Israel

In this brief attempt at interpreting the Saudi Arabian data set (Lamson and Leone, 1980) emphasis was put on the continental part of the profile--shotpoints 1 to 5.

The approach adopted was conventional. A first approximation of the crustal model comprising depths and velocities was derived from apparent velocities of the correlated phases and their intercept times. Branches used were Pg, Pn, P* where correlatable, and PmP in one instance. Of particular interest were the reversed segments between shotpoints 1-2, 3-4, and 4-5, which were used to establish the true velocities and depths at the shotpoints. Although these segments are relatively short, good Pn arrivals were recorded at distances of up to 250 km. The intercept-apparent velocity computations were checked by the use of a $\tau(p)$ inversion scheme for inclined layers (Loewenthal, personal communication). The calculated true velocities were 6.1-6.2 km/s for the Pg branch, 6.6 km/s for P*, and 8.1 for the Pn branch. These velocities and computed depths were used as an initial model in an iterative ray-tracing program (modified after Makris, 1977) which was used for the computation of the final model.

The interpretation presented here suffers from two limitations--one related to data quality and the other to the computational procedure used. The quality of the data deteriorates rather rapidly at distances beyond 250-300 km, and the first arrivals cannot be picked with certainty. The program used assumes the existence of a gradient within each layer. The gradients are quite gentle, and in cases of moderate heterogeneity do not affect the results. However, in cases of severe heterogeneity, such as between shotpoints 5 and 6 (fig. 23), the errors are quite large.

In the segments shotpoints 4 to 5 (figs. 18 and 19) and 4 to 3 (fig. 20), a good agreement was obtained between the forward and reversed profiles. Between shotpoints 1 (fig. 21) and 2 (fig. 22), a good agreement was obtained to a shot-to-detector distance of 250 km on the shotpoint 1 record section. The disagreement beyond that could well be due to unclear first arrivals or noisy traces. The arrivals beyond 400 km show a much lower apparent velocity and are probably reflected arrivals from an interface within the upper mantle. Such a phenomenon was observed by Ginzburg and others (1979) further north in the Arabian Shield (along the Gulf of Elat).

The overall model of the crust across the Arabian Shield is shown in figure 24. As can be seen, the crust thickens very gradually, reaching a maximum thickness of 41 km near shotpoint 5, and thins drastically towards the Red Sea where the crust beyond a narrow transition zone is oceanic.

REFERENCES

Ginzburg, A., Makris, J., Fuchs, K., Perathoner, B., and Prodehl, C., 1979, Detailed structure of the crust and upper mantle along the Jordan-Dead Sea rift: Journal of Geophysical Research, v. 84(B10), p. 5605-5612.

Lamson, R. J. and Leone, L. E., 1980, Saudi Arabia seismic refraction profile data set, volumes 1 and 2: U.S. Geological Survey Open-File Report, Miscellaneous Document 17.

Makris, J., 1977, Geophysical investigations of the Hellenides, Hamburg: Geophys. Einzelschriften, v. 34, p. 1-124.

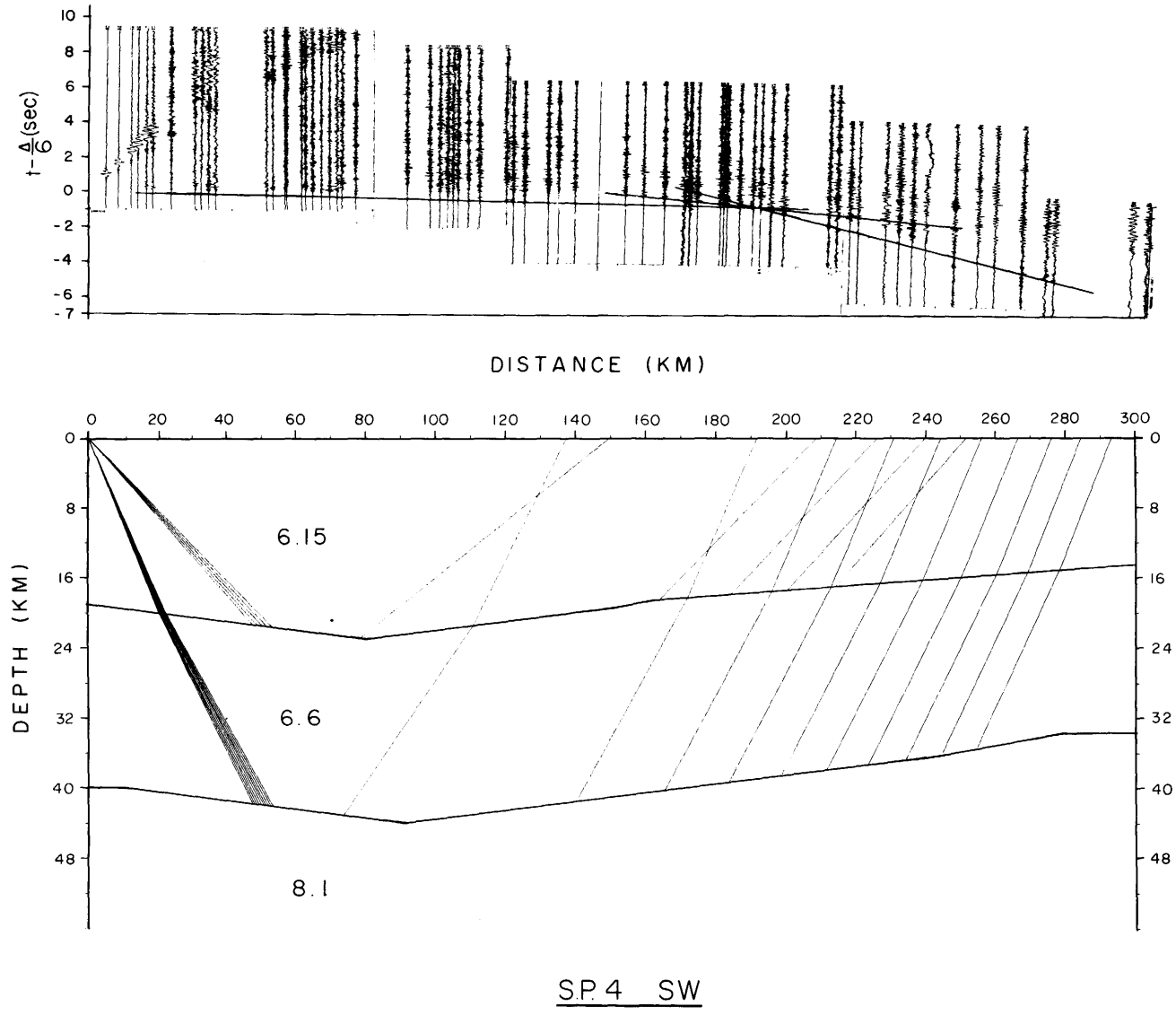

Figure 18. Shotpoint 4 SW: Seismic record section with calculated traveltimes (top); crustal velocity model and selected ray paths (bottom).

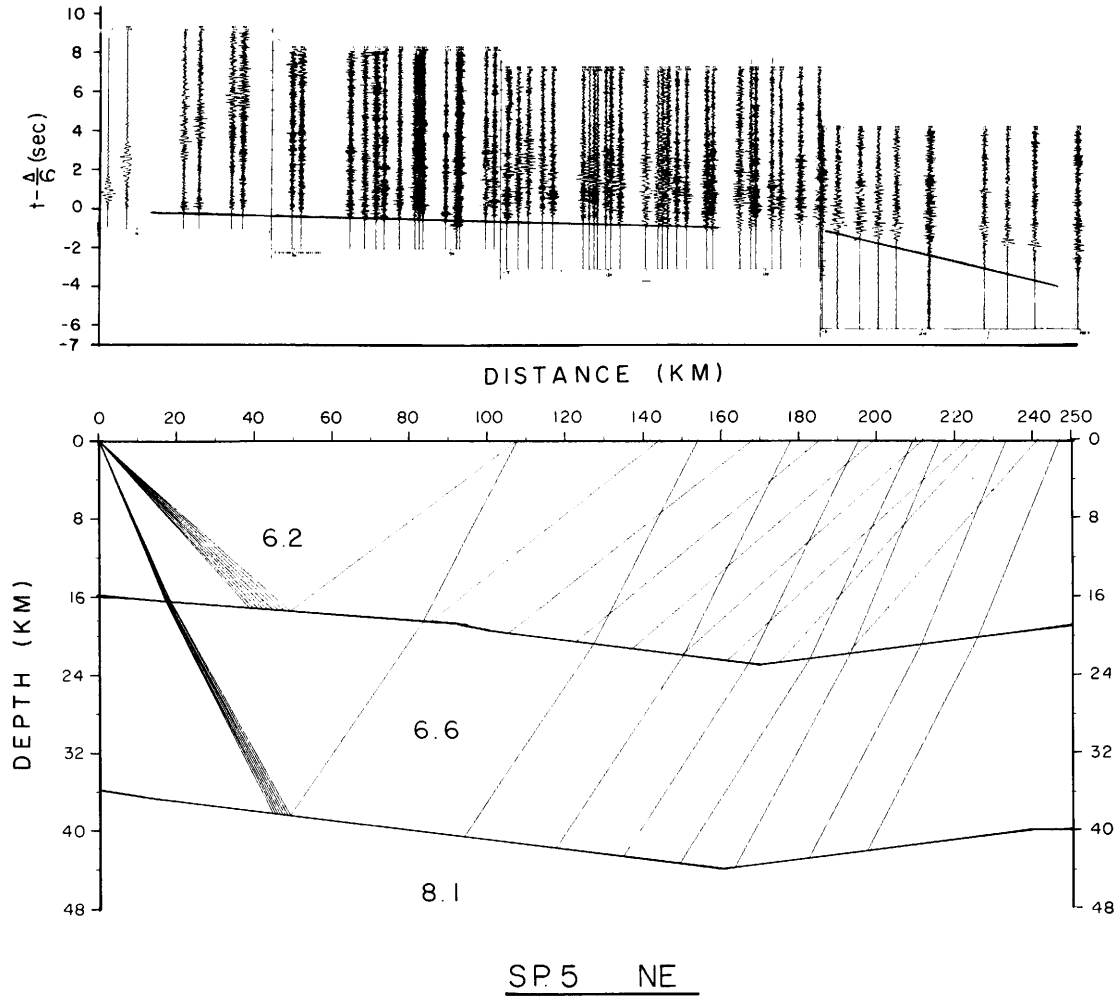

Figure 19. Shotpoint 5 NE: Seismic record section with calculated traveltimes (top); crustal velocity model and selected ray paths (bottom).

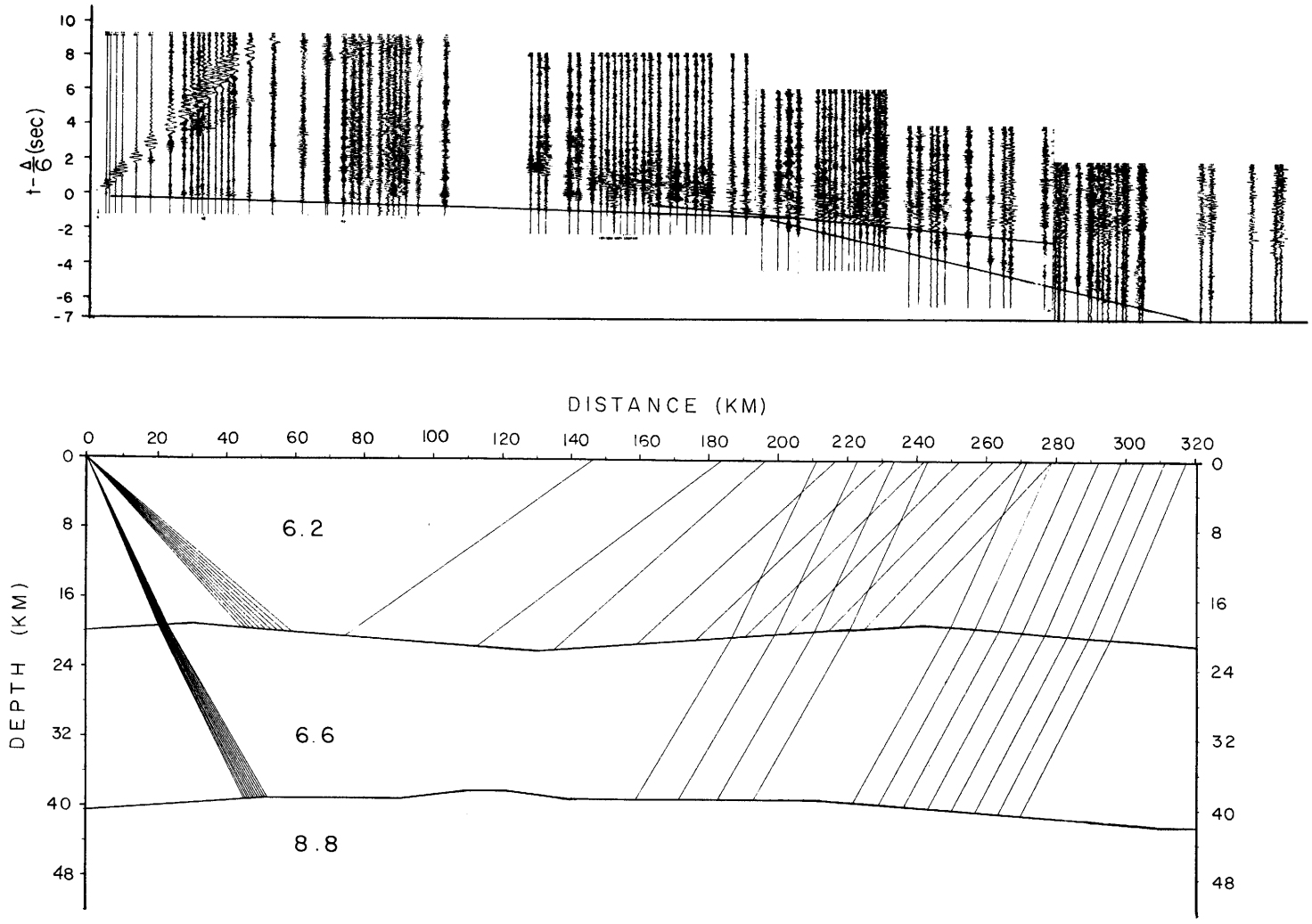

Figure 20. Shotpoint 4 NE: Seismic record section with calculated traveltimes (top); crustal velocity model and selected ray paths (bottom).

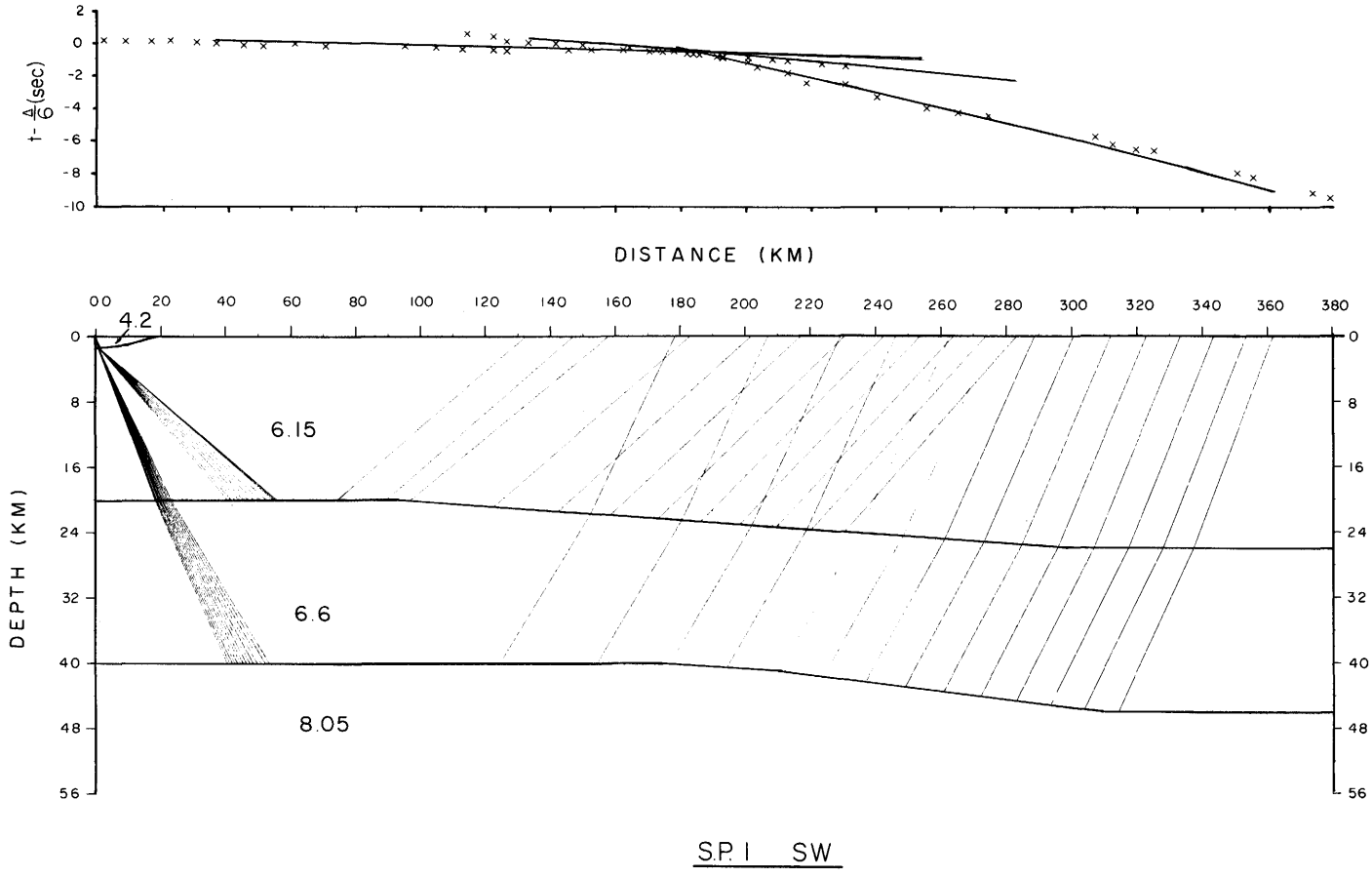

Figure 21. Shotpoint 1 SW: Arrival time picks with calculated traveltimes (top); crustal velocity model and selected ray paths (bottom).

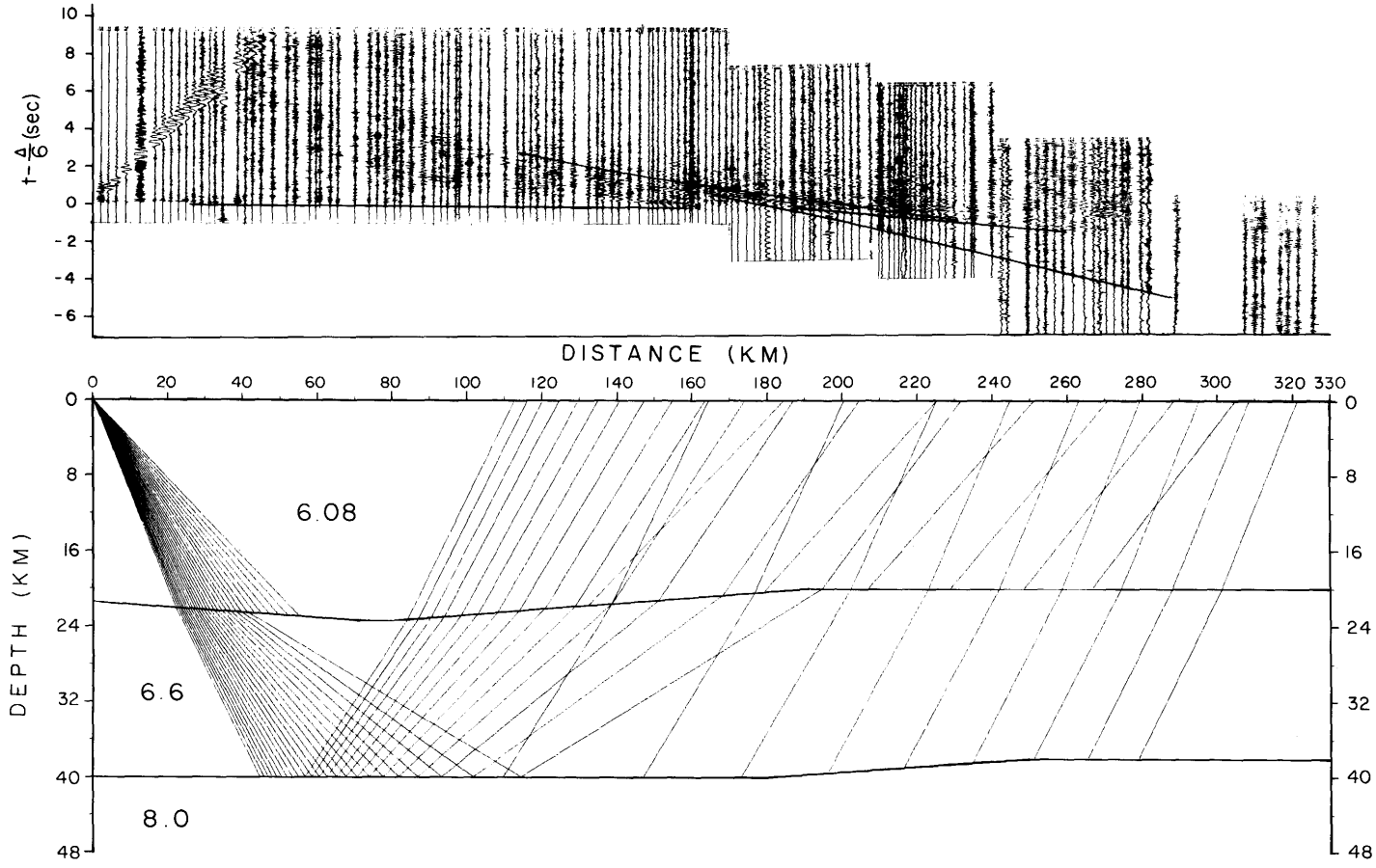

S.P. 2 SW

Figure 22. Shotpoint 2 SW: Seismic record section with calculated traveltimes (top); crustal velocity model and selected ray paths (bottom).

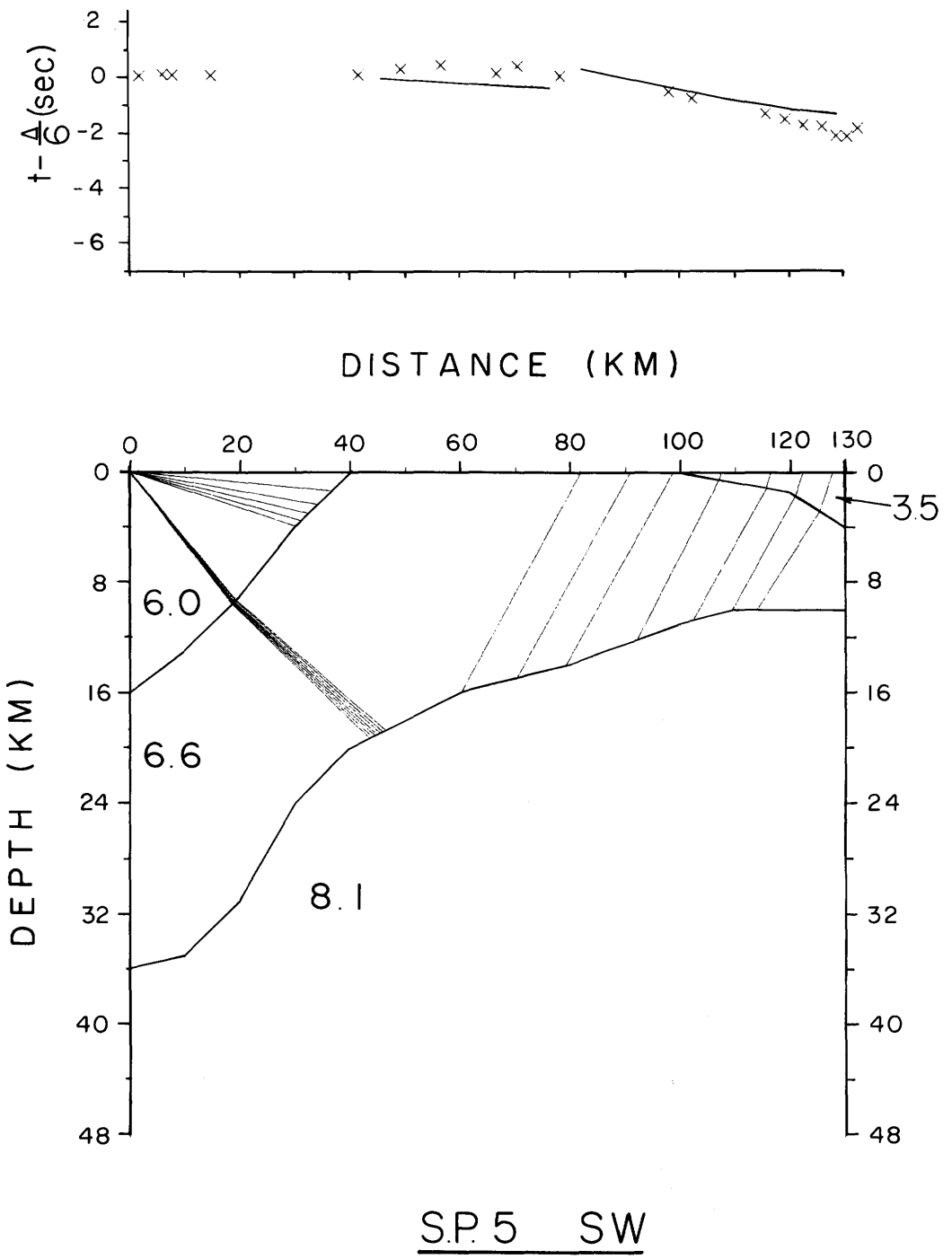

Figure 23. Shotpoint 6 NE: Arrival time picks with calculated traveltimes (top); crustal velocity model and selected ray paths (bottom).

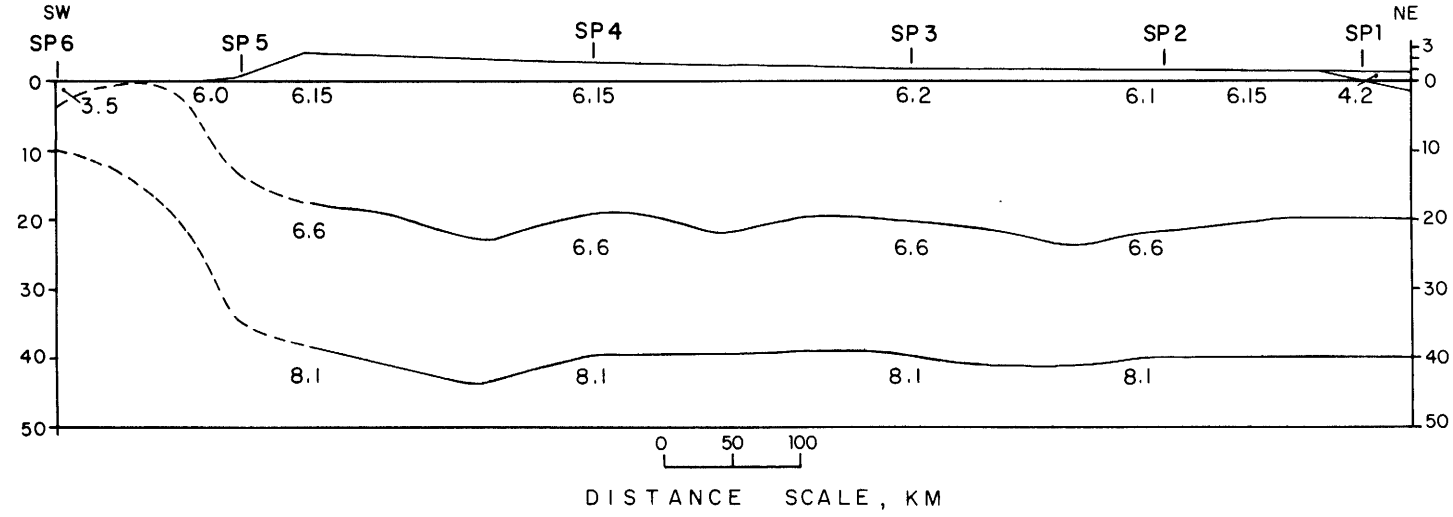

Figure 24. Crustal section across the Arabian Shield from seismic refraction data.

A PRELIMINARY EXAMINATION OF THE 1978 REFRACTION PROFILES IN SAUDI ARABIA

By P. K. H. Maguire

Department of Geology
University of Leicester
Leicester, LIE JRH, England

A "conventional" first interpretation of the data has been carried out. This involved a constant velocity, horizontal layer model derived from first-arrival data, supplemented by selected points from second-arrival prograde and retrograde branches. Smoothed local gradients of retrograde branches were also determined to allow definition of the type of transition across particular boundaries for later analysis.

The model type chosen presumes horizontal layers. This precludes the derivation of laterally heterogeneous structures unless the velocity contrasts across steeply dipping interfaces or transitions are large, particularly if the correlations used spread over large distances. In order to derive a first crustal section suitable for a trial-and-error ray-tracing analysis, it was decided to correlate arrivals over lengths comparable with possible crustal units, that is, on the order of 50 km, where necessary. It is probable that the resultant section contains more detail than is reasonable geologically, but it satisfies the data when analyzed using the particular geophysical model type chosen. As stated above, the derived section is to be used as a first attempt in a ray-tracing analysis, and the detail in the section is merely a guide to possible heterogeneities in the final model; it should not be considered definitive.

Initially, it was found that variation in the section "collages" could cause errors of approximately 15 percent in depth and 2 percent in velocity measurements. T and X scale conversion factors were determined from each shot into each northeast and southwest section. Straight lines were then fitted through the first arrivals on each section. In general, the straight line segments were offset, with later segments delayed relative to earlier ones, indicating possible low-velocity layers, but occasionally the later segments arrived early, indicating near-surface high-velocity structures beneath the receivers, or upwarped or faulted refractors. In some cases it was difficult to decide between one slow or two higher velocity arrivals. Occasionally very weak high-velocity arrivals occurred in low-velocity sections, indicating possible sawtooth velocity depth profiles. The apparent velocity and intercept time were derived for all segments. This allowed the detailing of approximate velocity-depth models for all sections, excluding low-velocity layers. By identifying the end of the prograde and beginning of the retrograde branches associated with the top and bottom of low-velocity layers, and presuming the layer was of constant velocity, and then using geometrical ray-path theory, a maximum thickness and velocity of the layer can be derived. The interpretation used was therefore based on a "useful" combination of straight and curved ray path theory. In order to determine the depth of a low-velocity layer within a particular higher velocity layer, the maximum depth to the top of the layer and the average overburden velocity was derived from the data point at the end of the prograde branch. In general, this gave too deep a depth point for the derived structure, so the low-velocity layers were placed at the base of their surrounding higher velocity layer. In order to fit the simple horizontal layer

interpretation, early arrivals (as mentioned above) were replaced by higher velocity arrivals where necessary. This only proved necessary for one or two near-surface segments. A set of velocity-depth models, including low-velocity layers, has been produced for all the shotpoints.

Two-dimensional depth points have been estimated from the distance coordinates of the various arrivals, and these were plotted in section form. These proved possible to contour, as in figures 25 and 26. The cartoon excludes much of the fine detail, particularly in the upper crust, and is occasionally somewhat speculative, in particular beneath the region between shotpoints 6 and 5, but would be suitable for a first attempt at ray tracing and as a means for identifying arrivals from particular horizons for delay-time analyses. The region between shotpoints 5 and 6 is speculative because a horizontal layer interpretation method is used to derive a structure of marked lateral variation. The contouring and resultant cartoon in this region is possibly influenced by ideas on the structure beneath mid-ocean ridges.

The other points of interest are: the proposed thickening of the crust just to the northeast of shotpoint 5, together with the inclusion of a high-velocity mid-crustal horizon; the thinning and exclusion of the upper crustal 6.4 km/s layer toward shotpoint 5; the deep crustal high-velocity 7.3 km/s layer (which is very tentative to the northeast of shotpoint 4); the presence of a thin high-velocity 8.4 km/s layer beneath the Moho underlain by a lower velocity 8.1 km/s layer to the southwest of shotpoint 3; and finally, the change in the Moho from a firm boundary (derived from first arrivals only) between shotpoints 5 and 4, to a sawtooth transition to the northeast of shotpoint 4. However, it should be emphasized that all these proposals are derived from the simplest possible interpretation, not allowing for lateral or continuous vertical variation in structure.

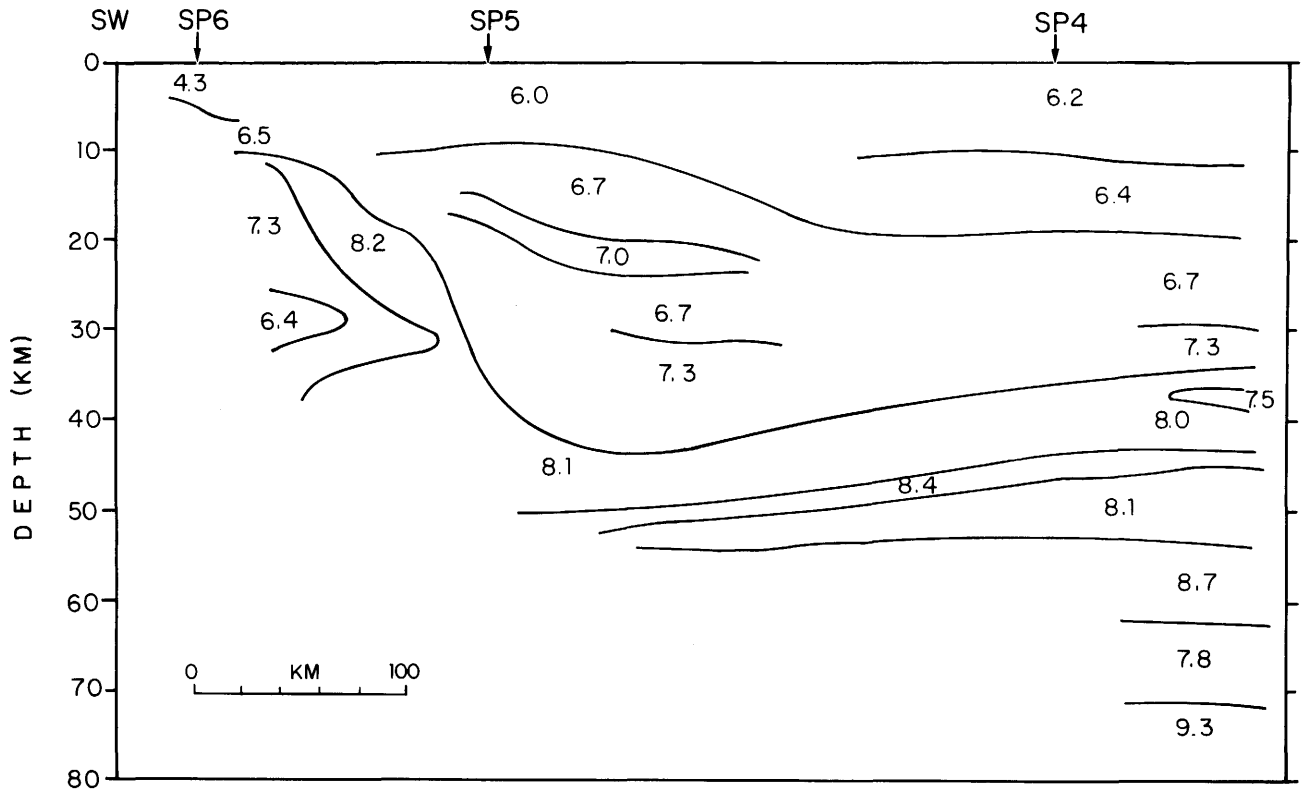

Figure 25. Cartoon from constant-velocity horizontal-layer interpretation for shotpoints 6, 5, and 4.

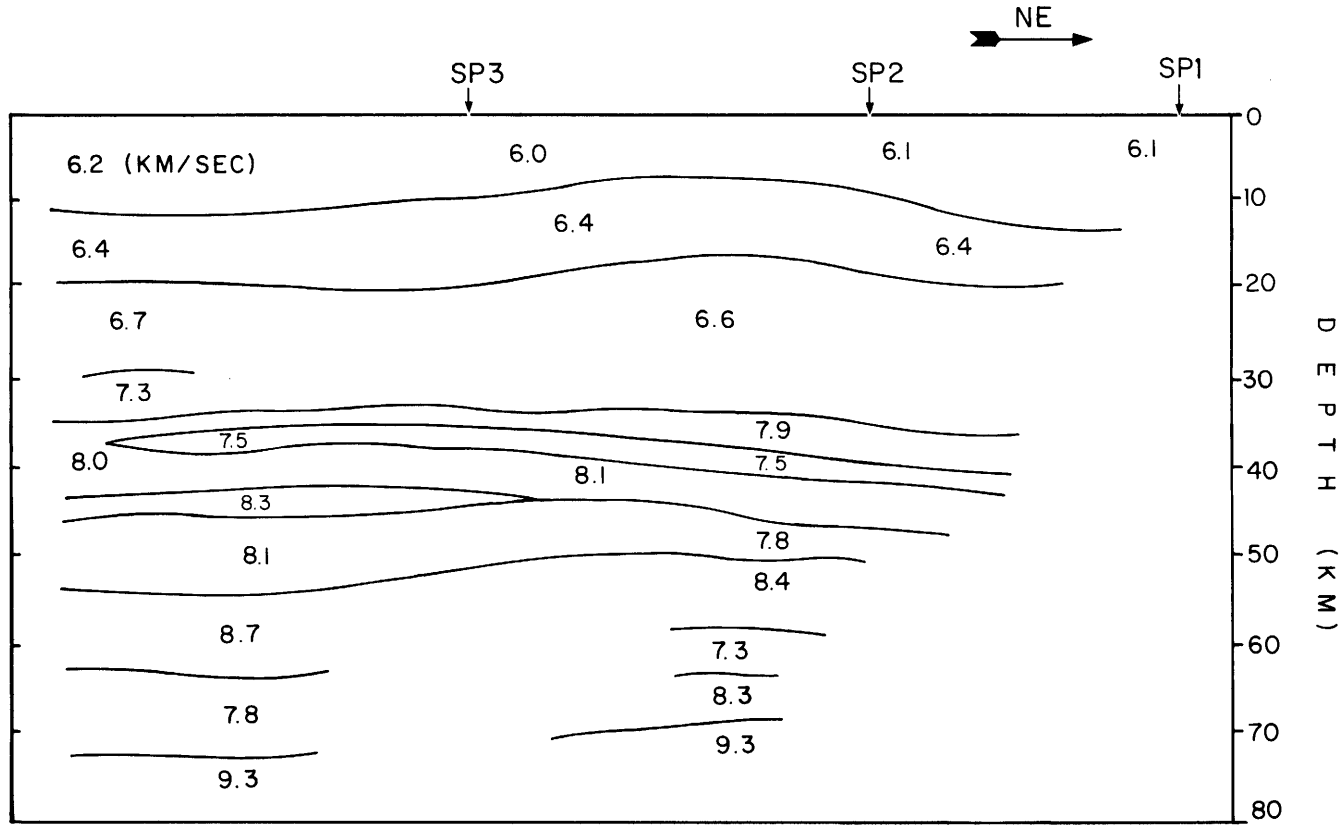

Figure 26. Cartoon from constant-velocity horizontal-layer interpretation for shotpoints 3, 2, and 1.

THE RIFTED MARGIN OF SAUDI ARABIA

By James S. McClain and John A. Orcutt

Geological Research Division
Scripps Institute of Oceanography
University of California, San Diego
La Jolla, California, 92093

The structure of rifted continental margins has always been of great scientific interest, and now, with dwindling economic oil deposits, these complex geological features assume practical importance as well. The ocean-continent transition is, by definition, laterally heterogeneous and likely to be extremely complicated.

The southernmost shotpoints (4, 5, and 6) in the U.S. Geological Survey seismic refraction profile in the Kingdom of Saudi Arabia lie within a transition region and thus provide a testing ground for methods that treat wave propagation in laterally heterogeneous media. This portion of the profile runs from the Farasan Islands in the Red Sea across the coast line and the Hijaz-Asir escarpment into the Hijaz-Asir tectonic province. Because the southernmost shotpoint is within the margin of the Saudi sub-continent, the full transition region is not sampled. Furthermore, such an experiment is precluded by the narrowness of the purely oceanic portion of the Red Sea.

Data from shotpoints 6 and 4 have been used to define the transition structure while shotpoint 5 data are used to further refine and confirm our resulting model. Traveltimes and amplitudes of the seismic arrivals are trial-and-error fitted using ray tracing in complex structures. Certainly, forward modeling is less satisfactory than the use of an inverse technique. However, present schemes are probably inadequate for this type of data. In such a local seismic refraction experiment the linearizing assumption that ray paths do not vary substantially from initial estimates is probably not valid. In other words, the models are not allowed to vary enough, through successive perturbations, to provide reliable error bounds.

Shotpoint 6 in the Red Sea, with receivers up to 470 km inland, provides some of the most interesting data. The initial interpretation (Blank and others, 1979) proposed that a sedimentary sequence overlies oceanic mafic rocks. That report suggested that first arrivals from beyond 65 km are refracted arrivals from the uppermost mantle with an apparent velocity of 8.2 km/s. This velocity is, of course, quite high for a "Moho" presumably becoming deeper beneath the continent. However, on several of these "Pn" arrivals the apparent velocity is low, about 7.0 km/s. Substantial lateral variations in the velocity structure must be present to explain the early arrival of these high-slowness rays. The true uppermost mantle velocity profile is obscured by the more complex ray paths.

For receivers in the Hijaz-Asir tectonic province, the seismograms are dominated by a large-amplitude arrival with apparent velocities between 7.7 and 8.7 km/s. Surprisingly, unlike the rapid amplitude decay of a head wave, the wave amplitudes persist from 180 to over 425 km. We interpret such continuity as evidence for large-scale lateral heterogeneity although immediately beneath the receivers the effects of inhomogeneities must be small. Furthermore, the impulsive and large, low-slowness arrivals are not apparent on any other portions of the profiles. In particular, shotpoint 4,

which reverses the shotpoint 6 data, shows no evidence of such an arrival. Large-scale heterogeneity, therefore, causes a sharp focusing of energy between the Farasan Islands and the Hijaz-Asir province. The high velocities are produced by this focusing and do not reflect a deeper sub-Moho boundary.

The Hijaz-Asir escarpment is apparently the surface expression of an important boundary in the transition from ocean to continent. This is confirmed by preliminary analyses of shotpoint 5 data, which show a substantial change in crustal thickness between receivers to the southwest and those to the northeast (Blank and others, 1979).

REFERENCE

Blank, H. R., Healy, J. H., Roller, J. C., Lamson, R. J., Fischer, F., McClearn, R., and Allen, S., 1979, Seismic refraction profile, Kingdom of Saudi Arabia--field operations, instrumentation and initial results: U.S. Geological Survey Saudi Arabian Mission Project Report 259, 49 p.

SAUDI ARABIAN REFRACTION PROFILE: CRUSTAL STRUCTURE OF THE RED SEA-ARABIAN SHIELD TRANSITION

By B. Milkereit and E. R. Flüh

Institut für Geophysik
Universität Kiel
D-2300 Kiel, Federal Republic of Germany

Analysis of the two southwesternmost shotpoints (5 and 6) of the Saudi Arabian refraction line (Blank and others, 1979) shows a great degree of lateral heterogeneity. Ocean-continent transition zones have been studied all over the world, always showing rather high or low apparent velocities of many traveltime branches and either large or small intercept times. Therefore, a two-dimensional ray-tracing program seems to be an appropriate method for the interpretation of the data set. Picking of the first arrivals for the two shotpoints led us to the identification of the following phases.

Shotpoint 6 SW:	4.2 km/s	(Sedimentary layer)	0-20 km
	7.1 km/s	(Oceanic layer 3)	10-30 km
Shotpoint 6 NE:	4.2 km/s	(Sedimentary layer)	0-30 km
	6.8 km/s	(Oceanic layer 3)	20-60 km
	8.9 km/s	Pn	60-120 km
	6.8 km/s	Pn	120-160 km
	8.2 km/s	Pn	170-400 km
	8.5 km/s	Pl (upper mantle layer, 70-80 km depth, similar to observation from shotpoint 1)	300-500 km
Shotpoint 5 SW:	6.0 km/s	Pg (between 35 to 85 km delayed-sediments?)	0-90 km
	8.4 km/s	Pn (between 70 to 85 km delayed-sediments? Velocity estimated in the 100-150 km range)	70-150 km
	8.4 km/s	Pn (later arrival, about 1 s later than first arrival)	100-150 km
Shotpoint 5 NE:	5.7 km/s	Pg	0-30 km
	6.6 km/s	Pg	30-90 km
	6.4 km/s	Pc (lower crustal boundary)	100-250 km
	7.7 km/s	Pn	100-250 km

Figure 27 shows the traveltime curves and the model, described as follows. We started our model calculation assuming an oceanic structure beneath shotpoint 6 and a continental structure beneath shotpoint 5. To fit the rather low apparent velocities for Pc and Pn from shotpoint 5 to the northeast, we assumed a dip to the northeast in both boundaries, thus proposing a root of the Asir mountain range in the Hijaz Asir province. The model explains the 6.6 km/s "Pg phase," which is very abruptly stopped at 90 km by a wedge of higher velocity material in the upper crust (possibly lower crustal material). Between 35 and 85 km southwest of shotpoint 5 we introduced a sedimentary

basin, reaching 3.5 km maximum depth overlying 6.1 km/s material (upper continental crust). This could well explain the delay of the Pg phase and the Pn/PmP critical point. Sediments beneath shotpoint 6 reach the same depth. We chose a velocity of 3.8 km/s at the top, increasing with a gradient of 0.04 km/s/km. Slightly decreasing sediment thicknesses southwest of shotpoint 6 fits the observed phase velocity of 7.1 km/s, which is a refracted arrival from the 6.7 km/s oceanic crust.

The observed high apparent velocity of 8.9 km/s is interpreted as a Pn arrival, Moho depth being about 12 km, and the thinning of the sediments to the northeast results in a higher apparent velocity. Where the sediments are completely absent the velocity is about 6.8 km/s (120-160 km northeast of shotpoint 6). The Moho has a down-dip in this region, too. The Moho, however, is overlain by 6.1 km/s material in the region 50-130 km northeast of shotpoint 6. The third and fourth phase of shotpoint 6 (>170 km) are explained by rays traveling along the continental crust-mantle boundary with an additional boundary (velocity increase of 0.2 km/s) in the upper mantle at about 75 km depth.

This upper mantle boundary can also be seen in the record section of shotpoint 1 SW. Synthetic seismograms show a good fit to the observed amplitudes when a small gradient (0.006 km/s/km) is assumed beneath both boundaries. Our model, as presented in figure 27, still fails to explain the clear Pn arrivals between 200 to 280 km northeast of shotpoint 6. The apparent velocity of some of these Pn arrivals is low (6.8 km/s), which agrees with the record section. Assuming that the northeastern part of the oceanic Moho is underlain by continental material, we matched the second Pn arrival southwest of shotpoint 5. The ray path then crosses this "nappe structure" and enters the oceanic Moho again at a greater depth, about 25 km. Here the Moho dips strongly to the northeast and reaches its continental depth beneath shotpoint 5.

Later low-frequency arrivals (about 4 s after the first arrival) from shot-points 5 SW and 6 NE have not been taken into consideration. We believe these are converted waves or double-bounce arrivals.

TECTONIC IMPLICATIONS

The breaking up of the Red Sea Rift about 25 m.y. ago induced strong tectonic forces against the margin of the Saudi Arabian Shield. Our model structure is in agreement with a new concept about the development of continental margins (Meissner, 1981). Plume material has a tendency to intrude at lower continental crust levels (viscosity minimum) at the beginning of rifting. The nappe structure of our model can be attributed to such an intrusion. This is overlain by continental material and shelf sediments, here consisting mainly of salt. Northeast of shotpoint 5, where we found a zone of higher velocity material (6.65 km/s) near the surface, there seems to be a zone of strong compression. Whether or not this high-velocity material corresponds to lower crustal material cannot be deduced, but the velocities seem to indicate that it does. In this region the strongest uplift recently occurred while volcanic activity ceased a few million years ago.

CRITICISM AND POSSIBLE IMPROVEMENTS OF THE MODEL

The most outstanding feature of our model is the double structure of the oceanic Moho, interpreted as an intrusion of plume material into the continental crust at a very early stage of rifting. This structure was derived from the record sections mainly by picking two Pn arrivals from shotpoint 5 SW,

which were rather clear on the first distributed record sections. This phase is rather difficult to identify on the second data set, and we would not have picked it if we had worked only with those sections. The velocity of 8.0 km/s, however, seems to be too high. One would expect a somewhat lower velocity, about 7.2 km/s. Also, the thickness of the shelf sediments, 3.5 km, is too small; drilling results show more than 4 km. As these sediments consist mainly of salt, our velocity of 3.2 km/s is too low.

If we do not take the second Pn phase of shotpoint 5 SW into consideration we would be able to flatten the transition from the oceanic to the continental Moho, and the remaining problems with the Pn phase of shotpoint 6 between 200 and 280 km could probably be resolved. If we decrease the 8.0 km/s velocity of the "nappe," perhaps by stronger dips along the boundary and elongation of oceanic layer 3 (6.7 km/s) to greater distances toward the northeast, we might again be able to fit the observed apparent velocities and traveltimes. Increasing the sediment thickness between shotpoints 5 and 6 and choosing a higher velocity more adequate to salt layers should not seriously affect the calculation.

REFERENCES

Blank, H. R., Healy, J. H., Roller, J. C., Lamson, R. J., Fischer, F., McClearn, R., and Allen, S., 1979, Seismic refraction profile, Kingdom of Saudi Arabia--field operations, instrumentation and initial results: U.S. Geological Survey Saudi Arabian Mission Project Report 259, 49 p.

Meissner, R., 1981, The development of continental margins--A consequence of plumes intruding a variable viscosity tectonosphere: submitted to Oceanologica Acta, special issue on continental margins, p. 115-127.

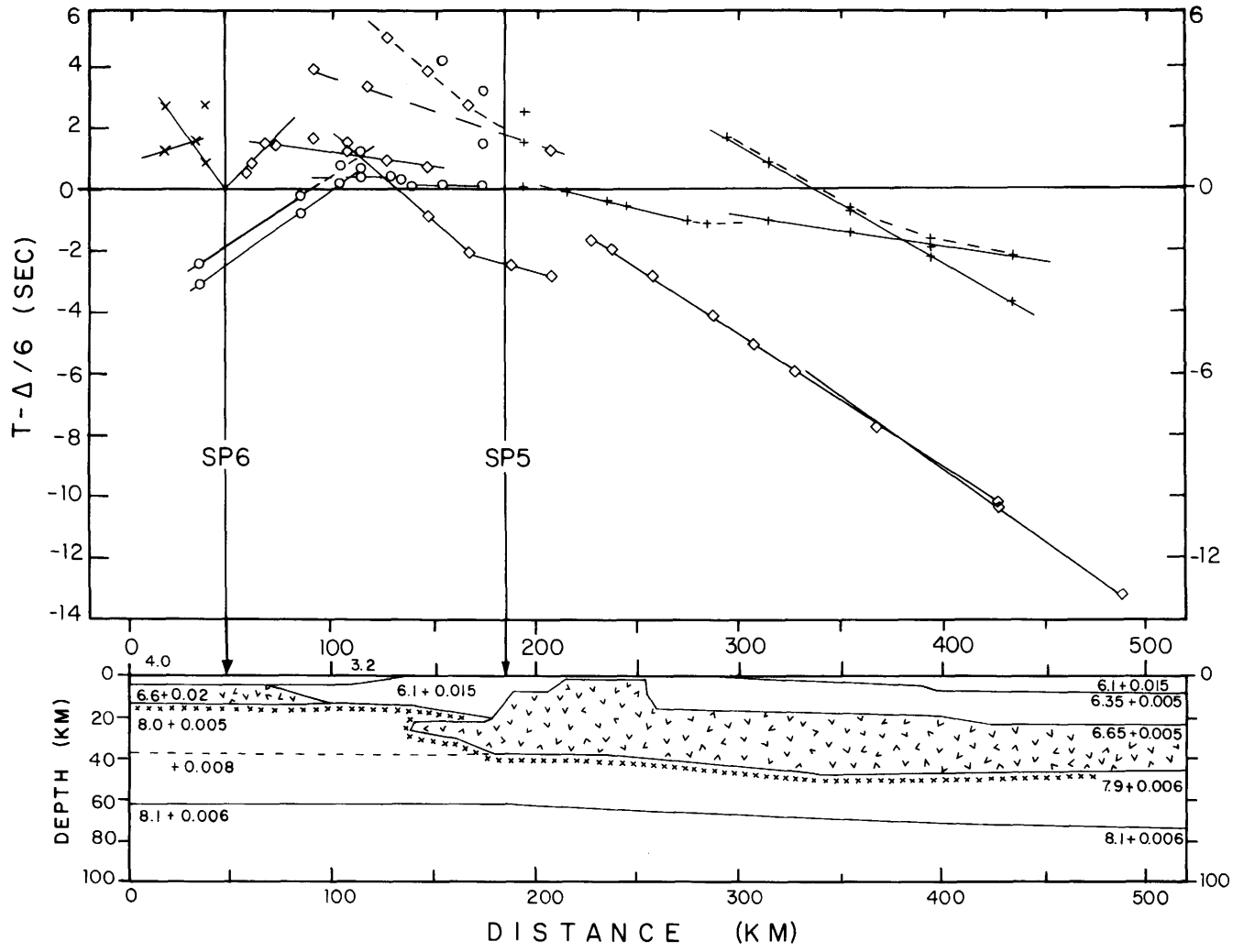

Figure 27. Traveltimes for shotpoints 5 SE and 6 NW (top) and crustal section derived from these observations (bottom). Lower crustal rocks with a seismic velocity of 6.65 km/s occur at shallow depths between 200 and 250 km on the distance scale.

SAUDI ARABIAN REFRACTION PROFILE: A PRELIMINARY INTERPRETATION FOR THE RED SEA-ARABIAN SHIELD TRANSITION

By H. Miller

Institut für Allgemeine und Angewandte Geophysik
Universität München
Munich, Federal Republic of Germany

An attempt was made to resolve the crustal structure between shotpoints 5 and 6 of the Saudi Arabian refraction seismic line. As is evident from the record sections, this part of the line has the greatest degree of lateral heterogeneity. The results obtained by ray tracing are of a very preliminary nature and only a general idea of the structure will be outlined.

In general, we have a very rapid increase in crustal thickness from south to north. With an average velocity of 4.2 km/s, the top part of the crust from shotpoint 6 to approximately 60 km to the north may consist of sediments or ocean layer 2 material or both. The crust is thin, the Moho being at a depth of 12 km. The Moho is modeled as a sharp discontinuity, below which a velocity inversion must exist in order to explain the traveltimes of the very prominent arrivals with apparent velocities of 8.4 km/s at distances beyond 200 km. South of shotpoint 5 the Moho is at a depth of some 27 km with a mean upper crustal velocity of 6.2 km/s and a mean lower crustal velocity of 6.8 km/s.

Little can be said at this stage about the transition between the two types of crust, and therefore the velocity contours of figure 28 in the region of the transition are not to be taken too seriously.

North of shotpoint 5 the crust thickens further and is characterized by relatively high average velocities.

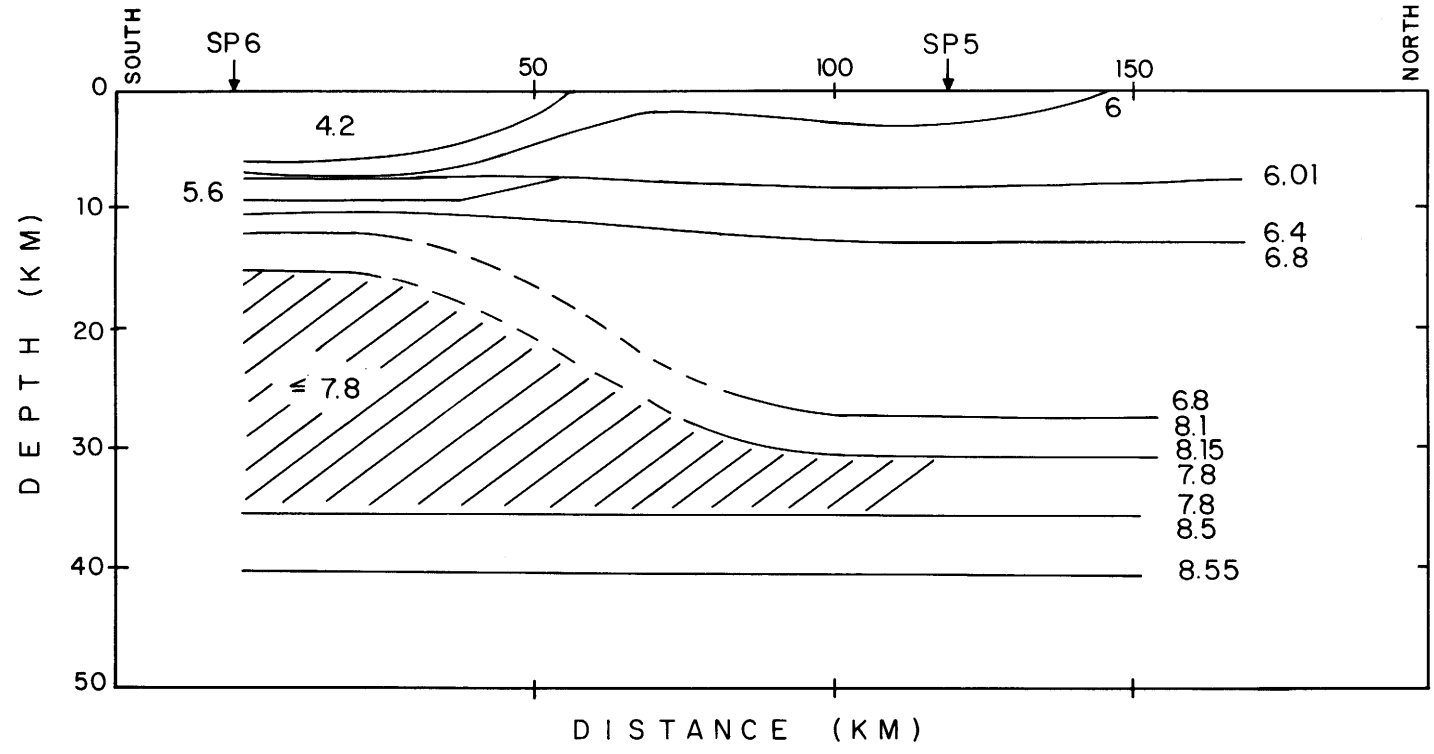

Figure 28. Cartoon crustal section between shotpoints 5 and 6.

A TRAVELTIME INTERPRETATION OF THE 1978 SEISMIC REFRACTION PROFILE IN THE KINGDOM OF SAUDI ARABIA

By Walter D. Mooney

U.S. Geological Survey
345 Middlefield Road
Menlo Park, California 94025

This report describes a traveltime analysis of the USGS/DGMR-conducted seismic refraction profile in Saudi Arabia. The analyzed data consist of reversing and overlapping profiles obtained from six shotpoints extending from the southern Red Sea nearly to the city of Riyadh on the Arabian Shield.

Data analysis consisted of the following steps:

1. Primary and secondary arrivals were determined from record sections reduced to 6.0 or 8.0 km/s.
2. The phases were identified as either refracted or reflected waves based on their amplitudes and traveltime behavior. Once the apparent velocities and time intercepts of the main refractors were identified, the slope-intercept method (Steinhart and Meyer, 1961) was used to obtain a starting model. Reflected phases were then fit by iterative one-dimensional ray tracing.
3. The one-dimensional models (velocity as a function of depth only) to the southwest and northeast of each shotpoint were combined to make preliminary two-dimensional models. The theoretical traveltimes for these models were compared with the observations using a modified version of a two-dimensional ray-tracing program (Červený and others, 1977).
4. Qualitative judgments were made concerning the relative sharpness of the seismic discontinuities on the basis of the apparent amplitude relations of the various phases, and these judgments were used to vary the two-dimensional model. For example, in order to shift critical points, sharp boundaries were converted into transition zones.

FLAT-LAYER, UNREVERSED MODELS

Calculating flat-layer models is only a first step in modeling seismic refraction data. These models are clearly only approximations because they do not take into account lateral changes in velocity (such as those resulting from dips and faults). Therefore, while the general features of the crustal structure presented here are reasonably accurate, many details will be changed in the following section on two-dimensional modeling.

The nomenclature of the phases identified in the data is as follows. "Pg" refers to a phase refracted through the basement, "Pi" refracts in the middle crust, "PiP" reflects from the middle crustal boundary (when more than one such reflections are identified they are numbered PiP1 and PiP2), "PmP" reflects from the crust-mantle boundary (variously referred to as the Moho, Mohorovičić discontinuity, or M-discontinuity), and "Pn" refracts through the upper mantle. Upper mantle phases that arrive after Pn are numbered and referred to as "P1" and "P2."

Shotpoint 1

Northeast (fig. 29): This profile is entirely within the Arabian Platform. The data, recorded only to about 85 km, reveal low velocities at the near-surface and an apparent high gradient in the uppermost basement. The apparent velocity of the first arrivals is about 5.9 km/s to a distance of 40 km, and then becomes about 6.3 km/s. There is considerable scatter in first arrival times between 70 and 85 km. One-dimensional modeling does not adequately represent these features where lateral changes are known to occur.

Southwest (fig. 30): This profile begins in the Arabian Platform and enters the shield 43 km southwest of the shotpoint. Data were recorded to a maximum of 655 km, nearly across the entire shield, with clear arrivals to as far as 550 km. In this discussion we consider only the data to 370 km. Low velocities are evident directly beneath the shotpoint, with the basement refractor apparently at about 1.0 km depth. Pg (basement) arrivals have been fit most accurately between 90 and 150 km. The arrivals between 20 and 80 km appear to be traveling through a medium with a higher average velocity than those beyond 90 km. The change to higher velocity occurs near the point at which the profile crosses the Al Amar-Idsas fault. Clear arrivals between 136 and 180 km are seen intermediate in time between the Pg and PmP/Pn phases. We refer to these phases as PiP if we believe them to be reflections from an intermediate crustal boundary, and as Pi if we believe them to be refractions from that boundary. In order to fit the high apparent velocity of these PiP arrivals, we have used a continuous velocity gradient increasing from 6.15 km/s at 1.5 km depth to 7.2 km/s at 39 km depth. A discontinuity occurs at 39 km depth where the velocity increases to 7.6 km/s. Below 39 km, the velocity increases slowly, reaching 7.7 km/s at 47 km depth, the crust-mantle boundary. The best fitting Pn velocity is 8.15 km/s at 47 km depth. The velocity model is unique among the shield profiles in that it lacks a velocity discontinuity at about 20 km depth, which may be in part due to a lateral change in crustal composition that occurs 120 km southwest of shotpoint 1.

Shotpoint 2

Northeast (fig. 31): This profile begins in the Shammar tectonic province of the shield (Greenwood and others, 1977) and enters the platform at a distance of about 100 km from the shotpoint. The first arrivals in the distance range 0-150 km (Pg) are fit with a velocity gradient in the upper crust from 6.2 km/s at 1 km depth to 6.5 km/s at 21 km depth. Clear intermediate arrivals (PiP) between 85 and 150 km are modeled as reflections from a discontinuity at 21 km depth where the velocity increases from 6.5 to 6.85 km/s. A mantle depth of 38 km matches only the average arrival time of presumed mantle (PmP) arrivals but fails to match the low apparent velocity of this phase. Comparing the velocity model for this profile with that of shotpoint 1 SW (fig. 30), we note that both indicate a velocity discontinuity at about 38 km depth, but neither clearly indicate that this is the M-discontinuity. This raises the possibility that a high-velocity lower crustal layer is present between shotpoints 1 and 2.

Southwest (fig. 32): This profile (and the next four to be discussed) was recorded entirely within the Arabian Shield, crossing three tectonic provinces and the faults that separate them. The data on this profile have some of the highest signal-to-noise ratios of all the data recorded during the project. The flat-layer model was very successful in modeling the arrival

times of both primary and secondary phases. Pg is modeled with a velocity gradient from 6.1 km/s at 1 km depth to 6.3 km/s at 18 km depth. This upper crustal velocity structure is remarkably different from those of the previous three profiles discussed, all of which indicate significantly higher velocities. The data from profile 1 SW, for example, have a traveltime that is 0.25 s faster at a range of 140 km than the data from profile 2 SW. Intermediate crustal arrivals are modeled as reflections (PiP) from a discontinuity at 18 km depth.

The profile provides crucial evidence that the M-discontinuity in this region is not a first-order discontinuity but is transitional. The evidence is the critical distance for the PmP arrivals of about 150 km, the high amplitudes of the post-critical PmP arrivals, and the low amplitudes of the pre-critical PmP arrivals. The transition from the crust to the mantle is modeled as occurring between 31.5 and 41 km depth, with the velocity increasing from 6.7 to 8.1 km/s. Clearly, comparison of synthetic seismograms with the true-amplitude record sections are needed to examine the validity of this structure. Partly because of this profile a crust-mantle transition zone (specifically, a velocity gradient followed by a small velocity discontinuity to mantle) is a feature of the two-dimensional ray-trace models discussed below. Pn arrivals on this profile have been fit with a mantle velocity that increases from 8.1 km/s at 41 km depth to 8.2 km/s at 60 km depth.

Shotpoint 3

Northeast (fig. 33): This profile was recorded entirely in the Najd tectonic province and crosses no major mapped faults. Data were recorded to a distance of 56 km. They indicate a refraction velocity of 6.0-6.1 km/s with essentially no (about 100 m) surficial cover. The shot length of this profile leaves profile 2 SW essentially unreversed.

Southwest (figs. 34 and 35): This profile extends across several important features of the shield. It begins in the Najd tectonic province, crosses the southwest Najd fault zone, and enters the Hijaz-Asir tectonic province. Within the last province it crosses the Nabitah zone (a region of ultramafic outcrops), the Al Qarah gneiss dome, and the Al Junaynah fault zone.

At near ranges Pg has an apparent velocity of 6.0 km/s. This apparent velocity is followed at greater range (30 km) by an apparent velocity of 6.3 km/s, which continues to 175 km. Intermediate arrivals (PiP) are clearly observed and are modeled by a discontinuity at 22.5 km depth from 6.45 to 6.7 km/s. The PmP arrivals are modeled with a sharp M-discontinuity at 35 km depth where the velocity increases from 6.7 to 8.0 km/s. In light of the low amplitudes of the PmP reflections, however, it is unlikely that the sharp M-discontinuity is real, and a transition zone has been used in the two-dimensional ray-tracing model. Pn arrivals have been fit by using a positive velocity gradient in the upper mantle of 0.008 km/s/km.

We have calculated an alternative model for profile 3 SW to attempt to explain some clear secondary arrivals that are observed at about 85 km range at a reduced traveltime of 0.0 s. These are modeled with a discontinuity at 13 km depth where the velocity increases from 6.35 to 6.65 km/s (fig. 35). Bringing this high velocity to shallow depth makes it difficult to fit other secondary arrivals that are observed between 140 and 175 km at a reduced traveltime of 0.5 s. These secondary PiP arrivals are important, for they appear to be from the boundary between the upper and lower crust. A possible model, as yet untested, is one with a low-velocity zone at 16-21 km depth. A

strong reflection that could fit the PiP arrivals would occur off the bottom of the low-velocity zone. Both PmP and Pn arrivals are adequately fit by the mantle depth (35.5 km) and velocity (8.0 km/s) used in this alternative model.

Shotpoint 4

Northeast (figs. 36 and 37): This profile starts in the Hijaz-Asir tectonic province and crosses into the Najd province; en route it crosses the Al Junaynah fault zone, the Al Qarah gneiss dome, and the Nabitah zone. A simple 6.2 km/s refractor fits the data up to 40 km, but beyond this point a traveltime advance of some 0.2-0.3 s is apparent. A laterally varying model is required to fit these traveltimes, which are advanced because of the high-velocity Al Qarah gneiss dome. We propose two models to fit the intermediate arrivals. In the first (fig. 36) we assume that two distinct phases are present (PiP1 and PiP2) and use two intracrustal discontinuities (at 13 and 34 km depth) to fit the arrivals. The Moho is modeled by a discontinuity at 42 km from 7.2 to 7.8 km/s. This model fits most of the data adequately, but the high-velocity of the lowermost crust (needed to fit the PiP2 arrivals) then causes the theoretical wide-angle PmP reflection to arrive early. A low-velocity zone beneath the lower crustal discontinuity could explain this. Alternatively, a simpler model (fig. 37) associates the PiP2 arrivals with wide-angle reflections from a single discontinuity at 13 km depth. In this case, the lower crust has a velocity of about 6.8 km/s, and the wide-angle PmP phase fits the observations at 240-280 km. Amplitude modeling would be effective in better resolving these uncertainties in structure.

Southwest (fig. 38): This profile crosses from the Hijaz-Asir tectonic province to the Red Sea. It reaches the Khamis Mushayt gneiss (about 35 km wide) at a distance of 130 km and the Hijaz-Asir escarpment at about 225 km. The Pg velocity is 6.1 km/s, and arrivals from a mid-crustal reflection (PiP) are evident at 100 km and beyond. These are modeled with a velocity discontinuity at 23 km, where the velocity increases from 6.6 to 7.1 km/s. It was very difficult to pick with certainty additional secondary arrivals on this profile due to the high dominant frequency throughout the seismograms. This may be due in part to the low seismic attenuation and large amount of scattering that occurs as the profile crosses the Khamis Mushayt gneiss (located at just the distance where secondary arrivals should be the strongest). The Pn arrivals were fitted with a mantle velocity of 8.15 km/s. All other phases are discontinuous and uncertain.

Shotpoint 5

Northeast (fig. 39): This profile begins just northeast of the Tihamat-Asir (coastal plain), extends across the Hijaz-Asir escarpment and Khamis Mushayt gneiss, and ends within 9 km of shotpoint 4. The Pg traveltime curve gives unmistakable evidence for high upper crustal velocities (about 6.45 km/s) beginning about 50 km northeast of the shotpoint. This higher velocity persists as the profile passes through the Khamis Mushayt gneiss. Secondary arrivals (PiP) are evident at 110-175 km and have been modeled by a discontinuity at 17 km depth where the velocity increases from 6.45 to 6.75 km/s. PmP (mantle reflection) arrivals are clear between 120 and 150 km but are very difficult to correlate at larger ranges which may be because the seismic energy passes through a disrupted lower crust beneath the Khamis Mushayt gneiss. The velocity in the lower crust increases from 6.75 to 7.1 km/s between 17 and 41

km depth. The available mantle arrivals (PmP and Pn) are fit reasonably well with the M-discontinuity at 41 km depth and a velocity of 8.1 km/s.

Southwest (fig. 40): This profile crosses the Tihamat-Asir and continues onto the Red Sea shelf, where several islands were used as recording sites. At the eastern edge of the Tihamat-Asir the profile crosses a dike complex intruded by gabbro and related rocks; this region may be considered the Arabian Shield-Red Sea boundary. The clearest evidence that these data were recorded in a region of strong lateral variation is given by the Pn velocity of about 9.0 km/s. Since this is an unreasonably high velocity for the uppermost mantle, it is obvious that either the crust is thinning toward the Red Sea so that the profile is shooting up-dip or that the average crustal velocity increases rapidly seaward. Despite this evidence that this region has strong lateral velocity variations, the profile was modeled with a flat-layer solution. Basement velocity (Pg) is the lowest observed on any profile in this data set, 5.85 km/s. In view of the local geology the basement rocks should have a velocity greater than 5.85 km/s, so we assume that the Pg apparent velocity is a down-dip measurement. Both the mantle refraction (Pn) and reflection (PmP) traveltimes indicate a much thinner crust (about 17.5 km) beneath the coastal plain than was observed on the shield. The flat-layer velocity model must include a broad transition zone from 5.9 to 8.0 km/s occurring between 11 and 24 km depth (mid-depth is therefore 17.5 km) in order to fit the critical reflection point.

Shotpoint 6

Northwest: This profile was not modeled with a flat-layer solution.

TWO-DIMENSIONAL MODELS

Using the results of the flat-layer modeling presented in the previous section, we have constructed two-dimensional velocity models for profile sets 3-2-1, 5-4-3, and 6-5. Combining the flat-layer velocity models required subjective decisions about how the velocity-depth functions for neighboring shotpoints should be made compatible. In order to obtain the simplest model consistent with the data, we decided to use as few layers as possible; this means that strictly local features were not included in the two-dimensional ray trace model.

The basic model chosen consists of an upper and lower crust, each with two layers, and a two-layer mantle. In the upper crust two layers are needed to model both the near-surface rocks (which often have velocities less than 6.0 km/s) and the basement rocks. In the lower crust two layers are needed to model the region just below the mid-crustal discontinuity (about 20 km deep) and the crust-mantle transition zone. Two mantle layers are used for most of the ray-trace calculations, the first directly beneath the crust (where the Pn phase propagates), and the second at about 60 km depth. An additional mantle layer at 70 km depth was used to model the data from shotpoint 6 NE.

Shotpoints 3-2-1

The profile sets for shotpoints 1, 2, and 3 (figs. 41-44) cover the transition from the Arabian Platform to the shield and encompass the Shammar and Najd tectonic zones.

The Pg arrivals from shotpoint 1 SW match the calculated traveltimes quite closely (fig. 41), but the velocity discontinuity at 21 km depth predicts PiP arrivals about 0.5 s ahead of the observed arrivals. However, the depth to this boundary was not increased because its position provided an excellent fit to the PiP arrivals recorded on profile 2 NE. Therefore, there are probably upper crustal heterogeneities between shotpoints 1 and 2 that have not been resolved in the present modeling.

The composite model fits the PmP and Pn phases for profile 1 SW reasonably closely, but it predicts a PmP phase where none is visible from shotpoint 2 NE. In addition, the phase Pl (which is labeled Pl (theory) in fig. 41) has not been successfully modeled with the deep mantle reflection. These difficulties in modeling the lower crust between shotpoints 1 and 2 suggest that strong lateral heterogeneity characterizes the entire crust in this region.

The composite model reasonably fits all arrivals from shotpoint 2 SW (fig. 42), which is not unexpected as the model is very similar to the successful flat-layer solution (fig. 32). The data from shotpoint 3 NE (the reverse of shotpoint 2 NE) provide only Pg arrivals (fig. 43). These indicate a near-surface velocity of about 6.0 km/s.

The average upper crustal velocity of profile 2 SW (6.2 km/s) is significantly lower than that used to model profile 2 NE (6.35 km/s). The mid-crustal discontinuity occurs at 21 km depth (fig. 44). A strong velocity gradient is seen in the lower crust between 31 and 43 km (from 6.8 to 7.9 km/s); the velocity contrast at the M-discontinuity is only 0.2 km/s. The effect of the high lower crustal gradient is shown quite clearly in the ray trace of Figure 42, where rays are focused between 128 and 160 km on the range scale. Synthetic seismogram calculations are needed to assess the validity of this velocity gradient.

In summary, strong lateral velocity variations are evident between shotpoints 1 and 2. To the west of shotpoint 2 is a region of refraction overlap (both profiles 1 SW and 2 SW extend into it), but not of refraction reversal. The differences in crustal structure northeast and southwest of shotpoint 2 seem resolvable; we suggest (fig. 44) that a major crustal boundary occurs near the shotpoint.

Shotpoints 5-4-3

The profile sets for shotpoints 3, 4, and 5 (figs. 45-48) cover the southwestern portion of the Najd and all of the Hijaz-Asir tectonic provinces, crossing several major crustal features including the Nabitah zone, the Al Qarah gneiss dome, and the Hijaz-Asir escarpment.

The arrivals through basement (Pg) have been reasonably well fit for the four profiles considered here, with the exception of the data from profile 5 NE across the Khamis Mushayt gneiss (fig. 47). For profile 3 SW the composite model gives reasonably good traveltime fits for all phases except the portion of the PmP reflection near the critical point (labeled A on fig. 45). This may indicate lateral heterogeneity in the lower crust southeast of shotpoint 3. Traveltimes of the composite velocity model fit the Pn arrivals very reasonably.

In discussing the data of shotpoint 4 NE and SW, we reemphasize an observation made previously: the seismograms on this profile have a high dominant frequency coda which makes phase correlation of secondary arrivals very difficult. Therefore, we gave greater weight to the traveltime models of profiles 5 NE and 3 SW in constructing the composite model.

Even considering the difficulty in identifying secondary arrivals in the data from shotpoint 4, the disagreement between the picked secondary arrivals and those calculated for the composite model is notable and is interpreted to indicate anomalous crustal material beneath shotpoint 4. The composite model does not account for prominent secondary arrivals at about 80 km northeast of shotpoint 4 (labeled A in fig. 46). The observed PmP arrivals northeast of shotpoint 4 are about 0.4 s later than the calculated arrivals, indicating that the composite velocity model (fig. 48) is too fast in the lower crust beneath shotpoint 4. The observed Pn arrivals are also not fit by the calculated model. In profile 4 SW, the mid-crustal reflector at 22 km appears to fit observed PiP arrivals reasonably well. Some PmP arrivals (labeled B in fig. 46) are about 0.6 s later than calculated from the model, indicating, as in profile 4 NE, that the velocity in the lower crust is lower than indicated in the composite velocity model (fig. 48).

The composite velocity model fits the data of profile 5 NE considerably more successfully (fig. 47). The gneiss body possibly has disrupted the middle crustal boundary because the predicted intermediate crustal phases Pi and PiP do not have observed arrival times to match. The ray-trace model fits the mantle reflection (PmP) and refraction (Pn) quite well, indicating that the average crustal velocity and thickness of the model are consistent with the data.

In summary, the composite velocity model for profile sets 3, 4, and 5 is an adequate representation of the velocity structure near shotpoints 3 and 5, but some significant deviations are seen beneath shotpoint 4, including lower-than-average lower crustal velocities of 6.7 km/s, which amounts to a reduction of 0.3 km/s from the shield average of 7.0 km/s. There is also evidence for a 13-km-deep reflector between shotpoints 3 and 4.

Shotpoints 6-5

The region between shotpoints 5 and 6 spans the ocean-continent transition zone at the southwest end of the profile (figs. 49-51). Shotpoint 5 is about 5 km northeast of the dike swarms of the Tihamat-Asir, which are believed to be at the margin of the Red Sea rift. Southwest of shotpoint 5 are the sediments of the coastal plain and Red Sea shelf, which have been drilled to more than 4 km depth in the offshore regions (Gillman, 1968).

The ray-trace diagrams for shotpoint 6 NE (fig. 50) are all for traveltimes reduced by 8.0 km/s, unlike the previous figures. The pattern of arrivals is extremely irregular; the only certain correlations are crustal arrivals between 1 and 26 km and Pn arrivals between 105 and 125 km. Between 26 and 105 km the data show a series of traveltime advances and delays that may in part be due to large variations in the thickness of low-velocity sediments. Between 18 and 27 km high-amplitude secondary arrivals follow the first arrival by 0.4 to 0.15 s. We interpret these secondary arrivals as mantle reflections (PmP). According to this correlation, the depth to mantle 22 km east of shotpoint 6 is 8 km. However, if the PmP critical point at 22 km is connected to the clear Pn arrivals at 105 km with a straight line, the line is approximately 1.0-1.5 s ahead of the visible first arrivals. Two possible explanations exist for this. The first is that the velocity varies strongly laterally between 26 and 105 km and large traveltime delays occur in that range due to the thickening of sedimentary rocks. The second is that the visible first arrivals are actually secondary arrivals and the mantle refractors are of extremely low amplitude due to irregular structure at the

crust-mantle interface. The record section indicates possible weak earlier arrivals between 58 and 105 km.

Regardless of these uncertainties, an initial, relatively simple model was derived by connecting the 8-km crustal thickness at shotpoint 6 to the 17.5-km crustal thickness southwest of shotpoint 5 that was determined by taking the midpoint of the velocity gradient derived in flat-layer modeling (fig. 40). We used iterative two-dimensional ray tracing to somewhat refine the initial model. The model fits the Pg arrivals and the mantle refractions (Pn) in the traveltime data of shotpoint 5 SW (fig. 49) reasonably well, but the mantle reflection arrivals (PmP) appear to be delayed by as much as 0.2 s.

For shotpoint 6 NE (fig. 50), the Pg and Pn arrivals at 105-125 km are fit rather well by the ray-trace calculations. The detailed traveltime behavior ofarrivals between 25 and 100 km is not well fit, the average traveltime error being 0.4 s.

In summary, the data from shotpoints 5 SW and 6 NE are interpreted to indicate a landward dip of the M-discontinuity of 4.6° (fig. 51). The Pn velocity is 8.0 km/s and the crustal structure consists of a 4.2 km/s layer on top of a thicker 6.2 km/s layer. More densely recorded data would be desirable to further reveal the structure in this important tectonic region.

In the region of the Arabian Shield-Red Sea transition, the especially weak and diffuse arrivals between 150 and 200 km from shotpoint 6 probably indicate extreme structural complications. Beyond this structural transition, strong Pn arrivals observed beginning at about 225 km from the shotpoint appear to show an en echelon pattern of first and secondary arrivals, with the secondary arrivals having high amplitudes at 250 and 400 km. Western European and Russian seismologists, who previously conducted long-range investigations, have determined that these phases indicate velocity gradients or discontinuities in the upper mantle. We have attempted to model only two of the en echelon mantle phases (fig. 50), showing them as first-order discontinuities at 56 and 68 km deep where the velocity increases from 8.0 to 8.3 km/s and 8.3 to 8.5 km/s, respectively.

It is of some interest to note in the ray trace (fig. 50) that there is no true Pn phase (head or diving waves traveling along the continental M-discontinuity). This observation raises the possibility that similar phases that may have been modeled in previous offshore-onshore investigations as head waves are, in fact, upper mantle phases.

REFERENCES

Červený, V., Molotkov, I. A., and Pšenčik, I., 1977, Ray method in seismology: Univerzita Karlova, Prague, 214 p.

Gillman, M., 1968, Primary results of a geological and geophysical reconnaissance of the Jizan coastal plain in Saudi Arabia: Society of Petroleum Engineers AIME, Saudi Arabia Section, Second Regional Technical Symposium, Dhahran, Saudi Arabia, March 27-29, p. 189-212.

Greenwood, W. R., Anderson, R. E., Fleck, R. J., and Roberts, R. J., 1977, Precambrian geologic history and plate tectonic evolution of the Arabian Shield: U.S. Geological Survey Saudi Arabian Project Report 222, 97 p.

Steinhart, J. S. and R. P. Meyer, 1961, Explosion studies of continental structure: Carnegie Institute Washington Publication 622, 409 p.

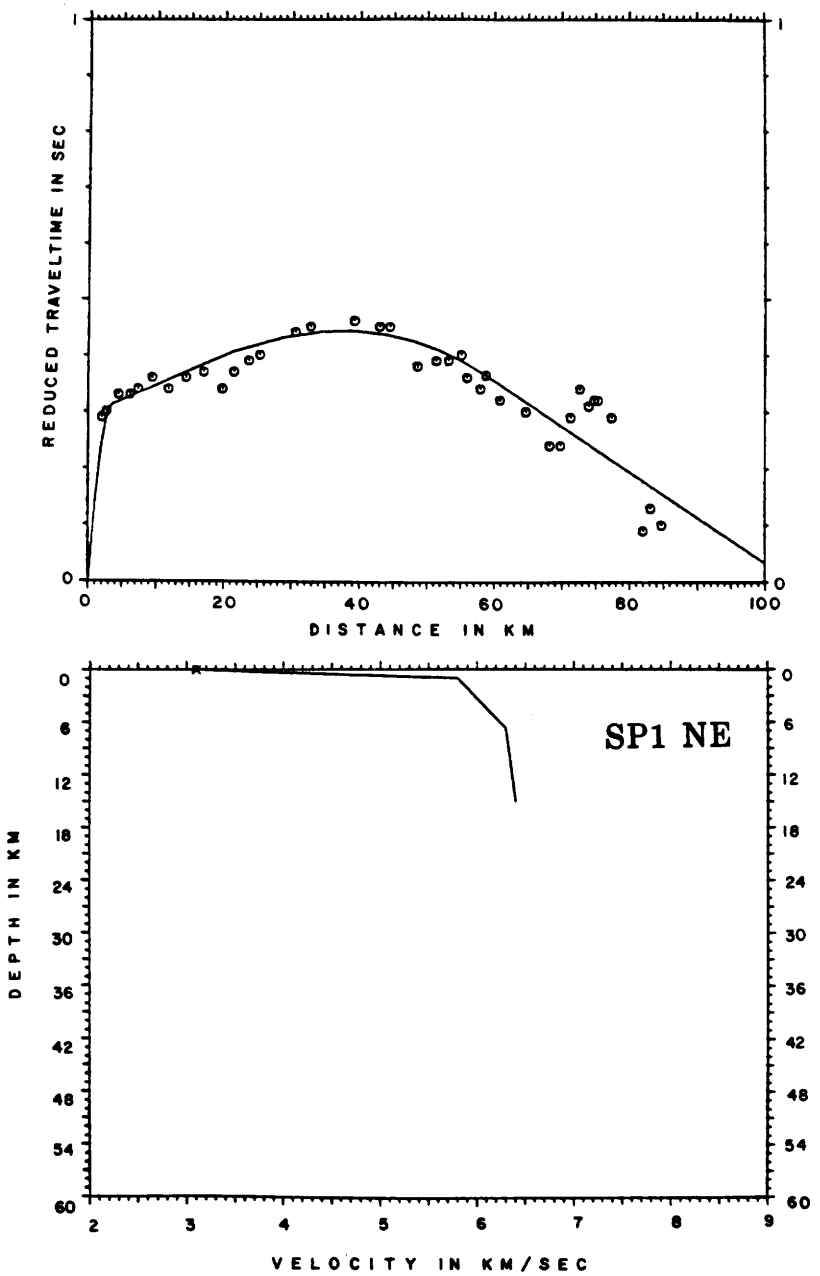

Figure 29. Flat-layer model for data from shotpoint 1 NE.

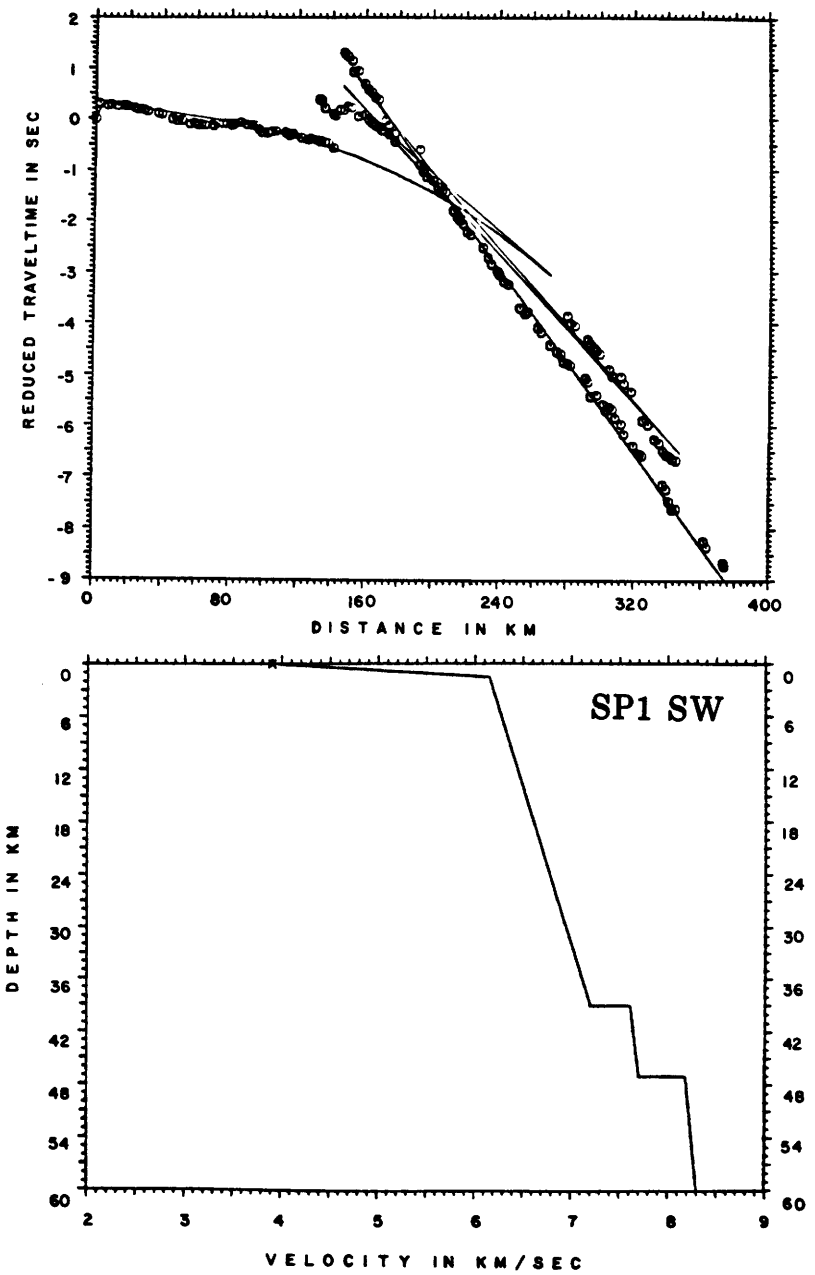

Figure 30. Flat-layer model for data from shotpoint 1 SW.

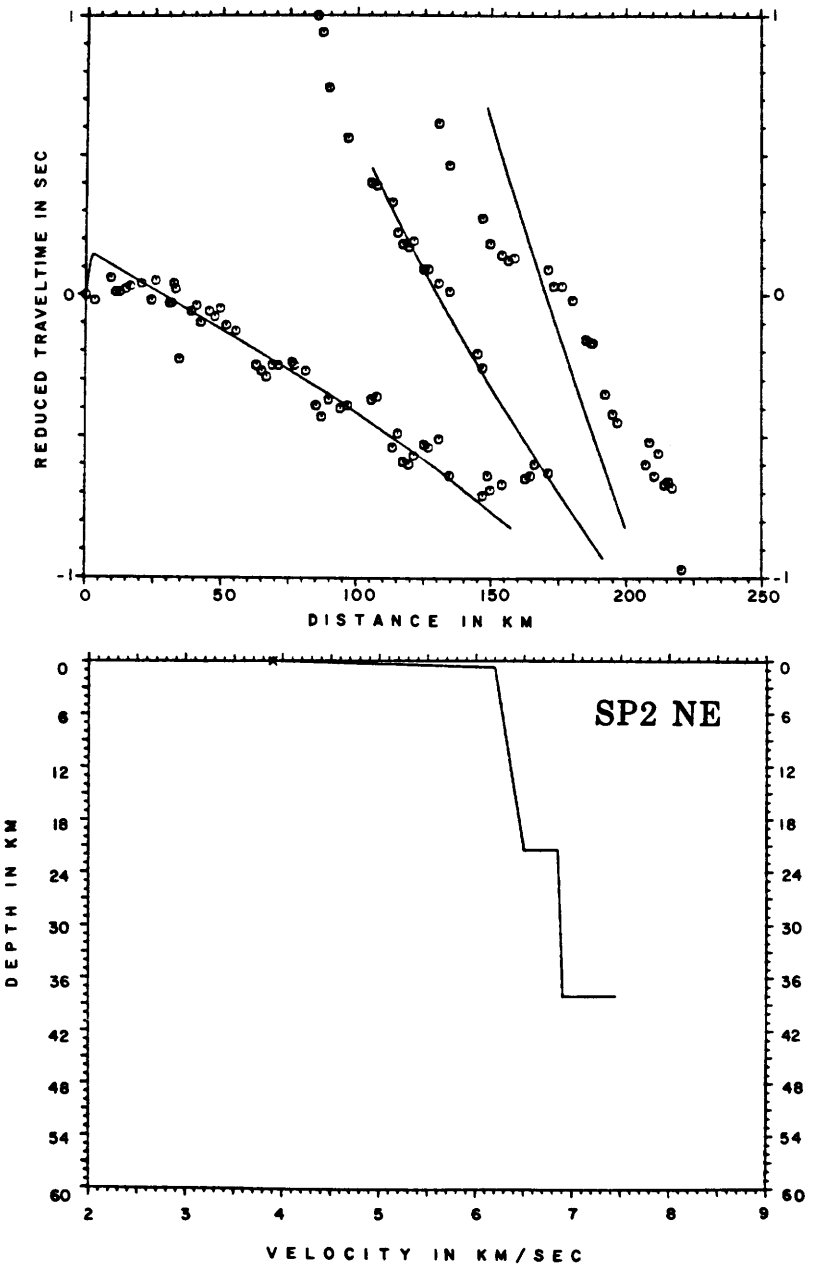

Figure 31. Flat-layer model for data from shotpoint 2 NE.

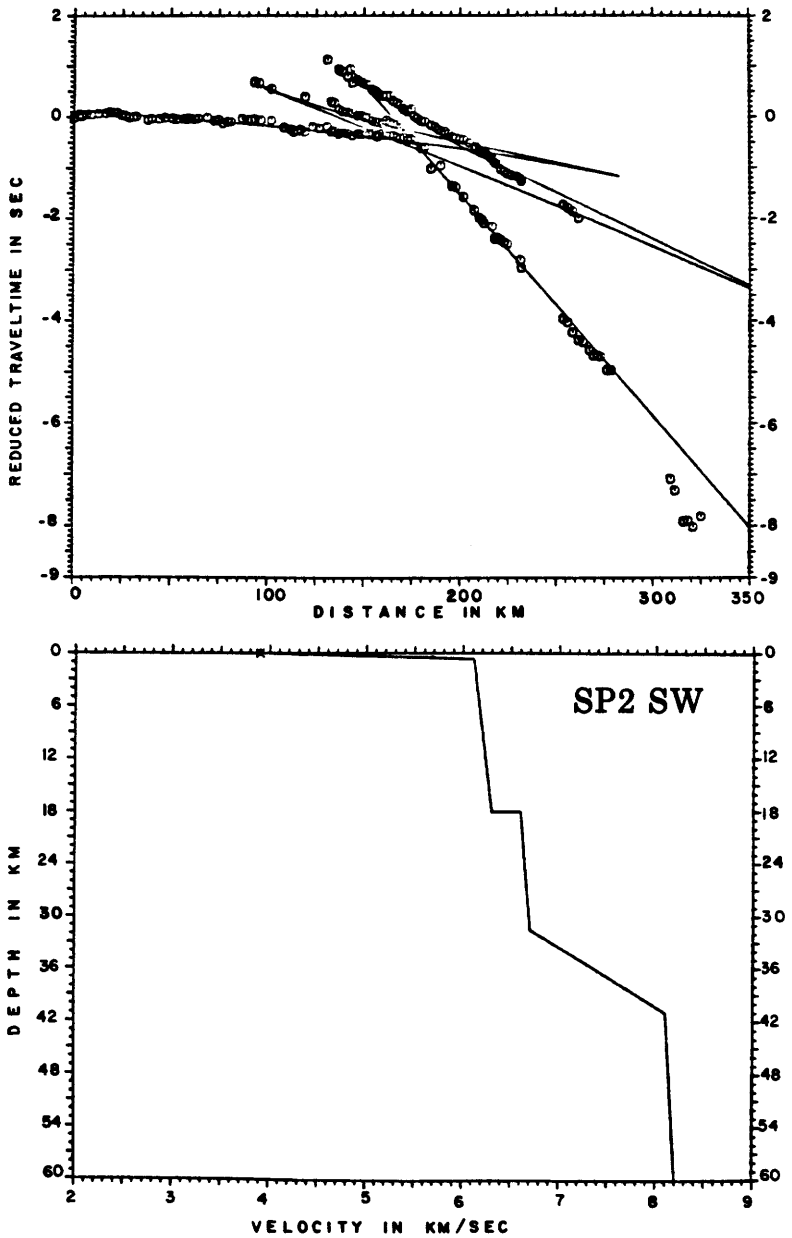

Figure 32. Flat-layer model for data from shotpoint 2 SW.

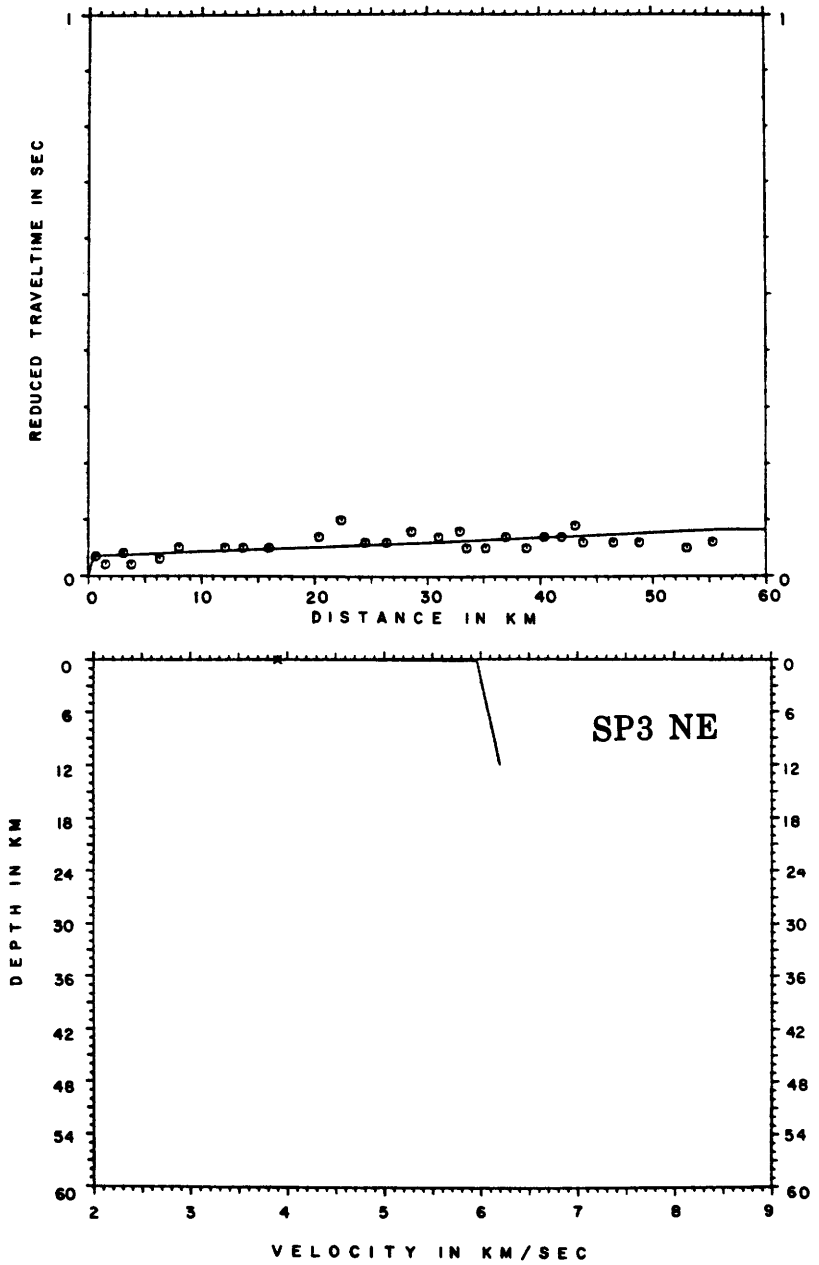

Figure 33. Flat-layer model for data from shotpoint 3 NE.

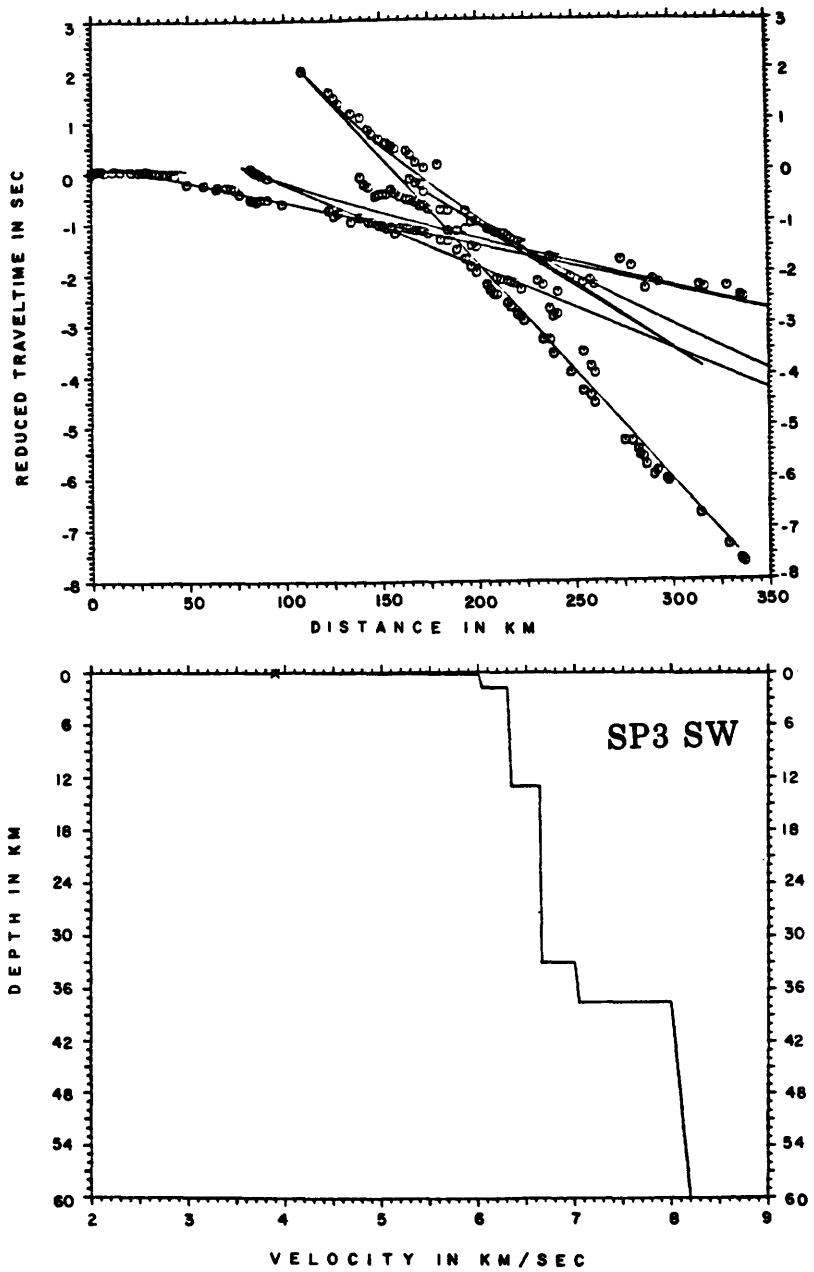

Figure 34. Flat-layer model for data from shotpoint 3 SW.

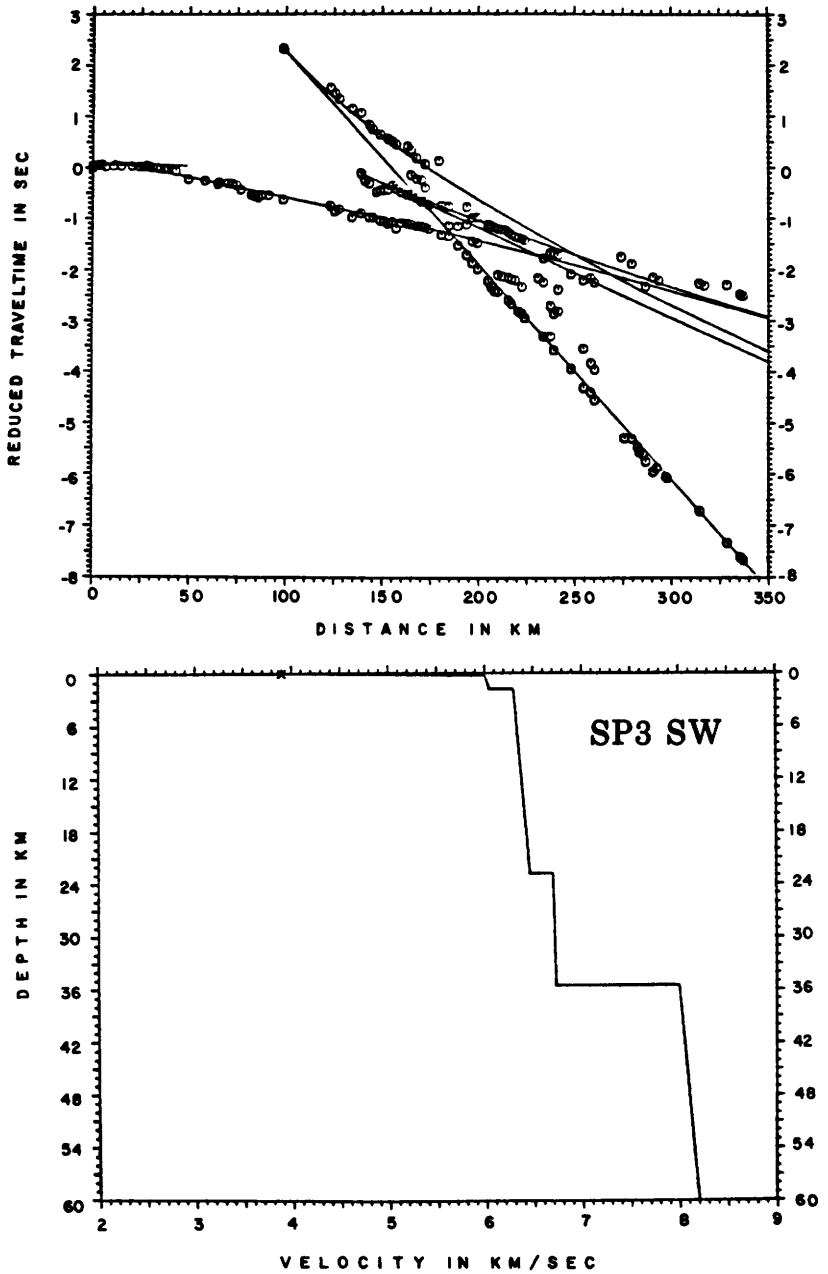

Figure 35. Alternate flat-layer model for data from shotpoint 3 SW.

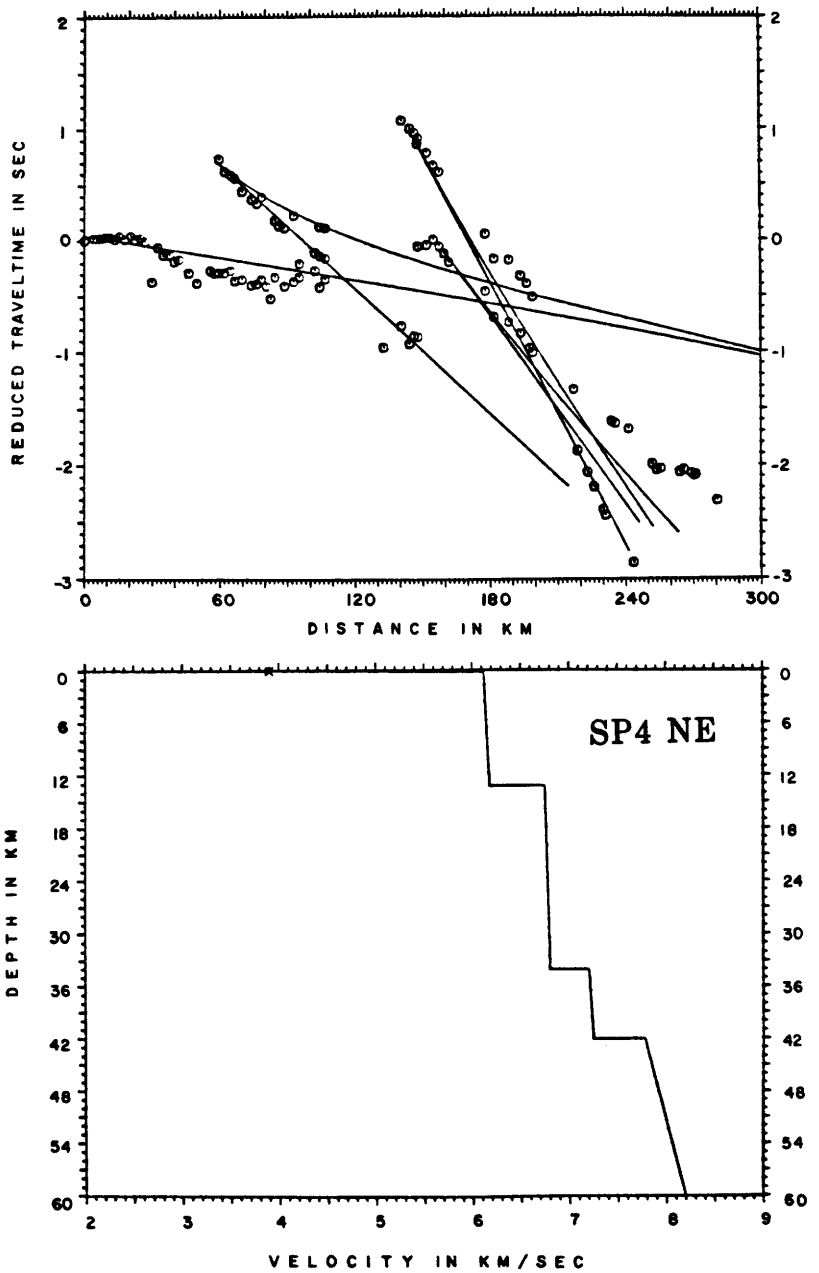

Figure 36. Flat-layer model for data from shotpoint 4 NE.

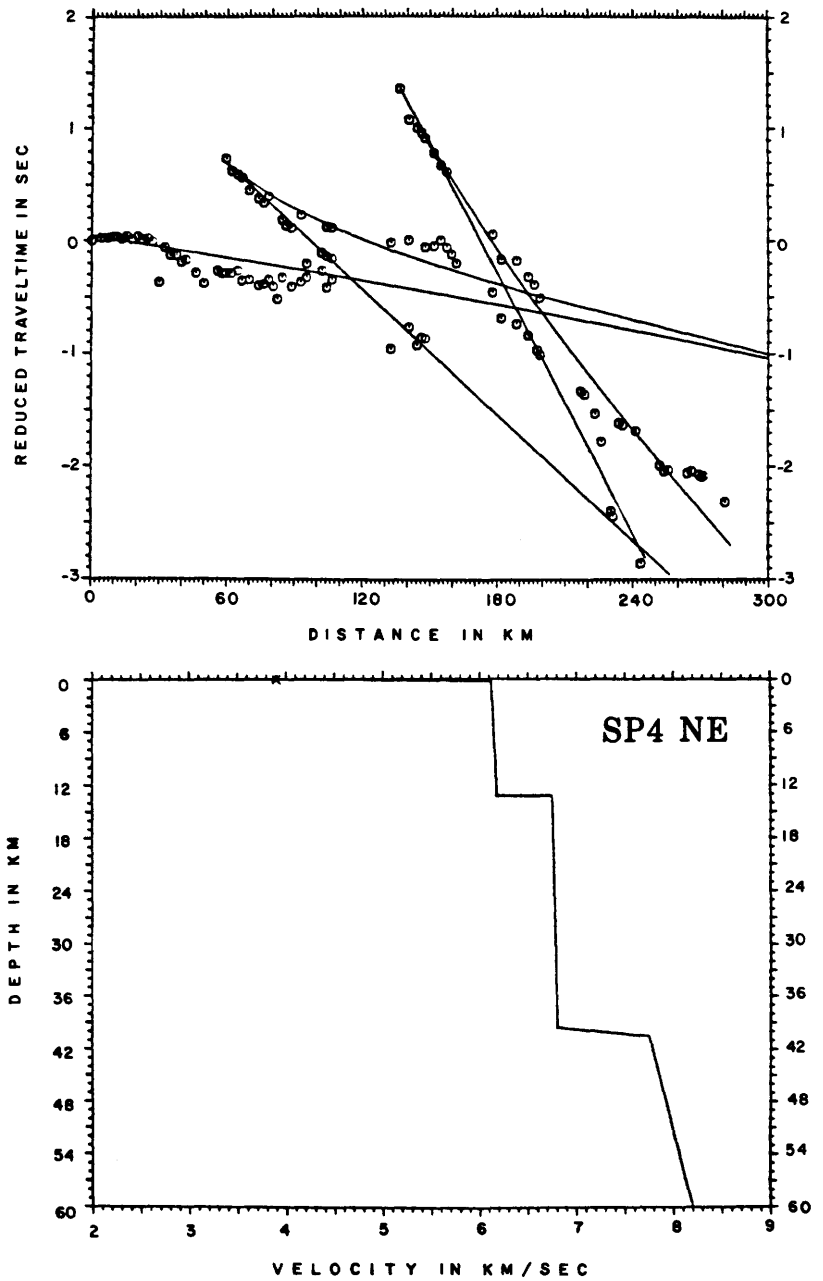

Figure 37. Alternate flat-layer model for data from shotpoint 4 NE.

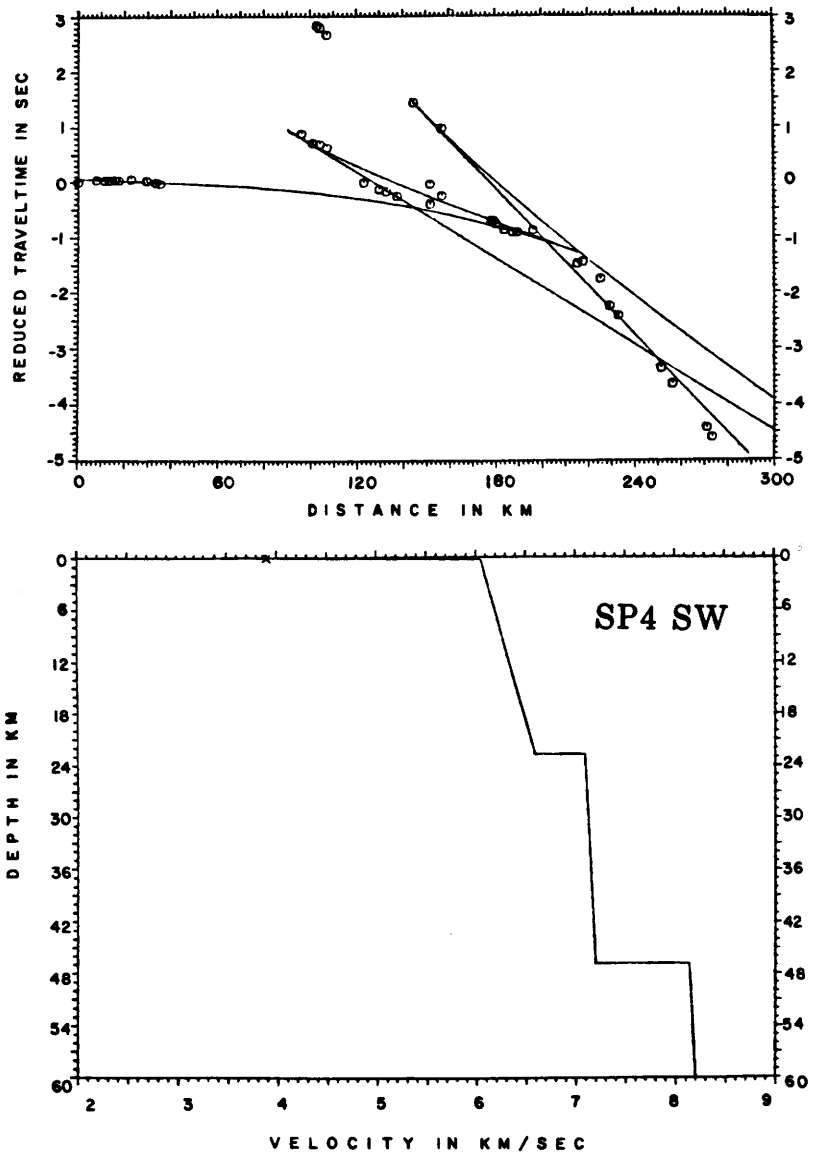

Figure 38. Flat-layer model for data from shotpoint 4 SW.

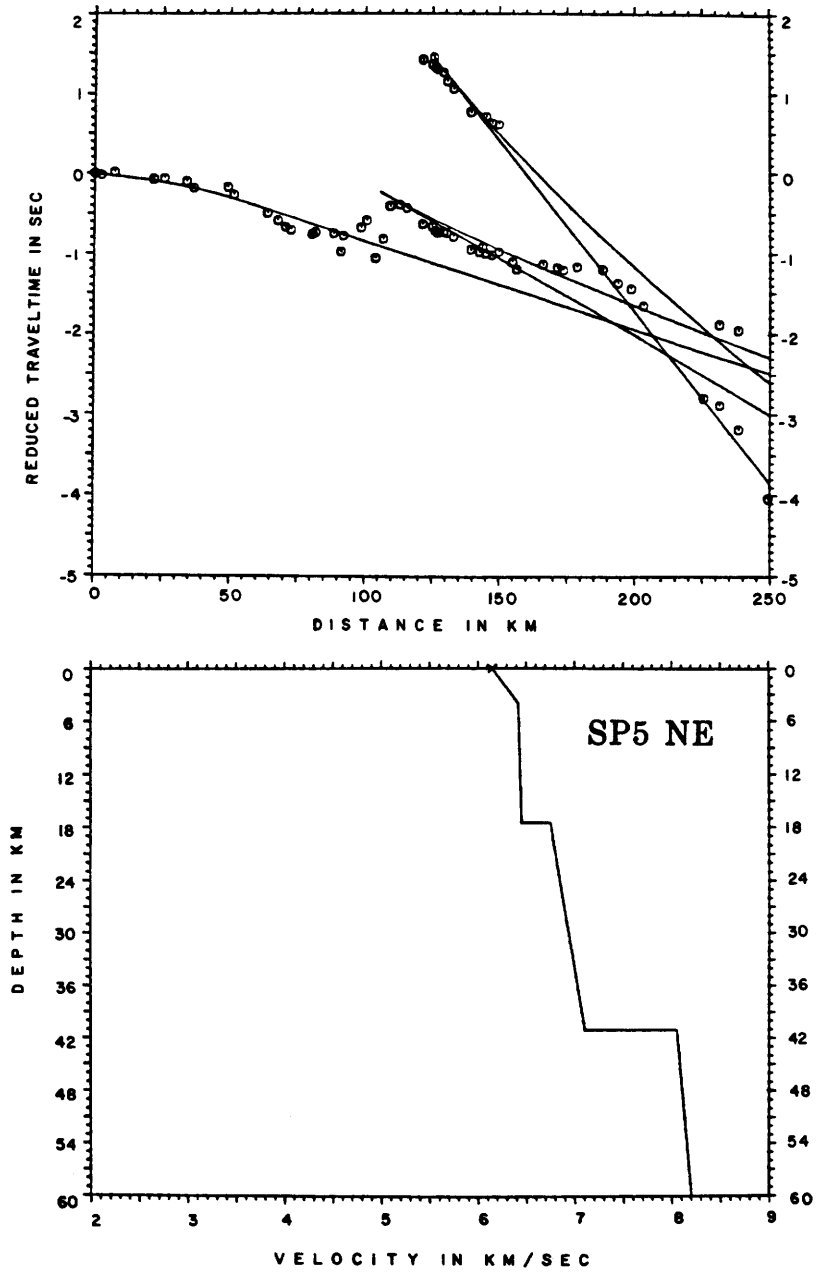

Figure 39. Flat-layer model for data from shotpoint 5 NE.

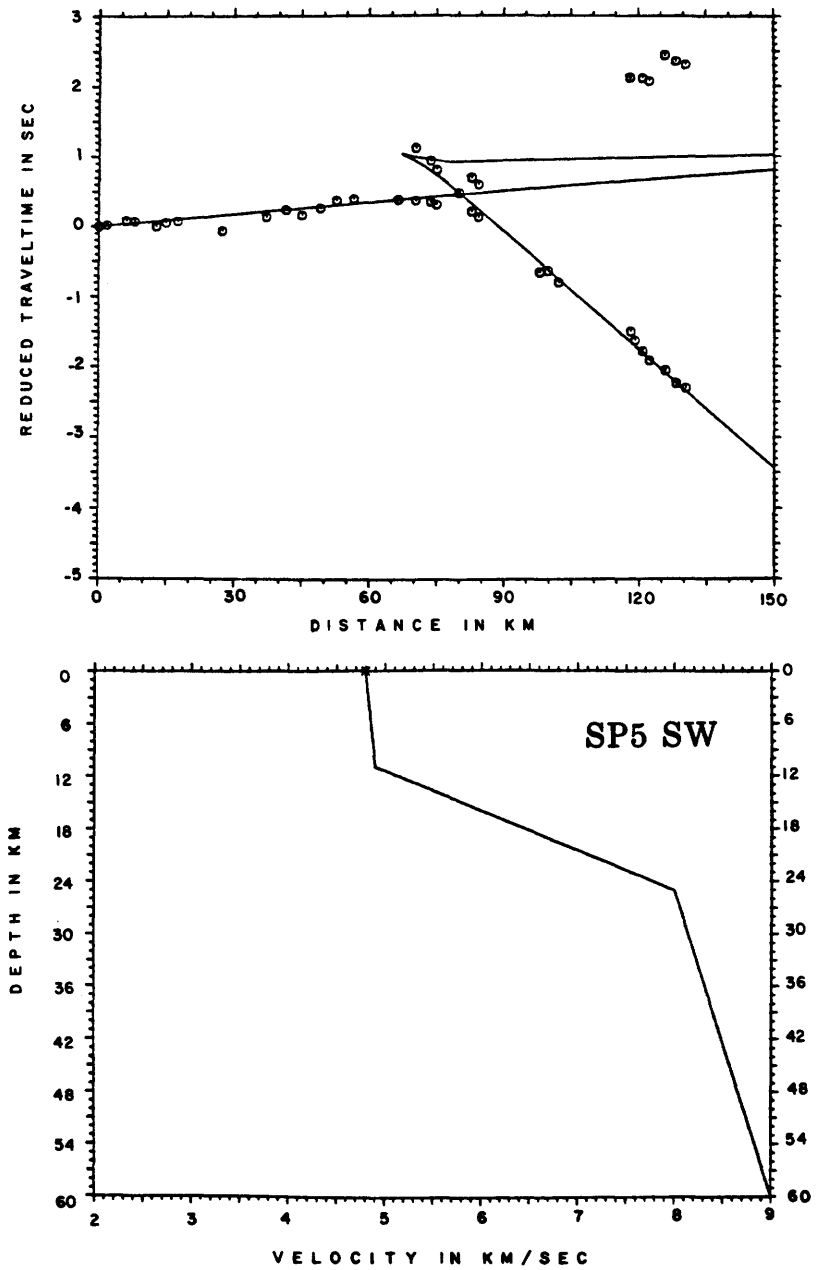

Figure 40. Flat-layer model for data from shotpoint 5 SW.

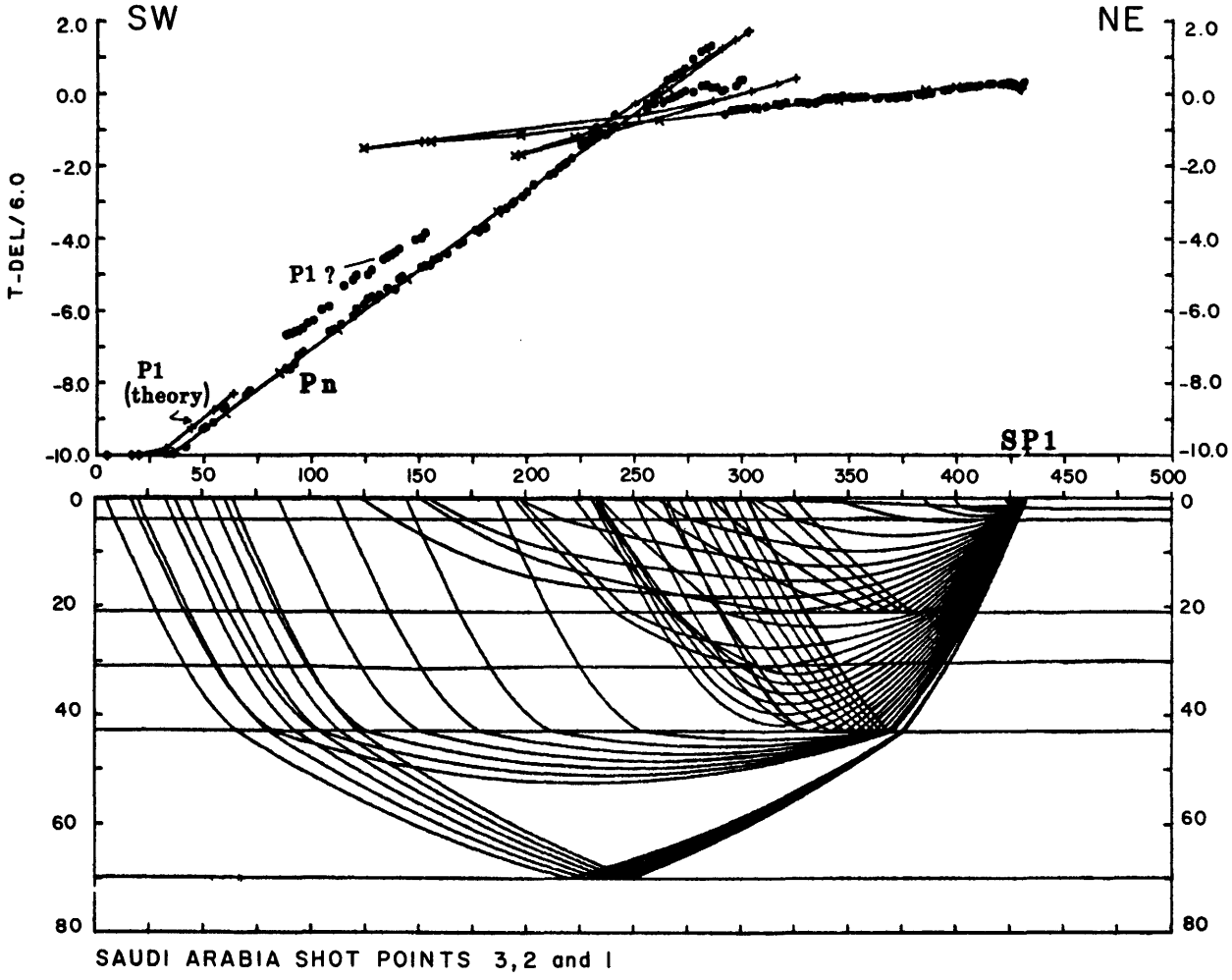

Figure 41. Two-dimensional ray trace diagram for the data from shotpoint 1 SW.

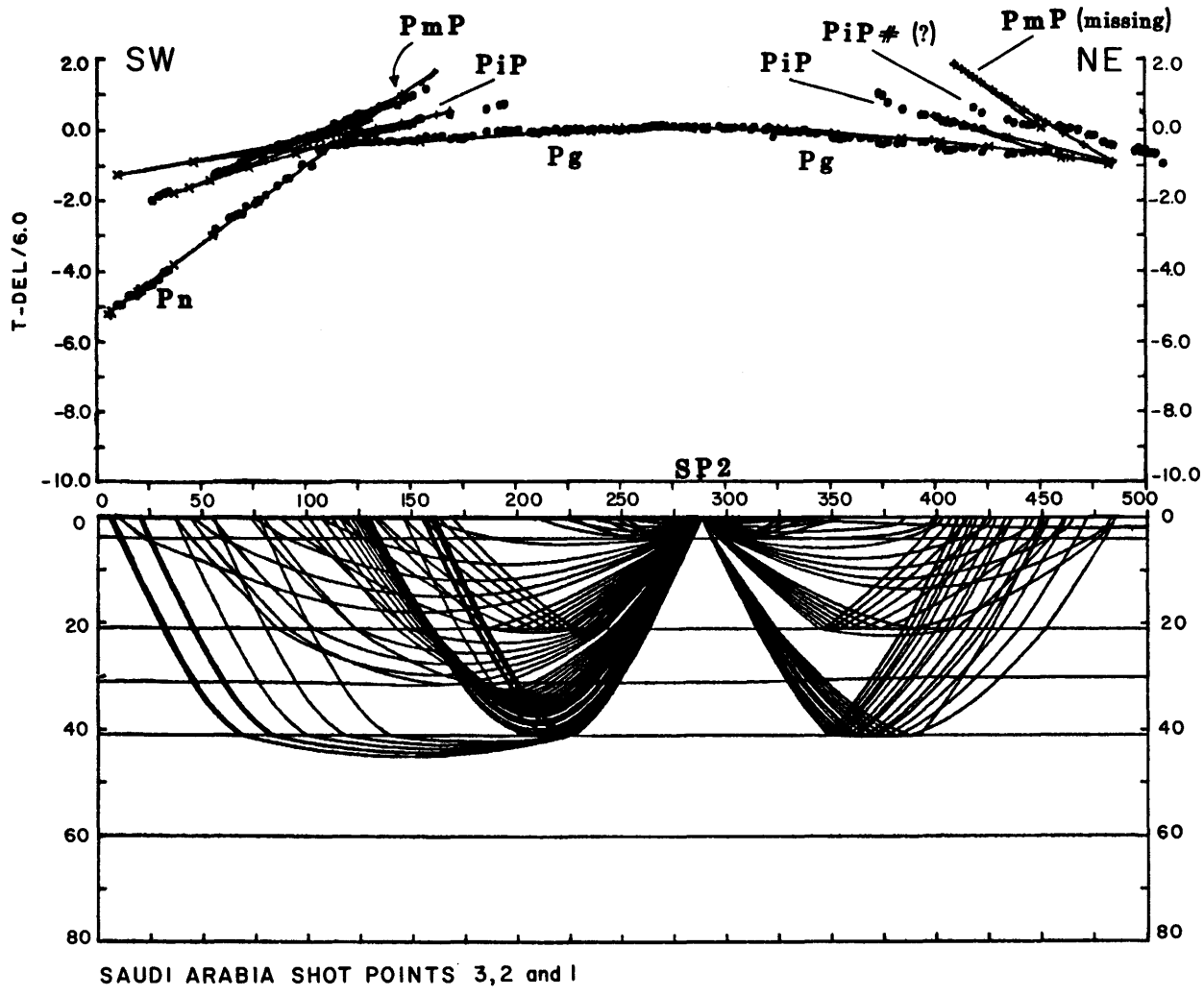

Figure 42. Two-dimensional ray trace diagram for the data from shotpoint 2.

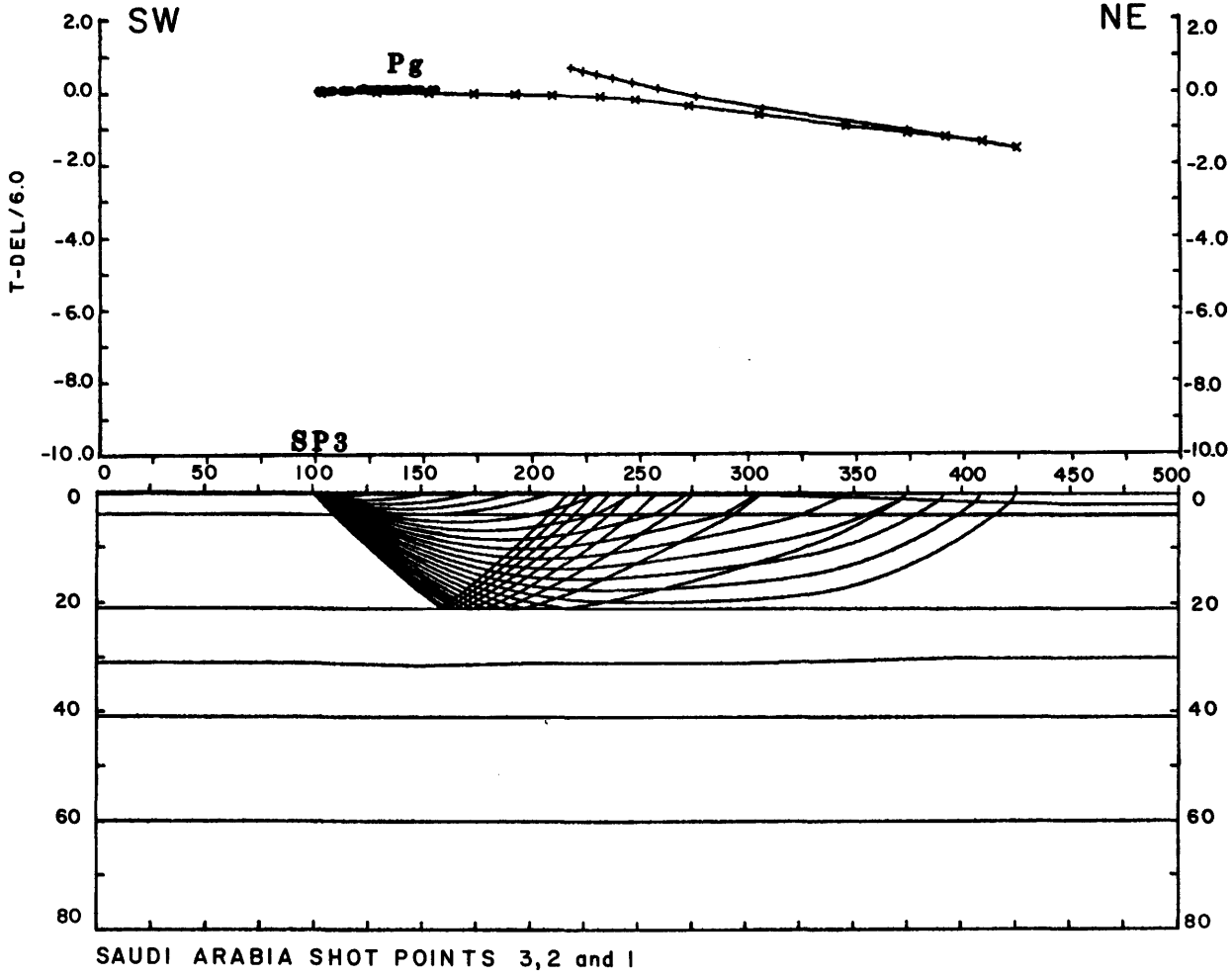

Figure 43. Two-dimensional ray trace diagram for the data from shotpoint 3 NE.

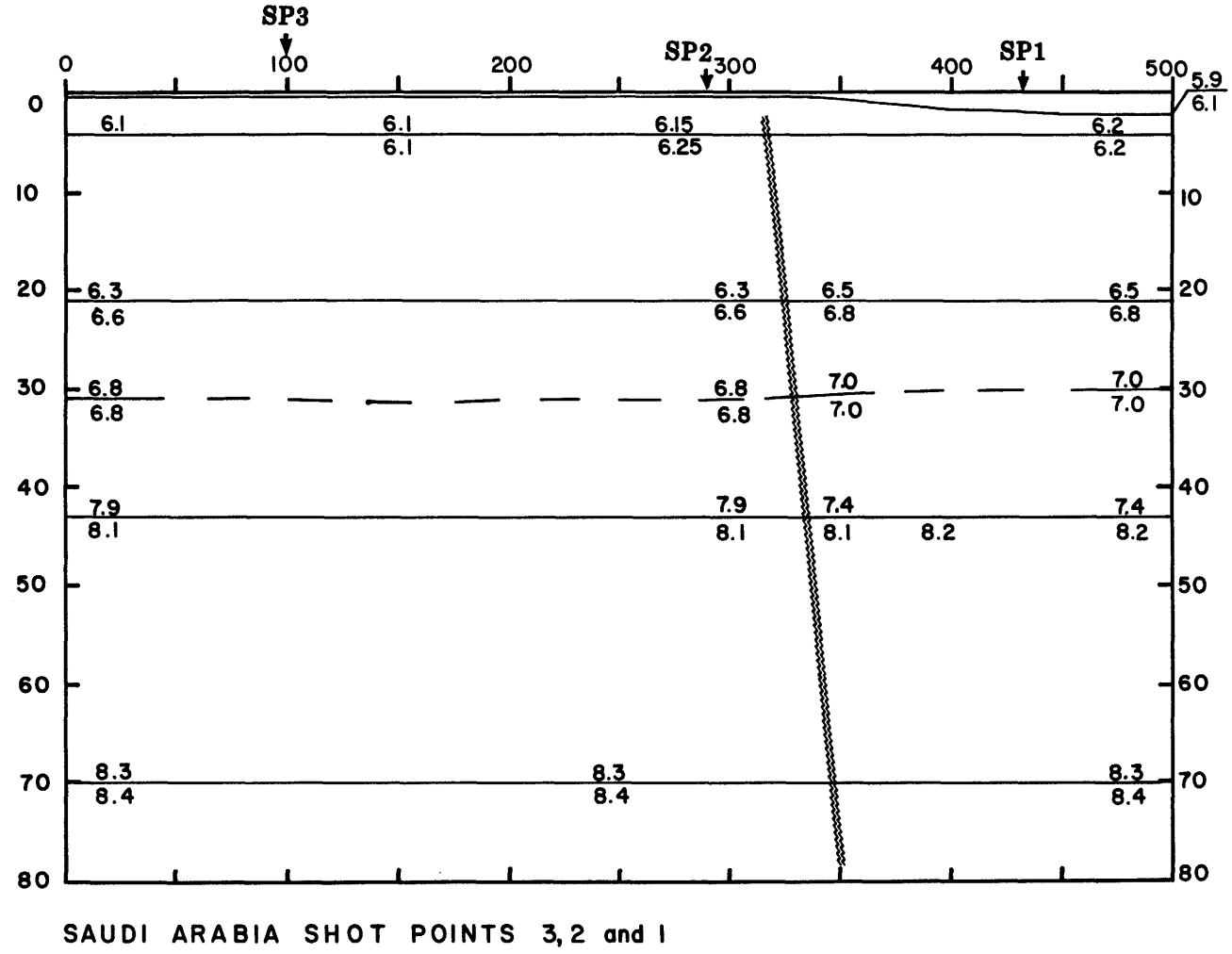

Figure 44. Velocity-depth structure beneath shotpoints 3, 2, and 1.

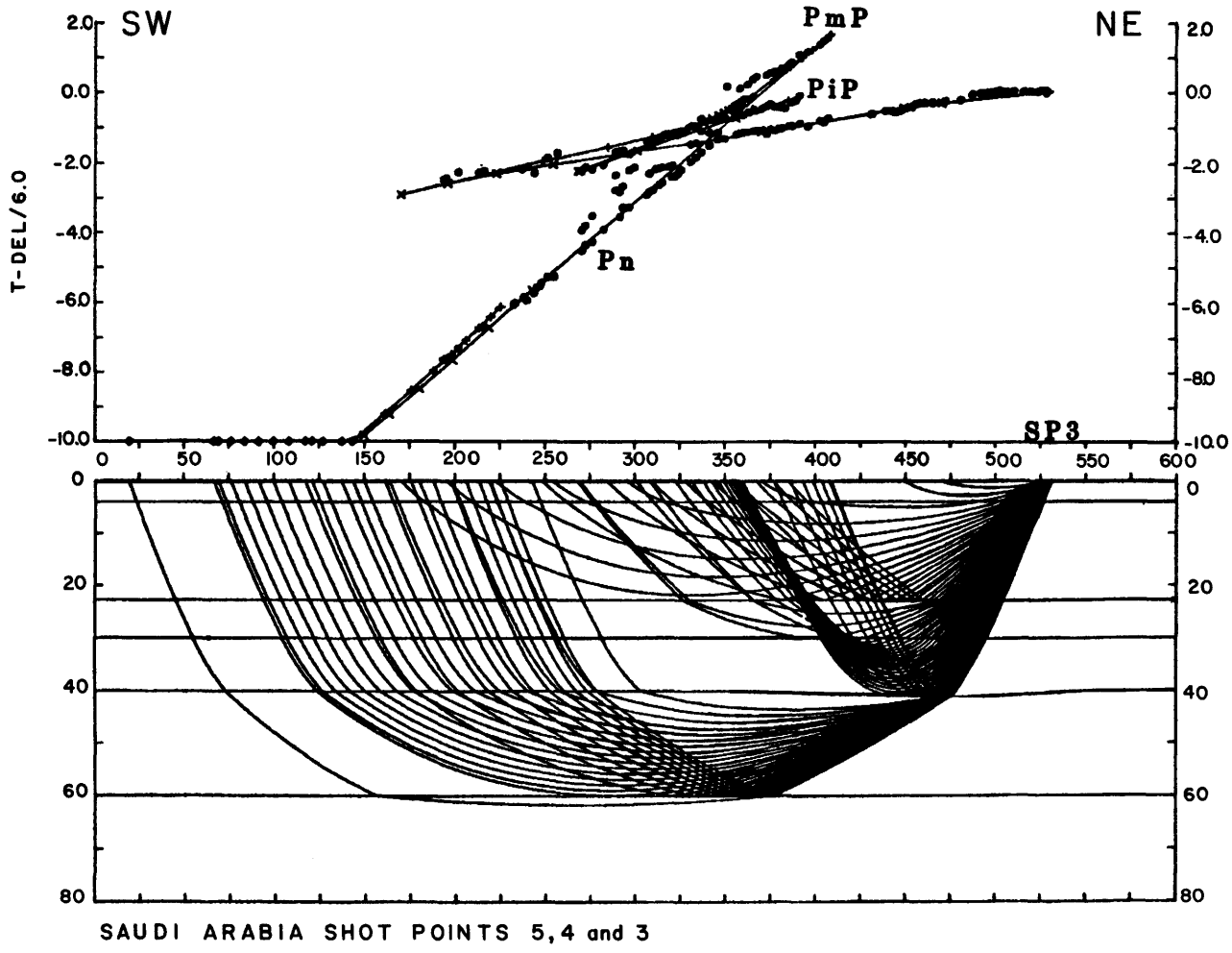

Figure 45. Two-dimensional ray trace diagram for the data from shotpoint 3 SW.

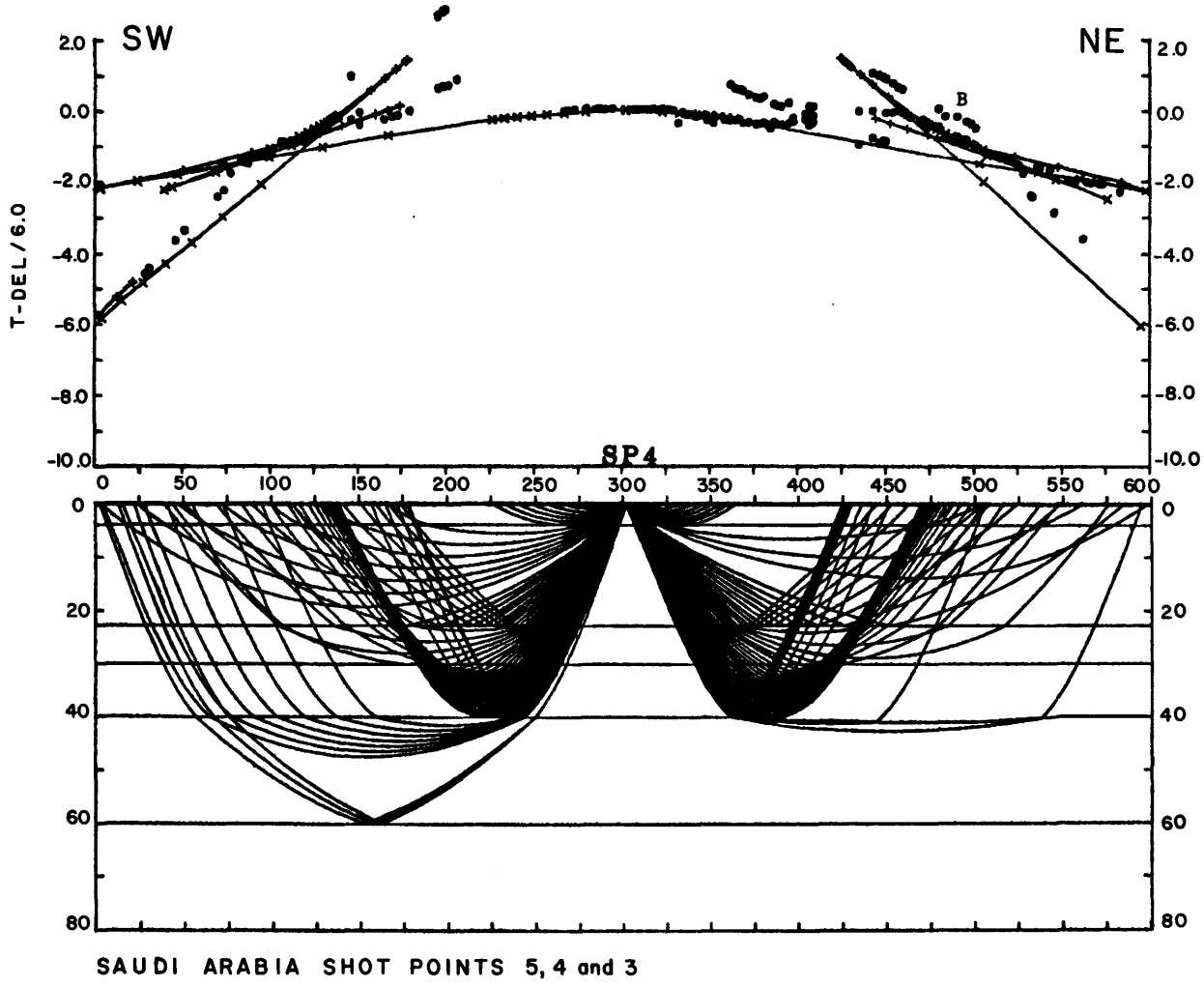

Figure 46. Two-dimensional ray trace diagram for the data from shotpoint 4.

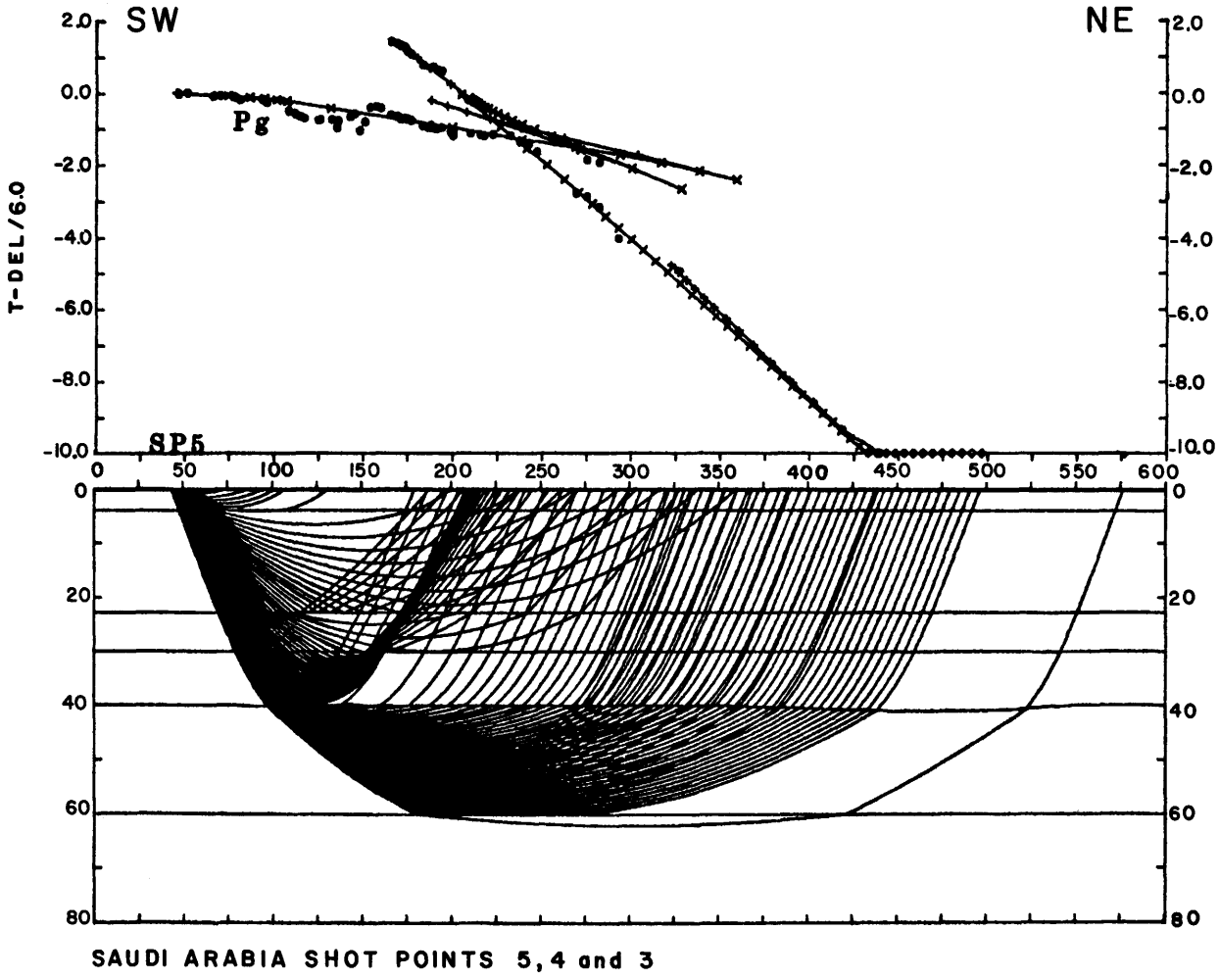

Figure 47. Two-dimensional ray trace diagram for the data from shotpoint 5 NE.

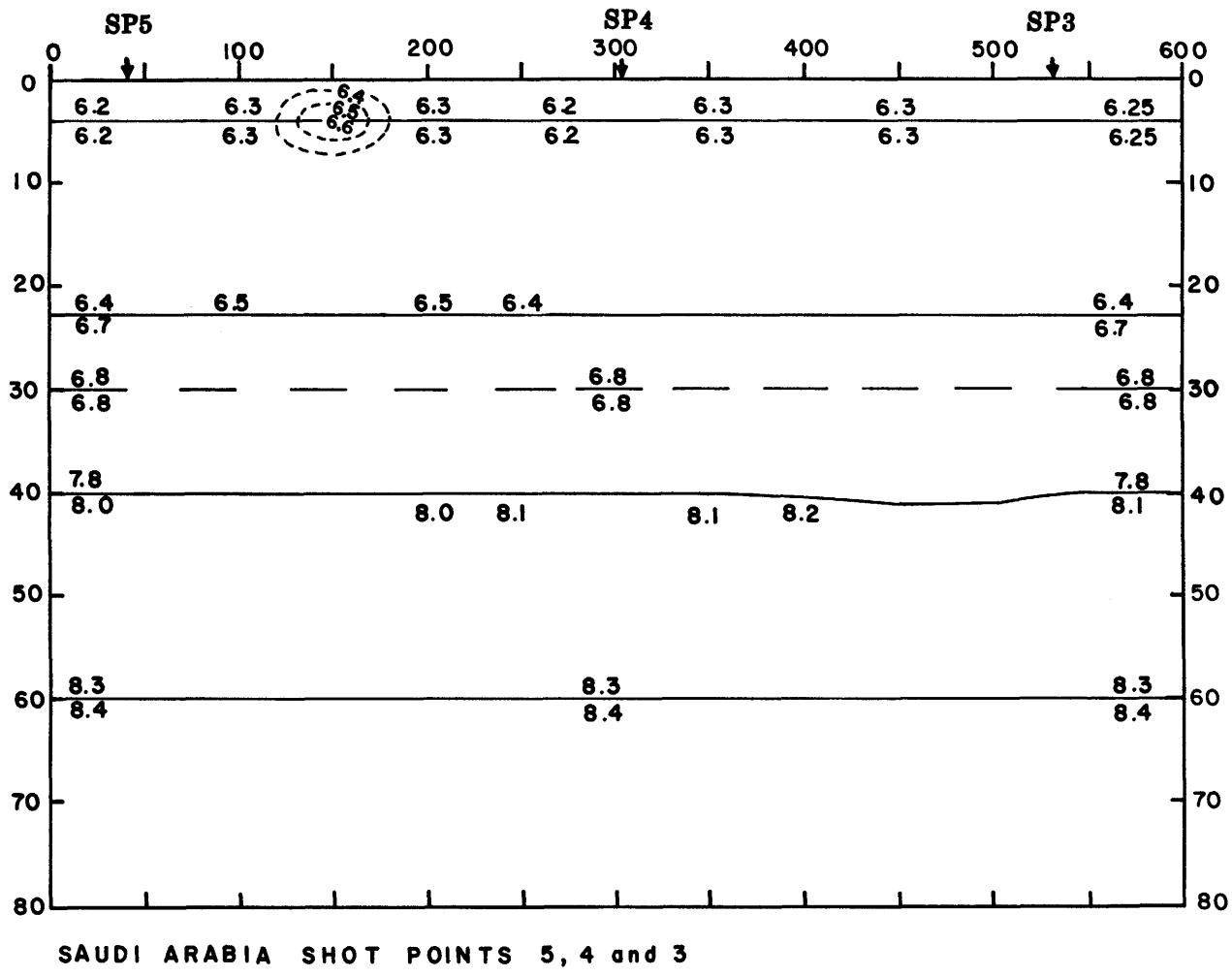

Figure 48. Velocity-depth structure beneath shotpoints 5, 4, and 3.

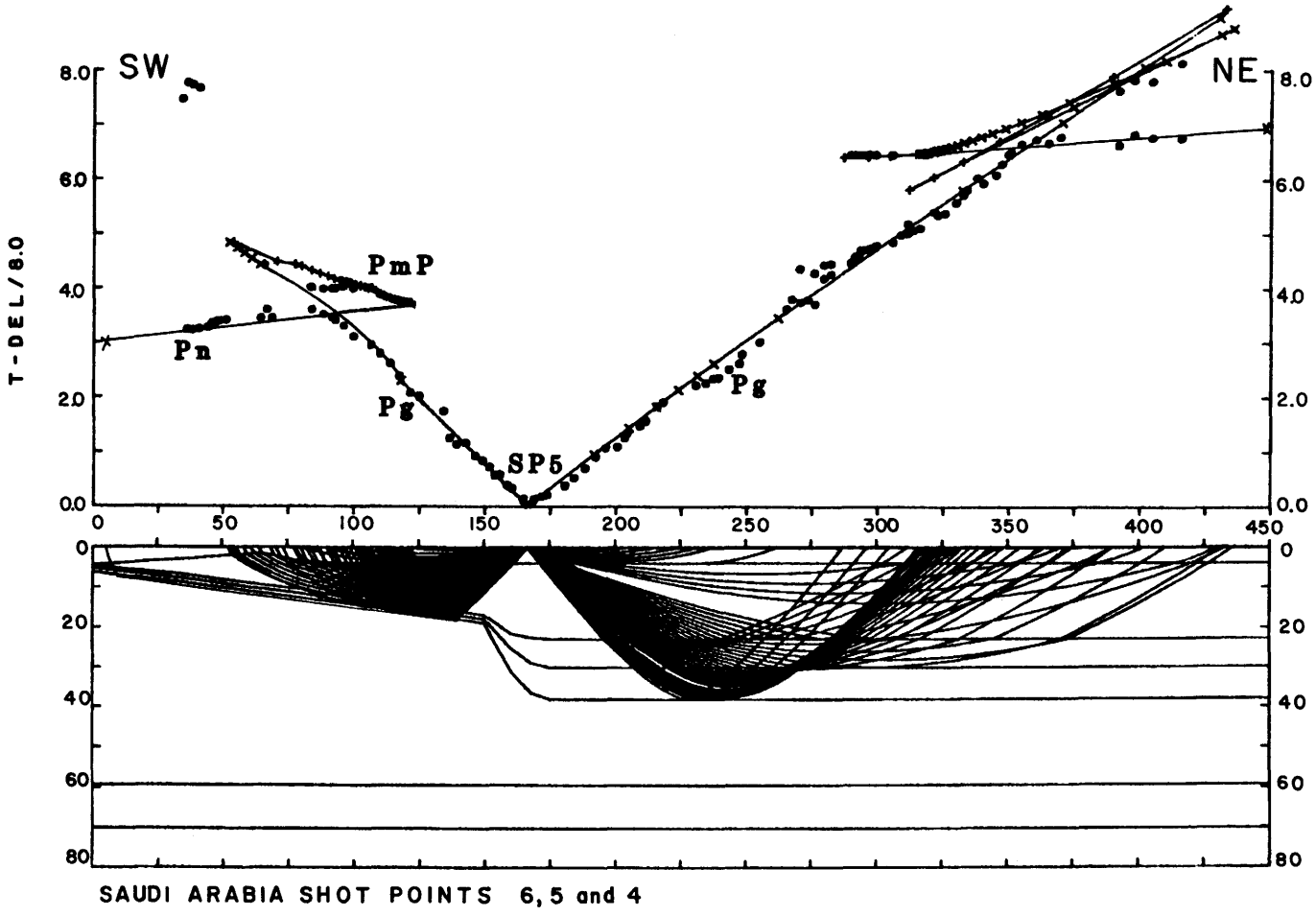

Figure 49. Two-dimensional ray trace diagram for the data from shotpoint 5.

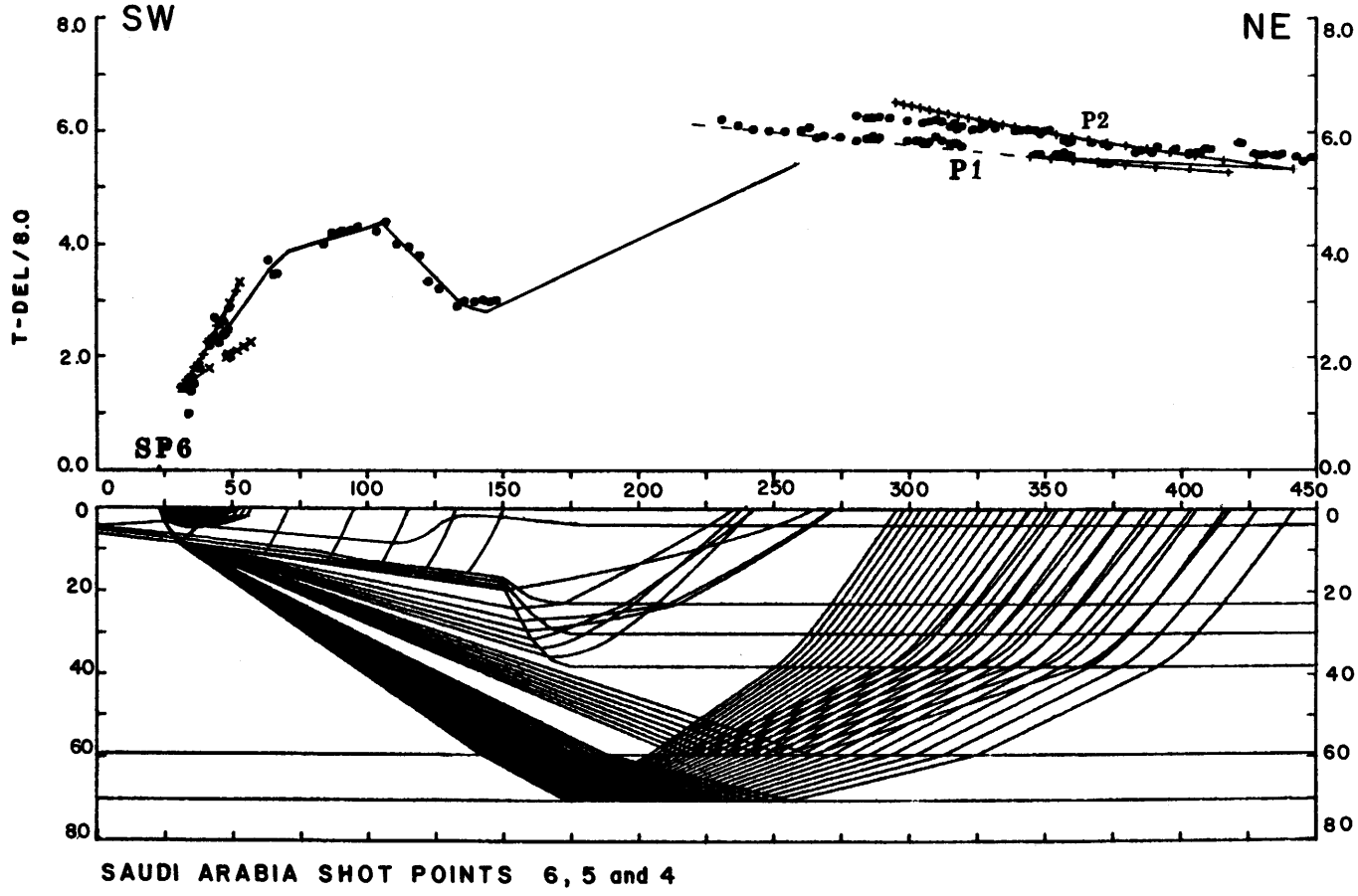

Figure 50. Two-dimensional ray trace diagram for the data from shotpoint 6 NE.

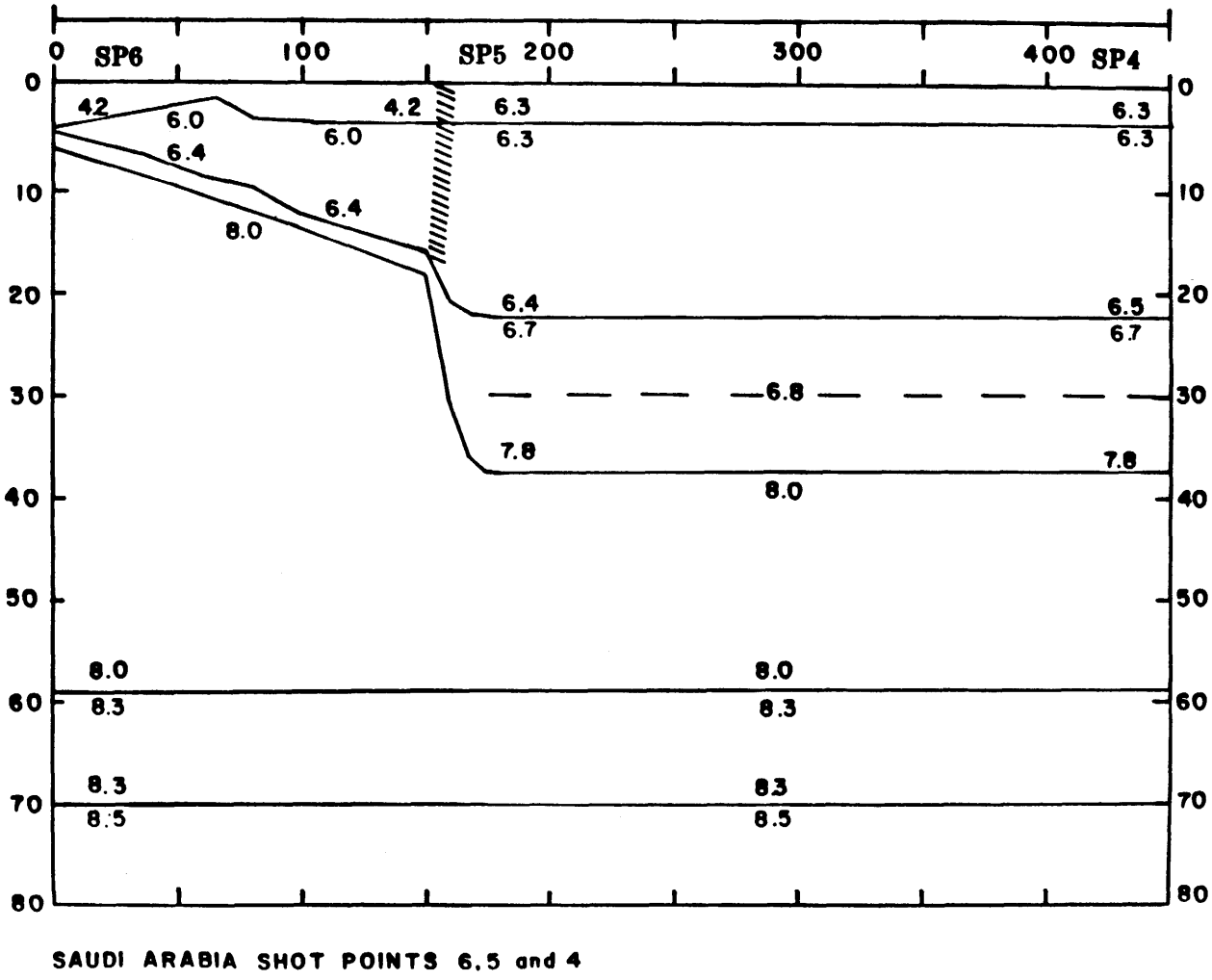

SAUDI ARABIA SHOT POINTS 6, 5 and 4

Figure 51. Velocity-depth structure beneath shotpoints 6, 5, and 4.

EXPLANATION OF RUSSIAN MODELS: SAUDI ARABIAN SEISMIC REFRACTION PROFILE

By N. I. Pavlenkova and I. P. Kosminskaya

USSR Academy of Sciences
Institute of the Physics of the Earth
Moscow, USSR

Three models were presented at the CCSS meeting, one by Krilov, Michenkin, Mishenkina, and Solovjeva (the Novosibirsk group), a second by Yurov, and the third by Pavlenkova.

1. The Novosibirsk group used the so-called time-field method which employs for depth calculation the times at equal distances for all shotpoint data. It was thereby possible to determine more accurately the relative depths of velocity isolines or boundaries. Their results were represented by a set of points derived from refractions and reflections and by a set of isolines connecting these points. The model also shows average velocities from reflections and boundary velocities from refractions. They derived the uplift of the M-discontinuity beneath the Red Sea but they have not tested the model using traveltime calculations.

2. Yurov employed one-dimensional models for all shotpoints. He used a formula for depth calculation from refractions and reflections which takes into account a multi-layered structure of the medium. Then all models were improved using an iteration process--calculation of traveltimes for velocity curves. The resultant models are shown in the cross section (shown in fig. 86) as a set of one-dimensional models (velocity-depth curves).

3. Pavlenkova solved a two-dimensional problem using the intercept time method for the initial model construction and then the ray-tracing method for improving the model. At the second stage of the interpretation a disagreement between the observed and calculated traveltimes was revealed for shotpoint 6. The model gave good agreement for the upper part of the crust and for the basement structure, but at distances of 120 km the calculated traveltimes show large, nearly constant delay (see fig. 52). An uplift of the M-discontinuity beneath the Red Sea and velocities beneath the M-discontinuity exceeding 8.0 km/s were obtained for the model.

The observed traveltimes have a peculiarity for shotpoint 6. At distances of 120 km the apparent velocities decrease and correlation of the first arrivals becomes difficult. At distances of about 180 km a new version of seismic energy comes to the surface. Calculations show that the simple model with uplifted mantle-velocity rocks in the Red Sea area cannot explain the observed pattern. A zone of decreasing velocity is needed to match the time delay and amplitude changes. An agreement is possible using the model with a low-velocity zone beneath the uplift, that is, the model with a separate mantle-velocity intrusion beneath the Red Sea. The form of this anomalous body is difficult to determine; the main conclusion from ray tracing is that a zone of decreasing velocity must be beneath this uplift. Considering the uncertainty of other seismic interpretation methods, models that have not been tested by the ray-trace method in two-dimensional versions cannot be considered as possible models.

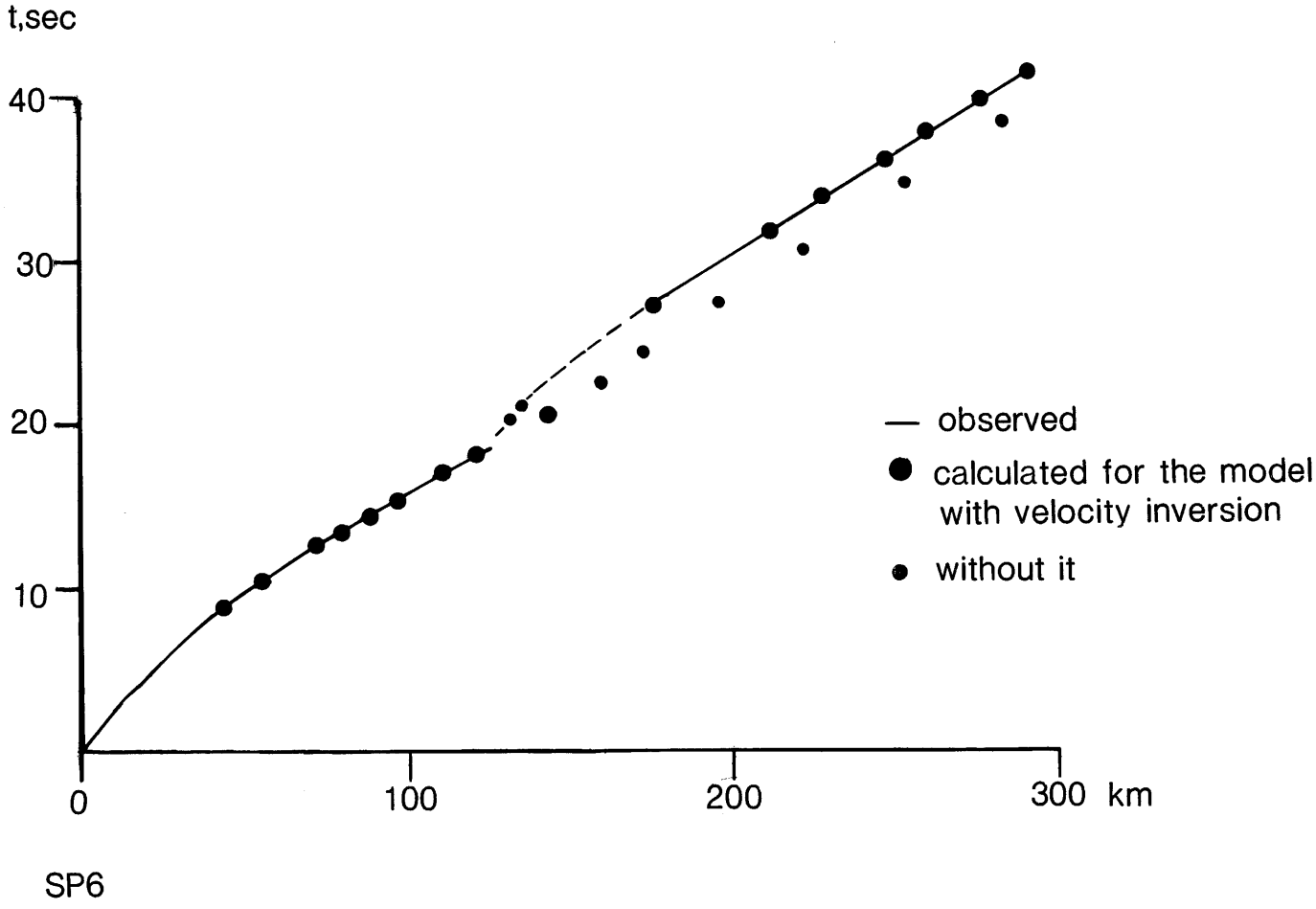

Figure 52. Traveltime curve for shotpoint 6 NE showing delay at 120 km. The observed delay is explained by a velocity inversion in the mantle.

INTERPRETATION OF THE DATA OF THE USGS SEISMIC REFRACTION PROFILE ACROSS THE ARABIAN SHIELD IN WESTERN SAUDI ARABIA

By Claus Prodehl

Geophysikalisches Institut
Universität Karlsruhe
Hertzstrasse 16
D-7500 Karlsruhe-21, West Germany

ABSTRACT

Based on the record sections distributed by the U.S. Geological Survey to the participants of a workshop for individual interpretation prior to the meeting, a preliminary traveltime interpretation assuming horizontally flat layering is presented (Part 1) in the form of velocity-depth functions and a corresponding cross section of the lithosphere to a depth of 60–80 km across the Arabian Shield in western Saudi Arabia.

The crust thickens abruptly from 15 km beneath the Red Sea Rift to about 40 km beneath the Arabian Shield. The upper crust of the western Arabian Shield yields relatively high-velocity material at about 10 km depth underlain by velocity inversions, while the upper crust of the eastern Shield is relatively uniform. The lower crust with a velocity of about 7 km/s is underlain by a transitional crust-mantle boundary. For the lower lithosphere beneath 40 km depth a laterally discontinuous lamellar structure may exist where high-velocity zones are mixed with zones of lower velocities. Beneath the crust-mantle boundary of the Red Sea Rift strong velocity inversions with velocities as low as 6.0 km/s may be encountered between 25 and 44 km depth. This model was prepared before the CCSS workshop.

The model was tested (Part 2) using ray-tracing and amplitude studies and agreed well with observed traveltimes, except between shotpoints 5 and 6. Discussion of the tests reflects the discussions at the CCSS workshop.

PART 1

Introduction

The data of a deep refraction profile recorded by the U.S. Geological Survey in February 1978 along a 1,000-km line across the Arabian Shield in western Saudi Arabia (fig. 53) were interpreted for the workshop meeting organized by the Commission on Controlled Source Seismology (CCSS) held in Park City, Utah, in August 1980. Details of the survey, instrumentation, and data preparation are described by Blank and others (1979). The data were prepared in the form of record sections which were distributed to all participants in January 1980. To guide the individual interpretations of the various participants, two volumes of data (Lamson and Leone, 1980) and a geological map (U.S. Geological Survey and the American-Arabian Oil Company, 1963) were also distributed.

The present report describes a traveltime interpretation based on the record sections distributed. The velocity-depth functions shown in figure 60 (see Part 2) fit the traveltime data shown in figures 54-59 (see Part 2) if one assumes that for the individual profile the hypothesis of homogeneous flat

layering in lateral direction is fulfilled. In future steps of interpretation, amplitude studies will have to be added which may be based on the same restrictions, and the model derived (fig. 60) will have to be checked by ray-tracing methods which allow for lateral variations of depths and velocities.

The record sections distributed are as follows: from shotpoint 1 (Quway'iyah) to the north-northeast up to 85 km and to the south-southwest up to 580 km recording distance (fig. 54), from shotpoint 2 (Sabhah) to the north-northeast up to 220 km and to the south-southwest up to 325 km distance (fig. 55), from shotpoint 3 (Mish'ab) to the north-northeast up to 55 km and to the south-southwest up to 340 km (fig. 56), from shotpoint 4 (Bishah) to the north-northeast up to 285 km and to the south-southwest up to 275 km (fig. 57), from shotpoint 5 (Ad Darb) to the north-northeast up to 250 km and to the south-southwest up to 135 km (fig. 58), and from shotpoint 6 (Farasan) to the north-northeast up to 475 km recording distance (fig. 59). All record sections contain "reduced" traveltimes; the reduction velocity used was 6 km/s.

Correlation and Interpretation of Phases

With the exception of profiles 1 NE, 1 SW, 5 SW, and 6 NE, the data indicate an almost complete absence of sediments, showing negative reduced traveltimes for the distance range of the Pg phase. The corresponding velocities of this phase, including the profiles from shotpoint 1, are relatively high, reaching values between 6.2 and 6.25 km/s from the northeastern shotpoints 1 and 2 and between 6.5 and 6.7 km/s on the profiles on the Arabian Shield from shotpoints 3, 4, and 5 at recording distances between 80 and 150 km. For all this first-arrival data it is characteristic that the energy is suddenly fading out and the first arrivals beyond that distance are delayed considerably with respect to a hypothetical continuation of the Pg traveltime curve.

This traveltime behavior can well be explained by a continuous increase of velocity with depth underlain by a zone of either constant or reduced velocity.

With the exception of the two profiles 5 SW and 6 NE within the Red Sea Rift zone, on all profiles between 120 and 230 km distance a bulk of energy in secondary arrivals is recorded that can be correlated by two traveltime curves to be interpreted as reflections from zones of increased velocity gradient at intermediate crustal depth or at the crust-mantle boundary. On the profiles in the Red Sea Rift such a reflection from the crust-mantle boundary can also be correlated, but at much smaller distances: between 40 and 75 km.

First arrivals in the distance range of 80-170 km on profiles 3 SW, 4 NE, 4 SW, and 5 NE, not interpreted here, could be explained by assuming the existence of high-velocity lamellae within the upper crustal low-velocity zone.

The velocity of the first arrivals beyond 180 km from shotpoints 1, 2, and 3, beyond 200 km from shotpoint 5, and to the northeast from shotpoint 5 generally exceeds 8 km/s. On the profiles 5 SW and 6 NE, a velocity greater than 8 km/s is already reached at 90 km distance.

On a few profiles reaching distances beyond 250-300 km, namely profiles 6 NE, 3 SW, 2 SW, and 1 SW, the Pn velocity seems to be replaced by other phases with increased velocities. On profiles 2 SW and 4 SW a smooth but clear increase in velocity is observed at about 250 km distance, on the other profiles such an increase is accompanied by an offset of the corresponding traveltime curve with respect to the Pn phase. Two branches following each

other with a more or less strong delay can be correlated to the largest recorded distances of 475 and 580 km, respectively.

In this traveltime interpretation these phases are discussed tentatively as originating from various layers within the lower lithosphere separated from each other by more or less strong velocity inversions (fig. 60).

In this context one particular phase recorded on profile 5 SW between 115 and 132 km with a reduced traveltime of about +2.0–2.5 s has to be considered.

This phase has been interpreted tentatively as a reflection from a very thick and pronounced low-velocity zone between 25 and 44 km depth beneath the Red Sea Rift with an average velocity of 6 km/s embedded between mantle material with velocities of 8.5–8.6 km/s (see fig. 60). Indications for such a phase at similar distance and reduced-time ranges can also be seen on the record section of the reversing profile 6 NE. We cannot ignore, however, the fact that these high-amplitude phases on profiles 5 SW and 6 NE may be multiple reflections from the crust-mantle boundary.

A Model of the Lithosphere

The model of the lithosphere based on traveltime interpretation assuming flat layering for each individual profile is shown in figure 60 and table 1. The lower part of figure 60 shows the velocity-depth functions, and the upper part shows the corresponding cross section.

Based on the earlier of the two reflections recorded between 120 and 230 km distance, as described above, a zone with a strong velocity gradient at a depth range varying between 20 and 35 km defines an intermediate crustal boundary separating upper and lower crustal material. While the upper crust seems to be represented by a uniform velocity of about 6.2–6.25 km/s beneath the Arabian Shield (profiles 1 SW, 2 NE, 2 SW), it shows velocities increasing from 6.0 to 6.5–6.7 km/s underlain by a zone where the velocity is reduced reaching values which may be as low as 6 km/s. In the lower crust the velocity is constant or slightly increasing. Its base is formed by a zone of strong velocity gradient where the velocity increases from about 7 to about 8 km/s over a depth range of several kilometers at about 40 km depth.

As the changes in crustal structure along the line within the Arabian Shield and adjacent Arabian Platform occur gradually over large distances, the velocity-depth functions derived on the basis of homogeneous flat layering may characterize the true situation rather accurately. However, this is not the case for the transition between the Arabian Shield and the Red Sea Rift, where crustal thickness changes from 40 to 15 km over a horizontal distance of a few tens of kilometers. The crustal models shown for profiles 5 SW and 6 NE can therefore be regarded only as a rough approximation. The data, on the other hand, are rather scarce and are biased by the fact that the profile crosses this complicated transition zone, so it seems doubtful that a detailed structure can be deduced at all with the data. The velocity-depth functions indicate the complications in structure. On both profiles of the reversed line between shotpoints 5 and 6 the velocity increases gradually from 6 to 8.2 km/s. However, the mantle velocity of 8.2 km/s is reached at different depths: at 25 km from shotpoint 5 and at 15 km from shotpoint 6.

As already discussed, only a few data allow a penetration into the uppermost mantle as is shown tentatively by the dashed lines of the velocity-depth functions of some of the profiles. With the exception of profiles 2 SW and 4 SW, a lamellar structure is indicated to exist beneath the crust-mantle

boundary where relatively thin zones of a few kilometers in thickness of higher and lower velocities follow each other with increasing depth.

Beneath the Moho of the Red Sea Rift, the data indicate a strong velocity inversion where the velocity may be as low as 6 km/s. In general a triangular form for zones of reduced velocity has been assumed. If one assumes a similar triangular shape of the low-velocity zone of profile 5 SW between 25 and 44 km depth, a low value of 4 km/s has to be introduced in order to fit the observed data. The lower part of the velocity-depth function of profile 6 NE below 40 km depth has to be attributed to the mantle of the Arabian Shield, as this zone is deduced from observations beyond 300 km distance and is directly comparable with the corresponding depth range deduced for profiles 3 SW and 1 SW.

Such a lamellar structure does not seem to exist along the entire line, as the continuous increase of velocity with depth on profiles 2 SW and 4 SW indicates. However, these observations allow only a penetration of the upper 10-20 km of the uppermost mantle beneath the Moho.

The cross section shown in the upper part of figure 60 summarizes the results. Here, lines of equal velocity are shown. The crust-mantle transition zone (rapid increase of velocity from about 7.4 to 8.2 km/s) dips rapidly from 15 km beneath the Red Sea Rift toward the east to about 40 km, reaching a maximum depth beneath the Hijaz-Asir province and rising slightly as the line enters the Najd province. The crust of the Hijaz-Asir province where the elevation of the Arabian Shield is highest is also characterized by rather high velocities at about 10 km depth and underlying velocity inversions, indicated by dots in the cross section. No crustal velocity inversion is found for the easternmost province of the Shield, the Shammar province. For the adjacent Arabian Platform to the east only limited information on the upper crust is available indicating a velocity inversion at 10-12 km depth.

The structure of the uppermost mantle is only sketched in the cross section. The strong velocity inversion indicated by profile 5 SW is concentrated on the Red Sea Rift. Beneath the Arabian Shield a laterally discontinuous lamellar structure is indicated beneath Ad Darb, east of Bishah and east of Sabhah below 40 km depth.

PART 2

The model presented in figure 60 and table 1 was tested by ray-tracing and amplitude studies. Much of the following discussion is based on the discussions held during the CCSS workshop of 10-16 August 1980 in Park City, Utah.

This section contains table 1 and the main parts of revised record sections of the data (figs. 54-59), including synthetic sections for selected examples.

Test of the Crustal Model by Ray Tracing

Only a first test of the western part of the model shown in figure 60 between shotpoints 4 and 5 as well as 5 and 6 was carried out. Although the model is based on a traveltime interpretation assuming horizontally flat layering, the agreement between traveltimes calculated for the real model of figure 60 and observed traveltimes is $\pm$ 0.05-0.2 s for the part between shotpoints 4 and 5. Such a deviation can easily be adjusted by slight modifications of the original model. Figure 61 shows the results of a test

run for rays traversing the model of figure 60 from shotpoint 4 toward the southwest. The crosses indicate the traveltimes for the corresponding rays. For comparison some selected arrivals of the main reflected phases are shown as triangles.

As was expected for the transition zone from the Arabian Shield to the Red Sea between shotpoints 5 and 6 the difference between observed and calculated traveltimes is up to 0.5 s; thus, the model for profiles 5 SW and 6 NE shown in table 1 can only be regarded as a rough first approximation.

Amplitude Studies

Based on the first test of ray tracing for the part between shotpoints 4 and 5 it can be concluded that the assumption of horizontally flat layering is not seriously violated for the area of the Arabian Shield between shotpoints 1 and 5. Therefore, synthetic seismograms using the reflectivity method of Fuchs and Müller (1971) and Kind (1976) were calculated for selected velocity-depth functions of table 1. As the data presented in the record sections are normalized, only the relative amplitudes can be considered.

As shown by Červený and others (1977, p. 190-193), for example, the largest amplitudes of the reflected phase do not coincide with the critical distance but are usually observed at slightly greater distance from the shotpoint. For crustal investigations, the difference between critical distance and distance of the theoretically largest amplitudes is of the order of 10 to several tens of kilometers. The greater the frequency of a phase the closer lies its amplitude maximum to the critical point. For a 40-km-thick crust and a main frequency of 8 Hz, Červený and others (1977) computed a difference of about 15 km and for 4 Hz a difference of about 25 km.

During the traveltime analysis we attempted to obtain traveltime curves for the reflected phases such that the critical distance was located within visible energy of the corresponding phase. Normally, in observed data the position of maximum energy cannot be located exactly, but can be assumed to be somewhere within the 20-30-km-wide band of well-recorded energy of the reflected phases near the critical point.

As the computed synthetic record sections (figs. 54-58) show, the agreement with the observed record sections is rather good. For example, on the synthetic sections computed for profiles 2 SW (fig. 55) and 3 SW (fig. 56) the main frequency used is about 5 Hz. The corresponding maximum amplitude is located at about 10-15 km greater distance than the critical point. According to Červený and others (1977), this difference should decrease for the observed data, which show a main frequency between 10 and 15 Hz. For comparison, a test study was made computing synthetic seismograms with different main frequencies (3.4, 6.7, and 13.4 Hz) for a crustal model typical for the area of investigation (fig. 62). It can well be seen that, for all frequencies, there is not only well-recorded energy at the critical point (about 15 km away from the amplitude maximum), but also energy still visible at a distance range of 10-20 km left of the critical point, a fact that is in good agreement with the traveltime curves correlated for the real data (figs. 54-59).

REFERENCES

Blank, H. R., Healy, J. H., Roller, J. C., Lamson, R. J., Fischer, F., McClearn, R., and Allen, S., 1979, Seismic refraction profile, Kingdom of Saudi Arabia--field operations, instrumentation and initial results: U.S. Geological Survey Saudi Arabian Mission Project Report 259, 49 p.

Červený, V., Molotkov, I. A., and Pšenčik, I., 1977, Ray method in seismology: University Karlova, Prague, 214 p.

Fuchs, K. and Müller, G., 1971, Computation of synthetic seismograms with the reflectivity method and comparison with observations: Geophysical Journal of the Royal Astronomical Society, v. 23, p. 417-433.

Kind, R., 1976, Computation of reflection coefficients for layered media: Journal of Geophysics, v. 42, p. 191-200.

Lamson, R. J. and Leone, L. E., 1980, Saudi Arabia seismic refraction profile data set, volumes 1 and 2: U.S. Geological Survey Open-File Report, Miscellaneous Document 17.

U.S. Geological Survey and Arabian-American Oil Company, 1963, Geologic map of the Arabian Peninsula: U.S. Geological Survey Miscellaneous Geologic Investigations Map I-270A, scale 1:2,000,000.

TABLE 1. Velocity-depth functions shown in figure 60

Profile 1 NE

depth (km)	velocity (km/s)
0.0	2.50
0.8	5.90
6.0	6.22
6.5	6.40
8.0	6.54
10.0	6.00
12.0	6.84

Profile 1 SW

depth (km)	velocity (km/s)
0.0	2.50
0.9	6.10
1.5	6.20
5.0	6.23
13.0	6.24
24.4	6.60
26.0	6.80
40.0	7.10
42.0	8.20
51.3	8.40
53.3	8.00
55.3	8.41
56.3	8.50
60.3	8.00
65.4	8.60
69.4	8.30
74.5	8.70
83.0	8.00
94.0	8.80

Profile 2 NE

depth (km)	velocity (km/s)
0.0	6.00
2.4	6.20
4.0	6.25
5.0	6.26
18.0	6.20
19.0	6.60
32.0	6.59
38.5	7.60
39.5	7.61

Profile 2 SW

depth (km)	velocity (km/s)
0.0	5.80
2.3	6.10
7.5	6.20
9.0	6.21
17.0	6.20
20.0	6.60
29.5	6.59
43.0	8.20
45.4	8.22
54.0	8.60
55.5	8.61

Profile 3 NE

depth (km)	velocity (km/s)
0.0	5.90
1.5	6.00
4.0	6.10

Profile 3 SW

depth (km)	velocity (km/s)
0.0	6.0
6.4	6.50
7.0	6.51
20.0	6.20
23.4	6.80
37.4	7.24
40.7	8.20
42.0	8.21
46.0	8.00
51.0	8.30
54.0	8.00
59.0	8.50

TABLE 1 (continued)

Profile 4 NE

depth (km)	velocity (km/s)
0.0	5.90
1.5	6.10
1.7	6.20
9.0	6.70
26.0	6.20
33.5	7.20
40.0	7.28
45.0	8.00
46.4	8.01

Profile 4 SW

depth (km)	velocity (km/s)
0.0	6.00
16.0	6.70
22.0	6.20
30.0	7.00
39.0	7.10
45.0	8.00
65.0	8.90
66.0	8.91

Profile 5 NE

depth (km)	velocity (km/s)
0.0	5.30
0.2	6.10
5.0	6.60
5.5	6.61
12.0	6.20
17.3	6.70
23.0	6.00
26.5	7.10
37.9	7.15
38.8	8.00
40.2	8.01

Profile 5 SW

depth (km)	velocity (km/s)
0.0	5.30
0.5	5.85
5.0	5.90
5.5	6.04
6.0	6.05
24.0	8.33
24.3	8.34
25.0	6.00
28.0	8.35
28.1	8.50
29.0	6.00
44.0	6.01
45.0	8.60

Profile 6 NE

depth (km)	velocity (km/s)
0.0	4.10
6.5	5.50
6.6	6.00
7.0	6.10
14.0	7.00
14.5	8.40
16.0	8.41
23.0	6.00
42.6	8.50
44.0	8.51
49.0	7.70
54.0	8.55
56.0	8.56
61.0	8.10
66.0	8.60
68.0	8.61

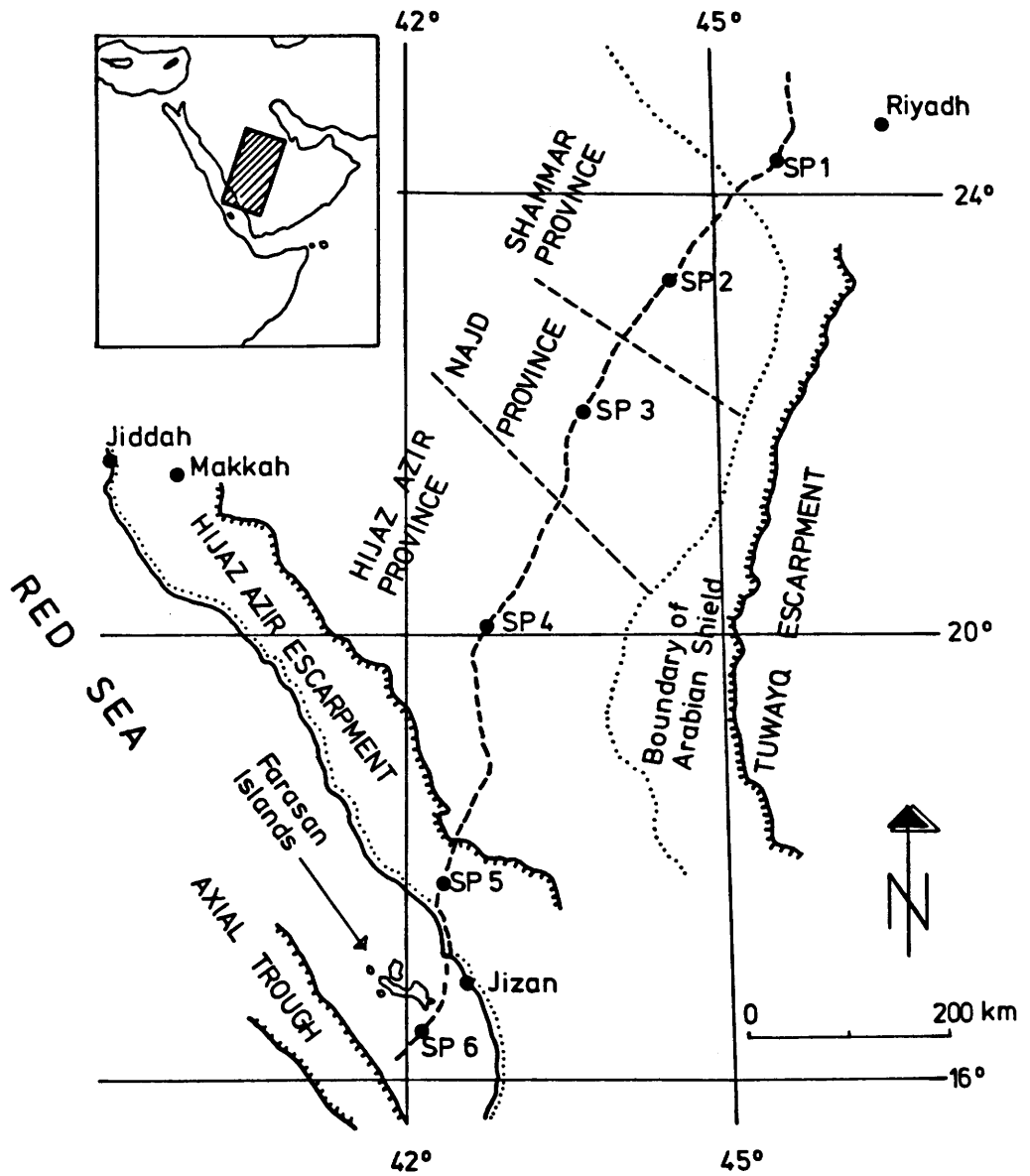

Figure 53. Location map of the seismic refraction profile (dashed line) across western Saudi Arabia and the southeastern Red Sea, showing the shotpoints (SP).

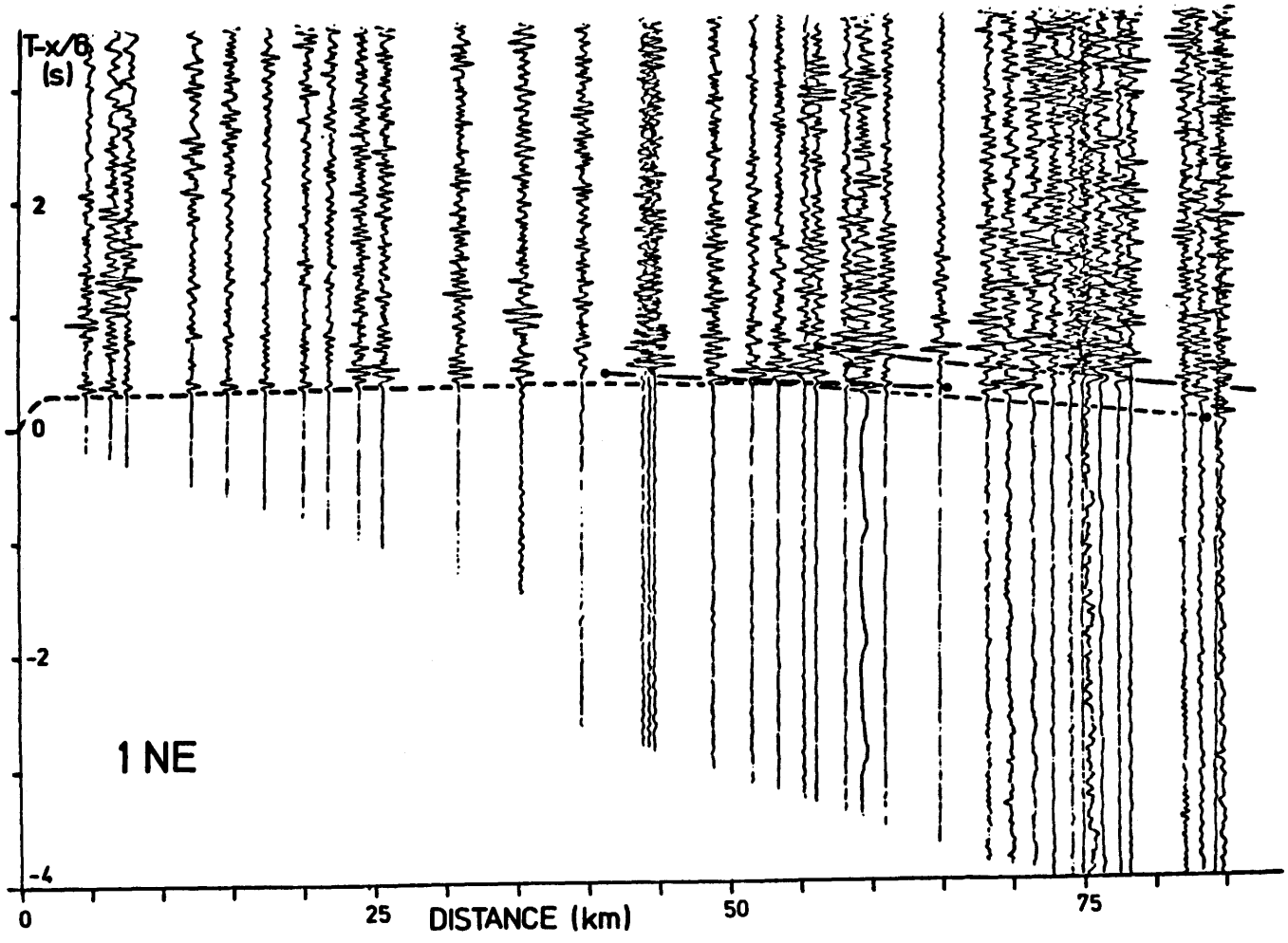

Figure 54a. Record section of profile 1 NE.

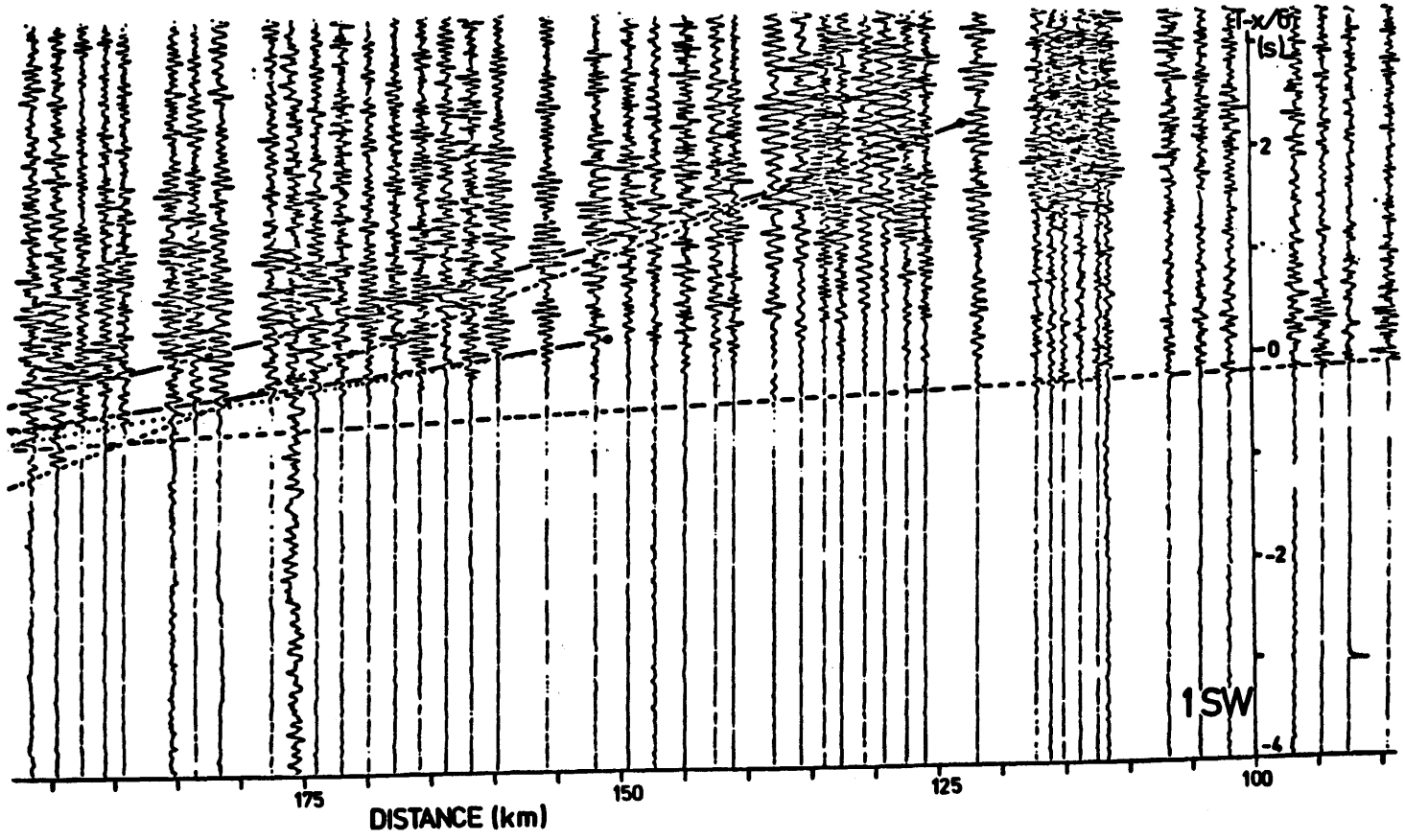

Figure 54b. Record section of profile 1 SW (v_r = 6 km/s).

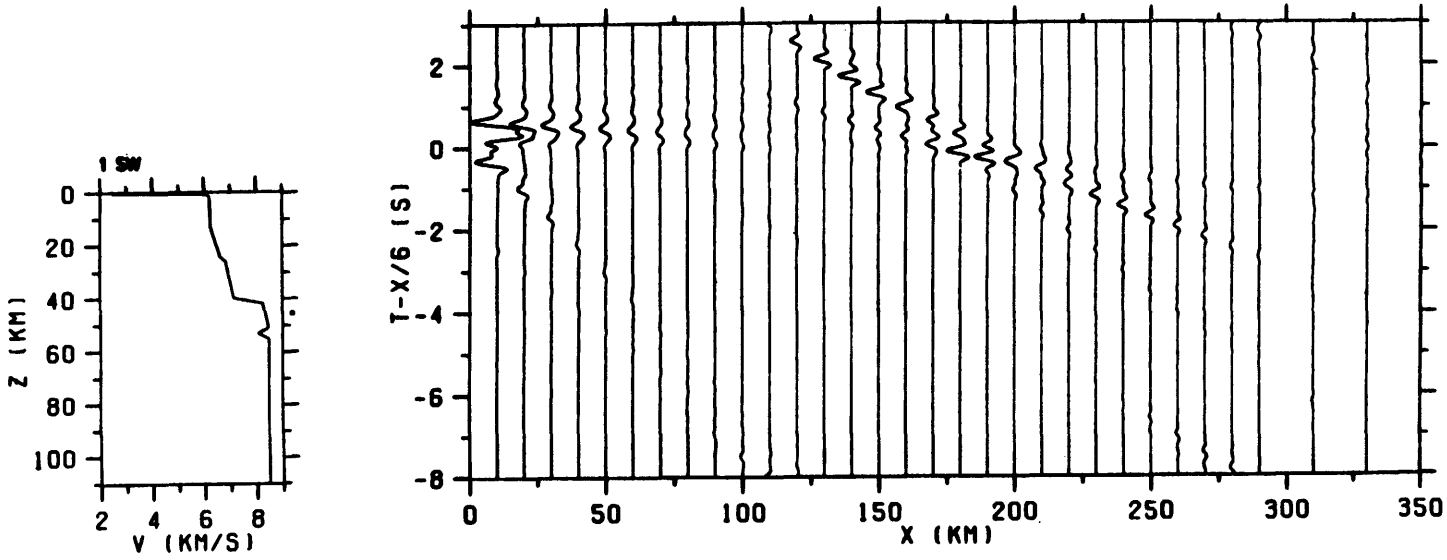

Figure 54c. Synthetic record section for profile 1 SW.

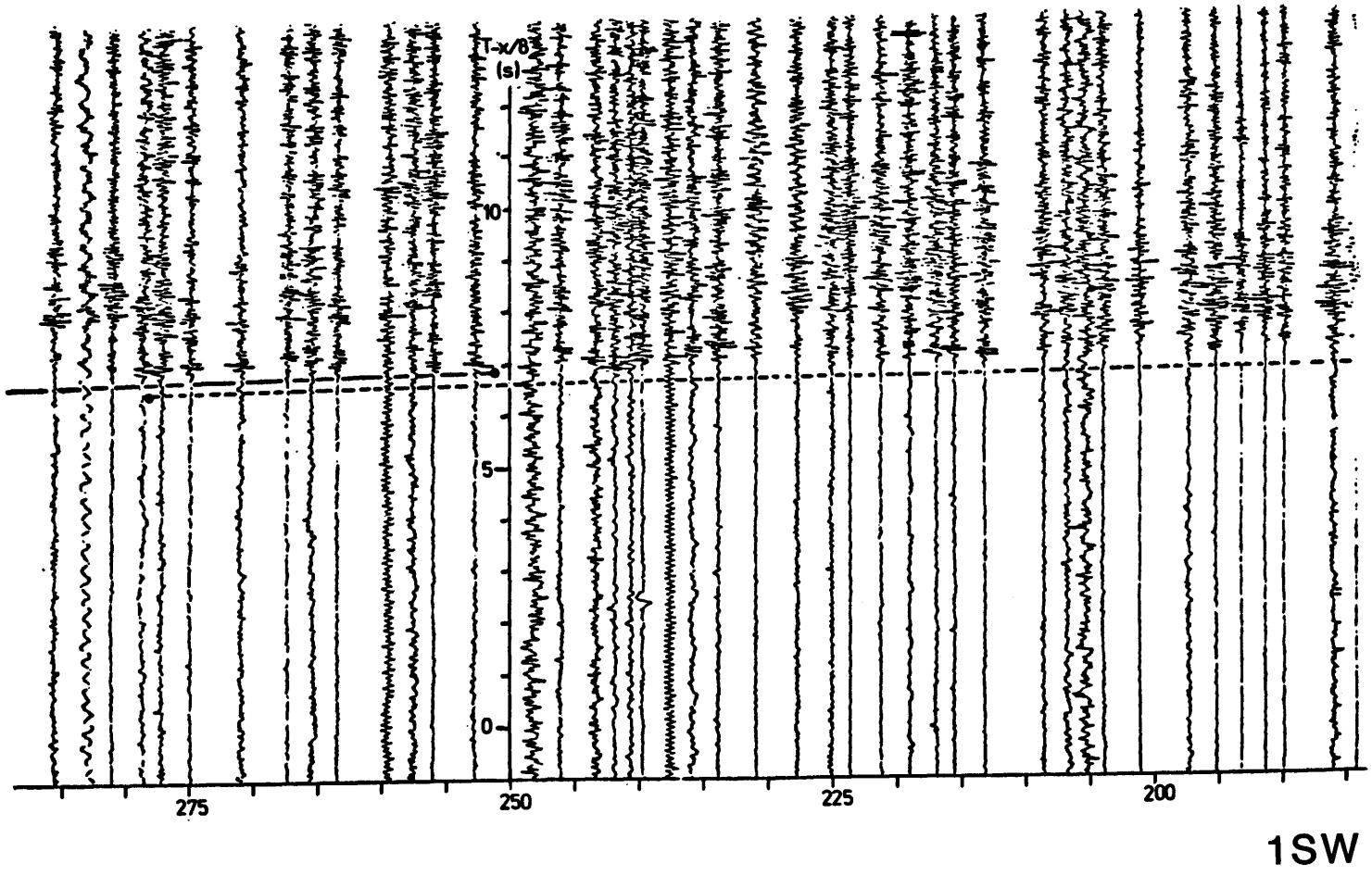

Figure 54d.1. Record section of profile 1 SW (v_r = 8 km/s), part 1 of 3.

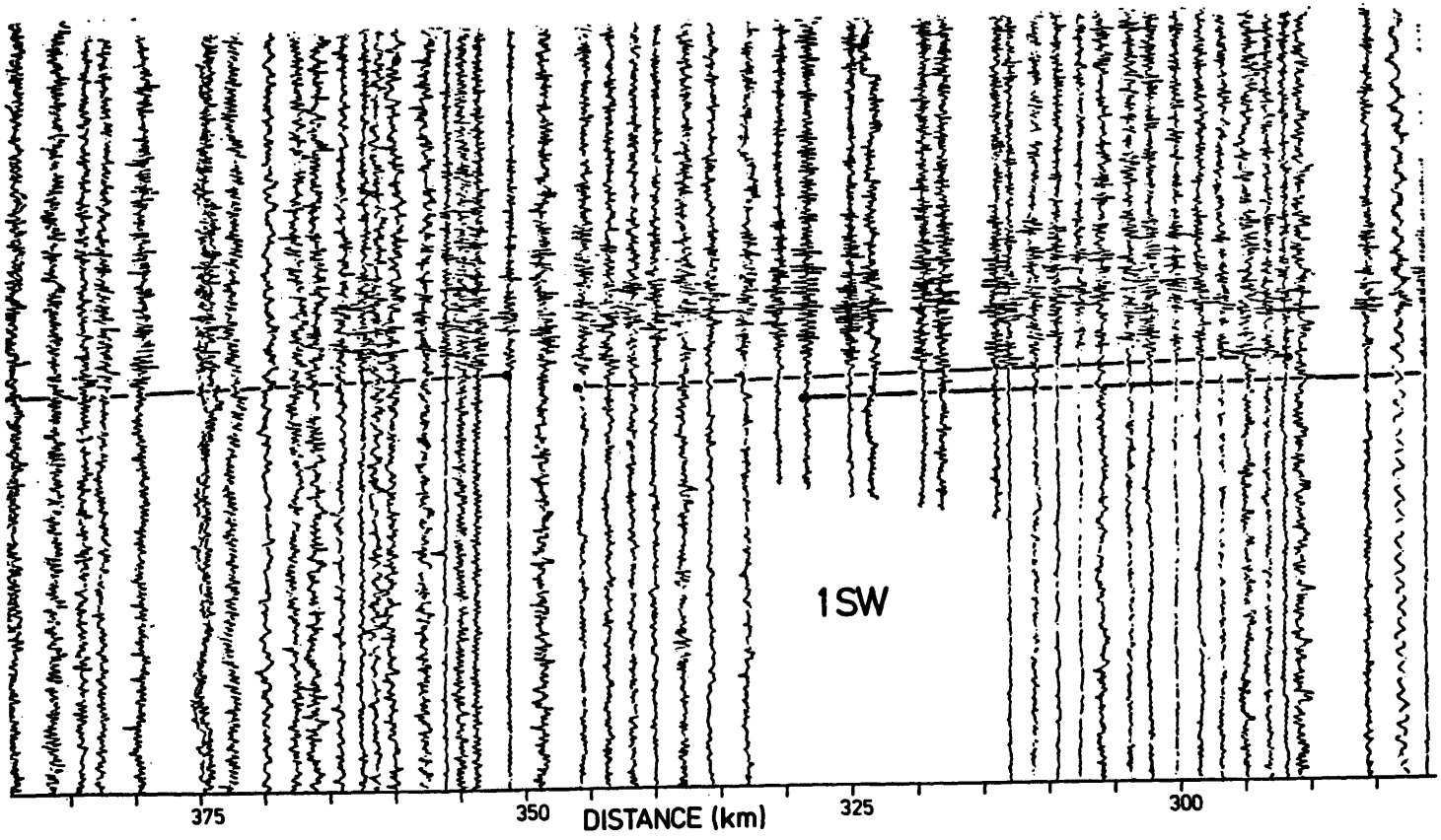

Figure 54d.2. Record section of profile 1 SW (v_r = 8 km/s), part 2 of 3.

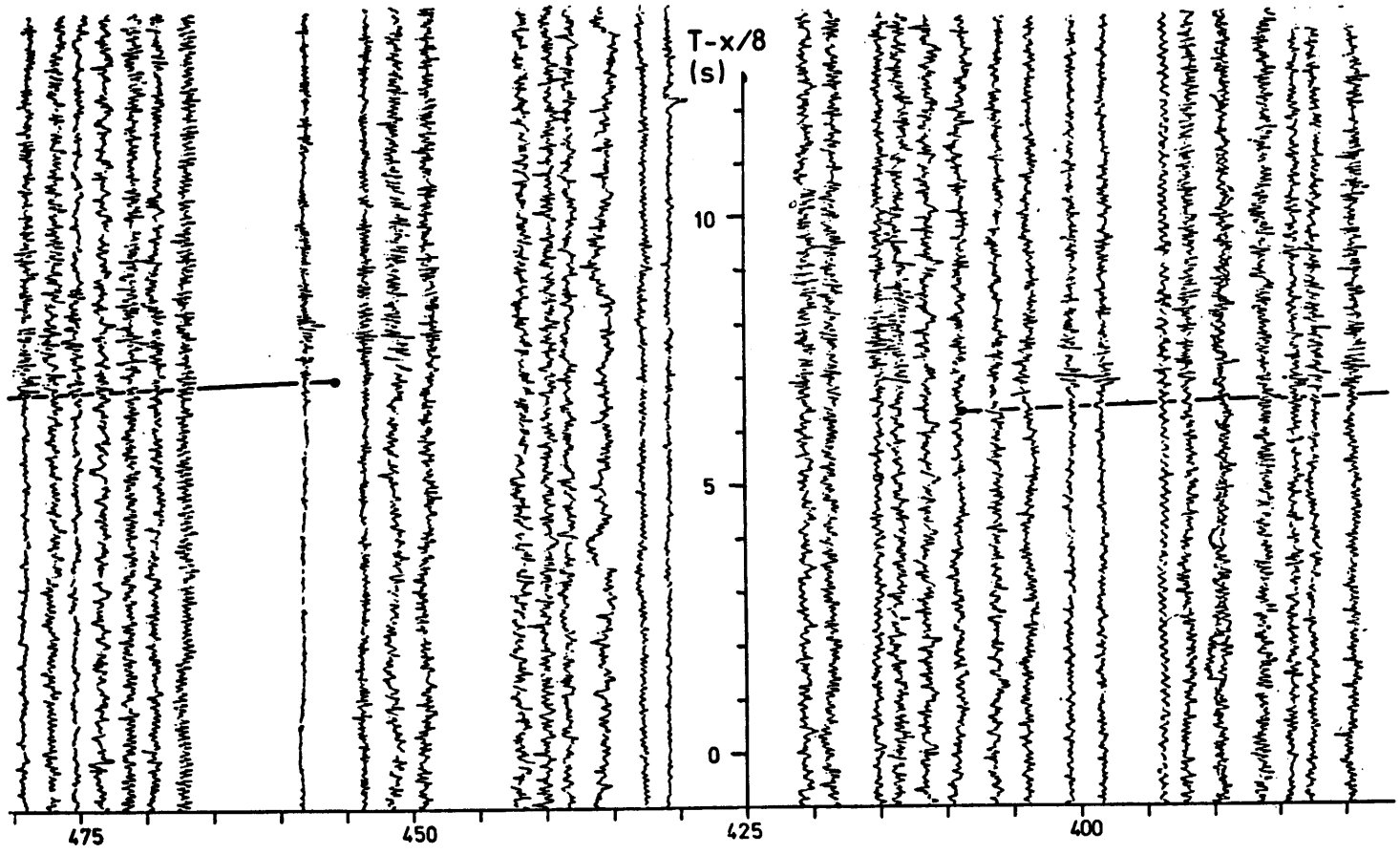

Figure 54d.3. Record section of profile 1 SW (v_r = 8 km/s), part 3 of 3.

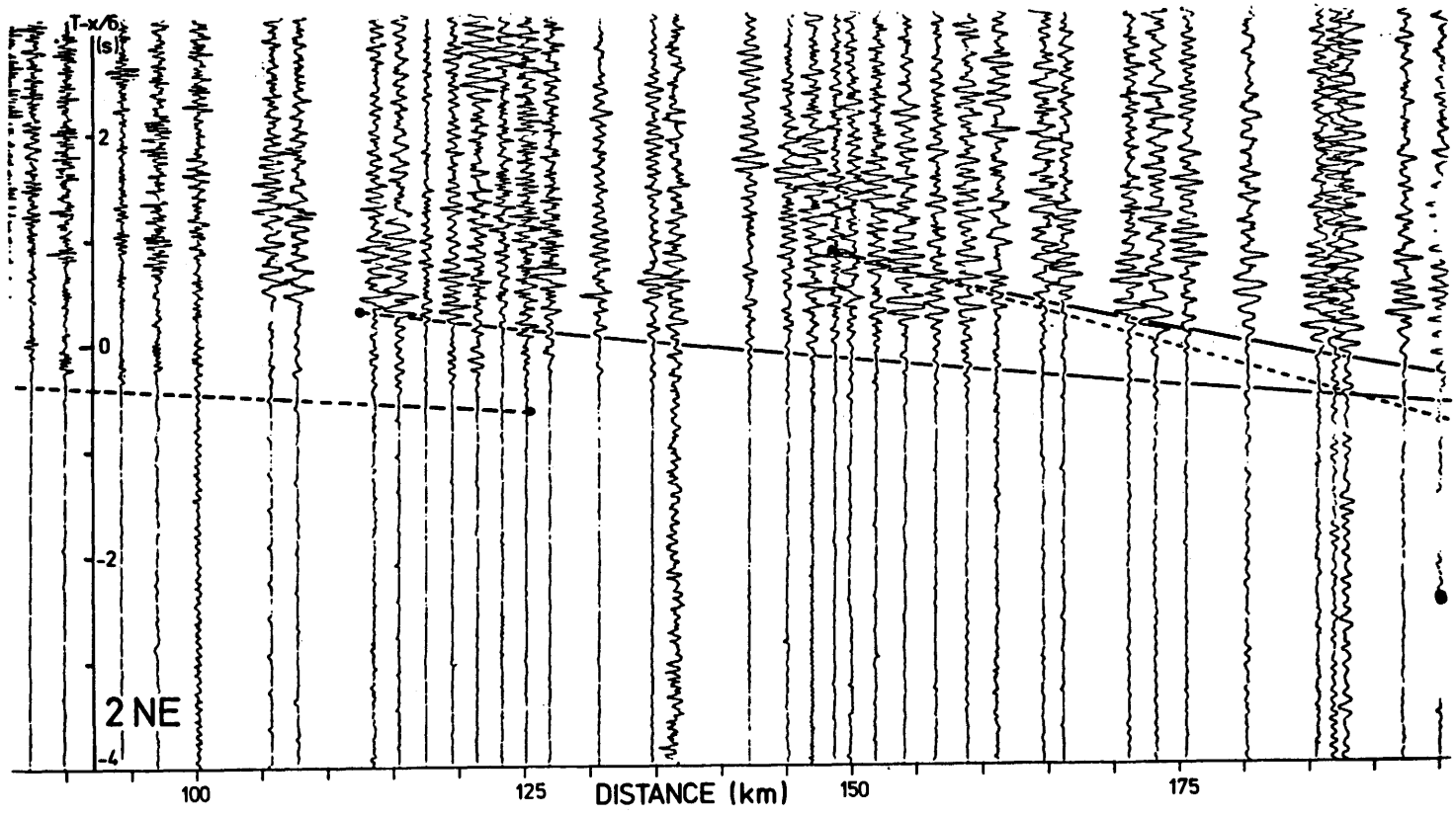

Figure 55a. Record section of profile 2 NE.

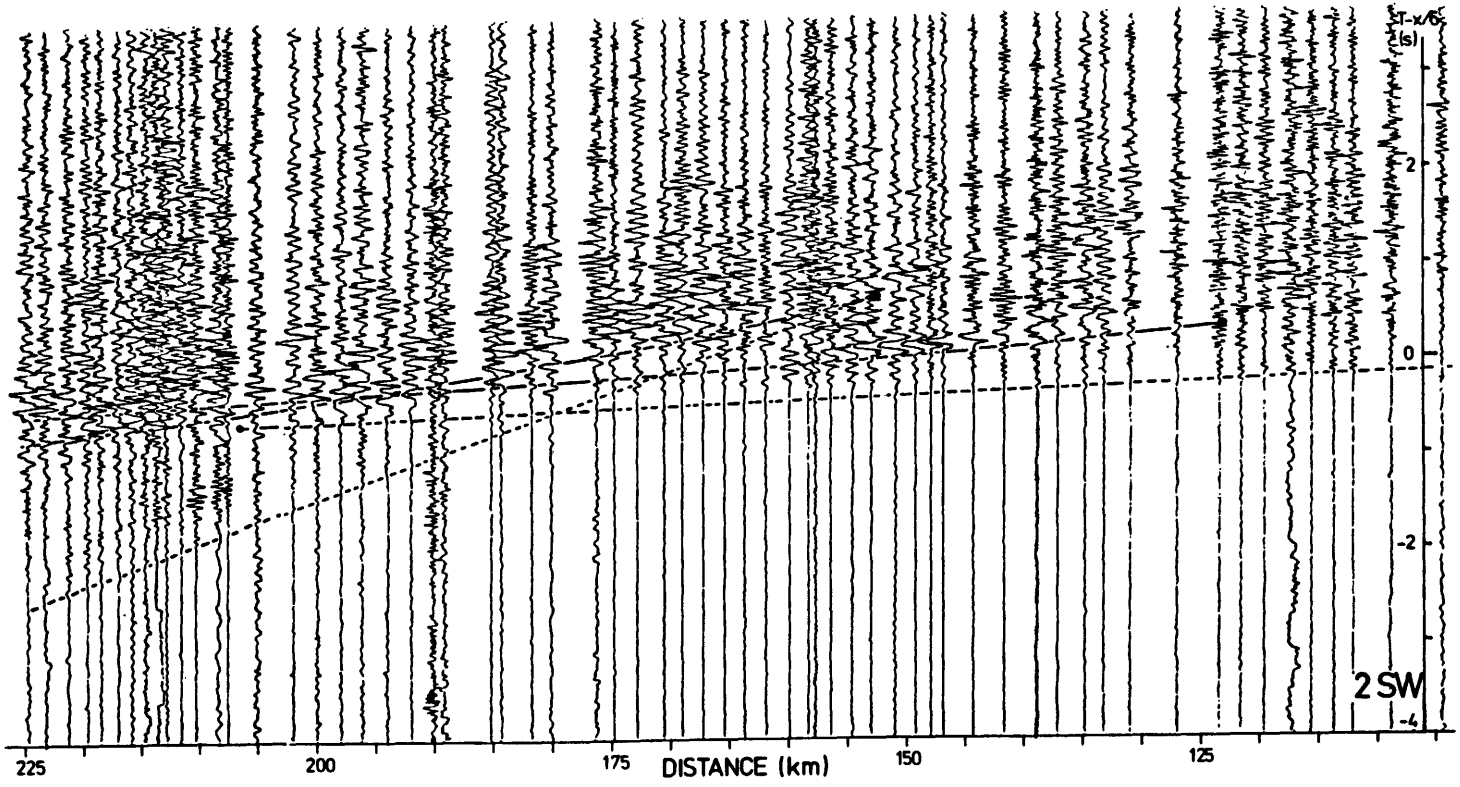

Figure 55b. Record section of profile 2 SW.

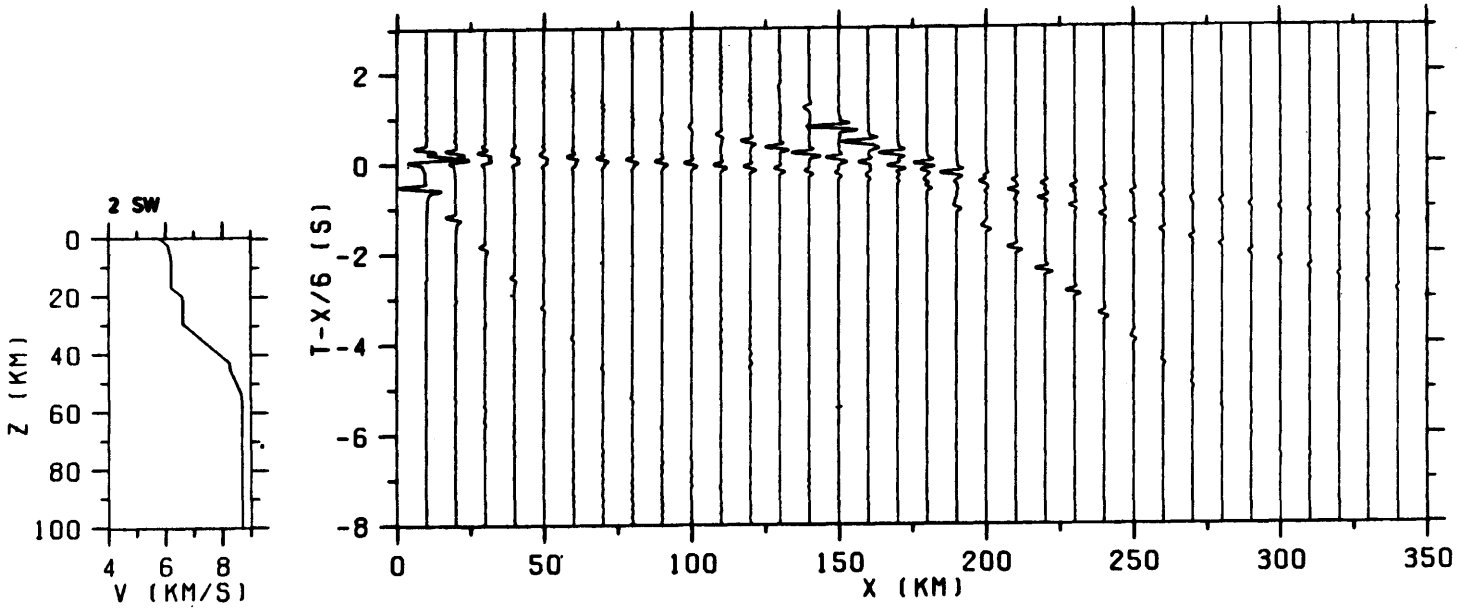

Figure 55c. Synthetic record section for profile 2 SW.

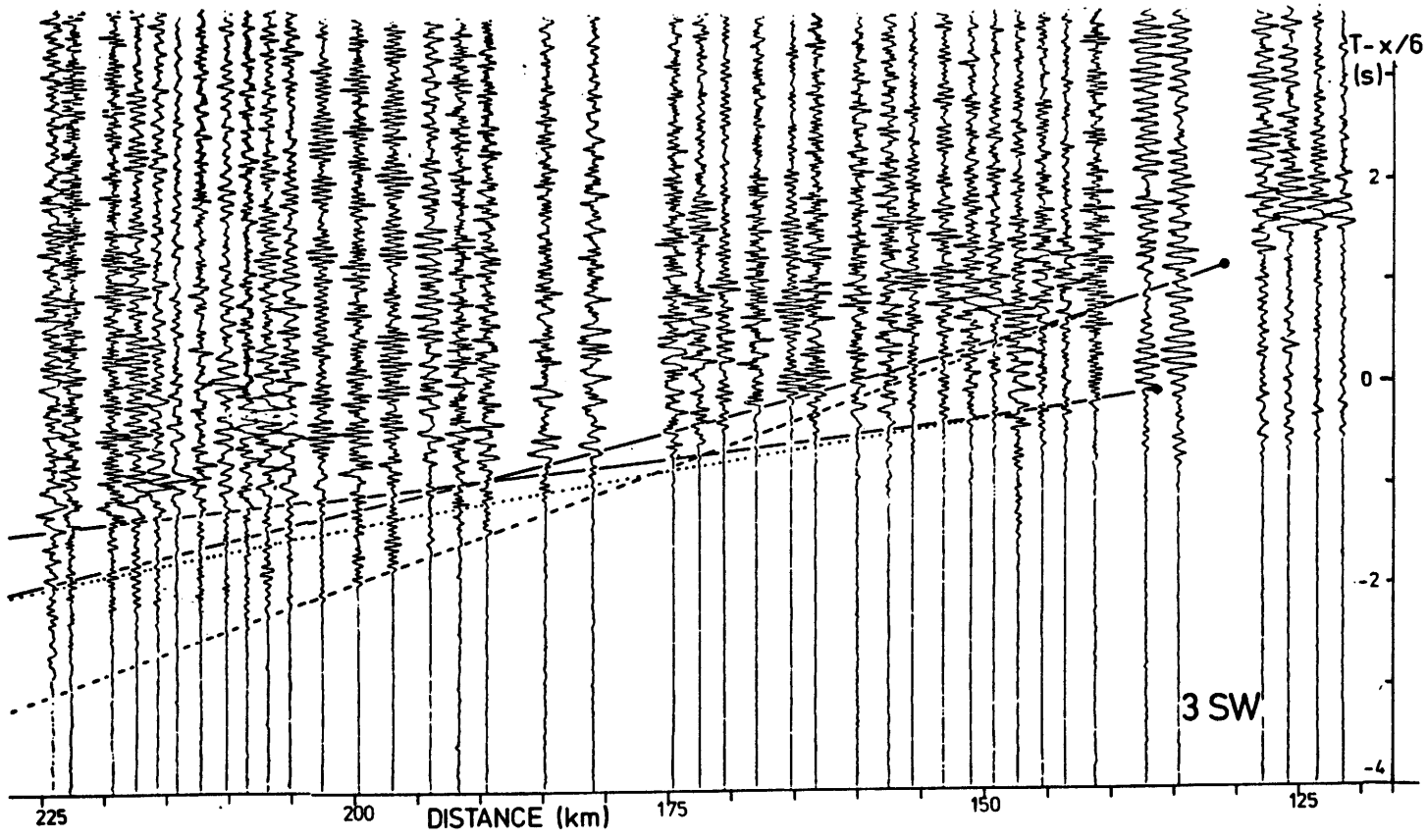

Figure 56a. Record section of profile 3 SW.

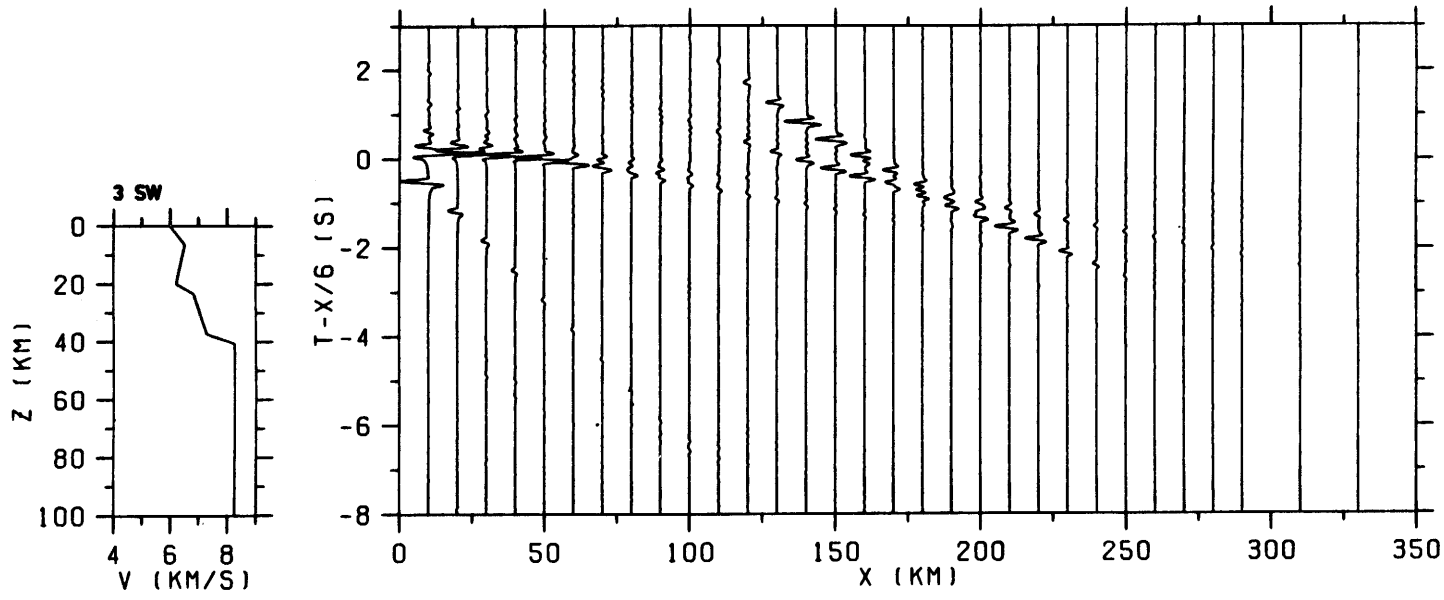

Figure 56b. Synthetic record section for profile 3 SW.

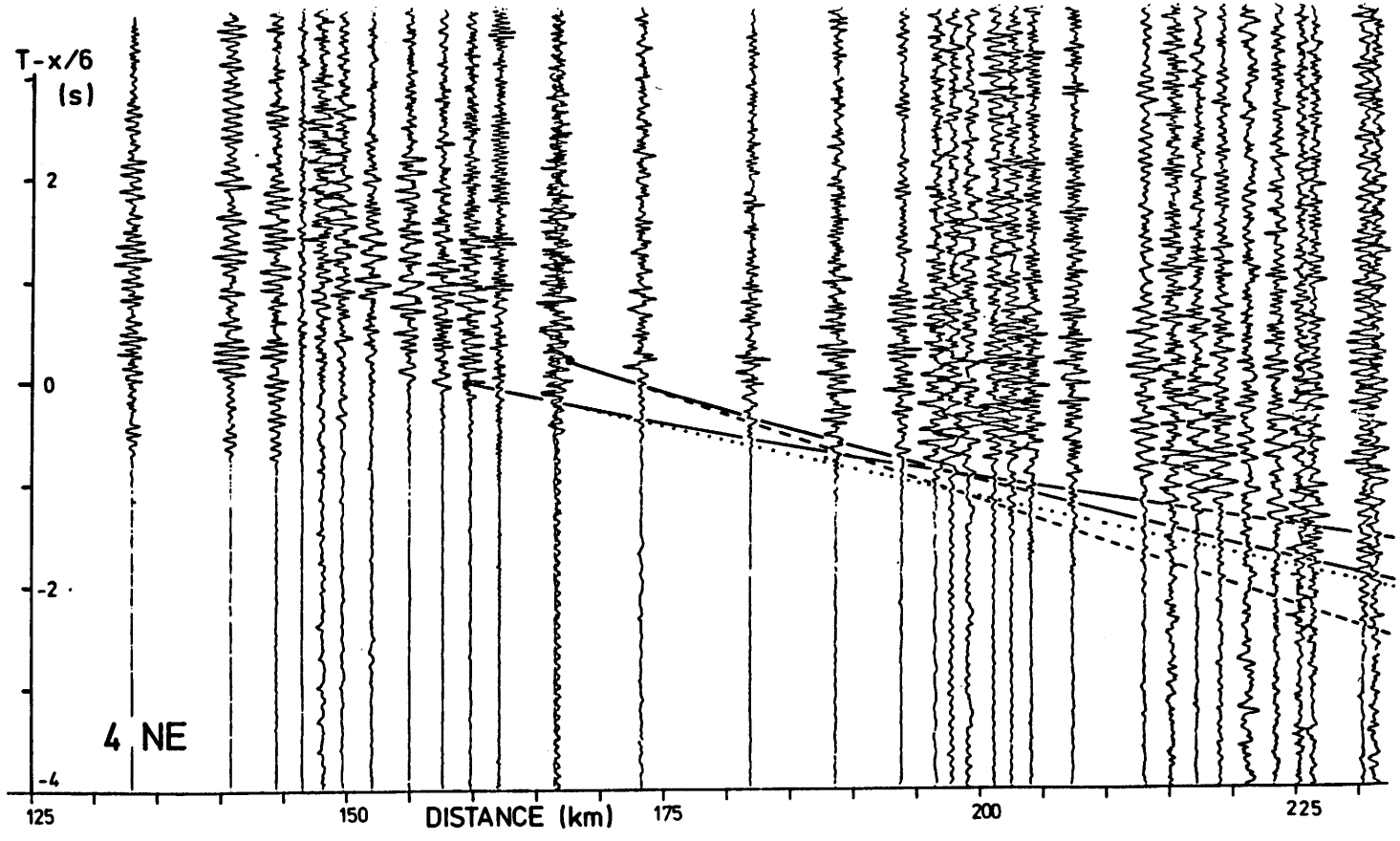

Figure 57a. Record section of profile 4 NE.

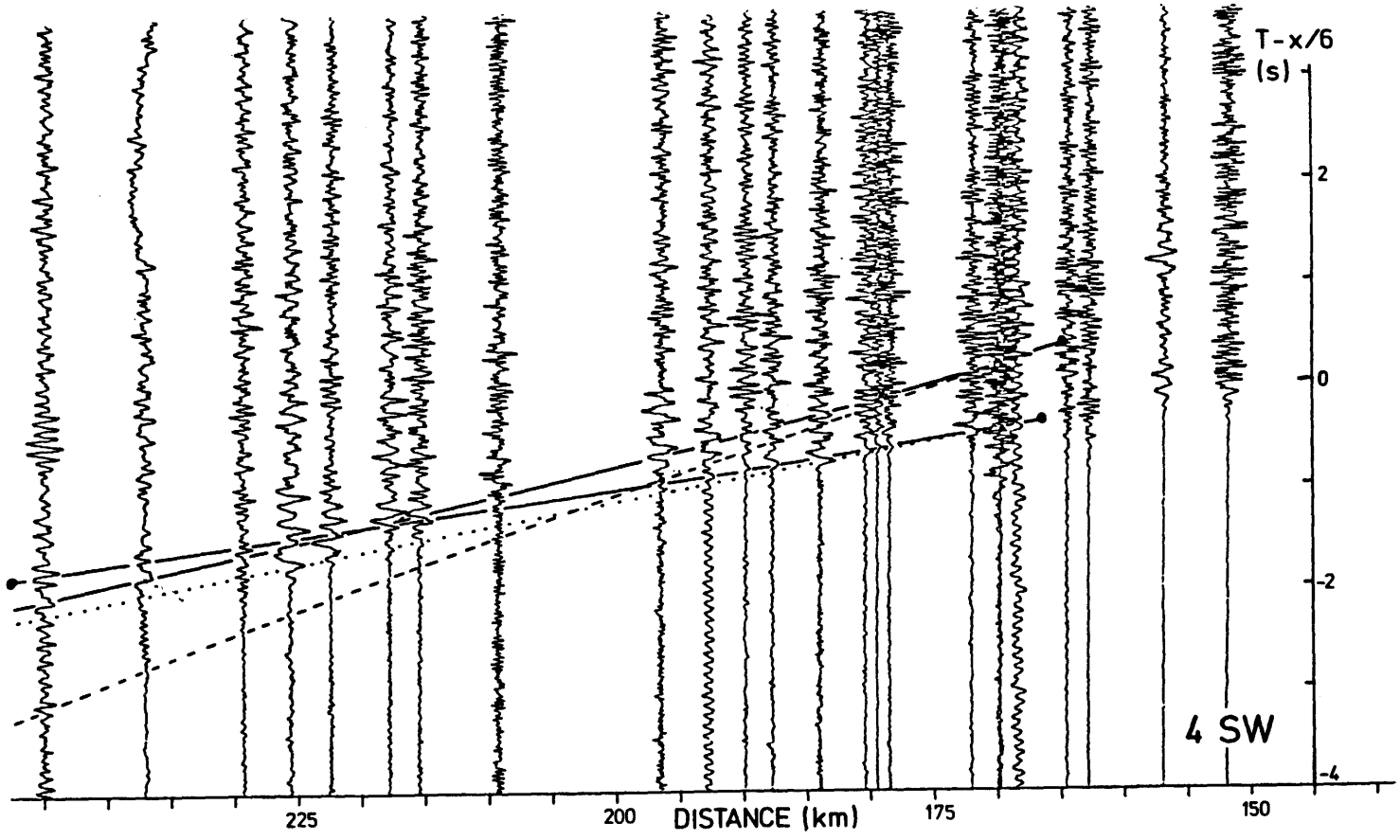

Figure 57b. Record section of profile 4 SW.

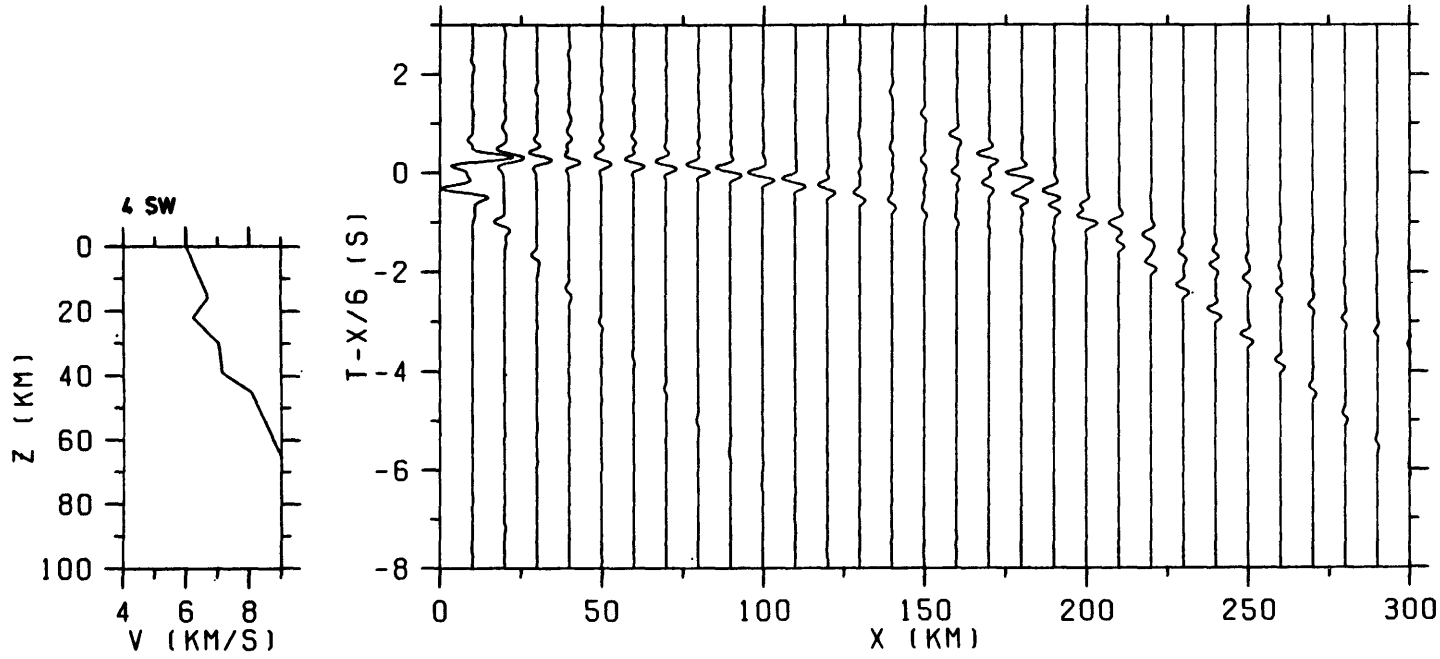

Figure 57c. Synthetic record section for profile 4 SW.

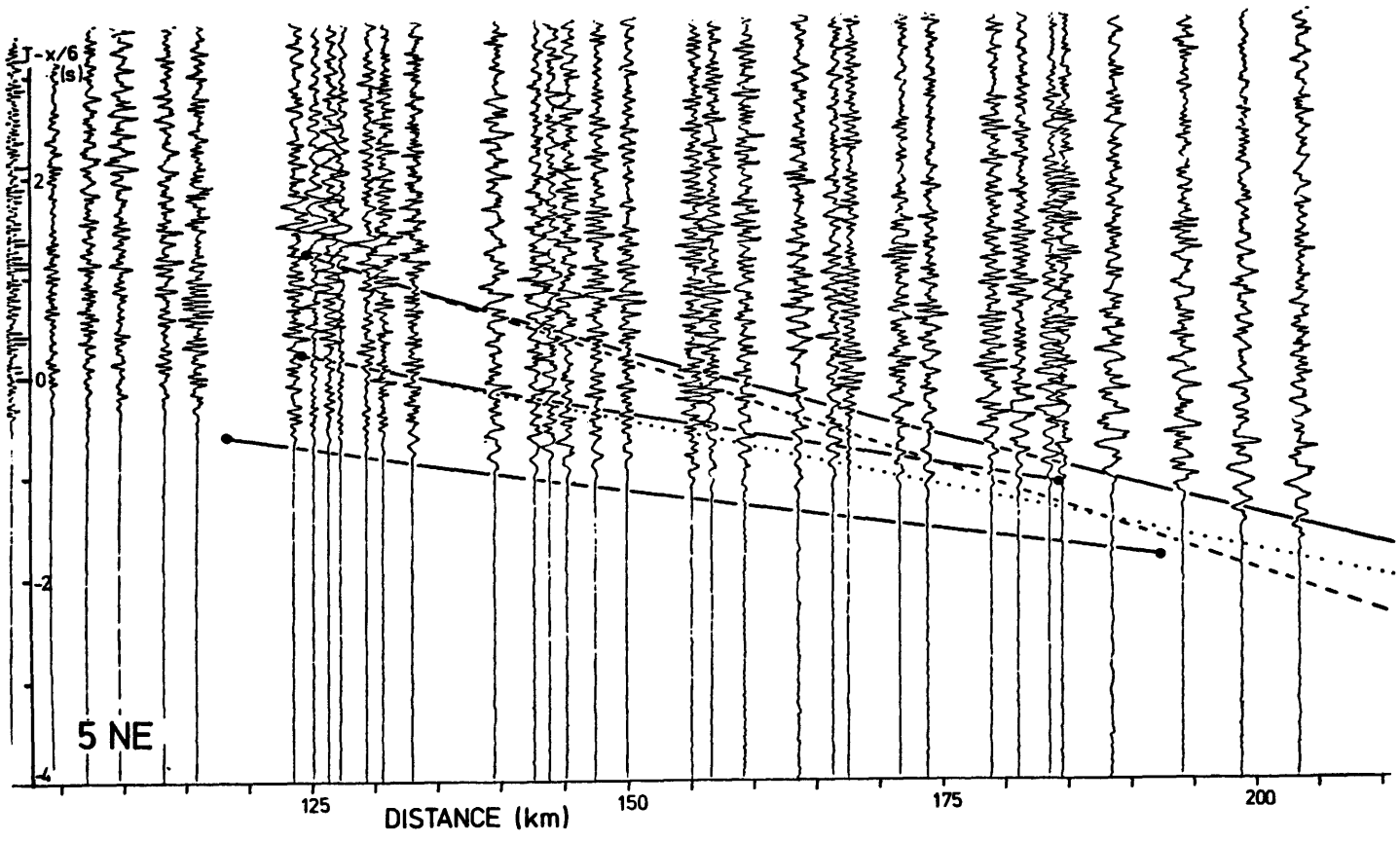

Figure 58a. Record section of profile 5 NE.

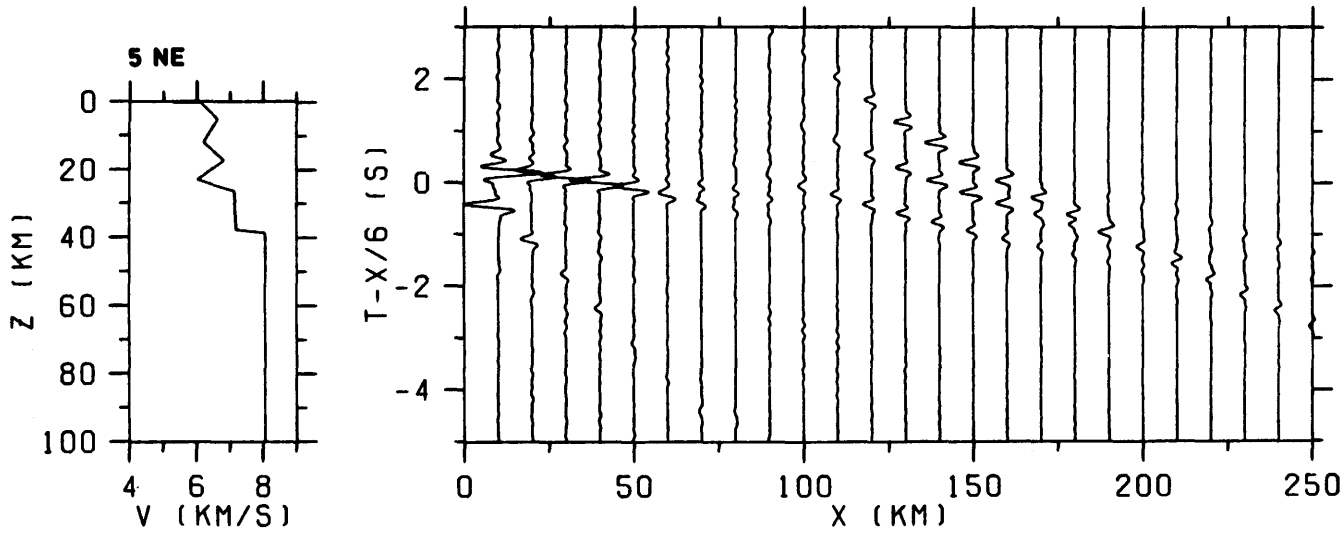

Figure 58b. Synthetic record section for profile 5 NE.

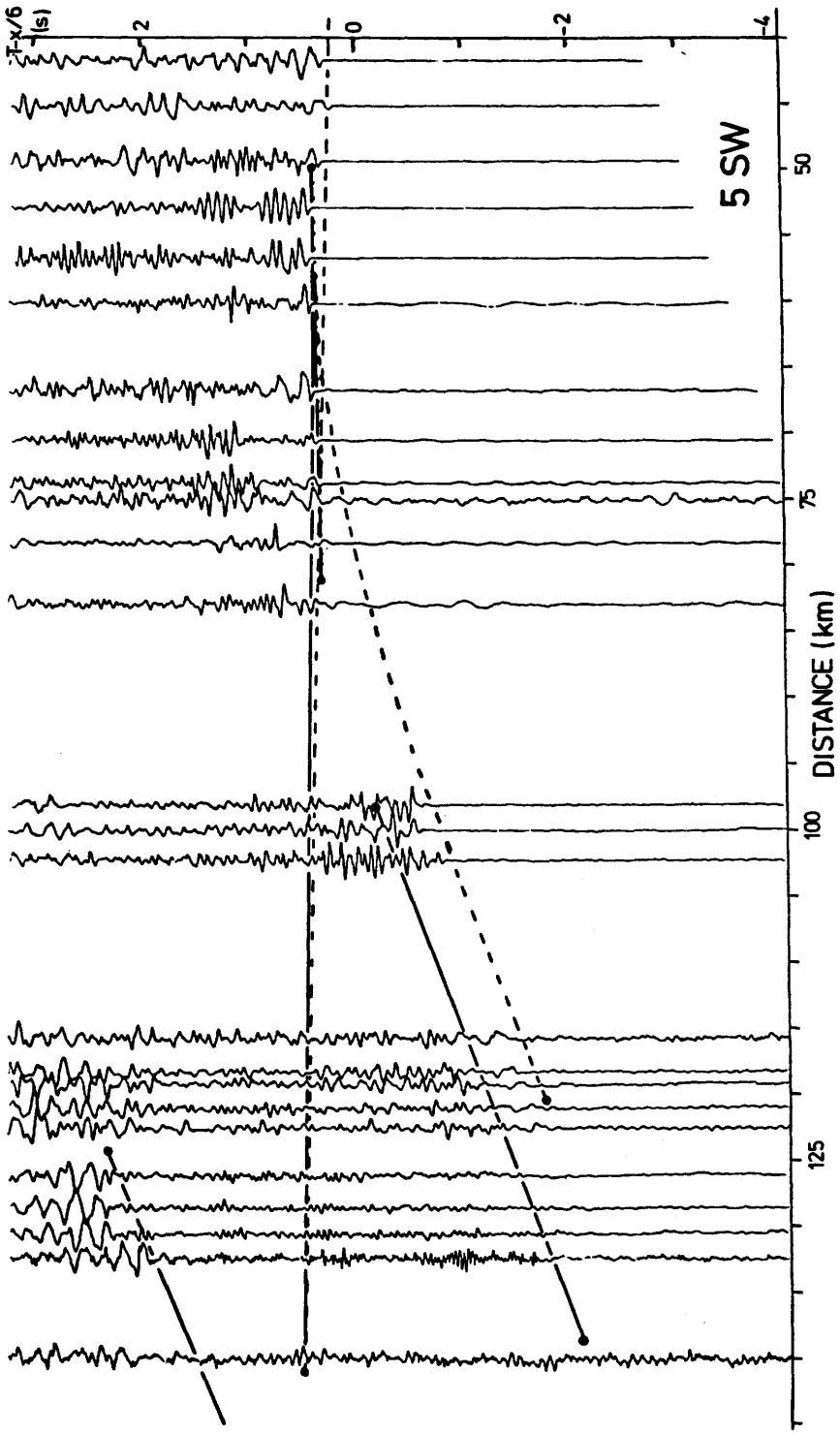

Figure 58c. Record section of profile 5 SW.

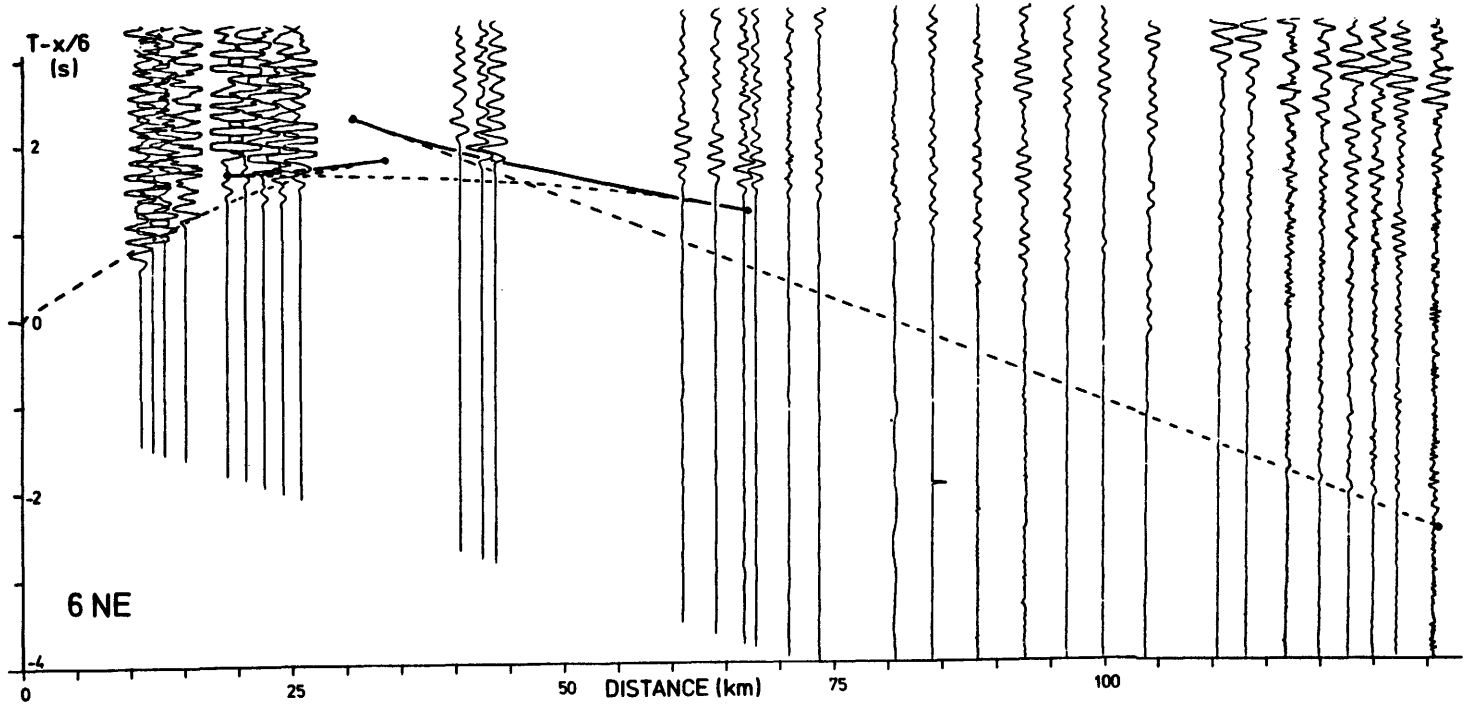

Figure 59a. Record section of profile 6 NE (v_r = 6 km/s).

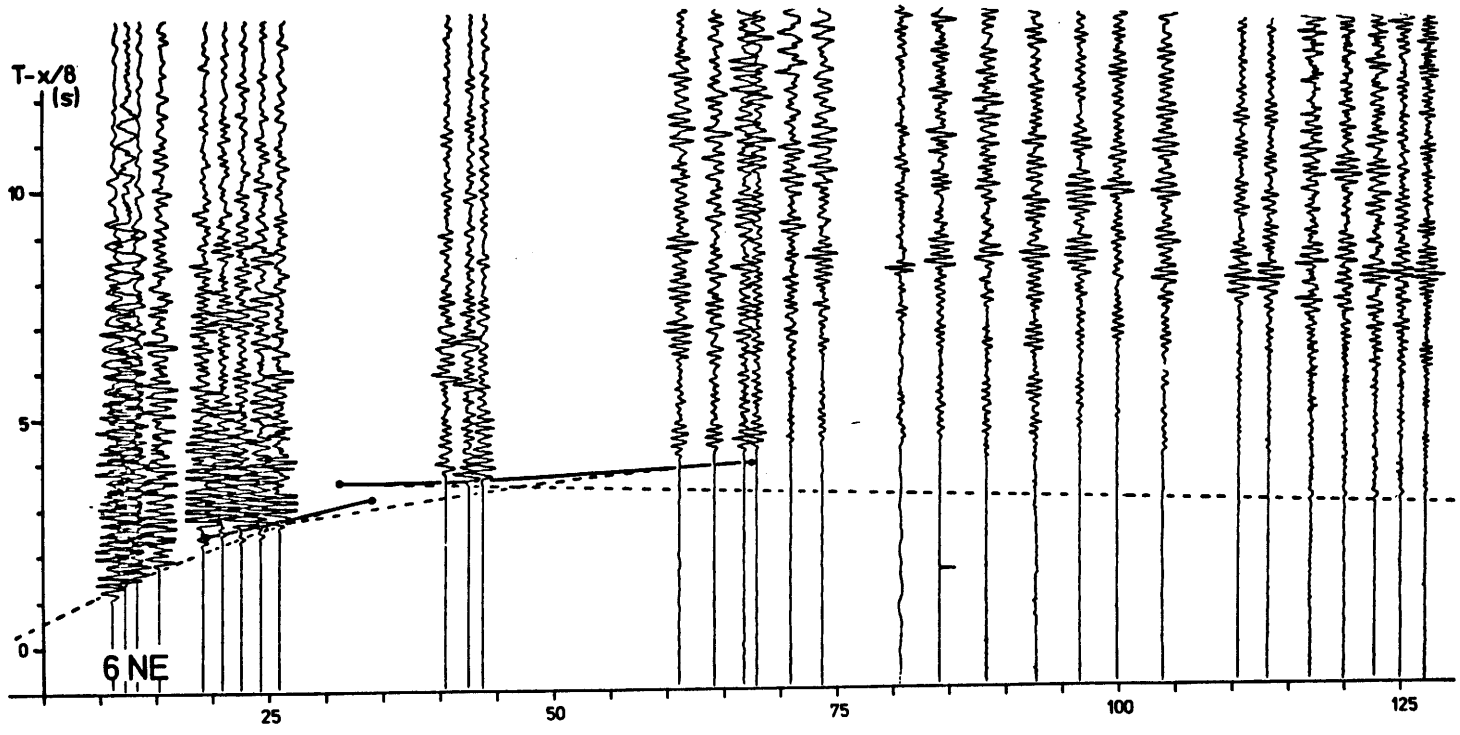

Figure 59b.1. Record section of profile 6 NE (v_r = 8 km/s), part 1 of 3.

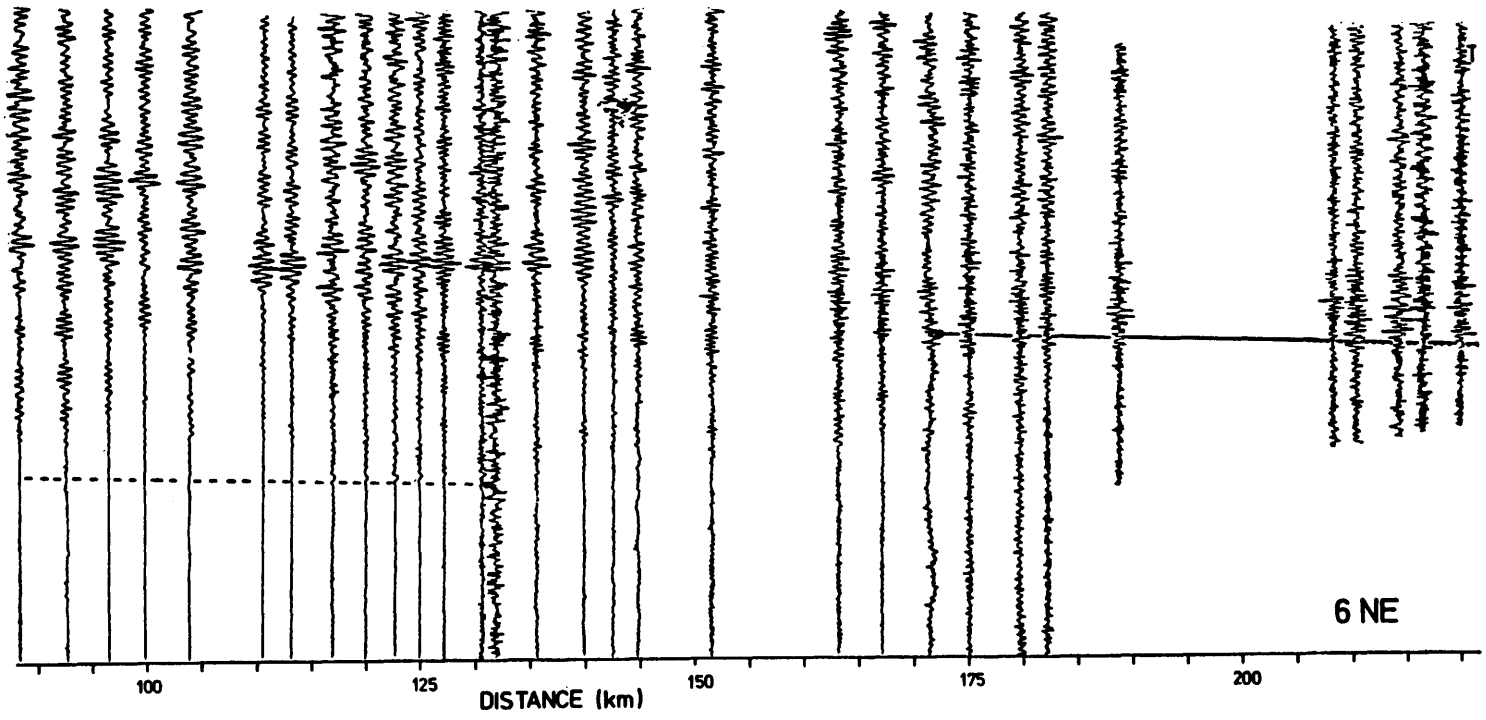

Figure 59b.2. Record section of profile 6 NE (v_r = 8 km/s), part 2 of 3.

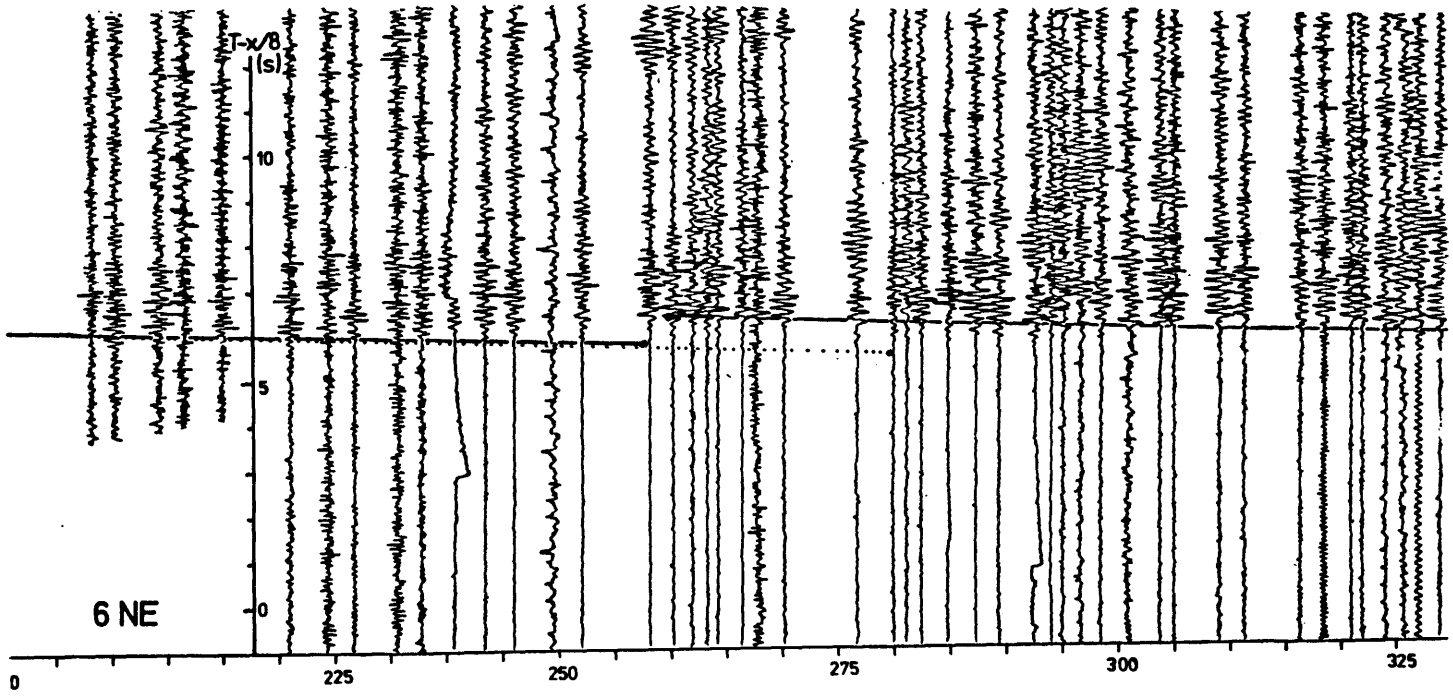

Figure 59b.3. Record section of profile 6 NE (v_r = 8 km/s), part 3 of 3.

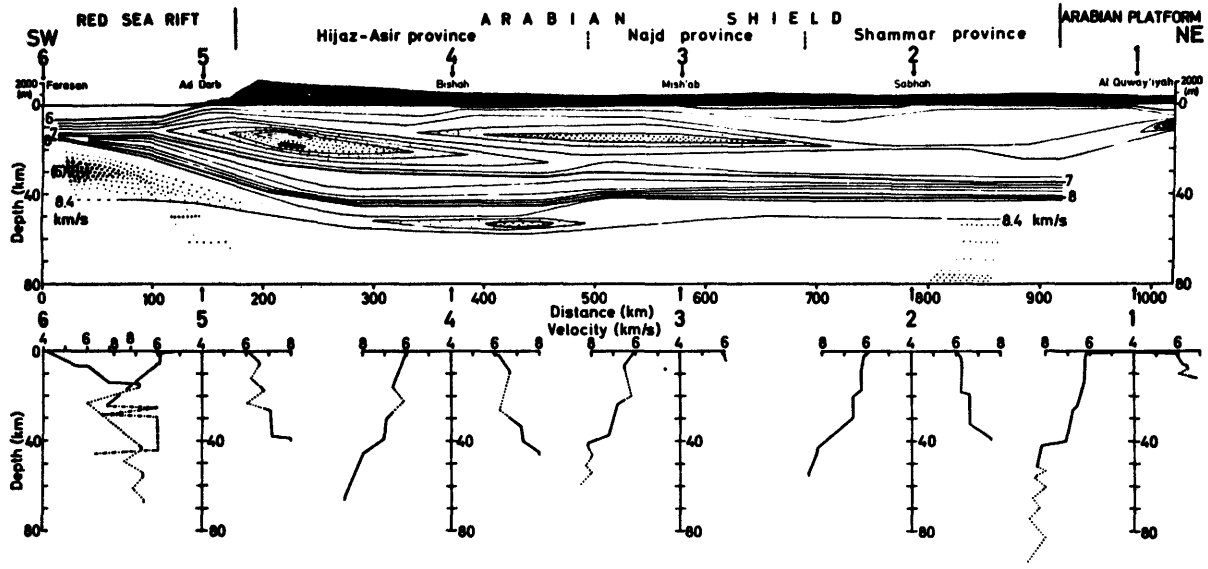

Figure 60. Model of the lithosphere beneath the Arabian Shield in western Saudi Arabia. See Part 1 for explanation.

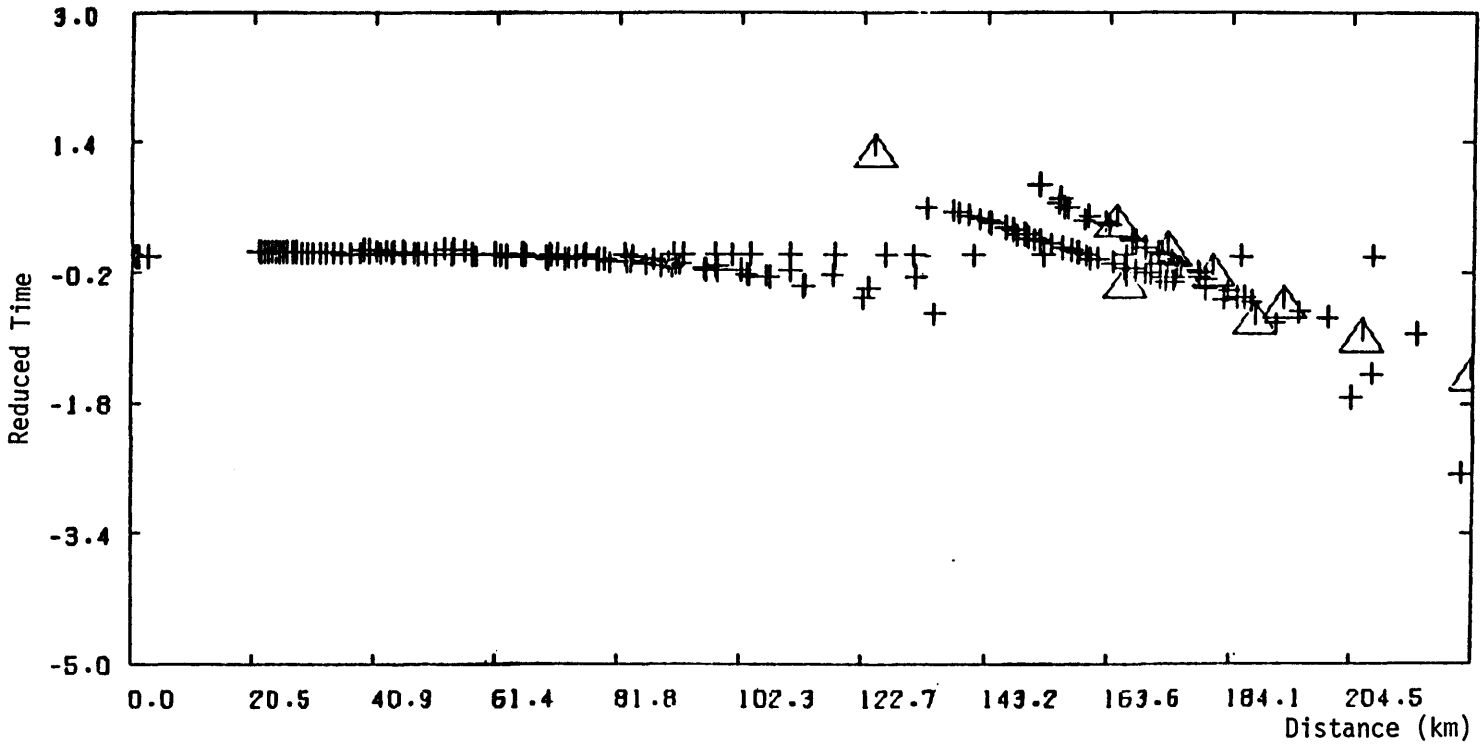

Figure 61. Traveltimes of rays (crosses) traversing the real model from shot-point 4 to the south-southwest compared with some observed traveltimes (triangles) of the main reflected phases.

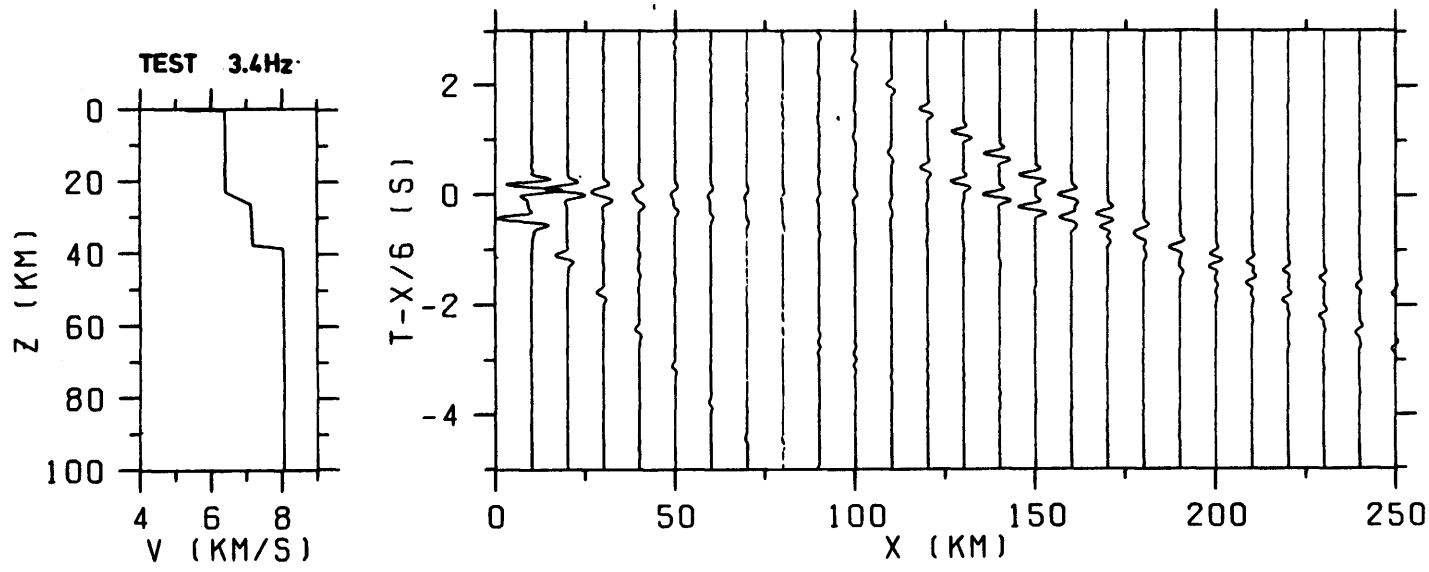

Figure 62a. Simplified model of profile 5 NE and synthetic record section computed for a main frequency of 3.4 Hz.

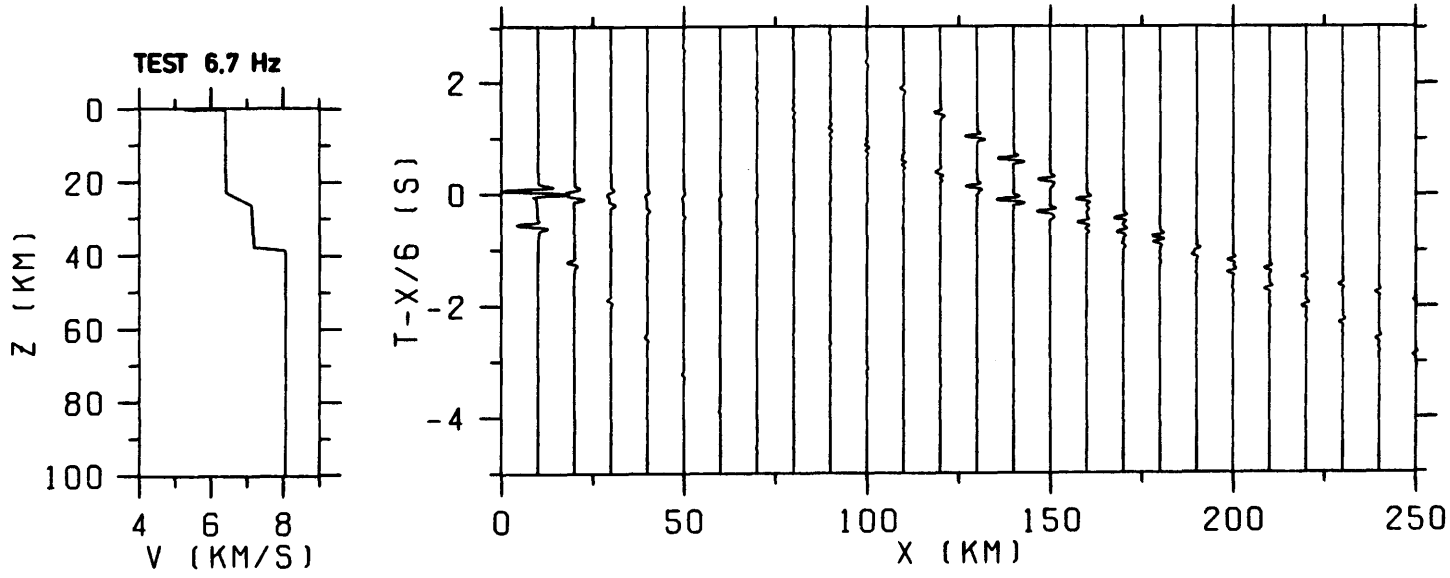

Figure 62b.1. Synthetic record sections computed for the main frequency of 6.7 Hz.

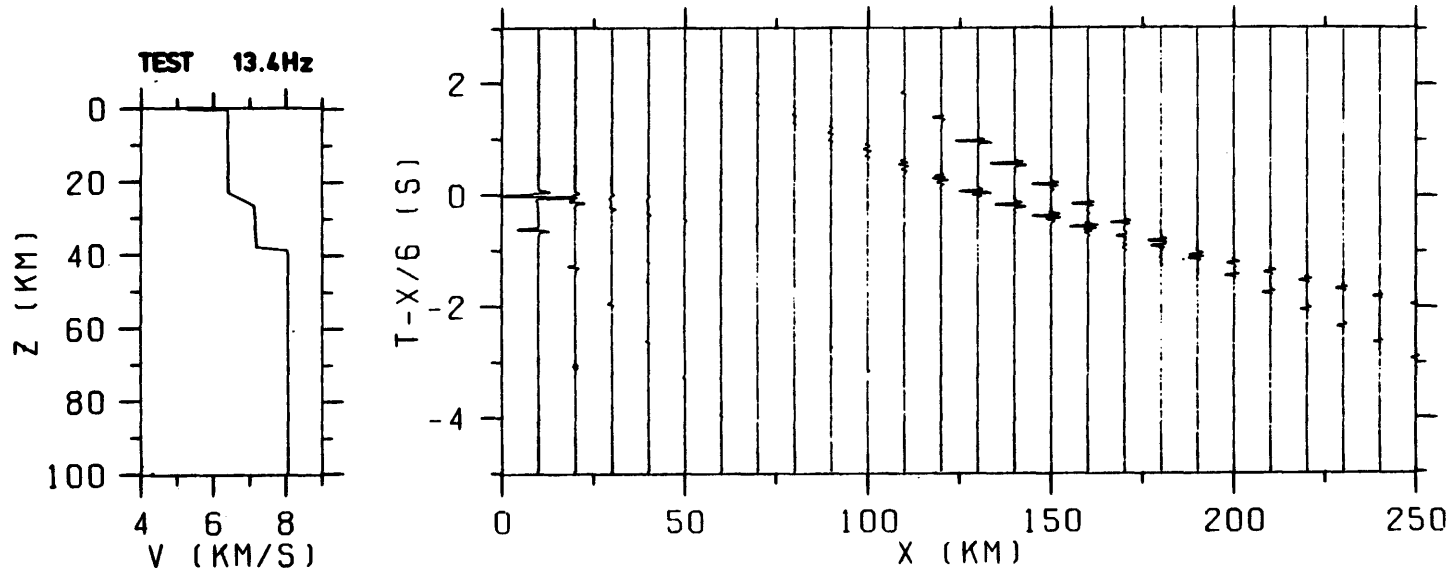

Figure 62b.2. Synthetic record sections computed for the main frequency of 13.4 Hz.

A PRELIMINARY ANALYSIS OF THE SAUDI ARABIAN DEEP SEISMIC SOUNDING DATA

By Zeng Rong-sheng, Hu Hong-siang, and Zhang Shao-quan

Institute of Geophysics
State Seismological Bureau of China
Beijing, China

CORRELATION OF PHASES AND TRAVELTIME CURVES

We have analyzed the data from shotpoints 1-4; the typical traveltime curve is shown in figure 63. P_1 is the refracted wave from the crystalline basement, showing an increase in velocity from 6.0 to 6.3 km/s. P_1 seems to stop at a distance of about 140 km from shotpoint 3.

Two reflections, P_3° and P_4°, can be identified in later arrivals in the record sections from nearly all the shotpoints. Other reflections may appear at varying distances, but they cannot be correlated with confidence.

At a distance greater than 180 km, three phases, P_ℓ, Pm, and Pn, can be distinguished. The first arrival, Pn, with a velocity of 8.1 km/s, can be traced to at least 500 km from shotpoint 3. P_ℓ has a velocity of 7.2-7.6 km/s; it intersects Pn at a distance of 180 km from the shotpoint. As shown below, P_ℓ is related to a boundary just a few kilometers above the ordinary Moho discontinuity; this is important in understanding the physical properties of the Moho discontinuity.

Pm is especially clear in the record sections from shotpoint 1 at a distance of 250-350 km from the shotpoint. It originates from a boundary in the upper mantle.

At a distance less than 50 km from the shotpoint, the transverse S wave (corresponding to P_1) and the Rayleigh waves of the superficial layer are very prominent.

THE SEDIMENTARY LAYER

Since there are no available data on the sedimentary layer, we tried to derive its velocity from the dispersion of the Rayleigh waves. Both the group and phase velocities are calculated by digital processing methods. The results for the group velocities of the Rayleigh waves are shown in table 1 and a typical group velocity curve is shown in figure 64. The parameters of the overburden layer at different shotpoints have been calculated by an inversion program. The thickness of the overburden layer is only about 200 m, with a corresponding P-wave velocity of 5.2 km/s, assuming that the corresponding P-wave velocity of the subterranean layer is 6.0 km/s. The result of the phase velocities is similar to that of the group velocities.

The intercept time of P_1 is about 0.4 s. Assuming that the velocity of the sedimentary layer is 5.2 km/s, the thickness of the sedimentary layer is about 1-2 km. Therefore, the Rayleigh waves are traveling in a guided layer much shallower than the sedimentary layer.

Table 1. Parameters of the overburden layer obtained from group velocities of Rayleigh wave dispersion.

Shotpoint	Distance (km)	Thickness (km)	Shear wave velocity (km/s)	Compressional wave velocity (km/s)
2 (SW)	21-39	0.22	3.07	5.31
3 (SW)	12.7-39	0.25	3.04	5.26
4 (SW)	9-27	0.33	2.99	5.17

THE UPPER CRUST

The velocity of P_1 appears to increase linearly from 6.0 km/s just below the crystalline basement boundary to 6.3 km/s at a depth where a velocity inversion may occur. The latter depth corresponds to the deepest points of the ray returning to the surface 140 km from the shotpoints and can be calcu- lated by using the Herglotz-Wiechert method (results shown in table 2). The depth of the velocity inversion tends to vary from 7 km at shotpoint 1 to 14 km at shotpoint 3.

Table 2. Depth of deepest penetration of P_1.

Shotpoint	Depth
1 (NE)	6.6 km
2 (NE)	10.9 km
2 (SW)	9.2 km
3 (SW)	14.7 km

DEEP REFLECTIONS AND REFRACTIONS

Two strong reflections, P_3° and P_4°, can usually be identified in later arrivals. The parameters corresponding to P_3° and P_4° at different shotpoints were calculated by inverting their traveltimes (results shown in table 3). It is interesting that the thickness between P_4° and P_3° decreases from 18 km at shotpoint 1 to 12 km at shotpoints 2 and 3, while the thickness between P_3° and P_1 increases from 12 km at shotpoint 1 to about 20 km at shotpoints 2 and 3.

P_ℓ, Pm, and Pn are considered to be refractions from three different boundaries in the crust and upper mantle. Their synthetic seismograms were calculated (fig. 65) and two possible models of the structure of these phases are compared, one with constant interval velocities, and the other with velocity gradients above the Pn boundary. The model with constant interval velocities between P_ℓ and Pn produces stronger reflections at longer receiving distance intervals, in agreement with actual observations.

Pn is the ordinary refraction from the Moho discontinuity. The depth of P_ℓ is always a few kilometers less than that of the Pn refractor. It is more

likely, therefore, that P_4° is an ordinary reflection corresponding to the shallower boundary P_ℓ than a diving wave in the medium just above the Pn boundary.

Table 3. Parameters from the reflections P_3° and P_4°.

	Shotpoint 1(SW)		Shotpoint 2(NE)		Shotpoint 2(SW)		Shotpoint 3(SW)	
	v(km/s)	h(km)	v(km/s)	h(km)	v(km/s)	h(km)	v(km/s)	h(km)
P_1	5.30	1.76	5.30	1.11	5.30	0.71	5.30	0.93
P_3°-P_1	6.23	12.38	6.40	22.18	6.21	18.62	6.36	20.27
P_4°-P_3°	6.65	18.27	(5.36)	(4.05)	6.63	12.65	6.60	11.95
	$\Sigma h = 32.5$		$\Sigma h = 27.3$		$\Sigma h = 31.98$		$\Sigma h = 33.15$	

RELIEF OF THE DEEP STRUCTURE

The relief on the boundaries corresponding to P_3° and P_4° are obtained by using the "common depth method" of reflection (fig. 66). The Moho boundary relief is obtained by using the Pn traveltimes, and a uniform velocity model has been adopted. A preliminary model of the Pn boundary relief is obtained by using the t_p and t_o method as proposed by Soviet geophysicists. Traveltimes are then calculated by the ray-tracing method. Successive modifications of the model are derived until an ideal fit of the calculated values with the observed values of the traveltimes has been obtained (fig. 67).

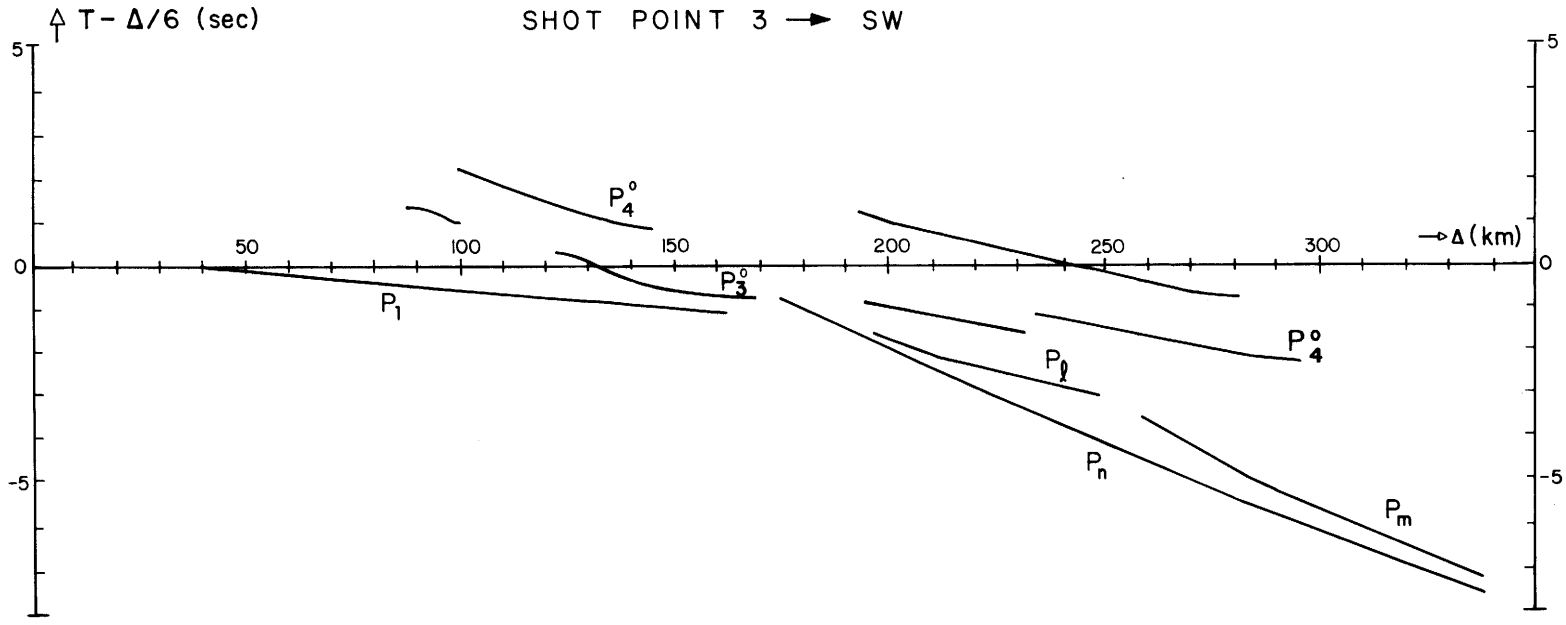

Figure 63. Typical traveltime curve for the seismic refraction profiles.

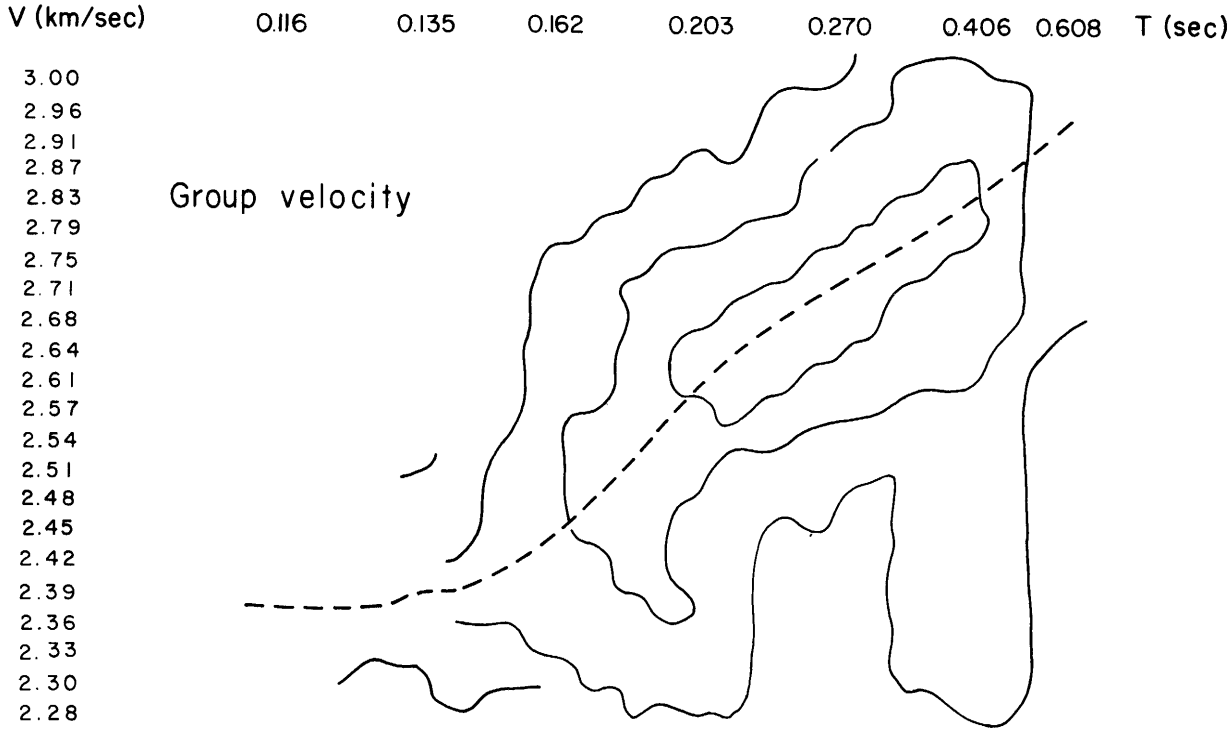

Figure 64. Dispersion of the Rayleigh waves.

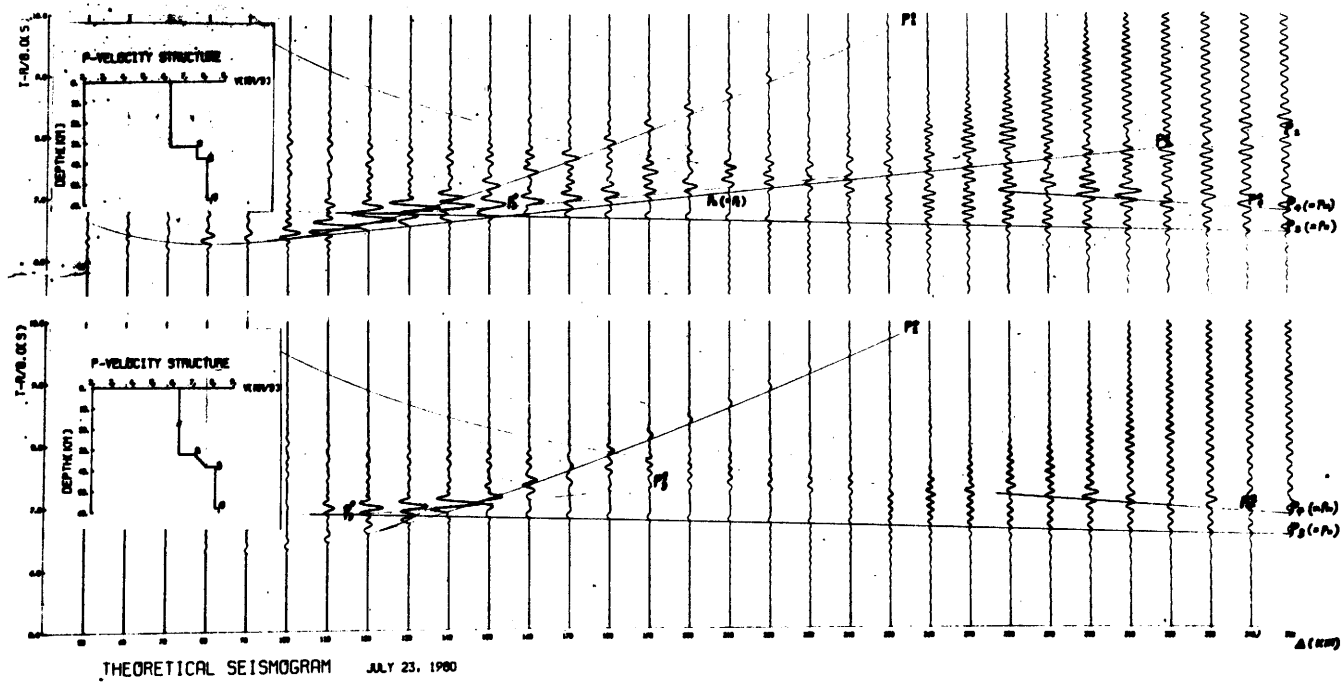

Figure 65. Synthetic seismograms for two different models.

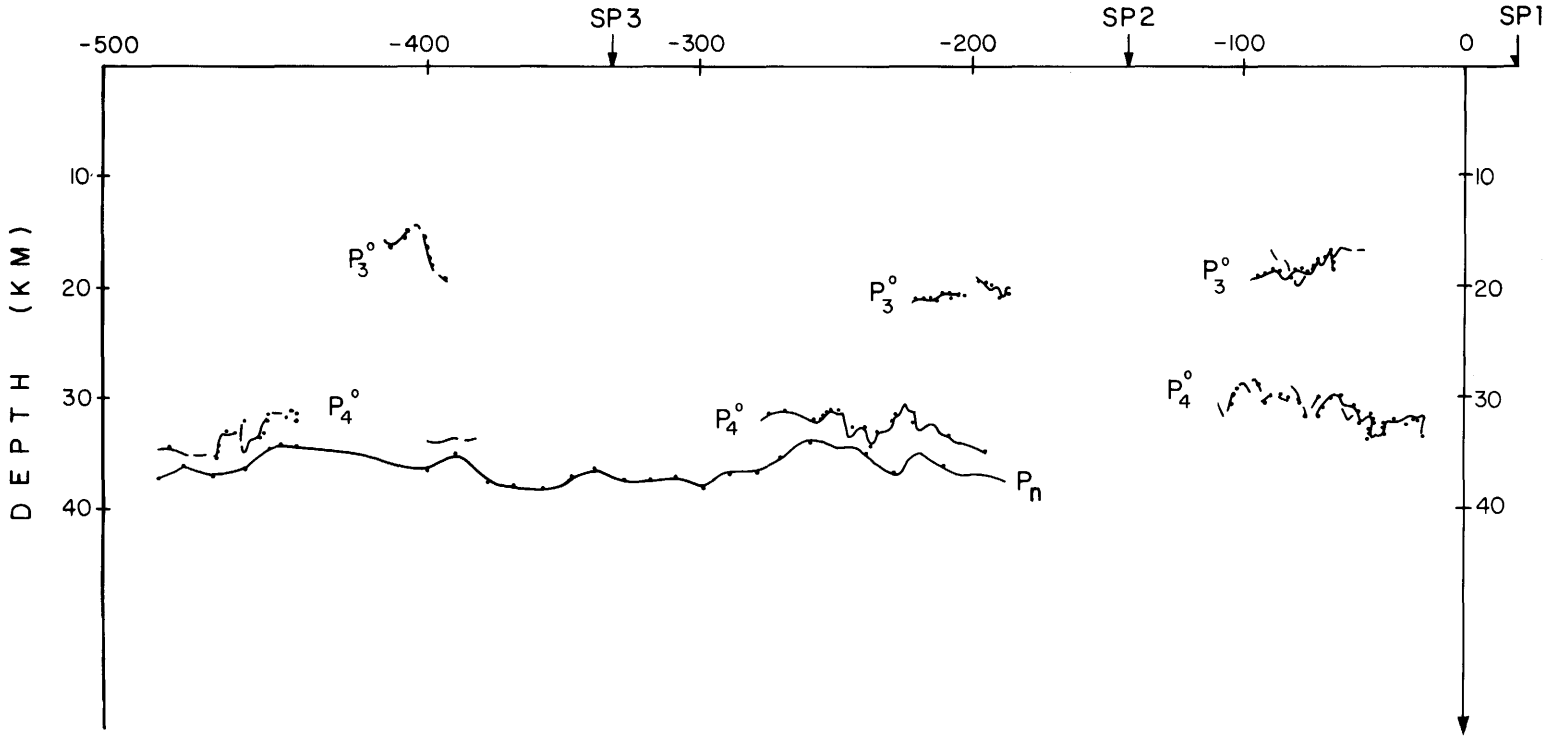

Figure 66. Relief of the P_3°, P_4°, and Pn boundaries.

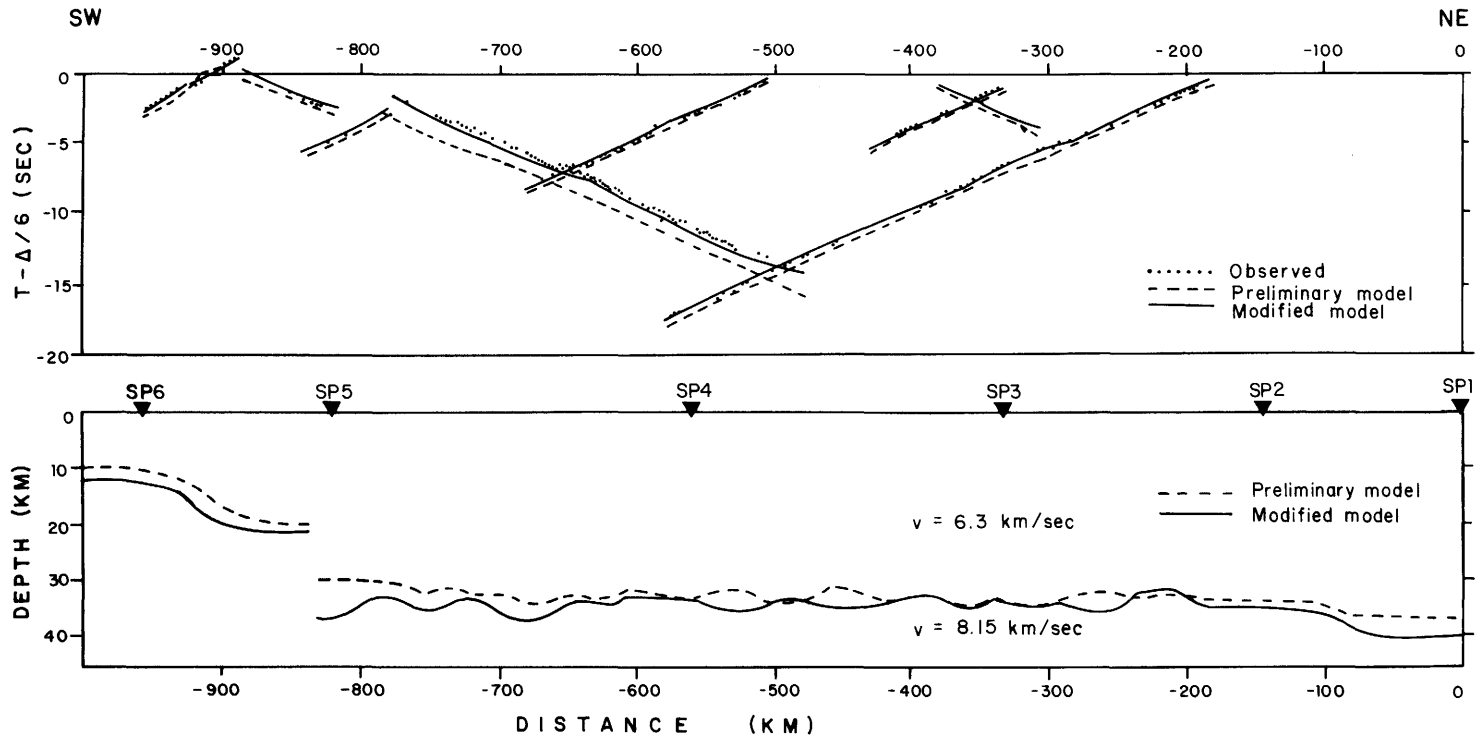

Figure 67. Relief of the Pn boundary obtained by the ray-tracing method.

ONE-DIMENSIONAL VELOCITY-DEPTH FUNCTIONS DETERMINED FOR THE ARABIAN SHIELD AND THE SOUTHWESTERN RED SEA: A COMPARISON OF MODELS

By W. D. Mooney, U.S. Geological Survey, Menlo Park, California, and
M. E. Gettings, U.S. Geological Survey, Jiddah, Saudi Arabia

INTRODUCTION

The use of the Saudi Arabian seismic refraction data (Blank and others, 1979; Healy and others, 1982) at the IASPEI Commission on Controlled Source Seismology Workshop resulted in as many as 14 interpretations of the velocity-depth structure along the profile. The bases for these individual interpretations forms the bulk of this workshop volume. We here compare and discuss these interpretations in order to identify the common aspects as well as those aspects with a significant diversity of interpretation. We expect that future analyses of these data will help resolve the structure in those portions of the crust and upper mantle with the greatest diversity of interpretation.

SHOTPOINTS 1 AND 2

We begin our comparison of the various crustal models presented at the CCSS workshop by considering those between shotpoints 1 and 2 (fig. 68). We have generalized the features of the original models in quoting average thicknesses and velocities. The models are generally in excellent agreement. The crust is shown as 40 $\pm$ 2 km thick with an upper crust about 20 km thick and an average velocity of about 6.15 km/s, and a lower crust also about 20 km thick and an average velocity of about 6.6 km/s. Many models do not show homogeneous crustal layers, but rather velocity gradients, discontinuities,and low-velocity zones. We also note that calculation of an "average" velocity of 6.15 km/s loses any physical significance in a crust composed of velocity layers of, say, 6.45 and 5.85 km/s; the average velocity actually does not exist anywhere in the model. Two of the models show low-velocity zones in the upper crust, although model 2 indicates only a slight velocity reduction (0.1 km/s) as compared with that of model 1, which indicates a significant velocity reduction (0.6 km/s). Within the upper crust there is considerable scatter in the details of the structures. Models 4, 5, and 12 have a one-layer upper crust, models 1, 2, 6, 8, 10, and 11 have two or more layers, and models 13 and 14 show the entire crust as being characterized by velocity gradients rather than layers. Likewise, in the lower crust the models range from a single layer to multiple layers to gradient models. The crust-mantle boundary is modeled as a first-order discontinuity in all but one of the models, where it is spread out over several kilometers (model 13). Only models 11, 13, and 14 show velocities in the lowermost crust greater than 7.0 km/s (model 2 did not reach the crust-mantle boundary). Model 13 shows considerable structure below the crust-mantle boundary, with successive regions of high and low velocity.

The source of the differences in the various interpretations shown in the crustal sections may be confusing. In the course of the presentations at the CCSS meeting, it became evident that the main source of differences in the

final models is the phase correlation of the data. As discussed in the introduction to the volume, the term "phase correlation" refers to the process of identifying, within a seismic record section, those arrivals which refract or reflect from the same feature of the crustal or mantle velocity structure. For example, the Pi phase refracts along the top of the lower crust, while the PmP phase reflects from the M-discontinuity. Knowledge of the expected amplitude and frequency of a particular phase, on the basis of experience and theoretical considerations, facilitates its correlation in the record section, but the complexity of the typically observed wave field leads to some subjectivity in the interpretation of the phases. Examples of phase correlations are given in the contribution by C. Prodehl (this volume). Different methods of traveltime and amplitude analysis of given identical phase correlations will produce nearly the same result. Conversely, different correlations will result in markedly divergent models. A comparison of models 5 and 6 (fig. 68) provides an example of a difference in interpretation resulting directly from a difference in phase correlation. The phase correlation of model 6 includes the identification of arrivals reflecting from a boundary within the upper crust at a depth of 12.5 km. Model 5 is not derived from this phase correlation. Both models 5 and 6 are apparently based on nearly the same phase correlation of mid-crustal and crust-mantle phases (arrivals returning from depths of about 20 and about 39 km, respectively). For this reason the depths and velocities of those portions of models 5 and 6 agree reasonably well. However, even these correlations must have been somewhat different because, for example, model 6 has both a higher average velocity of the entire crust and a thinner crust. These two factors imply that the phase correlations of the arrivals from the mantle were earlier in time than those of model 5. Examination of the record sections (see contribution by C. Prodehl) reveals how relatively small ($\pm$0.2 s) differences in phase correlation can arise, particularly when emergent secondary arrivals are being interpreted.

Another reason for differences in the interpretations is that most of them were prepared specifically for the CCSS workshop and are not final interpretations prepared after exhaustive trial-and-error modeling or direct inversion. Some interpretations show the simplest possible model consistent with the data, while others are based on the most detailed model permitted by the data. Therefore, the compiled sections should be considered with the informal nature of the workshop in mind.

Velocity-depth functions beneath shotpoints have been estimated by extrapolating the more reliable determinations made between shotpoints. The composite figure of the velocity-depth functions beneath shotpoint 1 (fig. 69) gives an estimate of the range of models permitted by the data. In this figure, the crust appears to be characterized by a simple crust from 0 to 15 km depth with an average velocity of 6.15 km/s, underlain by a zone of considerable scatter in estimated velocity between 15 and 20 km depth, and a simple crust from 20 to 40 km depth with an average velocity of 6.6 km/s. The crust-mantle boundary appears to be marked by a large velocity discontinuity in all but one model. The upper mantle velocity is 8.2 $\pm$ 0.1 km/s.

The comparison of the velocity-depth functions beneath shotpoint 2 (fig. 70) is of particular interest because long-range data were collected from shotpoint 1 southwest of shotpoint 2 that define both the crustal and upper mantle structure beneath the shotpoint. The average upper crustal velocity is 6.25 km/s, 0.1 km/s higher than that at shotpoint 1. Most interpretations of the mid-crustal boundary are clustered around 20 km depth, and the average lower crustal velocity is 6.6 km/s, the same as for shotpoint 1. The average depth

to the M-discontinuity is 2 km shallower than the average interpretation at shotpoint 1, and there is somewhat more scatter in the interpreted depths. There is considerable scatter in the estimated sub-Moho velocity, averaging 8.1 km/s. Between 40 and 50 km depth, there is general agreement for either an upper mantle velocity gradient or velocity discontinuities. Two of the three models that continue below 50 km show velocity discontinuities between 60 and 70 km depth.

SHOTPOINTS 3, 4, AND 5

Farther southwest along the profile, the comparison of velocity-depth functions beneath shotpoint 3 (fig. 71) shows a pattern virtually identical to that for shotpoint 2. Average crustal velocities and thicknesses are nearly identical to those beneath shotpoint 2 and the scatter in interpretations is similar in magnitude. There appears to be general agreement in a velocity increase in the upper mantle between 40 and 60 km depth, either gradually or discontinuously. Two models also show velocity discontinuities at 70 km depth, the latter interpretation based on the long-range data from shotpoints 1 and 6. One of the models shows a pronounced low-velocity zone between 60 and 70 km depth.

No comparison of crustal columns has been made for the region between shotpoints 2 and 3 because there is no refraction reversal (shotpoint 3 was recorded only 75 km to the northeast). The crustal columns between shotpoints 3 and 4 (fig. 72) show considerable scatter in the interpretation of layer thickness (for example, models 5 and 6, and 13 and 14), although some models are in extremely close agreement (for example, models 10, 11, and 12). Average crustal thickness is 40 km. The upper crust is generally agreed to be 22 ± 2 km thick with a 6.3 km/s average velocity. The lower crust has a velocity of 6.7 ± 0.13 km/s in eight cases and a velocity greater than 7.0 km/s below the 6.7 km/s material in three cases. The velocity of the uppermost mantle is 8.1 ± 0.1 km/s, and one or more upper mantle discontinuities are found in four of the 11 interpretations. It seems likely that much of the scatter in the interpretations of crustal thickness is due to the high dominant frequency (about 10 Hz) of the seismograms recorded from these shotpoints. The record sections from this part of the profile show unusually high amplitudes, presumably due to a high average Q (low seismic attenuation) in the upper crustal rocks. This has made phase correlation of the data particularly difficult. Bandpass filtering of the data would probably improve its usefulness.

The comparison of velocity-depth functions beneath shotpoint 4 (fig. 73) reveals a general consensus of an average velocity of 6.3 km/s and an upper crustal thickness of 22 km, as well as good agreement on the 6.7 km/s average velocity between 20 and 30 km depth. In the lower crust the models indicate that either the velocity continues at 6.7 km/s with depth, or the velocity increases rapidly with depth, reaching 7.6-7.8 km/s just above the M-discontinuity. Upper mantle velocity structure has been identified in several models, the velocity generally increasing with depth in either a smooth gradient or a series of high and low velocities. An upper mantle discontinuity is observed in at least two models at both 55 and 72 km depth.

The comparison of crustal columns between shotpoints 4 and 5 (fig. 74) shows a smaller scatter in crustal thickness, 40 ± 2 km, than was obtained between shotpoints 3 and 4. There is considerable disagreement as to whether there is an upper crustal boundary at about 15 km depth. Seven models show a

discontinuity at about that depth and five models do not. Seven models identify a discontinuity at about 22 km depth and four do not. Three models show discontinuities at both depths, and several models show changes in velocity gradient at those depths.

The lower crust is modeled with a nearly uniform velocity of 6.7 $\pm$ 0.15 km/s in seven models, and with velocities greater than 7.0 km/s in the lowermost crust in four models. Five models show velocity gradients or discontinuities in the upper mantle or both, based largely on the long-range data from shotpoint 6.

SHOTPOINTS 5 AND 6

Before discussing the comparison of the velocity-depth interpretations between shotpoints 5 and 6, it is appropriate to refer to a geologic map of the region where these profiles were recorded (fig. 75). For logistical reasons, records were obtained only on the coastal plain and on islands in the Red Sea, resulting in the largest interstation spacing in the region of strongest lateral heterogeneity (the ocean-continent transition). This factor should be considered when comparing the models.

Shotpoint 5 is located approximately 5 km east of the point at which Precambrian rocks meet the Tertiary mafic dikes of the Tihamat-Asir (coastal plain), marking the shield-Red Sea boundary. Considering its proximity to this important crustal boundary, it is most appropriate to discuss in terms of two-dimensional models.

In comparing the crustal columns between shotpoints 5 and 6 (fig. 76), all interpretations, except model 2, show a thin crust, 14 km thick being average. There is a wide scatter of values of upper crustal velocity; all but one model show velocities less than 6.7 km/s above 10 km depth. Below 10 km depth, four models show velocities above 7.0 km/s while others reach the M-discontinuity with no lower crustal velocities above 7.0 km/s. The upper mantle velocity shows considerable scatter, with values between 8.0 and 8.65 km/s. Five models show low-velocity zones in the upper mantle above 40 km depth and nine models show some upper mantle structure, either a low-velocity zone(s) or a velocity discontinuity.

The comparison of velocity-depth functions beneath shotpoint 6 (fig. 77) reveals a general agreement between models that the crust is as thin as oceanic crust, about 12 km. The velocity structure is very difficult to resolve in the crust itself, based on the available data. The consensus is that it increases rapidly from 4.5 to 6.7-6.8 km/s over the 12-km depth to Moho, a structure also typical of oceanic crust.

The interpretations of the upper mantle structure from shotpoint 6 NE show considerable scatter. It should be noted that for the long-range data from shotpoint 6 the ray paths do not bottom beneath the Red Sea, but rather beneath the continent (see fig. 49). Notable aspects of the interpreted velocity structure are an uppermost mantle velocity of 8.0 km/s, a low-velocity zone (6.0-6.7 km/s) between 18 and 35 km depth, an increase in velocity to 8.2 km/s at 35 km depth, and a velocity increase to 8.45 km/s at about 68 km depth. This complicated velocity structure in the upper mantle may be a direct consequence of the mantle convection process that is evidently operating near the Red Sea.

SUMMARY

We summarize this discussion of the CCSS interpretation of the Saudi Arabian data:

1. The 21-km-thick upper crust of the shield has an average velocity of 6.25 km/s. In some regions there are small velocity discontinuities and low-velocity zones.
2. The 19-km-thick lower crust of the shield is separated from the upper crust by a seismic discontinuity at which the velocity increases by 0.2-0.4 km/s. The average velocity of the lower crust is about 6.7 km/s. Velocities greater than 7.0 km/s may be present in the lowermost crust.
3. The M-discontinuity is probably a transition zone 2-5 km thick and occurs at an average depth of about 40 km. The uppermost mantle velocity is 8.0-8.2 km/s, and there is evidence that this velocity increases laterally from 8.0 km/s beneath the Red Sea to 8.2 km/s beneath the Arabian Platform.
4. There is considerable evidence for fine structure in the upper mantle, including low-velocity zones and velocity discontinuities between 40 and 70 km depth.
5. The detailed structure of the crust and upper mantle is difficult to resolve between shotpoints 5 and 6, the Arabian Shield-Red Sea transition zone. Models derived from the available data show a change in crustal thickness from 12 km in the Red Sea to 40 km on the shield, and considerable upper mantle structure.

RECOMMENDATIONS

A general consensus was reached at the CCSS meeting on recommendations for future seismic refraction and reflection work in areas of strong heterogeneous structure, such as the continent-Red Sea transition in western Saudi Arabia:

1. Parallel-to-structure refraction profiles are needed in regions of complex structure, such as along the coastal plain and in the Red Sea.
2. Perpendicular-to-structure profiles must be densely recorded and should include considerable data redundancy.
3. Critically placed seismic reflection profiles would help resolve details in the areas of greatest structural complexity. In the present case, reflection profiles crossing the Hijaz-Asir escarpment would help in understanding the structure across this rift boundary.

REFERENCES

Blank, H. R., Healy, J. H., Roller, J. C., Lamson, R. J., Fischer, F., McClearn, R., and Allen, S., 1979, Seismic refraction profile, Kingdom of Saudi Arabia--field operations, instrumentation and initial results: U.S. Geological Survey Saudi Arabian Mission Project Report 259, 49 p.

Healy, J. H., Mooney, W. D., Blank, H. R., Gettings, M. E., Kohler, W. M., Lamson, R. J., and Leone, L., 1982, Saudi Arabian seismic deep-refraction profile, final project report: U.S. Geological Survey Saudi Arabian Mission and Directorate General of Mineral Resources Open-File Report USGS-OF-02-37, 370 p., 9 plates.

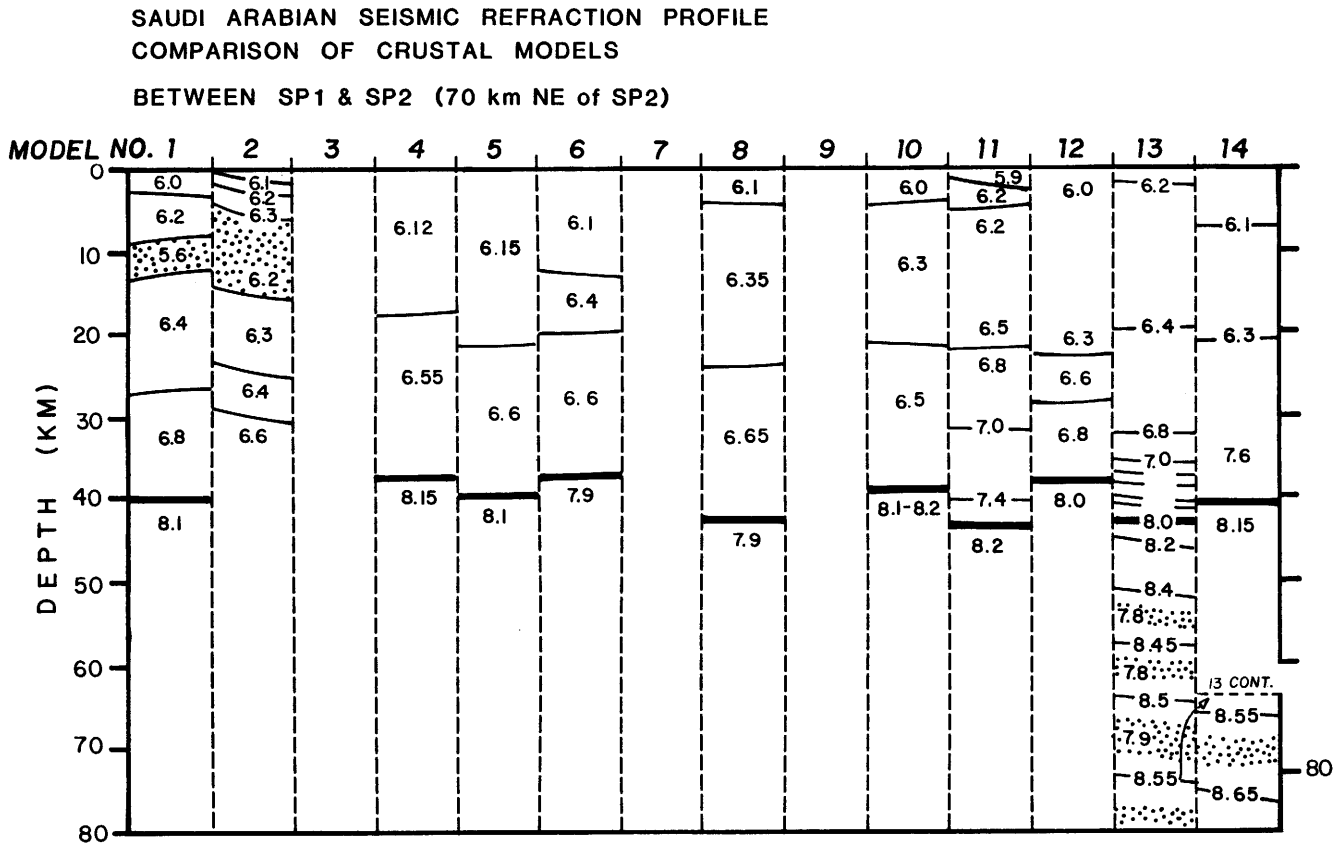

Figure 68. Comparison of crustal models between shotpoints 1 and 2. Velocities are in kilometers per second. Velocity discontinuities are indicated by solid lines with velocities above and below the line; isovelocity lines are indicated by velocities on the lines (for example, model 13). Moho is the thick solid line. Low-velocity zones are stippled. Key: 1 - Ansorge and others; 2 - Firbas; 3 - Forsyth and others; 4 - Gettings; 5 - Ginzburg; 6 - Maguire; 7 - McClain and Orcutt; 8 - Milkereit and Flüh; 9 - Miller; 10 - Mishenkin and others; 11 - Mooney; 12 - Pavlenkova and Yurov; 13 - Prodehl; 14 - Zeng.

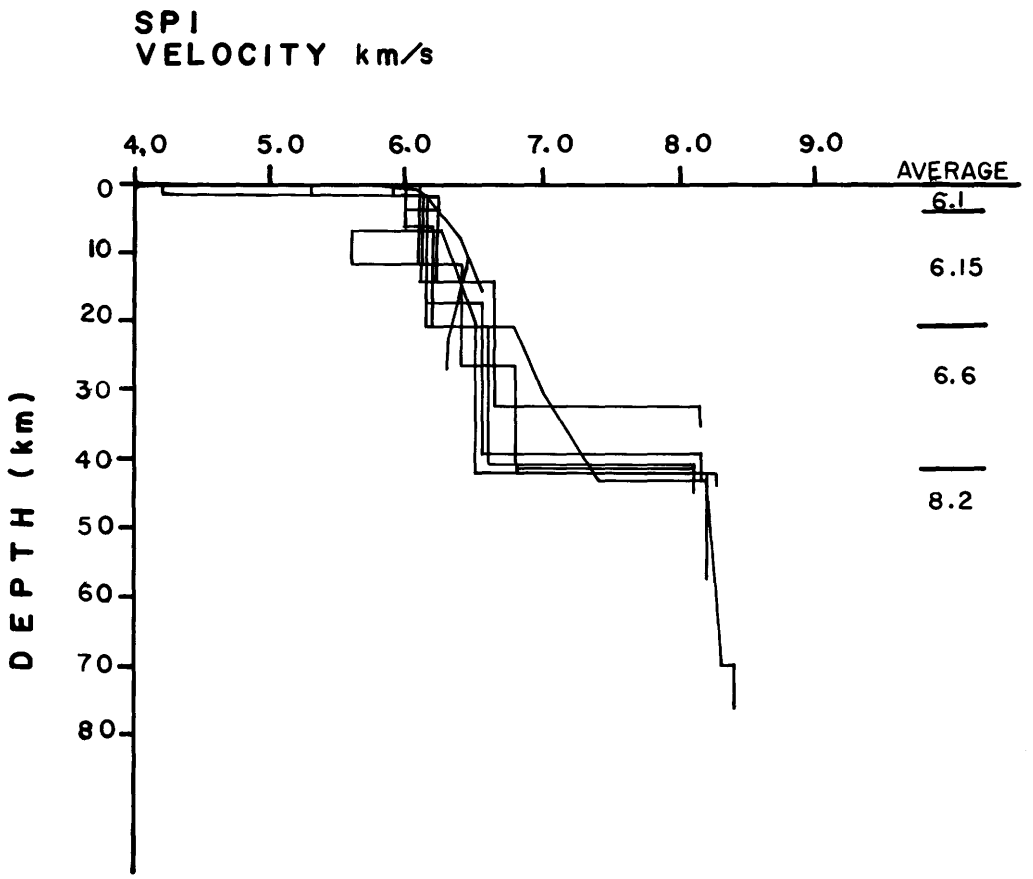

Figure 69. Comparison of velocity-depth functions beneath shotpoint 1. Average velocity section was obtained by inspection.

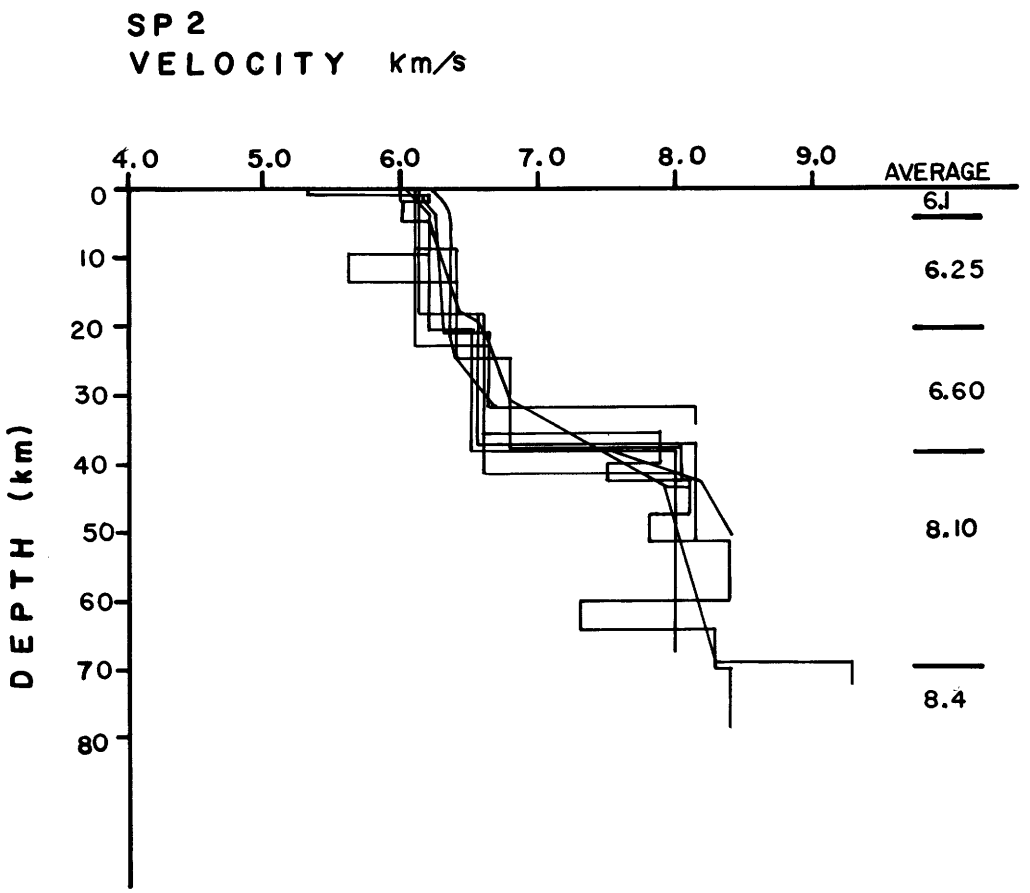

Figure 70. Comparison of velocity-depth functions beneath shotpoint 2. Average velocity section was obtained by inspection.

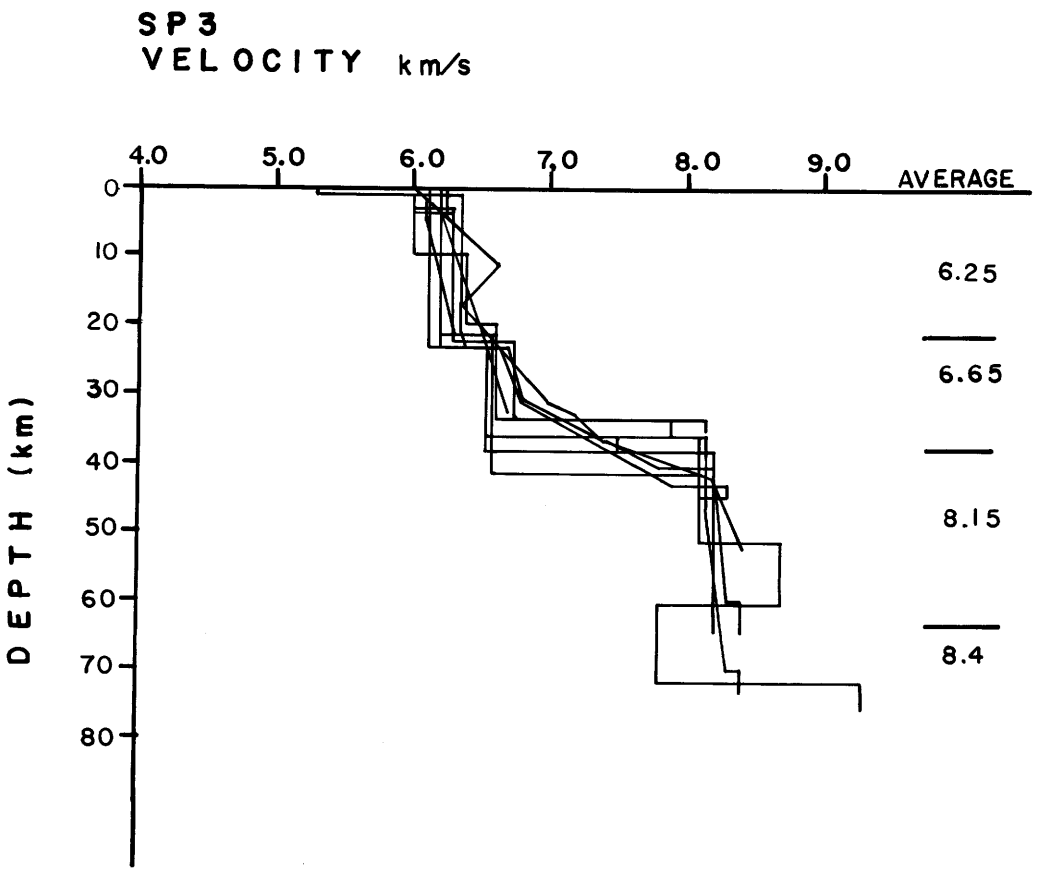

Figure 71. Comparison of velocity-depth functions beneath shotpoint 3. Average velocity section was obtained by inspection.

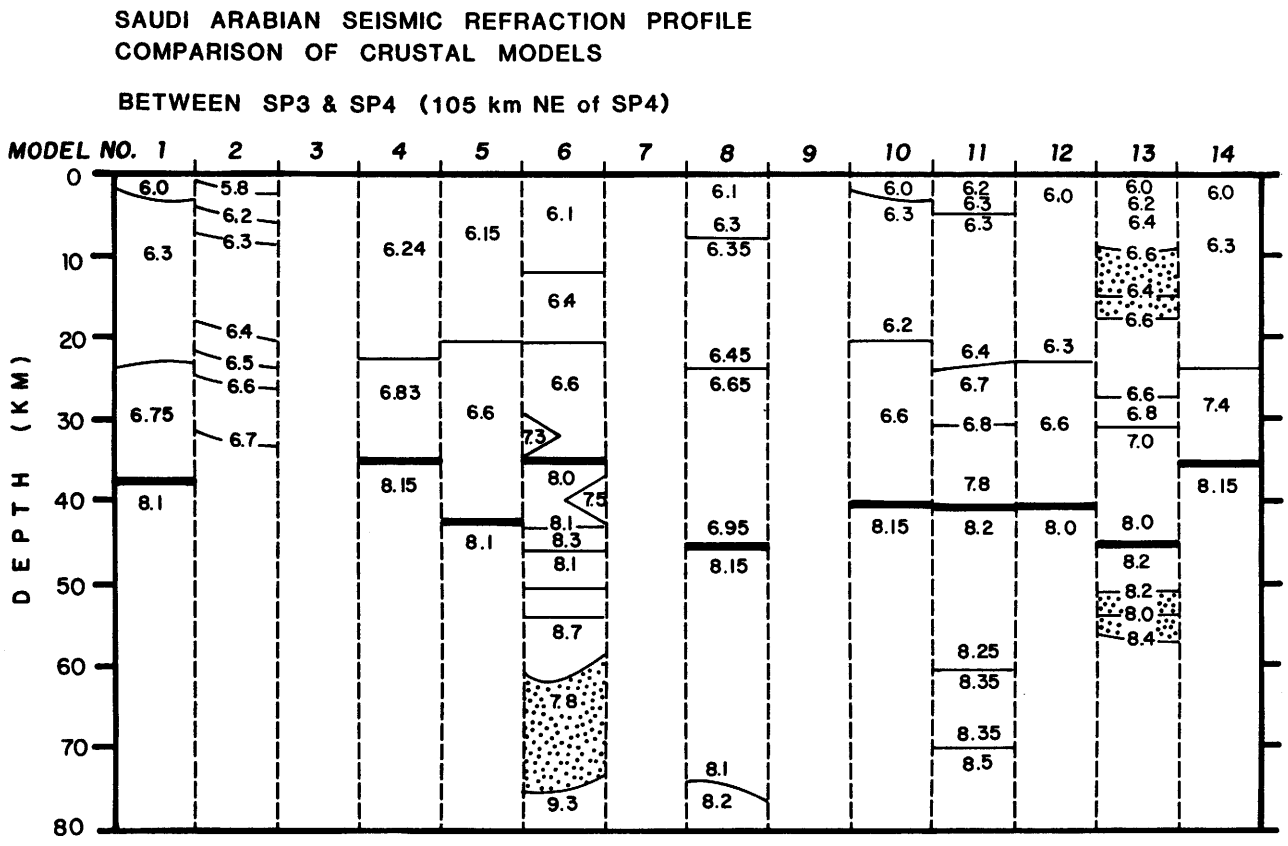

Figure 72. Comparison of crustal models between shotpoints 3 and 4. Symbols same as in figure 68.

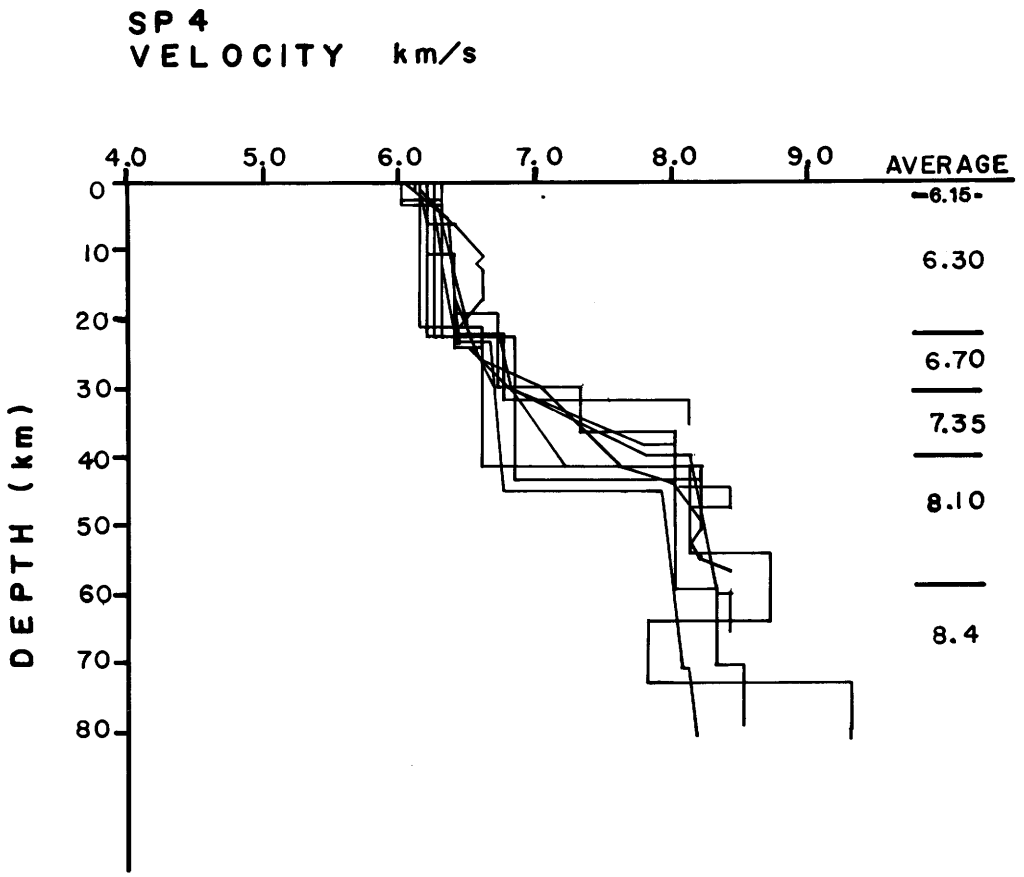

Figure 73. Comparison of velocity-depth functions beneath shotpoint 4. Average velocity section was obtained by inspection.

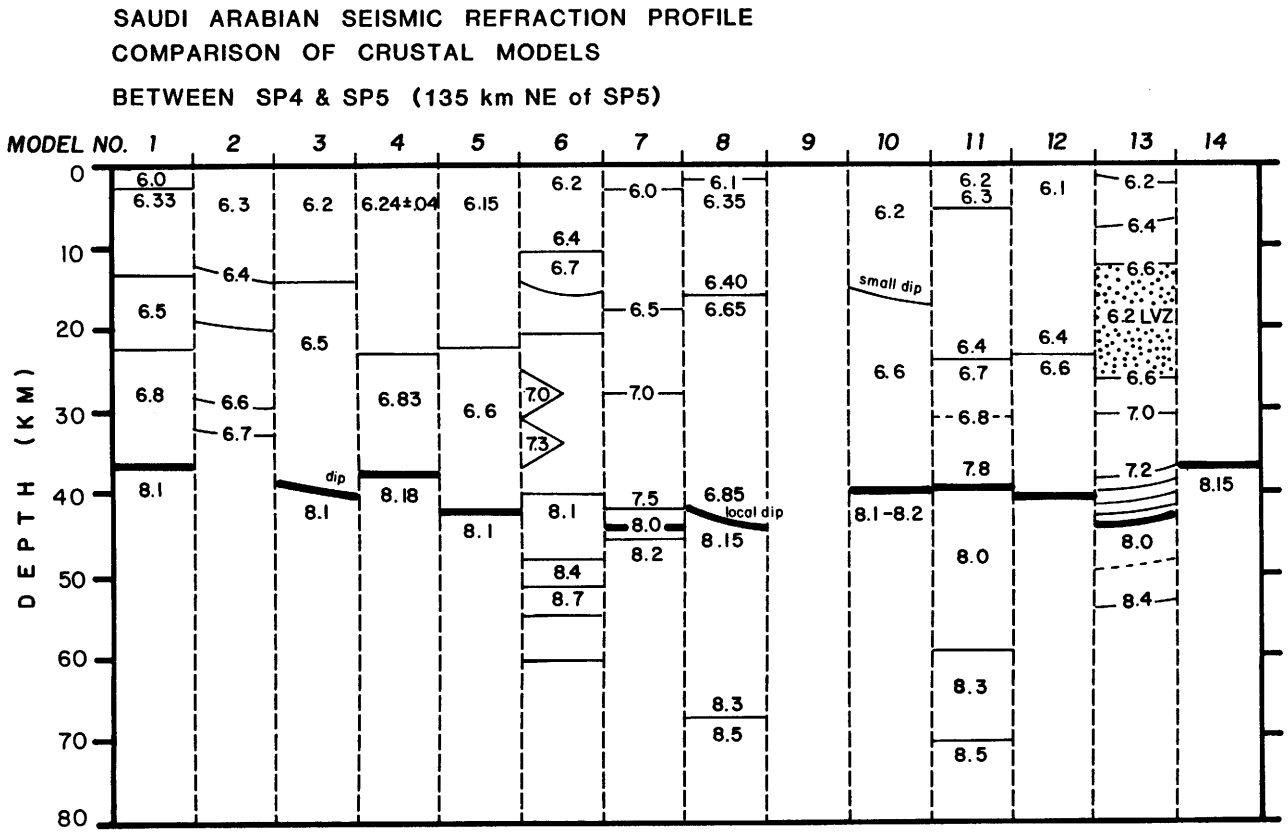

Figure 74. Comparison of crustal models between shotpoints 4 and 5. Symbols same as in figure 68.

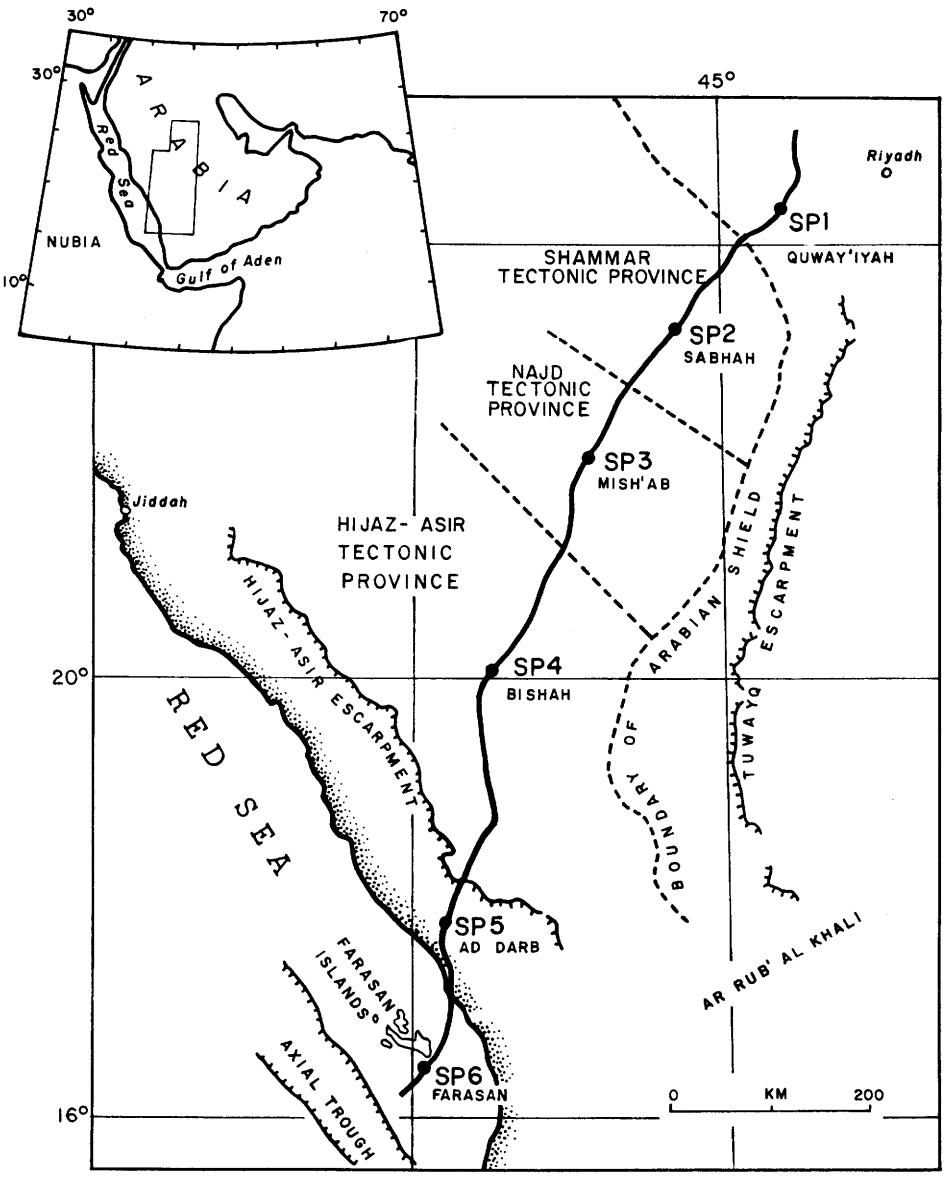

Figure 75. Location map of the 1978 seismic refraction profile across western Saudi Arabia and the southeastern Red Sea showing the shotpoints (SP), the profile line (heavy line), and the tectonic provinces.

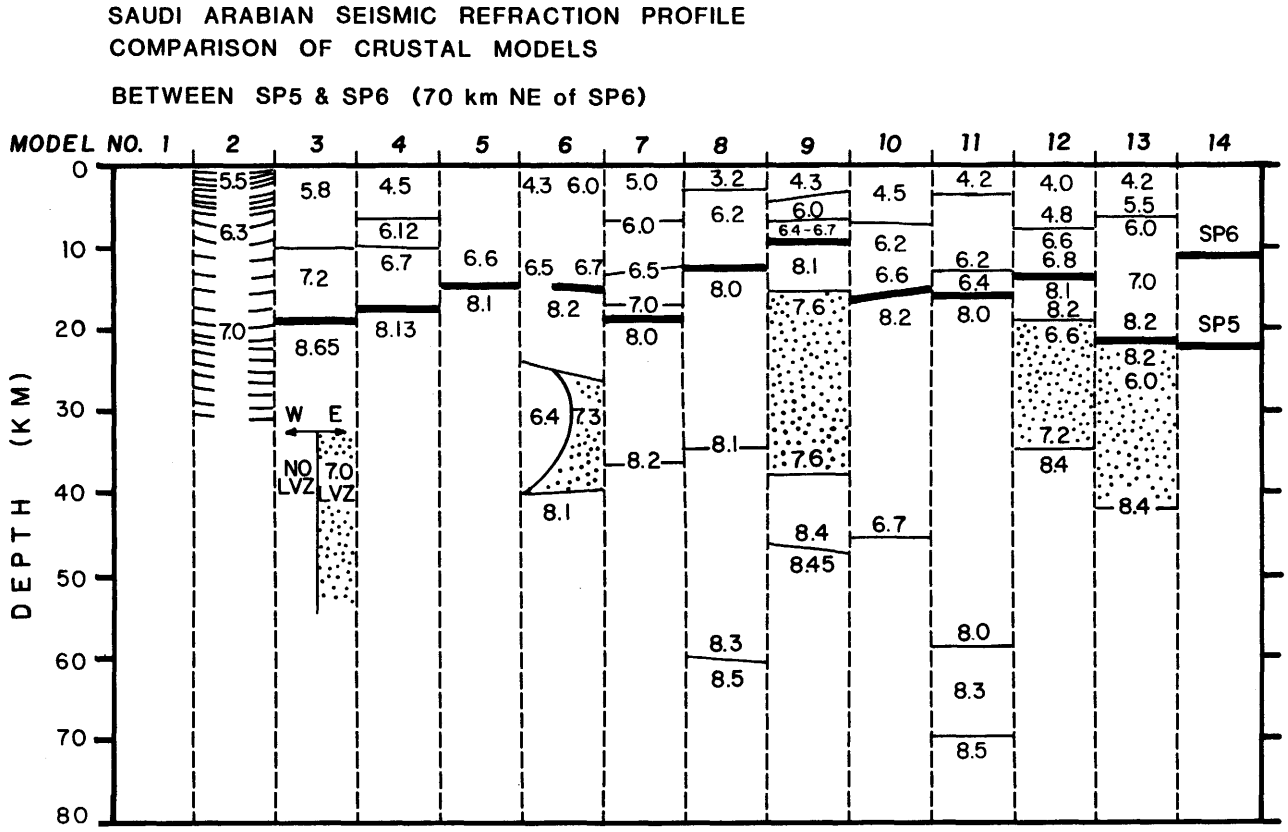

Figure 76. Comparison of crustal models between shotpoints 5 and 6. Symbols same as in figure 68.

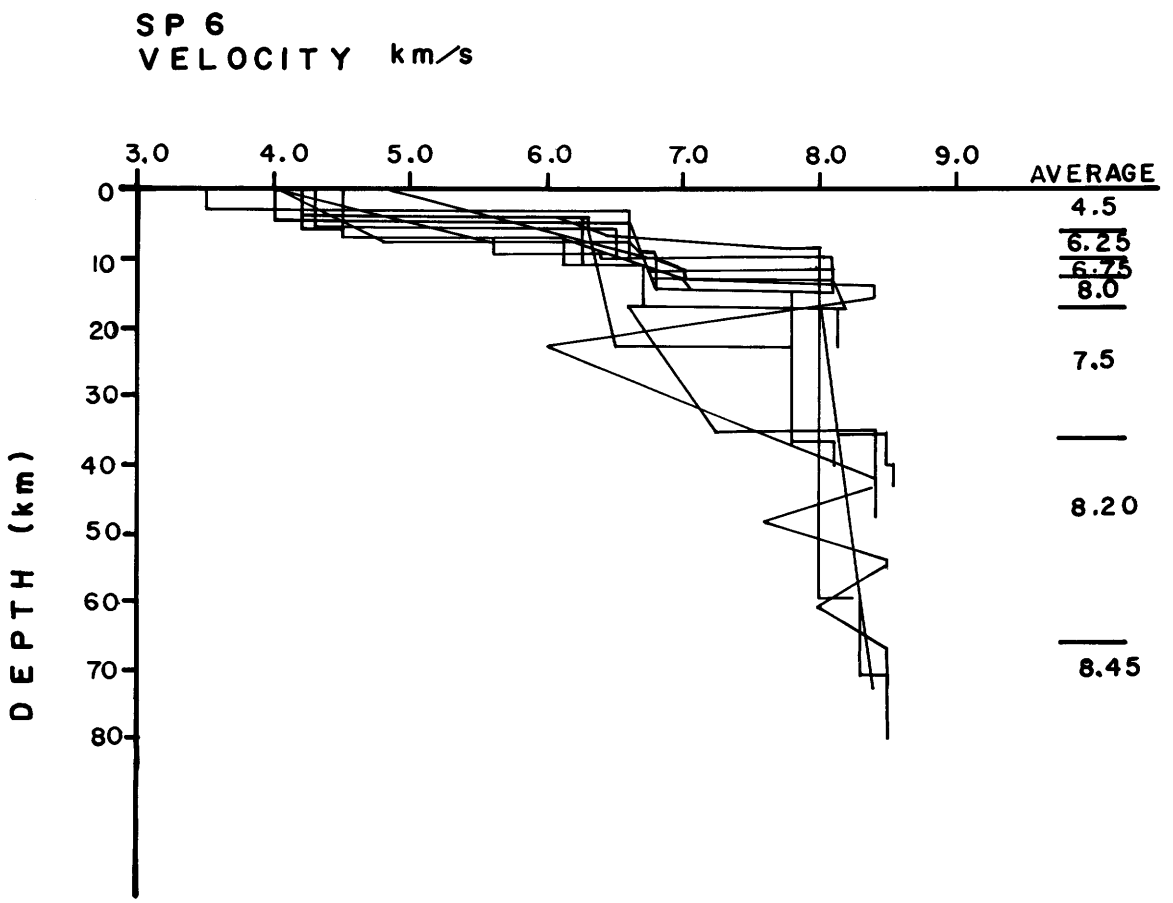

Figure 77. Comparison of velocity-depth functions beneath shotpoint 6. Average velocity section was obtained by inspection.

A COMPARISON OF CRUSTAL SECTIONS: ARABIAN SHIELD TO THE RED SEA

By Walter D. Mooney, U.S. Geological Survey, Menlo Park, California, and Claus Prodehl, University of Karlsruhe, Federal Republic of Germany

INTRODUCTION

The use of the Saudi Arabian seismic refraction data (Blank and others, 1979; Healy and others, 1982) at the IASPEI Commission on Controlled Source Seismology workshop made possible the compilation of ten complete crustal sections from the Red Sea across the Arabian Shield to the Arabian Platform. These sections (figs. 78-87) are presented on the same vertical and horizontal scale to facilitate a discussion of lateral variations in structure which were not evident in the previous figures of this workshop volume. The sections vary in detail from presenting only the general outline of the structure to more complete presentations of the crust and upper mantle.

We make no comparison of layer thicknesses and velocities, nor do we discuss the different methods of interpretation; the interested reader should refer to the previous section (Mooney and Gettings) for the former and to the individual contributions for the latter. The crustal sections presented here are as given at the workshop in August 1980. They may differ in detail with the revised contributions included in this volume or with the latest work of the investigators. In any case, the sections indicate the variation in possible interpretations.

Ansorge, Banda, Benz, Mueller, and Smith

The model of Ansorge and others (fig. 78) features a crust about 22 km thick at the eastern Red Sea and a mantle velocity of 7.8 km/s. These authors indicate the possibility of an upper mantle discontinuity at about 37 km beneath the Red Sea. Within the shield, their model consists of a three-layer crust that is locally perturbed by an extra high or low-velocity layer. Between shotpoints 4 and 5 they show a 6.5 km/s layer in the midcrust. The crust then consists of the basic three-layer model in the distance range 340 to 740 km from shotpoint 6, with an upper mantle velocity of 8.1 km/s. From 740 to 960 km, (mainly between shotpoints 1 and 2), the crust takes on an entirely different character; there are five layers, including a low-velocity zone. This change in interpreted structure may indicate a fundamental change in crustal composition and tectonic history for that portion of the profile.

Gettings

Gettings' model (fig. 79) describes the crustal structure in terms of a simple model, with statistical uncertainties assigned to the layer velocities. The Red Sea crust is modeled with three layers with velocities of 4.5, 6.12, and 6.7 km/s and a total thickness of 18 km. The mantle velocity is about 8.1 km/s. Between 140 and 370 km the shield crust thickens to 42 km, then thins to about 36 km toward the platform. The continental crust may be divided into two types in Gettings' model. From 140 to 600 km it consists of two layers with velocities of 6.24 and 6.83 km/s, while from 600 to 975 km it consists of two layers with velocities of 6.12 and 6.55 km/s. This lateral change in velocity structure implies an important change in crustal composition.

Ginzburg

Ginzburg's model (fig. 80) also describes the crustal structure in terms of a simple model. The Red Sea is modeled with a 12-km-thick crust with a westward-thickening sedimentary wedge. The crust thickens rapidly from 12 to 36 km between 80 and 140 km, which centers the Red Sea-shield transition 35 km west of shotpoint 5. Between 150 and 750 km the continental crust is modeled with two layers with velocities of 6.15 and 6.6 km/s. A possibly important lateral change occurs west of shotpoint 4 where the intracrustal and crust-mantle boundaries shallow abruptly by about 5 km. The crust is then rather homogeneous from shotpoint 4 to shotpoint 1. Thus, this model indicates three main crustal blocks: the Red Sea, shotpoint 5 to shotpoint 4, and shot point 4 to shotpoint 1.

Kosminskaya

The model presented by Kosminskaya (fig. 81) reveals several strong lateral variations. This model includes several features also seen in the models of Mishenkin, Mishenkina, and Solovjeva (fig. 84), and of Pavlenkova and Yurov (fig. 86). The essential features beneath the Red Sea are a 13-km-thick crustal layer which is underlain by normal mantle of 8.1 km/s velocity. The mantle layer extends to 17 km depth and is underlain by an 18-km-thick low-velocity zone (6.6-7.2 km/s). At about 35 km beneath the Red Sea the velocity discontinuously increases to 8.4 km/s and an additional mantle reflector is indicated at 47 km depth. The crust of the shield is composed of three layers with velocities of 6.0, 6.2-6.3, and 6.5-6.6 km/s. The largest lateral changes are the gradual thinning of the crust northeast of shotpoint 4 and the thickening of the 6.0 km/s layer northeast of shotpoint 3.

Maguire

Maguire's model (fig. 82) is characterized by strong lateral and vertical heterogeneities, including some within the upper mantle. The crust in the Red Sea is about 11 km thick near shotpoint 6, and the mantle velocity is 8.2 km/s. There is a low-velocity layer (6.4 km/s) centered at 30 km depth beneath shotpoint 6. The continental crust has three basic layers with velocities of 6.0-6.2, 6.4, and 6.6-6.7 km/s. This layered structure is significantly disrupted by higher and lower velocities in the region northeast of shotpoint 5 and beneath the escarpment, and a smaller high-velocity lens is depicted in the lower crust at 480 km. The velocity directly beneath the crust-mantle boundary decreases systematically from 8.2 km/s beneath the Red Sea to 7.9 km/s at the northeast end of the cross section. The upper mantle is shown with high- and low-velocity laminations ranging from 7.3 to 9.3 km/s. The laminations presumably correspond to zones of partial melt separated by eclogite or other high-velocity materials.

Milkereit and Flüh

Milkereit and Flüh presented a velocity cross section (fig. 83) derived from two-dimensional ray tracing. Their layer velocities are given as the velocity at the top of a boundary and the velocity gradient in km/s/km. The crust in the Red Sea is 13 km thick near shotpoint 6 and has a 6.6 km/s lower crustal layer. This layer extends only about 40 km to the northeast of

shotpoint 6 and is replaced by a 6.1 km/s velocity layer. Mantle velocity is 8.0 km/s beneath the Red Sea. An 8.1 km/s mantle layer underlies the entire profile and increases in depth from 62 km at the southwest end to 80 km at a point about midway along the profile (600 km from shotpoint 6). There are three main crustal layers with velocities of 6.1, 6.35, and 6.65 km/s and positive velocity gradients. There are several important lateral changes in the continental crustal structure. The 6.65 km/s layer, which has a regional depth of about 23 km in the shield, rises to as shallow as 2 km below sea level in the region northeast of shotpoint 5. Several changes in crustal structure occur between 300 and 410 km from shotpoint 6; the mantle becomes nearly flat northeast of 300 km, the 6.65 km/s layer deepens abruptly at 350 km, and the 6.1 km/s layer begins to thicken at 300 km and again at 410 km. These changes result in a different average crustal structure in the southwest end of the shield as compared with the central and northeast portions of the shield (400 to 910 km). This crustal section, like several others, shows a lateral change in structure 30 km southeast of shotpoint 2. Here, the lateral change is restricted to the upper crust and consists of a northeastward thinning of the 6.1 km/s layer.

Mishenkin, Mishenkina, and Solovjeva

The velocity cross section of Mishenkin, Mishenkina, and Solovjeva (fig. 84) describes the structure with as few layers as possible. The crust in the Red Sea is 15 km thick and the upper mantle velocity is 8.2 km/s. Although the authors have not modeled the upper mantle in detail, they indicate that there is a region in the upper mantle with an average velocity ($\bar{v}$) of 6.7 km/s. The continental crust is described in three layers with velocities of 6.0, 6.2, and 6.6 km/s, and the mantle velocity is 8.1-8.2 km/s. There is some indication of lateral discontinuities in the crust near shotpoints 4 and 2, and a lower crustal low-velocity zone is implied by the 6.2 km/s average velocity at 38 km depth at 540 km.

Mooney

The velocity section presented by Mooney (fig. 85) was derived by two-dimensional ray tracing. The crust beneath the Red Sea is shown as thickening toward the shield, increasing from 9 km at shotpoint 6 to 18 km near shotpoint 5. The Red Sea crust has three layers, the thickest with an average velocity of 6.2 km/s; the upper mantle velocity is 8.0 km/s. Unlike many other interpretations, there is no upper mantle low-velocity zone beneath the Red Sea. The ocean-continent transition occurs over a relatively short distance, about 25 km. The continental crust is modeled with three layers, all with positive gradients. The near-surface velocity varies from 6.1 to 6.3 km/s; the upper crustal layer (22 km thick) is laterally continuous and has an average velocity of 6.3-6.4 km/s. The lower crust thickens to the northeast and consists of a layer with two distinct gradients; the first is a low gradient from 6.7-6.8 km/s, and the second is from 6.8-7.8 km/s, both occurring over about 9 km in depth. The only major discontinuity within the crust itself is beneath shotpoint 2 where a strong lateral velocity discontinuity appears. One of the vertical velocity discontinuities in the upper mantle is laterally continuous.

Pavlenkova and Yurov

The velocity cross section of Pavlenkova and Yurov (fig. 86) describes the crust in relatively simple terms. The crust of the Red Sea is 13 km thick and includes a 5-km-thick layer with an average velocity of 6.7 km/s. The 8.1 km/s mantle is underlain at 18 km depth by a layer with a velocity of 6.6-7.2 km/s, which constitutes an upper mantle low-velocity zone. However, it is also possible to consider this layer as a continuation of the continental lower crust, with a mantle sill injected above it from the Red Sea axis. Mantle velocities (8.4 km/s) are attained once again at 35 km depth.

The continental crust is described in two layers with average velocities of 6.25 and 6.9 km/s, although two of the three velocity depth profiles (at 620 and 800 km) indicate some variations from this simple structure. Mantle velocity decreases from 8.2 km/s at 200 km to 8.0 km/s beneath the platform.

Prodehl

The crustal section of Prodehl (fig. 87), described by isovelocity lines, depicts the crust and upper mantle as vertically and laterally inhomogeneous. The crust is as thin as 15 km in the Red Sea and thickens to 45 km over a distance of 280 km. The upper mantle beneath the Red Sea contains a large low-velocity zone (stippled, ≥ 6.0 km/s) underlain by an 8.4 km/s upper mantle layer. There are several important lateral changes in the structure within the continental crust. Between shotpoints 5 and 4 the 6.6 km/s isovelocity contour rises to a depth of as little as 6 km (compare the model of Milkereit and Flüh, fig. 83). In this region there is also an elongate low-velocity zone (from 120 to 450 km) centered at about 15 km depth. The velocity in the lower crust gradually increases to mantle velocity. A second low-velocity zone is depicted in the upper crust between shotpoints 4 and 3, below which the velocity gradually increases to mantle values. Another lateral change in the crust occurs at 880 km (60 km northeast of shotpoint 2). Here the 6.4 and 6.6 km/s velocity contours begin to rise from about 20 km depth to about 10 km. Northeast of shotpoint 1 the basement increases in depth and a low-velocity zone appears in the upper crust.

The upper mantle structure for this cross section includes a low-velocity zone beneath shotpoint 4. Alternating high- and low-velocity layers are shown in the upper mantle (50-80 km), but no details can be derived from the available data for lateral variations below the 8.4 km/s contour.

REFERENCES

Blank, H. R., Healy, J. H., Roller, J. C., Lamson, R. J., Fischer, F., McClearn, R., and Allen, S., 1979, Seismic refraction profile, Kingdom of Saudi Arabia--field operations, instrumentation and initial results: U.S. Geological Survey Saudi Arabian Mission Project Report 259, 49 p.

Healy, J. H., Mooney, W. D., Blank, H. R., Gettings, M. E., Kohler, W. M., Lamson, R. J., and Leone, L., 1982, Saudi Arabian seismic deep-refraction profile, final project report: U.S. Geological Survey Saudi Arabian Mission and Directorate General of Mineral Resources Open-File Report USGS-OF-02-37, 370 p., 9 plates.

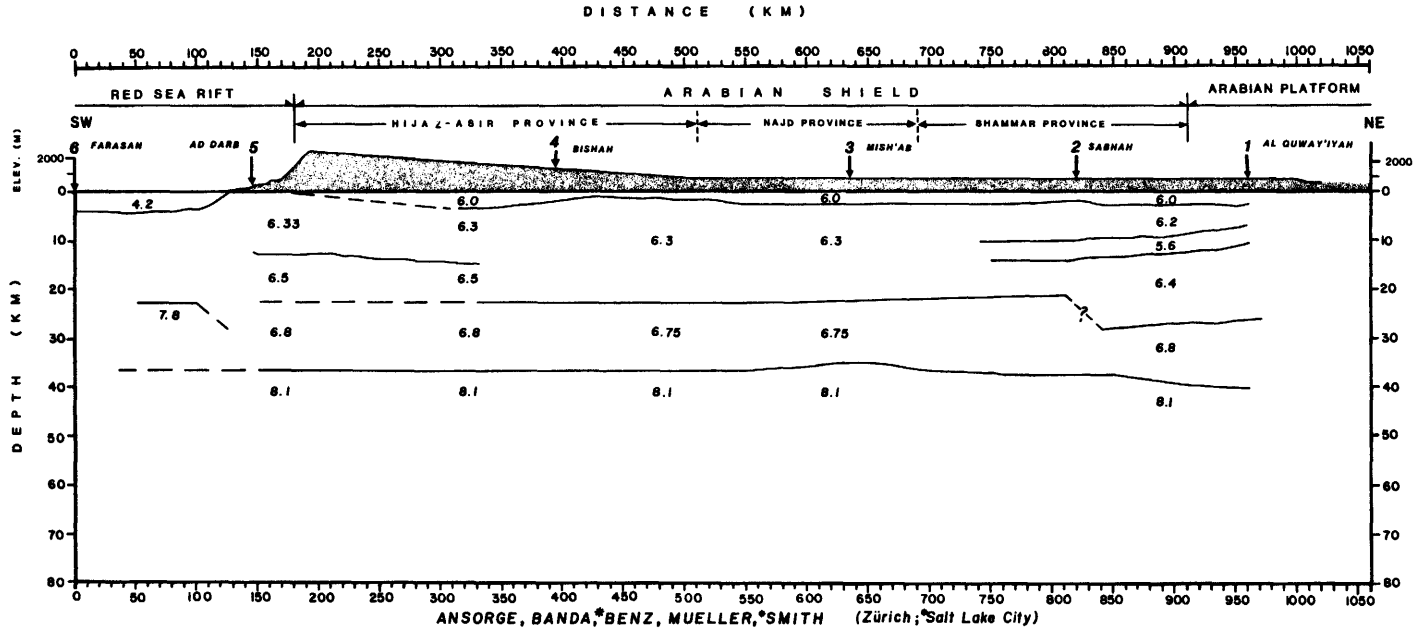

Figure 78. Crustal section of Ansorge, Banda, Benz, Mueller, and Smith.

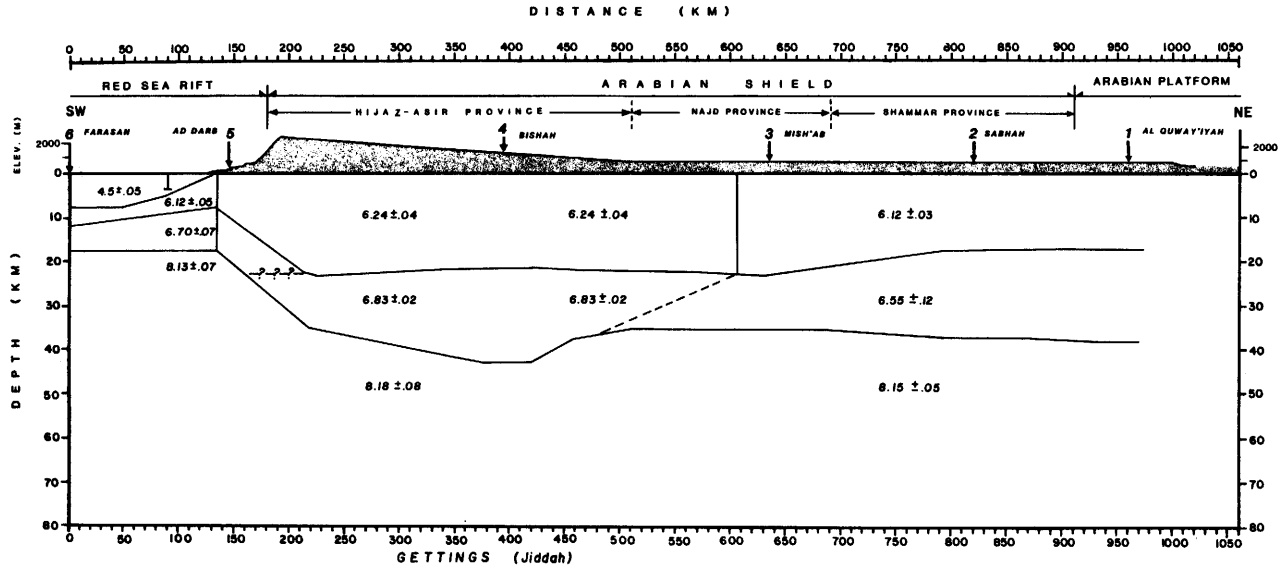

Figure 79. Crustal section of Gettings.

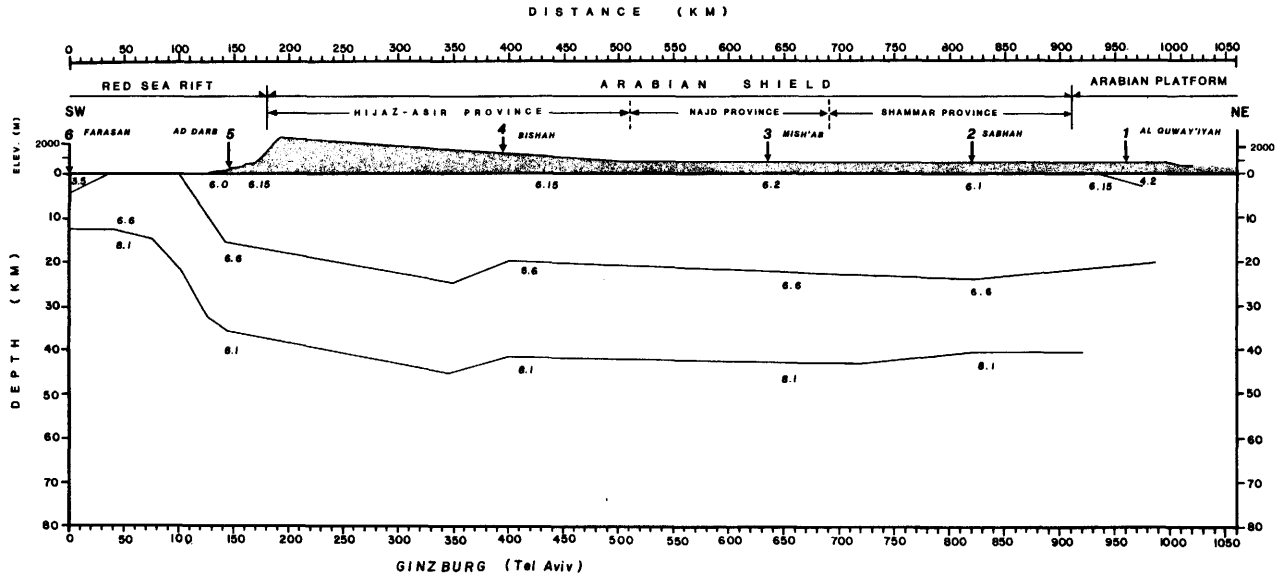

Figure 80. Crustal section of Ginzburg.

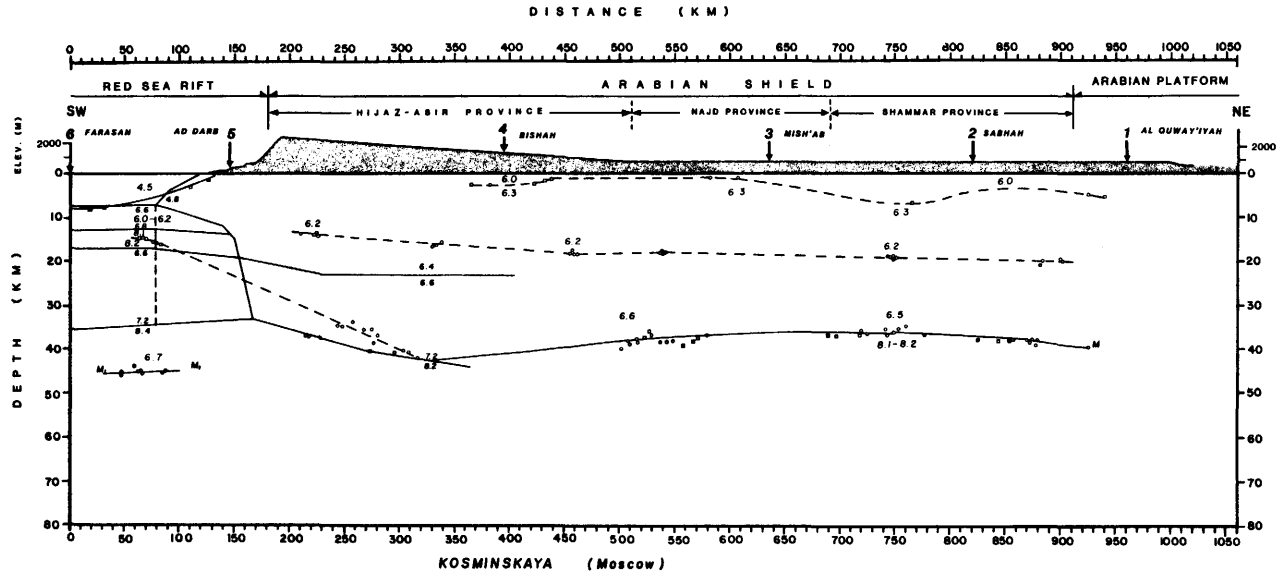

Figure 81. Crustal section of Kosminskaya. Small circles indicate individual boundary depth estimates.

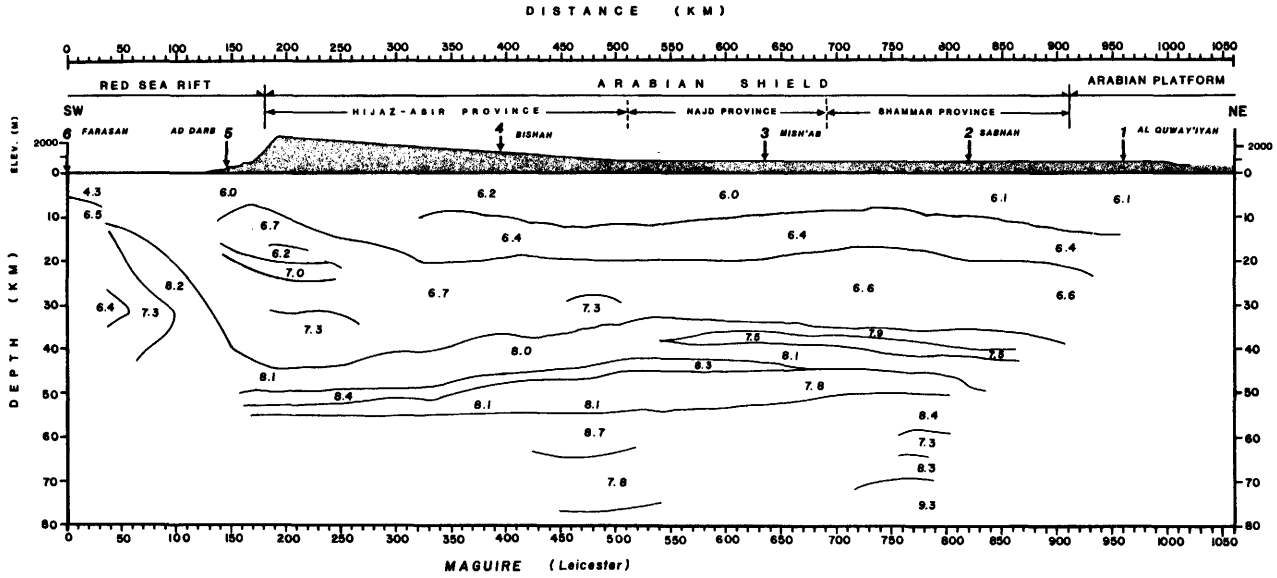

Figure 82. Crustal and upper mantle section of Maguire.

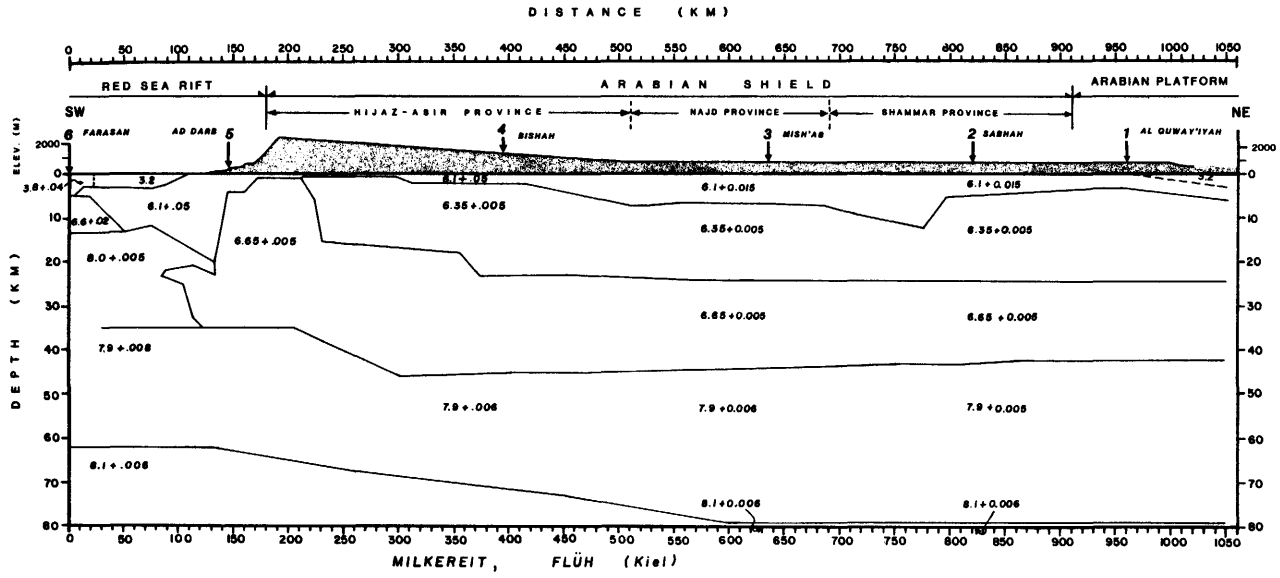

Figure 83. Crustal and upper mantle section of Milkereit and Flüh.

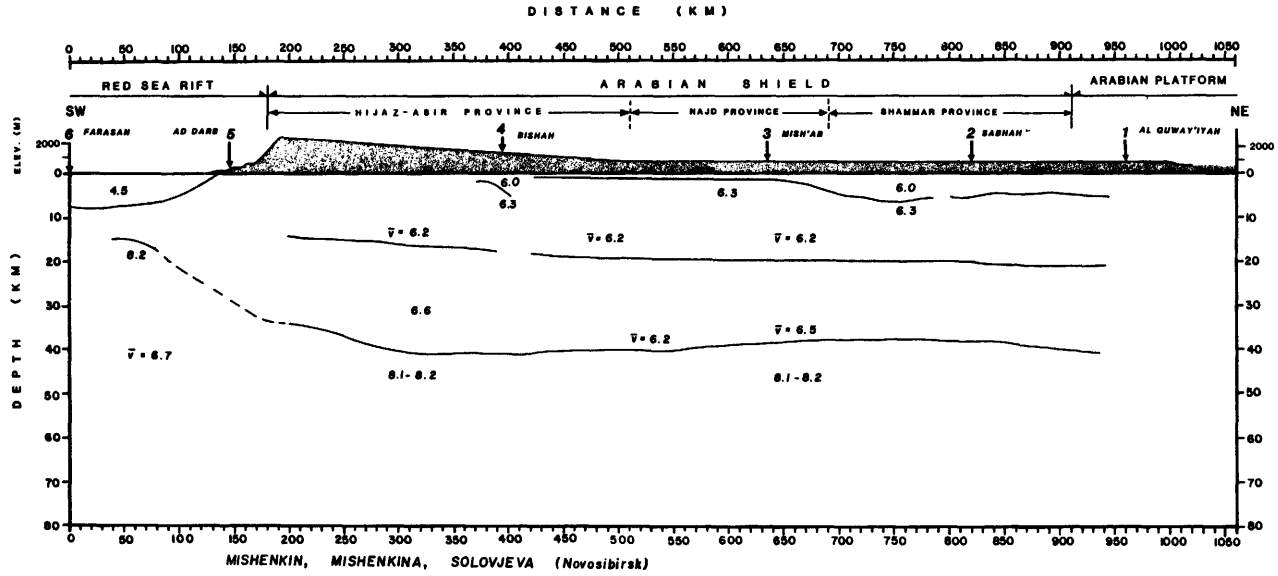

Figure 84. Crustal section of Mishenkin, Mishenkina, and Solovjeva.

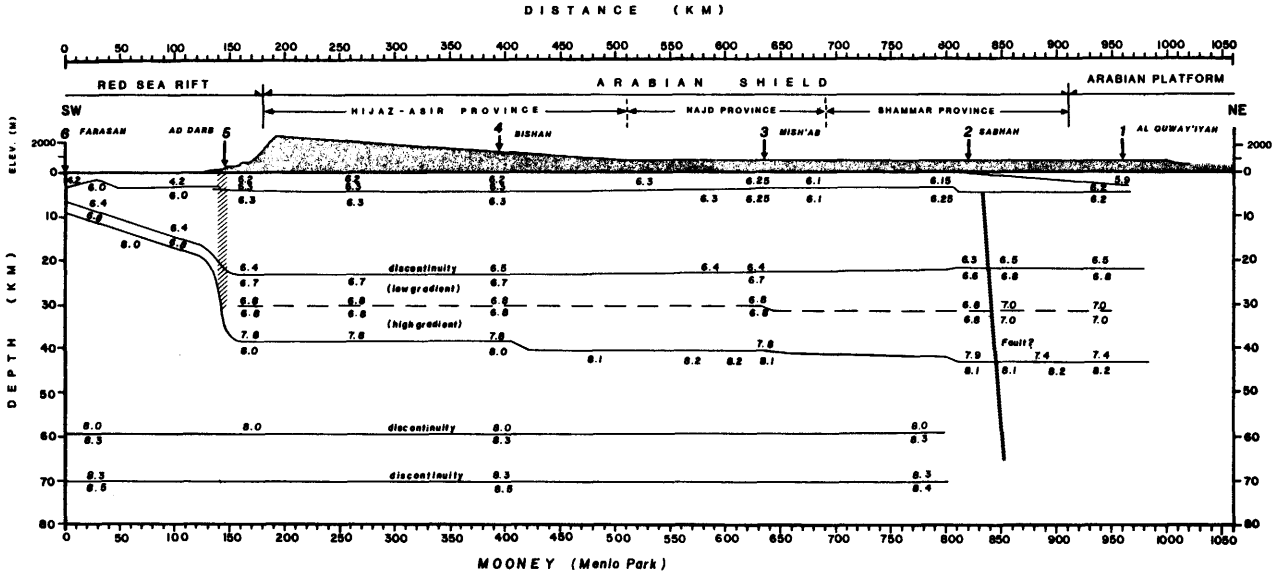

Figure 85. Crustal and upper mantle section of Mooney.

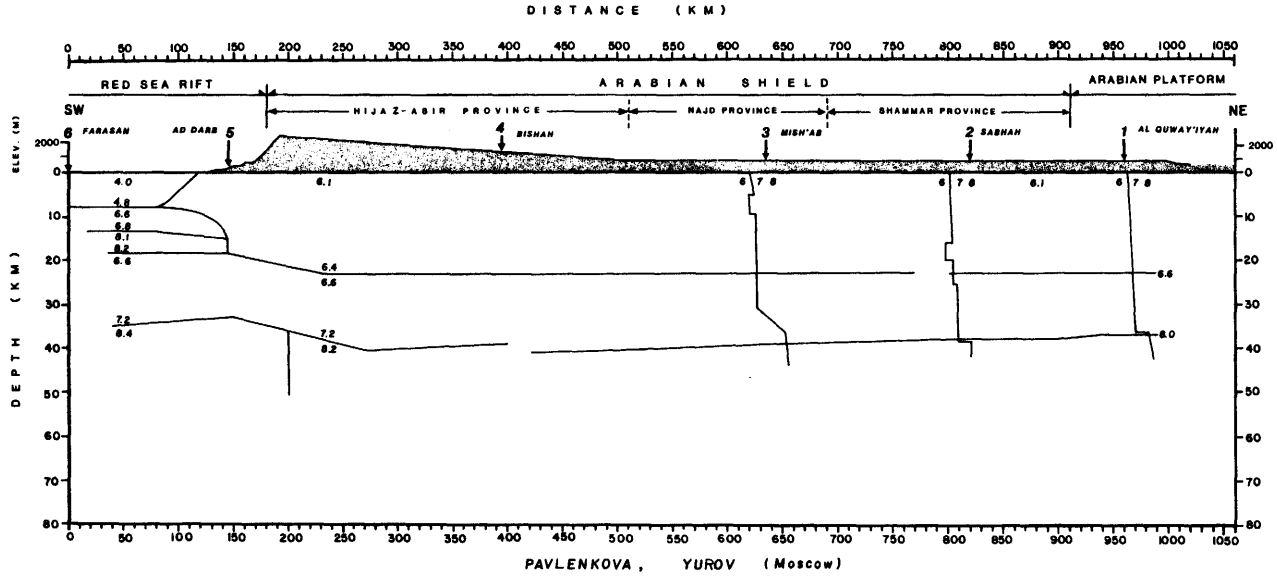

Figure 86. Crustal and upper mantle section of Pavlenkova and Yurov.

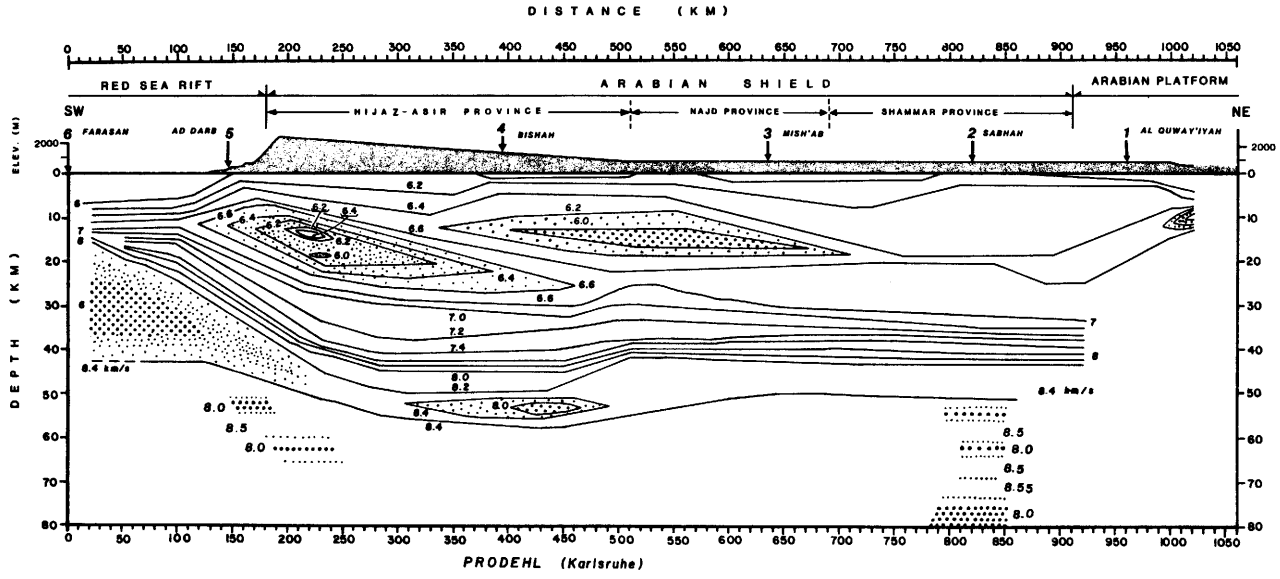

Figure 87. Crustal and upper mantle section of Prodehl.

REPORTS FROM THE DATA OF THE 1978 SAUDI ARABIAN SEISMIC REFRACTION PROFILE
[Published or in press as of November 1983]

Blank, H. R., Healy, J. H., Roller, J. C., Lamson, R., Fischer, F., McClearn, R., and Allen, S., 1979, Seismic refraction profile, Kingdom of Saudi Arabia, field operations, instrumentation, and initial results: U.S. Geological Survey Saudi Arabian Mission Project Report 259, 49 p.

Gettings, M. E., 1981, A heat flow profile across the Arabian Shield and Red Sea (abs.): EOS, American Geophysical Union Transactions, v. 62, no. 17, p. 407.

Gettings, M. E., 1982, Heat flow measurements at the 1978 Saudi Arabia deep-seismic refraction line shot points II. Discussion and interpretation: Saudi Arabian Deputy Ministry for Mineral Resources Open-File Report USGS-OF-02-40, 40 p.

Gettings, M. E., Blank, H. R., Mooney, W. D., and Healy, J. H., 1983, Crustal structure of southwestern Saudi Arabia: Saudi Arabian Deputy Ministry for Mineral Resources Open-File Report USGS-OF-03-59, 51 p.

Gettings, M. E. and Showail, A., 1982, Heat flow measurements at the 1978 Saudi Arabia deep-seismic refraction line, Part I. Results of the measurements: Saudi Arabian Deputy Ministry for Mineral Resources Open-File Report USGS-OF-02-39, 98 p.

Healy, J. H., Mooney, W. D., Blank, H. R., Gettings, M. E., Kohler, W. M., Lamson, R. J., and Leone, L., 1982, Saudi Arabian seismic deep-refraction profile, final project report: U.S. Geological Survey Saudi Arabian Mission and Directorate General of Mineral Resources Open-File Report USGS-OF-02-37, 370 p., 9 plates.

Kohler, W. M., Lamson, R. J., and Healy, J. H., 1980, A study of P-wave attenuation in the Arabian Shield using spectral ratios (abs.): EOS, American Geophysical Union Transactions, v. 60, no. 46, p. 881.

Lamson, R. J. and Blank, H. R., 1978, USGS/DGMR Geophysical Investigations in Saudi Arabia: Seismic refraction profile--status report no. 2, 15 January 1978.

Lamson, R. J., Blank, H. R., Mooney, W. D., and Healy, J. H., 1979, Seismic refraction observations across the oceanic-continental rift zone, southwest Saudi Arabia (abs.): EOS, American Geophysical Union Transactions, v. 60, no. 46, p. 954.

Lamson, R. J. and Leone, L. E., 1980, Saudi Arabia seismic refraction profile data set, volumes 1 and 2: U.S. Geological Survey Open-File Report, Miscellaneous Document 17.

Merghelani, H. M. and Gallanthine, S. K., 1980, Microearthquakes in the Tihamat-Asir region of Saudi Arabia: Bulletin of the Seismological Society of America, v. 70, no. 6, p. 2291-2293.

Mooney, W. D., 1980, IASPEI workshop--seismic modeling of laterally varying structures (Arabian Shield to the Red Sea): EOS, American Geophysical Union Transactions, v. 61, p. 19.

Mooney, W. D., Gettings, M. E., Blank, H. R., and Healy, J. H., 1983, Saudi Arabian seismic-refraction profile: A traveltime interpretation of crustal and upper mantle structure: Tectonophysics, in press.

U.S. Geological Survey, 1976, USGS/DGMR Geophysical Investigations in Saudi Arabia: Seismic refraction profile--status report no. 1: U.S. Geological Survey Mission, internal report, 19 p., 6 figs.

APPENDIX 1

IASPEI WORKSHOP ABSTRACT

[Presented at the July 1981 IASPEI meeting, London, Ontario, Canada]

Commission on Controlled Source Seismology, Reporters:
S. Mueller, Zurich; W. D. Mooney, Menlo Park; C. Prodehl, Karlsruhe; R. B. Smith, Salt Lake City; D. P. Hill, Menlo Park; J. A. Orcutt, La Jolla; J. Ansorge, Zurich

The third triennial meeting of the IASPEI Commission on Controlled Source Seismology was convened in Park City, Utah, from August 11 to 17, 1980, to explore and assess the progress of controlled source techniques and to evaluate its significance in terms of current models of the seismic velocity structure and composition of the crust and upper mantle.

Two and one half days of the five-day conference were used to discuss different interpretations of the seismic refraction data collected in Saudi Arabia by the U.S. Geological Survey in 1978. The format of this portion of the meeting was unlike most other scientific workshops. The complete refraction data set had been distributed to the participants well in advance of the meeting, giving time to thoughtfully analyze the same data. The use of a common data base allowed for a kind of in-depth examination of issues of interpretation that is not possible in traditional workshops which are based on diverse data sets.

In the course of the different presentations it became evident that the main source of differences in the final models is the phase correlation of the data. The term "phase correlation" refers to the process of identifying, within a seismic record section, those arrivals that refract or reflect from the same feature (or portion) of the crustal or mantle velocity structure. Given identical phase correlations, different methods of traveltime and amplitude analysis of these phases will produce nearly the same result. Conversely, different correlations will result in markedly divergent models. These points can be appreciated from the comparison of the models of the Arabian Shield to those of the transition from the Red Sea to the Arabian subcontinent. A few highlights on the interpretation are summarized below.

1. The upper crust (21 km thick) of the shield has a near-surface velocity of 6.1 km/s and, in most regions, a positive velocity gradient of 0.01-0.02 km/s/km. Low-velocity zones may be present in some regions.

2. The lower crust (19 km thick) of the shield is separated from the upper crust by a seismic discontinuity or smooth transition of 0.2-0.4 km/s. The average velocity of the lower crust is about 6.7 km/s.

3. The M-discontinuity is probably a transition zone 2-5 km thick and occurs at a nearly constant depth of about 40 km. The velocity of the uppermost mantle is 0.8-8.1 km/s, and there is evidence for fine structure within the lithosphere.

4. The structure of the Red Sea-continent transition remains uncertain with the currently available data.

APPENDIX 2

IASPEI-CCSS PARTICIPANTS

G. E. Andreasen, Reston, Virginia
J. Ansorge, Zurich, Switzerland
M. Qusai Assad, Jiddah, Saudi Arabia
E. Banda, Zurich, Switzerland
H. Benz, Salt Lake City, Utah
M. J. Berry, Ottawa, Canada
H. R. Blank, Jiddah, Saudi Arabia
L. W. Braile, West Lafayette, Indiana
S. Clawson, Salt Lake City, Utah
N. Deichmann, Zurich, Switzerland
E. R. Flüh, Kiel, Federal Republic of Germany
L. N. Frazer, Honolulu, Hawaii
J. D. Garmany, Seattle, Washington
M. E. Gettings, Jiddah, Saudi Arabia
S. K. Ghosh, Minneapolis, Minnesota
A. Ginzburg, Tel Aviv, Israel
R. E. Hanson, Falls Church, Virginia
J. H. Healy, Menlo Park, California
D. P. Hill, Menlo Park, California
S. Kaufman, Ithaca, New York
I. P. Kosminskaya, Moscow, USSR
L. E. Leone, Menlo Park, California
P. K. H. Maguire, Leicester, England
J. S. McClain, La Jolla, California
T. V. McEvilly, Berkeley, California
F. McKisic, Washington, D.C.
H. M. Merghelani, Jiddah, Saudi Arabia
B. Milkereit, Kiel, Federal Republic of Germany
H. Miller, Munich, Federal Republic of Germany
T. A. Mokhtar, Jiddah, Saudi Arabia
W. D. Mooney, Menlo Park, California
St. Mueller, Zurich, Switzerland
K. H. Olsen, Los Alamos, New Mexico
J. A. Orcutt, La Jolla, California
N. I. Pavlenkova, Moscow, USSR
R. A. Phinney, Princeton, New Jersey
K. Posgay, Budapest, Hungary
K. Priestley, Dunedin, New Zealand
C. Prodehl, Karlsruhe, Federal Republic of Germany
R. B. Smith, Salt Lake City, Utah
S. B. Smithson, Laramie, Wyoming
R. A. Stephen, Woods Hole, Massachusetts
R. M. Stewart, Reston, Virginia
R. W. Ward, Richardson, Texas
G. Zandt, Salt Lake City, Utah
R.-S. Zeng, Beijing, China

APPENDIX 3

INTERNATIONAL ASSOCIATION OF SEISMOLOGY

AND PHYSICS OF THE EARTH'S INTERIOR

COMMISSION ON CONTROLLED SOURCE SEISMOLOGY

Resolution 1

The International Association of Seismology and Physics of the Earth's Interior,

Recognizing the substantial progress made in the past decade in determining crustal and upper mantle structure through the application of "Controlled Source Seismology," and

Noting that the results obtained indicate considerable heterogeneity in structure,

Urges that, in detailed regional studies of the crust and upper mantle, refraction and reflection methods be used, when possible, in combination, supplemented by observations from deep sources wherever available.

Canberra (Australia)

12 December 1979

GPO 787-042/10005